THE UNIVERSITY *of* EDINBURGH

This thesis has been submitted in fulfilment of the requirements for a postgraduate degree (e. g. PhD, MPhil, DClinPsychol) at the University of Edinburgh. Please note the following terms and conditions of use:

- This work is protected by copyright and other intellectual property rights, which are retained by the thesis author, unless otherwise stated.
- A copy can be downloaded for personal non-commercial research or study, without prior permission or charge.
- This thesis cannot be reproduced or quoted extensively from without first obtaining permission in writing from the author.
- The content must not be changed in any way or sold commercially in any format or medium without the formal permission of the author.
- When referring to this work, full bibliographic details including the author, title, awarding institution and date of the thesis must be given.

THE UNIVERSITY *of* EDINBURGH

Defining Metabolic Zonation as a Determinant of Hepatocyte Plasticity

Caitlin McCaffrey

Doctor of Philosophy

University of Edinburgh

2025

Declaration

I declare that this thesis has been composed solely by myself. Any contribution by another person has been explicitly referenced and acknowledged. This work is entirely my own and has not been submitted in any previous degree application.

Signed,

Caitlin McCaffrey

Abstract

Liver regeneration following injury occurs through several well-defined mechanisms, including the hypertrophy or hyperplasia (proliferation) of epithelial cells and the recruitment and differentiation of hepatic progenitor cells. In specific contexts, experimental evidence suggests that mature hepatocytes have the capacity for transdifferentiation in order to contribute to biliary repair; however, it remains unknown whether all hepatocytes possess this propensity or whether lineage plasticity is zonated within the lobule.

This study aimed to investigate whether the position of hepatocytes along the axis of the lobule is a determinant of hepatocyte plasticity. This was achieved through two independent approaches, the first being the design and breeding of two mouse models, which facilitated *in vivo* lineage tracing of hepatocyte populations from opposite poles of the liver lobule. These mouse models enabled fluorescent labelling of Glutaminase (Gls2)-expressing periportal (zone 1/2) or Glutamine Synthetase (GS)-expressing pericentral (zone 3) hepatocytes, utilising a dual-fluorescent mT/mG CreER-loxP system. Based on established methods described in published studies, intrahepatic cholangiocarcinoma (iCC) was induced via hydrodynamic tail vein delivery of Notch intracellular domain 1 (NICD1) and Akt overexpression, thereby stimulating cell fate change in the two hepatocyte populations of interest. The second approach involved the development of a spheroid culture model from primary murine hepatocytes (PMH) isolated from control mice and lineage-traced Gls2CreER-mT/mG and GSCreER-mT/mG mouse models. This complementary approach enabled the *in vitro* modelling of zonated hepatocyte gene expression, providing a platform to evaluate hepatocyte plasticity via NICD1/Akt upregulation *ex vivo*.

The data presented in this study reveal that periportal hepatocytes, originating from zone 1/2, specifically those expressing Gls2, undergo transdifferentiation and phenotypic changes that contribute to biliary repair more readily than GS-expressing hepatocytes from the Wnt-high pericentral zone. Additionally, primary murine hepatocyte (PMH) spheroid models not only preserve zonated gene expression profiles of constituent hepatocytes *ex vivo* but also demonstrate that the zonated phenotypic markers can be influenced through changes in culture media composition. The PMH spheroid platform appeared to recapitulate the transdifferentiation seen *in vivo* upon NICD1/Akt upregulation, with gene expression analyses indicating a shift from a hepatocyte to a biliary lineage, closely mirroring changes in targeted hepatocyte populations in the mouse models. Importantly, these findings suggest that hepatocyte plasticity in biliary repair is zonally restricted and can be modelled and experimentally manipulated *ex vivo*, providing new insight into the determinants and modulation of hepatocyte fate in regeneration and disease.

Lay Summary

It is widely known that the liver has the unique ability to repair itself after injury, and it does so by exploiting several well-defined mechanisms involving the cells that make up the organ's tissue. These cells include hepatocytes, which comprise the bulk of the liver and are responsible for performing its metabolic functions, and biliary cells, which form the tubular bile ducts and drain bile from within the liver. Usually, these cells have distinct roles, but under certain conditions, hepatocytes can exhibit "plasticity" – meaning that they can change their identity and function to help repair damage.

In this study, an investigation was conducted to determine whether this plasticity depends on the location of hepatocytes within the liver. Although hepatocytes appear similar and share many functions, they differ depending on their location within the liver, which enables the organ to perform multiple metabolic tasks simultaneously. Using mouse models, hepatocytes from different areas of the liver were tagged with fluorescent markers, allowing their movements and any changes in shape to be tracked after an injury was induced that mimics the development of bile duct cancer. This revealed that hepatocytes that reside near the branches of the portal vein were more likely to change their shape and function, adopting characteristics that made them appear more like biliary cells. In contrast, hepatocytes found around the central vein at the opposite end of the liver's microscopic functional units, known as lobules, showed little to no plasticity.

A three-dimensional lab-grown cell culture system called primary murine hepatocyte spheroids was also developed. These are spherical clusters of thousands of hepatocytes isolated from mouse livers, which enabled analysis of these changes outside the body. These spheroids preserved the shape and function of hepatocytes for several days, and the hepatocyte type could be influenced by the cell culture medium in which they were kept, driving them to exhibit either more portal- or more central vein hepatocyte traits. When exposed to the same stimuli used in the mouse model to induce bile duct cancer, the hepatocytes making up the spheroids exhibited similar changes in appearance and function.

Overall, this work demonstrates that hepatocyte plasticity is influenced by their location within the liver and can be effectively modelled in the laboratory using advanced cell culture techniques. By improving understanding of how cellular location affects hepatocyte behaviour and by replicating these processes in cell cultures, insight is provided into early events in bile duct cancer development, which may guide new strategies for treating liver injury and disease.

Acknowledgments

First and foremost, I would like to thank my supervisor, mentor, and friend, **Rachel Guest**, for taking a chance on me and providing me with the opportunity to move across the world to embark on this PhD journey. I could not have achieved any of this without your tireless guidance and support throughout these years. You are a force of nature and an inspiration; I am constantly in awe of everything you have accomplished and everything you have yet to achieve.

I am equally grateful to my co-supervisor, **Luke Boulter**, for helping me become a better scientist and for offering guidance whenever needed. Your kindness and the warm, welcoming environment you fostered made my transition so much easier, and I will always appreciate that.

To the lab friends I have made along the way, **Nathalie**, **Bea**, **Kitty**, **Chloe, Rosie, Emily**, **Alex**, **Steve**, **Paul**, **Varun**, and **Joseph**. Your unwavering friendship and support helped me through challenges I couldn't have faced alone.

My gratitude also extends to the **Edinburgh Baseball Club**, **Saltire Sluggers**, and **Dalmeny Dodgers** and all their members – some of whom have become more like family than friends. Arriving in a new country alone, I had no idea how much joining this wonderful community of hooligans and playing these silly sports would change my life for the better. You have taught me resilience and the true meaning of unconditional friendship. No Scotland, No Party!

Speaking of changing things for the better, **Ryan Macfarlane**, the impact you've had on my life is beyond anything words could capture. You have been my rock, my shoulder to cry on, my voice of reason (even when I didn't want it), and, most importantly, my partner. Thank you for choosing to be the Marco to my Polo.

To my family – **Kevin**, **Nana**, **Walt**, **Sam**, **Steve**, **Justine**, **Lauren**, **Nick**, **Sean**, **Emma**, **Charlie**, **Fiona**, and **Laura** – thank you for your unwavering support through all the highs and lows. Your collective encouragement and kindness inspire me every single day.

Finally, to my mom, **Sarah McCaffrey** – my forever best friend and pillar of strength. To paraphrase Gilmore Girls: "My mother never gave me any idea that I couldn't do whatever I wanted to do or be whomever I wanted to be… As she guided me through these incredible 30 years, I don't know if she ever realised that the person I most wanted to be was her." I love you endlessly and miss you every day.

This thesis is dedicated to my lost loved ones: **Savannah Merrick (Lynch)**, **Toni-lee Kirkbride**, **Barrie Wardill**, and **John McCaffrey**.

Contents

List of Abbreviations

Abbreviation	Definition
2D	Two Dimensional
3D	Three Dimensional
ADME	Absorption, Distribution, Metabolism and Excretion
Akt	Akt Serine/Threonine Kinase
BP	Biological Processes
CCl_4	Carbon Tetrachloride
cDNA	Complementary DNA
Ct	Threshold Cycle
CV	Central Venule
DAB	3,3'-Diaminobenzidine
DDC	3,5-Diethoxycarbonyl-1,4-Dihydrocollidine
Dex	Dexamethasone
ECM	Extracellular Matrix
FACS	Fluorescence-Activated Cell Sorting
Gls2	Glutaminase 2
GOI	Gene of Interest
GS	Glutamine Synthetase
H&E	Haematoxylin & Eosin
HCC	Hepatocellular Carcinoma
HKG	Housekeeping Gene
HPCs	Hepatic Progenitor Cells
HR	Hour/s
HSD	Honestly Significant Difference
HTVI	Hydrodynamic Tail Vein Injection
iCC	Intrahepatic Cholangiocarcinoma
IF	Immunofluorescence/Immunofluorescent
IgG	Immunoglobulin G
IHC	Immunohistochemistry/Immunohistochemical
iPSCs	Induced Pluripotent Stem Cells

IR/DR	Inverted Repeat/Direct Repeat
LB	Lysogeny Broth
MASLD	Metabolic Dysfunction-Associated Steatotic Liver Disease
MF	Molecular Functions
mGFP	Membranous Green Fluorescent Protein
mT/mG	Membranous Tomato/Membranous Green Fluorescent Protein
mTom	Membranous Tomato
NAFLD	Non-Alcoholic Fatty Liver Disease
NASH	Non-Alcoholic Steatohepatitis
NICD1	Notch Intracellular Domain 1
p.adj	Adjusted P-value
PAS	Periodic Acid-Schiff
PBS	Phosphate Buffered Saline
PFA	Paraformaldehyde
PHH	Primary Human Hepatocytes
PMH	Primary Murine Hepatocytes
PMHS	Primary Murine Hepatocyte Spheroids
PV	Portal Venule
qPCR	Quantitative Polymerase Chain Reaction
RLU	Relative Light Units
RNA-seq	Ribonucleic Acid Sequencing
SB	Sleeping Beauty
scRNA-seq	Single-cell Ribonucleic Acid Sequencing
SD	Standard Deviation
SEM	Standard Error of Mean
SRA	Sequence Read Archive
TAA	Thioacetamide
TC	Tissue Culture

Figures

Tables

CHAPTER 1

Introduction and Literature Review

1.1 The Structure and Functional Anatomy of the Liver

The liver is a highly organised organ composed anatomically of repeating hexagonal units called lobules. These lobules consist of several portal triads, each of which comprises a branch of the hepatic artery, bile duct, and portal vein, that encircle the branches of the central vein (Figure 1.1a) [1]. This architecture has evolved to channel oxygen- and nutrient-rich blood from the portal and systemic circulations towards the central venous drainage, establishing gradients of oxygen, nutrients, and morphogens across the lobule. Hepatocytes comprise the principal functional cells of the liver parenchyma and account for ~70–80% of the liver mass. They are arranged in plates radiating from the portal triads. These plates are traversed by hepatic sinusoids, which enable exchange between blood and hepatocytes. The exchange occurs across the space of Disse, a narrow perisinusoidal region that separates the sinusoidal endothelium from the hepatocyte surfaces [1,2]. Within this space reside hepatic stellate cells, a mesenchymal population that, under homeostatic conditions, secretes extracellular matrix components to provide structural and biochemical support rather than constituting the matrix itself [3,4]. Hepatocytes coordinate essential metabolic, synthetic, and detoxification processes, while biliary epithelial cells (BECs), the other primary epithelial cell type in the liver, line the intrahepatic ducts to regulate bile modification and flow [5].

Despite being morphologically and functionally distinct, these polarised epithelial cell types originate from a shared bipotential progenitor cell type within the embryo known as hepatoblasts [6-10]. The bipotent hepatoblasts emerge from the ventral foregut endoderm during embryogenesis and are the founding cells of the developing liver bud [6,11]. Following hepatic specification, these cells invade the septum transversum mesenchyme and undergo lineage allocation in response to local cues. Hepatoblasts located adjacent to portal tracts are preferentially directed towards a BEC fate, while those positioned more centrally differentiate into hepatocytes, establishing early parenchymal and ductal domains (Figure 1.1b) [7,8,11-14]. Spatial and temporal signalling gradients orchestrate this regionalised cell fate choice. Zong *et al.* (2009) demonstrated that the asymmetric expression of Jag1 and Hes1 across the liver bud regulates hepatoblast specification [15]. Hepatoblasts near portal veins show heightened sensitivity to ectopic Notch signalling, favouring a biliary fate, whereas those within parenchymal regions remain committed to hepatocyte differentiation [15]. This positional bias has been proposed to be reinforced by local TGFβ signalling, which modulates Notch responsiveness, helping to establish ductal zones versus hepatocyte plates even at these early stages of organogenesis [16].

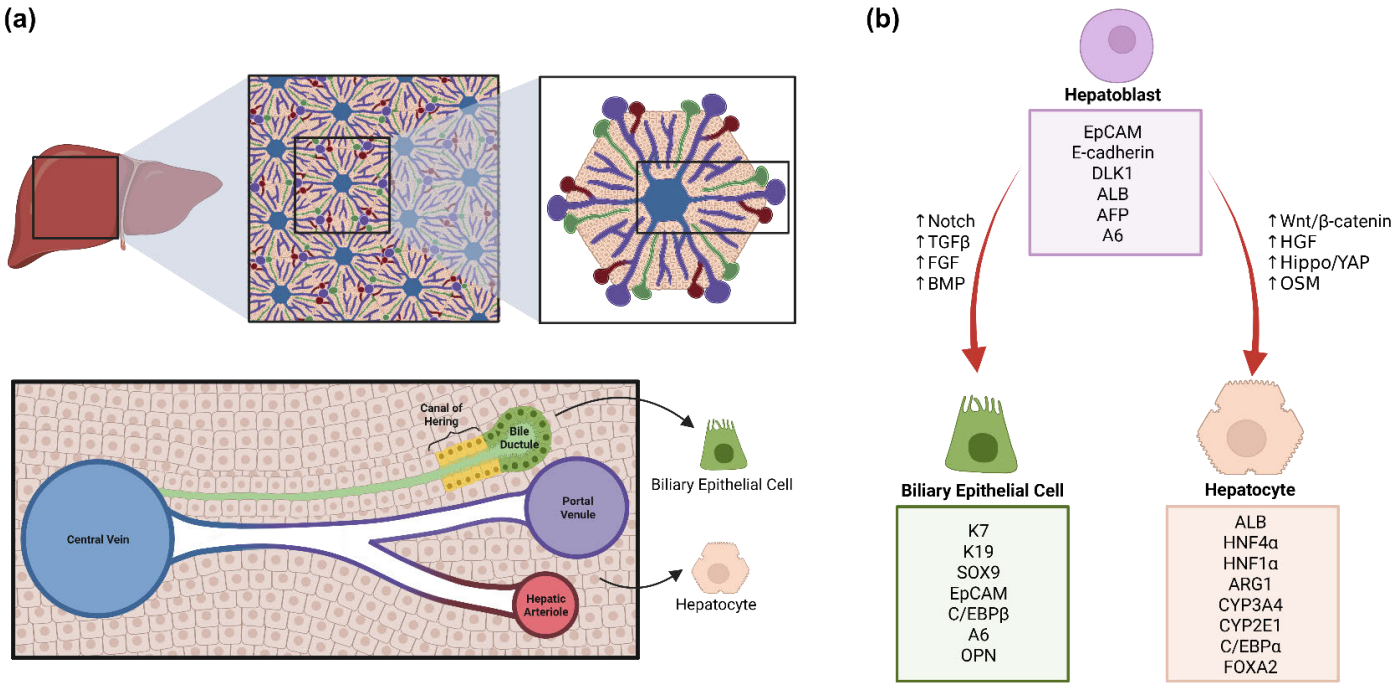

Figure 1.1: Liver Architecture and Lineage Specification of Hepatocytes and Biliary Epithelial Cells. (a) *Schematic overview of the hexagonal lobular structure of the liver, illustrating the arrangement of portal triads (portal venule, hepatic artery, and bile ductule) at the periphery and a central vein at the core, highlighting the spatial relationship between hepatocytes and biliary epithelial cells.* ***(b)*** *Summary of key signalling pathways directing bipotential hepatoblasts towards hepatocyte or biliary epithelial fates, emphasising molecular markers and transcriptional regulators of each lineage (Created with BioRender).*

1.1.1 Definition of a Biliary or Hepatocyte Lineage

The Notch signalling pathway is required for the specification of a BEC lineage during liver development. Canonical Notch signalling operates as a juxtacrine mechanism mediated by interactions between transmembrane receptors (Notch 1-4) and ligands from the Jagged (Jag1, Jag2) and Delta-like (DLL1, DLL3, DLL4) families, facilitating precise communication between adjacent cells to regulate key processes such as cell fate specification, proliferation, and morphogenesis (Figure 1.2) [15,17-21]. When membrane-bound Notch ligand engages a Notch receptor on a neighbouring cell, this interaction triggers two sequential proteolytic cleavages: the first mediated by ADAM-family metalloproteases, removing the Notch extracellular domain (NECD), and the second by γ-secretase, which releases the Notch intracellular domain (NICD). The NICD translocates to the nucleus, where it associates with the transcription factor CSL and co-activators such as MAML, converting CSL from a repressor to an activator of transcription and initiating the expression of Notch target genes [15,17-21]. Within the developing liver, portal mesenchymal cells and BECs surrounding the portal triads express

the Notch ligand Jagged1, which engages Notch receptors on neighbouring bipotential hepatoblasts, triggering a transcriptional program activating biliary lineage markers such as Sox9 and Hnf1β [8,15,17,22].

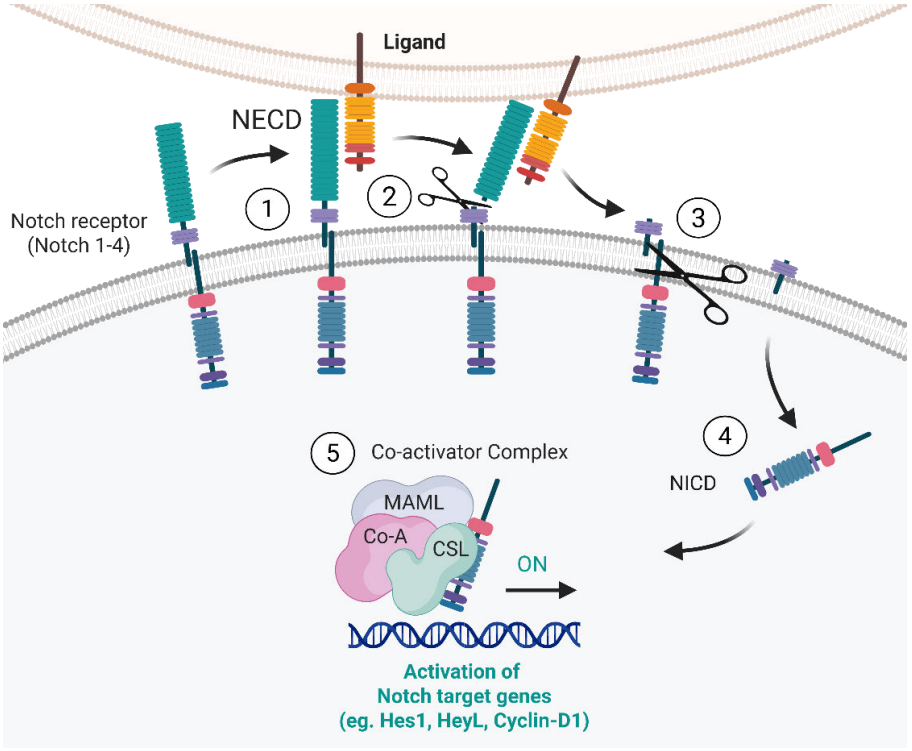

Figure 1.2: Schematic Overview of the Canonical Notch Signalling Pathway. ***(1)*** *Binding of Notch ligand to receptor induces cleavage and shedding of Notch extracellular domain (NECD).* ***(2–3)*** *Subsequent proteolytic processing releases Notch intracellular domain (NICD), which translocates to the nucleus.* ***(4–5)*** *NICD associates with the co-activator complex (CSL, Co-A, MAML) to drive activation of Notch target genes such as Hes1, HeyL, and Cyclin-D1 (Created with BioRender).*

Clinical studies have pinpointed mutations in key components of the Notch pathway – particularly in Jag1 and Notch2 – as causative for Alagille syndrome, a congenital disorder characterised by bile duct paucity and abnormal biliary development in affected humans [23,24]. These findings are based on sequencing analyses from large patient cohorts, which revealed that the vast majority of Alagille syndrome cases harbour either protein-truncating or missense mutations in Jag1, with a smaller subset exhibiting Notch2 mutations, confirming a direct link between Notch pathway disruption and human biliary disease [23,24]. Mechanistic insights have come from mouse models in which conditional, hepatoblast-specific deletion of Notch1 and Notch2 (such as $N1N2^{F/F}$ AlbCreER lines) produces disorganised and hypoplastic ductular structures accompanied by inflammation and fibrosis, thus underscoring the pathway's essentiality for bile duct morphogenesis [24,25].

Zong *et al.* (2009) further elucidated the molecular basis of this pathway by employing Foxa3-Cre-driven deletion of RBP-Jκ, a pivotal Notch transcriptional effector, in developing mouse livers [15]. Foxa3 is a pioneer transcription factor of the forkhead box family that is broadly expressed in hepatoblasts during embryonic liver development, prior to lineage segregation into hepatocyte and biliary fates. Its early and widespread expression in hepatoblasts makes it an ideal driver for Cre-mediated recombination to study liver development. The authors utilised lineage tracing, immunohistochemistry for biliary markers such as Sox9, cytokeratin 19 (K19), and Hnf1β, and serial section analysis to quantify both precursors and mature ducts. Their results demonstrated that RBP-Jκ deletion leads to a dramatic reduction in Sox9+ ductal plate cells and mature bile ducts, as evidenced by both decreased marker expression and structural analysis of the ductular network. Conversely, activation of Notch via NICD expression in hepatoblasts induced extensive ectopic expression of biliary markers and generated abnormal duct-like structures, directly showing that Notch is sufficient to drive a BEC fate and biliary morphogenesis *in vivo*. These experiments revealed that Notch signalling functions in a dose-, spatial-, and temporally restricted manner, orchestrating both the initiation of biliary lineage identity and the morphogenic processes necessary for the formation and maturation of the biliary network. Additionally, Notch2-deficient and RBP-Jκ knockout mice exhibit impaired biliary regeneration following liver injury by biliary toxins or resection, highlighting the pathway's ongoing role in repair and plasticity beyond embryonic development [15].

Notch signalling collaborates closely with other developmental pathways, notably TGFβ and Wnt/β-catenin, to orchestrate hepatoblast fate decisions and liver architecture. TGFβ2, secreted by portal mesenchymal cells, activates the SMAD2/3–SMAD4 cascade in adjacent hepatoblasts, upregulating BEC markers such as Sox9 and repressing hepatocyte determinants like Hnf4α [26,27]. Genetic and pharmacological studies have demonstrated that amplification of TGFβ signalling promotes the expansion of immature BECs. In contrast, pharmacological inhibition of TGFβ receptors disrupts this pipeline and favours hepatocyte differentiation, underscoring TGFβ's instructive role in establishing the biliary lineage [26]. These functional studies, including fate-mapping, gene knockout, and inhibitor experiments, illuminate how TGFβ acts as a regional instructive cue at the portal tract, operating in synergy with Notch to bias local hepatoblasts toward BEC identity.

In contrast, hepatoblasts that are not exposed to periportal cues such as Jagged1-mediated Notch activation from portal mesenchymal and biliary epithelial cells, TGFβ2 secreted by portal mesenchyme, and the high-oxygen, nutrient-rich environment of the portal circulation are biased toward the hepatocyte fate, primarily through the action of Wnt/β-catenin signalling [28-31]. In the earliest stages of liver development, Wnt/β-catenin – together with fibroblast growth factor (FGF) from the

adjacent cardiac mesoderm – drives the specification of hepatic fate in the foregut endoderm, initiating hepatic gene expression and supporting the expansion of hepatoblasts [28]. The essential function of this pathway during hepatic induction is exemplified by studies in zebrafish, where genetic ablation of Wnt2b causes a profound failure in liver bud formation (known as the "Prometheus phenotype"), confirming Wnt's requirement early in liver organogenesis [32]. As liver development advances, the role of Wnt/β-catenin becomes more dynamic, as demonstrated by the targeted deletion of Apc, a negative regulator in the β-catenin destruction complex, in murine hepatoblasts. This results in persistent β-catenin activation, promoting hepatomegaly while simultaneously disrupting terminal hepatocyte differentiation [33,34]. Conversely, complete loss of β-catenin prevents hepatocyte specification and leads to severely hypoplastic livers. Mechanistically, Wnt/β-catenin signalling acts by stabilising β-catenin – by inhibiting destruction complex components such as GSK3β and Axin – thereby enabling nuclear translocation and activation of hepatocyte-defining transcription factors, including Hnf4α, FOXA1/2, and C/EBPα [9,29,30].

Wnt/β-catenin also antagonises Notch-driven biliary specification, creating spatial compartmentalisation within the liver lobule that aligns with either hepatocyte or biliary cell fates [31,35,36]. This antagonism ensures robust lobular patterning, as cells exposed to high Wnt/β-catenin signalling commit to hepatocyte differentiation, while cells nearer the portal region, exposed to Notch and TGFβ, differentiate into biliary epithelial cells. Beyond Wnt, additional signalling pathways – including Oncostatin M (OSM) from hematopoietic cells [37,38], hepatocyte growth factor (HGF) [39-41], and glucocorticoids [42-45] – collectively reinforce the hepatocyte programme by stimulating proliferation and suppressing biliary gene expression. The Hippo/YAP pathway further balances proliferation and differentiation, with the loss of YAP inducing hepatocyte death, whilst overactivation drives dedifferentiation and the expression of biliary markers via Notch modulation [26,46-48]. Collectively, these integrated and stage-dependent pathway interactions, dissected through a wide array of genetic and pharmacological experiments in zebrafish and murine models, provide a detailed mechanistic and temporal map of how Notch, Wnt, TGFβ, and additional signals coordinate the specification and maturation of liver cell lineages, shaping the unique and functional architecture of the mammalian liver.

1.1.2 Metabolic Zonation in the Liver Lobule

Upon maturation, hepatocytes do not exhibit uniform function across the lobule; instead, their gene expression and metabolic activity are regionalised – a phenomenon termed liver zonation. Along the porto-central axis of the liver lobule (between the portal and central venules), hepatocytes are exposed

to gradients of oxygen, nutrients, and hormonal signals, resulting in spatially distinct roles (Figure 1.3) [49]. Periportal hepatocytes, located in 'Zone 1' adjacent to the portal triads, are richly supplied with oxygen and are therefore optimised for energetically demanding, oxidative processes. These cells preferentially carry out gluconeogenesis, β-oxidation of fatty acids, and urea synthesis, thereby supporting systemic glucose homeostasis and nitrogen disposal under conditions of ample oxygen availability [50-56]. In contrast, pericentral hepatocytes residing in 'Zone 3', near the central vein where oxygen tension is lower, are specialised for more anaerobically favourable and detoxification-related pathways, including glycolysis, xenobiotic metabolism via cytochrome P450 enzymes, and glutamine synthesis [50-56]. This configuration not only maximises the efficiency of hepatic metabolism but also protects the organism by compartmentalising potentially toxic reactions, such as drug and xenobiotic processing, to sites distal from the bloodstream entering via the portal vein [57,58]. Metabolic liver zonation begins to emerge during late gestation and is progressively established in the postnatal period. Spatially restricted expression of key zonation markers, such as glutamine synthetase (GS), is first detected around the central vein just prior to birth (embryonic day E17.5–E18.5 in mice), and this pattern becomes fully mature during the early postnatal weeks [31,59-61]. Studies employing metabolic enzyme reporters and single-cell transcriptomics have revealed that while some zonated gene expression can be observed perinatally, the sophisticated, adult-like zonation architecture – including both metabolic and non-metabolic regionalisation – relies on additional cues from the postnatal environment and reaches its final configuration only after birth [59-61].

In addition to oxygen and nutrient gradients shaping the metabolic functions in hepatocyte populations, Wnt/β-catenin signalling emerges as a pivotal molecular regulator orchestrating hepatic zonation [30,31,54,62-64]. This signalling pathway is predominantly active in Zone 3, around the central vein, where endothelial cells and hepatic stellate cells serve as key sources of Wnt ligands, particularly Wnt2 and Wnt9b, with hepatic stellate cells also contributing as secondary contributors of ligands such as R-spondin 3 (RSPO3) (Figure 1.3) [3,65]. Specifically, these analyses demonstrate evolutionarily conserved, pericentral zonation of Wnt2 and Wnt9b expression in both mouse and human livers. mRNA mapping and cell marker co-localisation confirm that these ligands are predominantly produced by central vein and sinusoidal endothelial cells. In contrast, stellate cell expression is much more limited [3,65] Functional studies, such as conditional deletion of Wntless (an essential gene for Wnt ligand secretion) or targeted knockout of Wnt2 and Wnt9b in endothelial cells, result in loss of pericentral β-catenin activation and corresponding ablation of canonical targets like GS and cytochrome P450 enzymes, thereby disrupting hepatic zonation and confirming the necessity of local endothelial Wnt2/9b delivery [65]. While hepatic stellate cells express some Wnt ligands, genetic ablation

experiments indicate that they are not required for steady-state zonation; however, they may provide context-dependent paracrine signalling during liver regeneration or fibrosis [49,51,66].

In contrast, periportal hepatocytes, exposed to lower levels of Wnt activity and additional inputs such as MAPK/ERK signalling and oxygen availability, preferentially express genes including Gls2, SDS, and Cyp2F2, thereby sustaining gluconeogenesis and oxidative functions [49,51,66-69]. Studies indicate that approximately 50% of hepatocyte genes exhibit spatial zonation, with expression levels subject to the effects of signalling pathways such as Wnt/β-catenin and oxygen gradients, effectively shaping a transcriptional landscape where metabolic and detoxification processes are tightly compartmentalised within the liver lobule [55,66,70,71].

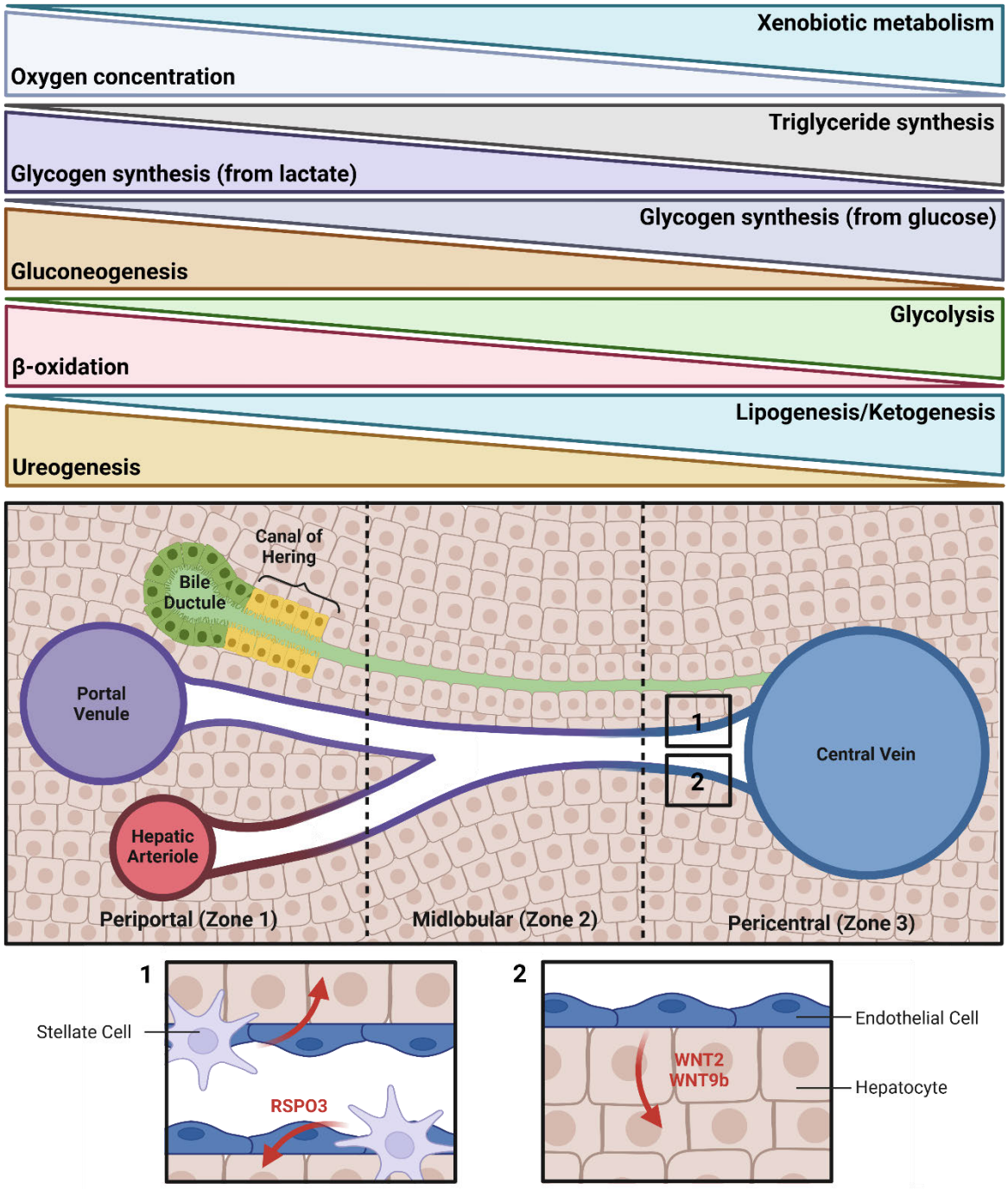

Figure 1.3: Spatial Gradients of Metabolic Functions and Endothelial- and Stellate-Derived Wnt Ligands in Liver Lobule Zonation. *Schematic illustrating oxygen and metabolic gradients across periportal to pericentral zones, along with (1) hepatic stellate cell- and (2) endothelial cell-derived Wnt modulators (such as RSPO3, Wnt2, and Wnt9b) that maintain β-catenin activity and zonal gene expression in hepatocytes (Created with BioRender).*

Glutamine synthetase (GS), encoded by the GLUL gene, is a well-established marker of pericentral hepatocytes and is directly regulated at the transcriptional level by β-catenin/TCF complexes. The spatial restriction of Wnt/β-catenin signalling across the hepatic lobule is maintained by the tumour suppressor gene APC, which is selectively enriched in periportal hepatocytes, where it acts as a negative regulator of the pathway [34]. By suppressing Wnt/β-catenin signalling in the periportal zone, APC ensures that pathway activity and the expression of pericentral genes such as GS remain confined to zone 3 hepatocytes. The conditional loss of APC in hepatocytes results in the ectopic activation of Wnt/β-catenin throughout the lobule, leading to the aberrant expansion of pericentral gene expression (including GS) into periportal territories and concomitant repression of periportal gene sets. Thus, APC is indispensable for establishing and maintaining the boundaries of metabolic zonation in the liver, locally restricting Wnt pathway activation and enabling the reciprocal expression of periportal and pericentral genes essential for hepatic metabolic homeostasis and nitrogen balance [34].

Complementing this, recent research has significantly advanced the ability to visualise and resolve liver zonation at both single-cell and spatial levels, thereby expanding upon classical biochemical mapping. Building on the findings of Preziosi *et al*. (2018), who defined endothelial cells as the primary sources of pericentral Wnt ligands, Sugimoto *et al*. (2025) further established the instrumental role of hepatic stellate cells as additional Wnt producers in the pericentral niche, particularly during regeneration and homeostasis [3]. Their work demonstrates that stellate cell-derived Wnts contribute to β-catenin signalling gradients, reinforcing metabolic zonation and supporting efficient recovery post-injury. These discoveries highlight a sophisticated paracrine network in which endothelial and stellate cells cooperatively regulate local Wnt ligand availability to sculpt the spatially distinct metabolic and detoxification functions across the lobule [53,64,65]. Through this mechanism, Wnt signalling drives the expression of enzymes involved in glycolysis, xenobiotic metabolism, and glutamine synthesis, while simultaneously repressing periportal functions, such as gluconeogenesis and urea synthesis [63]. Disruption of this balanced zonal architecture has been implicated in various liver diseases, underscoring the importance of signalling pathways, such as the Wnt/β-catenin pathway, in maintaining hepatic homeostasis (Figure 1.4).

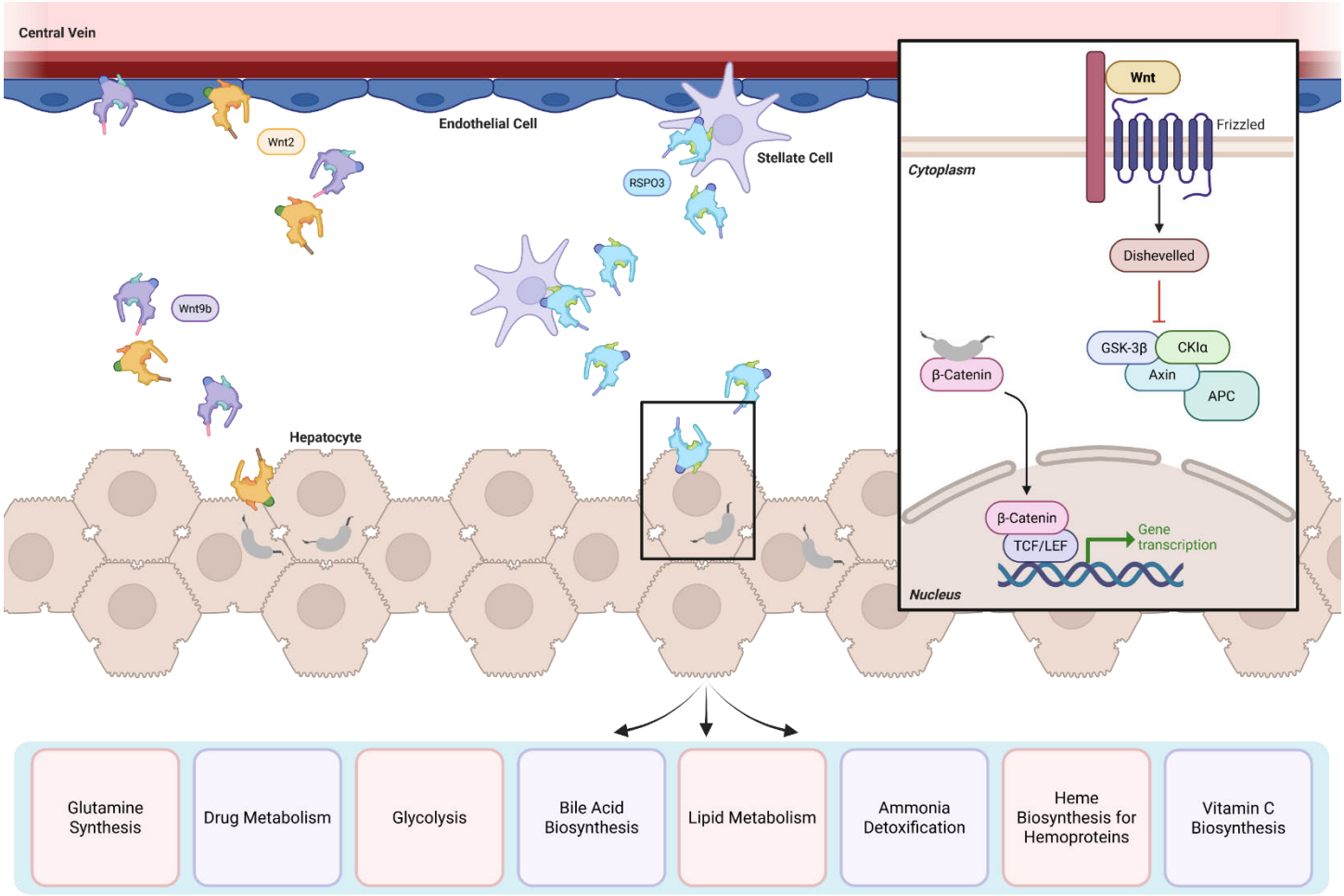

Figure 1.4: Spatial Regulation of Hepatocyte Metabolic Functions by Wnt/β-catenin Signalling in the Liver Lobule. *Pericentral endothelial and stellate cells secrete Wnt ligands (Wnt2, Wnt9b) and R-spondin 3 (RSPO3), activating canonical Wnt/β-catenin signalling in adjacent hepatocytes, as depicted in the inset. This signalling axis modulates zonated gene transcription and underlies the pericentral compartmentalisation of key metabolic processes, including glutamine synthesis, drug metabolism, glycolysis, bile acid biosynthesis, lipid metabolism, ammonia detoxification, heme biosynthesis, and vitamin C biosynthesis (Created with BioRender).*

Recent advances in genetic lineage tracing and the development of single-cell sequencing technologies have enabled unprecedented resolution in the study of liver zonation. Wei *et al.* (2021) generated a comprehensive series of zonally restricted CreER knock-in mouse lines, targeting genes with well-defined spatial expression – for example, Gls2 and Arg1 (zone 1), Hamp2 and Mup3 (zone 2), and GS, Cyp1A2, and Oat (zone 3) – allowing for the precise labelling and fate mapping of hepatocyte populations according to their metabolic position within the lobule [66]. These tools provide a robust genetic framework to interrogate the relationship between spatial gene expression, metabolic function, and ultimately, the behaviour of specific hepatocyte subpopulations in both physiological and pathological settings.

Comprehensive single-cell and spatial multi-omic datasets have further elucidated zonation hierarchies. The landmark study by Halpern *et al*. (2017) employed single-cell RNA-seq and spatial reconstruction to reveal that over 50% of hepatocyte-expressed genes exhibit robust zonated expression patterns, with non-monotonic and midzonal peaks also prevalent [49]. Gola *et al*. (2021) reported the pronounced zonation of both metabolic and non-parenchymal populations, including endothelial and immune cells, using paired-cell sequencing and advanced spatial transcriptomics [72]. Notably, Ben-Moshe *et al*. (2019) summarised how these technological advances enabled the reconstruction of proteome, transcriptome, and even noncoding RNA zonation maps, firmly linking spatial gene regulation to liver tissue function [51]. Most recently, González-Blas *et al*. (2024) used single-cell multi-omics and spatial mapping in the mouse liver to show that over 2,600 genes and thousands of enhancers are zonated along the porto-central axis [73]. They identified a core set of transcription factors, including Hnf6, Hnf4α, Hnf1α, C/EBPα, and FOXA1, as key regulators driving spatial gene expression. At the same time, the repressors TBX3 (pericentral) and TCF7L1 (periportal) restrict enhancer activity to their respective zones. Using a massively parallel reporter assay, they validated that these enhancer elements are responsive to zone-specific regulatory logic. Their `DeepLiver` deep learning model accurately predicted enhancer function and zonation, and motif analyses highlighted Hnf6 as a major driver of pericentral enhancer usage. Experimental mutagenesis further confirmed that disrupting TBX3 or TCF7L1 motifs alters spatial enhancer activity. Together, these results demonstrate that enhancers encode and enforce liver zonation patterns through the combinatorial action of core transcription factors and zonally restricted repressors, with Hnf6 playing a prominent role in establishing pericentral identity [16,73-75].

1.2 Liver Regeneration and Hepatocyte Plasticity

1.2.1 Evidence for Hepatocyte Plasticity in Liver Regeneration

Cellular plasticity, in the context of the liver, refers to the ability of hepatocytes and other liver cells to flexibly modulate their identity or functional phenotype in response to environmental signals – not necessarily altering their genome, but expressing alternative gene programmes according to the needs of tissue repair or adaptation to disease states. In the liver, this may encompass classic processes such as dedifferentiation (where mature hepatocytes reacquire progenitor-like features), transdifferentiation (direct conversion to another lineage such as biliary), metaplasia (acquisition of novel functional traits), or in some cases the loss of metabolic zonation – where hepatocytes from one lobular zone begin to co-express markers and perform functions typical of other zones.

The metabolic compartmentalisation is progressively disrupted in pathologies, including acute injuries such as acetaminophen toxicity and chronic diseases, including cirrhosis and non-alcoholic steatohepatitis (NASH) [76-78]. In injury states, surviving hepatocytes have been observed to lose their zonal identities and often adopt hybrid zone profiles, with the co-expression of typically segregated markers, such as Cyp2F2 and Gls2 (periportal) and Cyp2E1 and GS (pericentral), thereby compensating for tissue loss and functional deficits [79]. Disease-specific responses can further amplify these changes; for instance, pericentral cells are more susceptible to drugs and toxins (such as carbon tetrachloride (CCl_4) or thioacetamide (TAA)), whereas periportal injury predominates in autoimmune hepatitis and iron overload [80-84]. Chronic pathologies such as cirrhosis not only disrupt zonation but also drive hepatocytes to downregulate mature metabolic genes and activate stress-response and proliferative states, thereby impairing nitrogen, lipid, and xenobiotic metabolism [85,86]. Ben-Moshe and colleagues (2019) demonstrated, using single-cell analyses, that injury exerts zone-specific effects within the liver, which give rise to distinct pathological phenotypes [51]. These spatially resolved transcriptomic and proteomic analyses reveal that the highly zonated expression pattern is underscored by both mRNA and protein levels for most hepatocyte genes, with certain exceptions where post-transcriptional regulation further diversifies zonal identity [51]. Significant zonated genes highlighted in their data include the pericentral Wnt receptors Fzd7 and Fzd8, which are enriched in the central layers of the lobule and are crucial for mediating Wnt signalling governing metabolic specialisation [51]. Conversely, periportal hepatocytes express higher levels of Wnt inhibitors such as Tcf7l1 and CTNNBIP1, supporting their distinct metabolic profile and shielding them from Wnt pathway activation. Notably, the study showed that while markers such as Hnf4α are strongly expressed in periportal regions at the protein level, their mRNA abundance does not always correlate spatially, underscoring the role of post-transcriptional regulation in diversifying hepatocyte identity.

Hepatocyte responses to injury extend far beyond simple self-duplication, involving a rich diversity of subpopulations and remarkable plasticity spanning all regions of the liver lobule. Lin *et al*. (2018) identified a subset of hepatocytes with high telomerase expression (TERTHi), which comprises ~3–5% of the hepatocyte pool and is enriched in periportal and midlobular zones [87]. These cells demonstrated a greater proliferative and self-renewal capacity both at homeostasis and during injury, with ablation of this population being noted to impair regeneration and increase fibrosis. This discovery directly challenged the prevailing paradigm of strict zonal restrictions – such as models proposing that regeneration is driven solely by pericentral (AXIN2+) hepatocytes [88] – and opened the door for further exploration of hepatocyte heterogeneity and distributed regenerative potential. Subsequent studies have reinforced this broadened view, with one such study by Sun *et al*. (2020) performing

comprehensive lineage tracing using bacterial artificial chromosome (BAC)-transgenic Axin2CreERT2 mice and demonstrating that AXIN2+ pericentral hepatocytes do not exhibit superior proliferative capacity or behave as stem cells during homeostasis or regeneration [89]. Instead, hepatocytes throughout the liver, across all zones, were shown to upregulate AXIN2 and LGR5 and contribute equally to maintenance and repair following diverse forms of injury, with no evidence of zonal dominance. When pericentral AXIN2+ hepatocytes were tagged for ablation using a tamoxifen-inducible CreER/DTA system, their targeted loss only transiently disrupted the pericentral zone before surrounding hepatocytes converted phenotype and proliferated to restore this region, signifying a robust, widespread plasticity rather than zone-specific dominance [89]. Supporting these findings, a more recent study by May *et al*. (2023) revisited the Axin2CreERT2 lineage tracing model and again found no evidence for the predominant expansion or preferential contribution of pericentral hepatocytes to homeostatic regeneration [90]. In both the BAC-based and knock-in Axin2CreERT2 models, regeneration of the liver mass following partial hepatectomy was observed to have been achieved through coordinated contributions from hepatocytes distributed across all zones, rather than a dominant role for any single subpopulation [89,90].

A growing body of research has delineated the molecular signalling pathways driving hepatocyte-to-biliary transdifferentiation that appears to occur in response to tissue injury in mouse models, underscoring the importance of coordinated changes in the regulators of cell fate. These include Notch, YAP/Hippo, IL-6–STAT3, Sox4/Sox9, and TGF-β, which act to orchestrate the transition from a hepatocyte to BEC identity (Figure 1.5) [91]. Activation of Notch signalling within hepatocytes has been shown to initiate biliary reprogramming by upregulating key lineage determinants, including Sox9 and Hnf1β, with YAP activity acting upstream to promote the transcriptional induction of Notch2 and Sox9 following injury [92]. Concurrently, the role of Kupffer cell-derived IL-6/STAT3 signalling has been elucidated through a series of mouse studies that utilise models of chronic liver injury, such as 3,5-diethoxycarbonyl-1,4-dihydrocollidine (DDC) or CCl_4 administration [93]. The DDC diet selectively damages bile ducts and induces periportal fibrosis, whilst CCl_4 primarily injures hepatocytes and/or biliary ductules through the generation of reactive oxygen species (ROS) and free radicals during its metabolism [94,95]. In these experiments, researchers employed lineage-tracing and chromatin immunoprecipitation assays. Following tissue injury, Kupffer cells were observed to increase the secretion of IL-6. This cytokine acts on neighbouring hepatocytes, triggering the phosphorylation of STAT3. Upon activation, STAT3 mediates enhancer chromatin remodelling at the Sox9 and Spp1 gene loci [93]. As a result, these genes are upregulated, which supports the stabilisation of intermediate progenitor-like cells during the process of transdifferentiation. These conclusions were reinforced by

conditional depletion of Kupffer cells or hepatocyte-specific knockout of IL-6 or STAT3, which diminishes Sox9+ hybrid cell formation and impedes the hepatocyte-to-BEC fate transition [93]. Epigenetic factors like Arid1A, a core subunit of the SWI/SNF chromatin-remodelling complex, further maintain the permissive state necessary for hepatocytes to undergo YAP- and STAT3-mediated transdifferentiation, whilst Sox4 and Sox9 function as pioneer factors to repress hepatocyte enhancers and open loci for biliary gene regulation, enabling sequential dedifferentiation and acquisition of biliary characteristics [96]. The role of TGFβ signalling appears to be context-specific, with Smad4 deletion in specific mouse models enhancing the generation of biphenotypic hepatocyte-derived BECs but not complete conversion [97]. Collectively, the interplay of these canonical pathways establishes a plastic, injury-responsive landscape in which mature hepatocytes can undergo robust transdifferentiation towards a biliary fate.

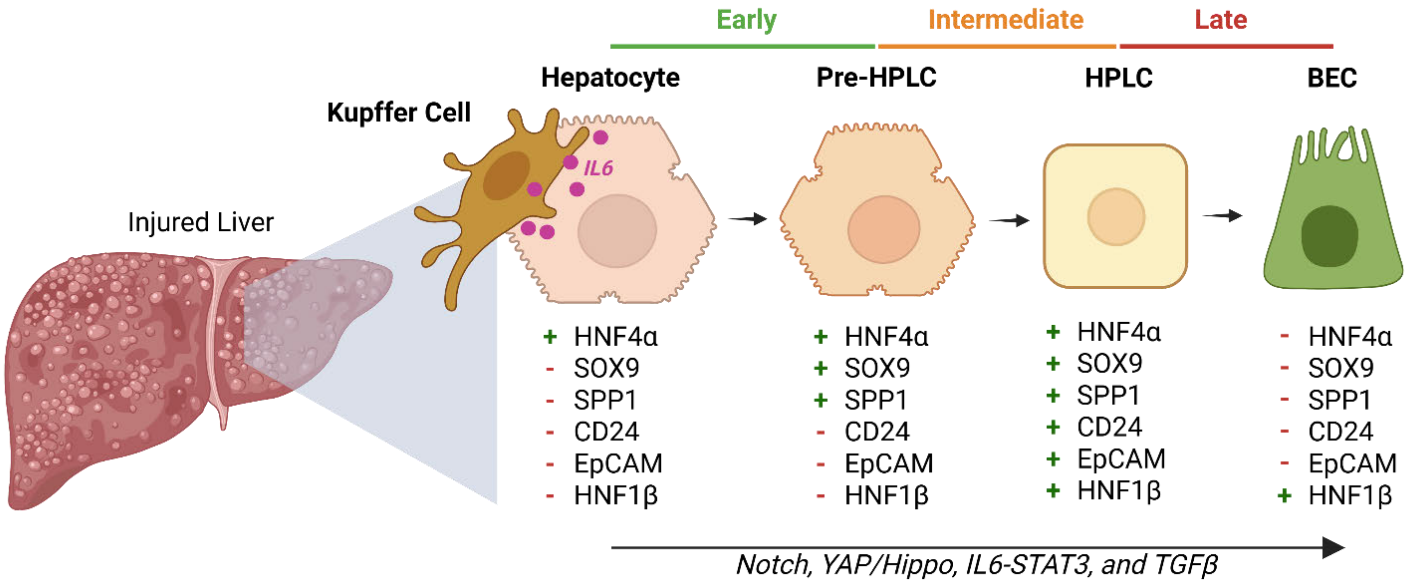

Figure 1.5: Schematic Representation of Hepatocyte-to-Biliary Reprogramming in Injured Liver. *Kupffer cell–derived IL-6 and other signals drive progressive cellular transitions from hepatocyte through pre-HPLC and HPLC states to generate biliary epithelial cells (BECs), marked by stage-specific changes in lineage markers (Hnf4α, Sox9, SPP1, CD24, EpCAM, Hnf1β). Key pathways—including Notch, YAP/Hippo, IL-6-STAT3, and TGFβ—govern the sequential early, intermediate, and late phases of reprogramming (Created with BioRender).*

Yanger *et al*. (2013) provided mechanistic evidence for injury-induced hepatocyte reprogramming using RosaNICD/YFP mice, in which Notch signalling is conditionally activated in hepatocytes [92]. Hepatocyte lineage changes were tracked following both chemical injuries, including a DDC diet and CCl_4 treatment, and mechanical injuries, including partial hepatectomy, bile duct ligation, and hepatic cryoinjury, each of which produced tissue loss, biliary obstruction, or localised necrosis. Strikingly,

hepatocyte-to-biliary reprogramming occurred only with bile duct–selective (BEC-derived) injury, most clearly seen following DDC diet. In this context, fluorescently tagged hepatocytes downregulated classic hepatocyte markers (Hnf4α), upregulated biliary markers such as Sox9, A6, Osteopontin (OPN), and K19, and underwent structural remodelling toward a biliary epithelial morphology, forming new canalicular structures consistent with hepatocyte-to-BEC transdifferentiation [92,98,99]. This bipotentiality, or capacity for lineage reprogramming, was further corroborated by Tarlow *et al.* (2014), who used Fah-/- mice repopulated with fluorescently labelled hepatocytes [100]. Following chronic chemical injury induced by a DDC diet, which causes selective bile duct injury and periportal fibrosis [95], these labelled hepatocytes demonstrably gave rise to new ductular cells with biliary identity, providing direct lineage evidence that mature hepatocytes can contribute to the bile duct epithelium during regeneration [100].

Another study that contributes to the growing evidence for regeneration-competent hepatocyte subpopulations is that by Font-Burgada *et al*. (2015), which focused on the periportal side of the lobule and identified a population termed “hybrid periportal hepatocytes” (HybHP) [101]. This cell population is described as being situated near the bile ducts (periportal) and marked by concomitant low-level expression of the biliary lineage marker Sox9 with classic hepatocyte markers such as Hnf4α. Upon chronic fibrotic injury (DDC diet), these HybHPs were shown to expand and repopulate hepatocyte mass clonally, all while retaining full hepatic function and displaying no signs of oncogenic transformation, suggesting that a periportal-derived bipotential state is particularly relevant for liver resilience and adaptation under pathological stress [101,102]. By making use of the zonally targeted fate-mapping CreER models mentioned previously, Wei *et al*. (2021) demonstrated that midlobular (Zone 2) hepatocytes, particularly those marked by Hamp2, are the major contributors to hepatocyte renewal during both homeostasis and injury [66]. In addition, they confirmed that LGR5+ hepatocytes – a small hepatocyte population primarily found in Wnt-high pericentral and midlobular regions – also exhibit robust proliferative activity after injury, in an attempt to repopulate damaged areas [66].

Recent advances in spatial transcriptomics have further corroborated and expanded upon these observations, with a study by Ang *et al*. (2025) demonstrating that both Cyp2E1+ (pericentral) and Gls2+ (periportal) hepatocytes display bidirectional plasticity in response to injury [103]. In their study, they employed highly specific genetic lineage-tracing mouse models to label Cyp2E1+ and Gls2+ hepatocytes and directly track their fates following various zone-specific liver injuries. Pericentral injury was induced using CCl_4 or diethylnitrosamine (DEN), both of which selectively damage hepatocytes near the central vein. To model periportal injury, a DDC diet was used. During both physiological homeostasis and following partial hepatectomy, each zonal hepatocyte population

predominantly sustained itself through self-renewal, with minimal interaction between pericentral and periportal lineages. However, after the selective injuries, they observed striking bidirectional plasticity, with periportal Gls2+ hepatocytes regenerating damaged pericentral regions following CCl_4 or DEN injury, and pericentral Cyp2E1+ hepatocytes replenishing periportal zones after DDC-induced injury [103]. These results demonstrate that, although zonal hepatocytes are self-maintaining during homeostasis, severe, zone-specific injury can drive reciprocal conversion and regeneration between pericentral and periportal hepatocyte populations. Collectively, these studies have transformed the classical understanding of liver regeneration from simple, zone-specific proliferation to a complex, dynamic process involving phenotypic flexibility and cross-lineage support among diverse hepatocyte subpopulations.

The "ductular reaction" – a hallmark response in chronic liver disease – refers to the histological observation of a proliferation and expansion of small duct-like epithelial structures, called bile ductules, in response to sustained injury or disease [104-106]. Morphologically, the ductular reaction is characterised by the appearance of newly formed ductules, frequently surrounded by inflammatory cells and myofibroblasts, especially at the portal tracts [104-106]. The response is especially pronounced under conditions where mature hepatocyte or BEC proliferation is insufficient for effective liver repair, such as in chronic viral hepatitis, biliary obstruction, or toxic injury [106-108]. Functionally, the ductular reaction is not only an alternative repair pathway – potentially generating new hepatocytes or BECs as needed – but also drives fibrogenesis via crosstalk with inflammatory and stromal cells [104,106,109-111]. Adding to this, recent work has identified a specialised population of neutrophils that appear to accumulate at sites of ductular reaction and closely interact with biliary epithelial cells – referred to as ductular reaction-associated neutrophils (DRANs) [104]. Their abundance increases with disease severity, and mechanistic studies show that DRANs adopt a pro-inflammatory, pro-proliferative phenotype and directly promote biliary cell proliferation through the release of neutrophil extracellular traps and elastase [104]. Pharmacological inhibition or depletion of DRANs reduces ductular reaction and fibrosis, highlighting these neutrophils as central drivers of maladaptive wound healing and as promising therapeutic targets in chronic liver disease [104]. Whilst targeting DRANs highlights the role of immune-mediated crosstalk in maladaptive ductular expansion, definitive proof of epithelial plasticity has required tracing the fate of specific cell populations *in vivo*.

For many years, this proliferative response was attributed almost exclusively to the expansion of hepatic progenitor or "oval" cells, which are thought to be capable of differentiating into either hepatocytes or biliary epithelial cells in response to severe or chronic injury [112]. However, using lineage tracing, Furuyama and colleagues utilised a tamoxifen-inducible CreERT2 knock-in into the Sox9 locus

to label Sox9-expressing cells and their progeny, demonstrating that these Sox9+ cells principally contribute towards the biliary compartment both during homeostasis and after injury, supporting their ductal identity [112]. Subsequent lines of evidence have significantly expanded this paradigm of ductular reaction origins, revealing that mature, lineage-committed hepatocytes – not just hepatic progenitors – can undergo "ductular metaplasia" by transdifferentiating into biliary-like epithelial cells and acquiring morphological and molecular characteristics of bile ductules in chronic injury settings [106,111,113]. This process is especially evident in the periportal region, where hepatocytes exposed to inflammatory cues and chronic damage can be reprogrammed to acquire biliary features such as upregulation of Sox9 signalling and directly give rise to new ductular structures [100,114]. Mechanistically, Choi and Diehl (2009) proposed that inflammatory injury induces hepatocytes to undergo a two-step transition: first, hepatocytes undergo epithelial-to-mesenchymal transition (EMT), losing polarity and acquiring migratory and mesenchymal characteristics; this is then followed by mesenchymal-to-epithelial transition (MET), in which the cells adopt a BEC-like epithelial phenotype [115]. EMT and MET are now recognised as context-dependent, reversible, and highly modulated by the hepatic microenvironment, reflecting the remarkable plasticity of adult hepatocytes.

In parallel, complementary plasticity is observed in the opposite direction under conditions where hepatocyte proliferation is severely impaired. For instance, Manco *et al.* (2019) used lineage tracing of OPN+ BECs to show that, during chronic CCl_4-induced liver injury, reactive biliary cells can clonally expand and differentiate into fully mature, proliferative hepatocytes [106,111,116]. These ductular reaction-derived hepatocytes integrate into the hepatic parenchyma and may constitute up to 12% of the hepatocyte pool in advanced injury, representing a robust example of BEC-to-hepatocyte fate conversion and highlighting the bidirectional potential of epithelial plasticity in chronic liver disease [116]. This phenomenon is supported by Español-Suñer *et al.* (2012), who used tamoxifen-inducible lineage tracing of LPCs and biliary cells to demonstrate that, during specific models of liver injury – including chronic CCl_4 or DDC diet – these ductular cells can differentiate into functional hepatocytes that integrate into hepatic cords and exhibit mature hepatic functions [117]. Similarly, Raven *et al.* (2017) showed that in mouse models where hepatocyte proliferation is experimentally impaired, BECs undergo lineage conversion and contribute significantly – up to 25% of new hepatocytes – to parenchymal regeneration, further substantiating the capacity of biliary cells to reconstitute hepatocyte populations following severe injury [118]. Together, these studies demonstrate that BECs can serve as a facultative source of hepatocytes when proliferation of the native hepatocyte pool is compromised, reinforcing the concept of dynamic bidirectional plasticity within the liver epithelium in chronic injury contexts.

Importantly, this form of cellular reprogramming often serves an adaptive function, enabling the rapid replacement of biliary epithelial cells lost during chronic injury. However, when dysregulated, ongoing plasticity may destabilise hepatocyte identity and increase the risk of dysplasia or malignant transformation; for example, hepatocellular carcinomas with aberrant K19 expression tend to be more invasive and portend poorer outcomes [119-121]. Consequently, unravelling the cellular and molecular networks underlying hepatocyte plasticity is critical for understanding both normal tissue repair and the origins of liver cancers.

1.2.2 The Role of Notch and PI3K/AKT Signalling in Hepatocyte Plasticity and Cholangiocarcinoma

Recent research has further refined this mechanistic landscape by revealing that both Notch and PI3K/AKT signalling serve as pivotal platforms for not only regenerative plasticity but also the malignant transformation underlying hepatocyte-derived intrahepatic cholangiocarcinoma (iCC). Cholangiocarcinoma represents a highly heterogeneous group of bile duct cancers, previously assumed – due to the biliary-like architecture and expression of BEC-specific markers such as K19, EpCAM, and Sox9 – to originate exclusively from BECs [122]. However, common risk factors such as cirrhosis, chronic viral hepatitis, alcohol use, diabetes, and obesity frequently precede both iCC and hepatocellular carcinoma (HCC), raising the possibility that these primary liver cancers may share a cellular origin [123-129]. Clinical and epidemiological observations have demonstrated that patients with viral hepatitis often develop iCC, further supporting the hypothesis that transformed hepatocytes can serve as a cell-of-origin for cholangiocarcinoma [91,127].

A pivotal study by Fan *et al.* (2012) provided direct functional proof for this hypothesis: by introducing constitutively active AKT and Notch intracellular domain (NICD) into hepatocytes via a hydrodynamic tail vein injection (HTVI)-mediated transposon system (Figure 1.6) in R26R-EYFP mice, they induced the rapid emergence of iCC directly from lineage-traced hepatocytes [124]. This work established that hepatocytes, when subject to oncogenic signals that mimic regenerative reprogramming, can function as a cell-of-origin for iCC. Expanding on this, Wang *et al.* (2018) used genetic models to show that Notch2 is required for AKT/YAP-driven iCC – hepatocytes lacking Notch2 predominantly developed hepatocellular adenomas rather than cholangiocarcinoma, underscoring the role of Notch2 in enforcing biliary fate specification in the oncogenic context [130]. Further highlighting the importance of Notch signalling, Guest *et al*. (2016) demonstrated that Notch3 is robustly upregulated in human and experimentally induced models of cholangiocarcinoma and that genetic or shRNA-mediated suppression of Notch3 – but not Notch1 or other paralogues – strongly inhibits tumorigenesis [131].

Notch3 reportedly drives tumour survival and proliferation through a non-canonical, RBPJ-independent pathway reliant on PI3K/AKT signalling, as evidenced by decreased AKT phosphorylation when Notch3 is inhibited [131]. In regeneration, Minnis-Lyons *et al.* (2021) showed that Notch1 and Notch3 coordinate the expansion and biliary fate specification of BECs during repair, largely through the IGF1R/PI3K/AKT axis [132]. Interestingly, activation of this pathway supports BEC expansion but, when hyperactivated, restricts their differentiation into hepatocytes – demonstrating a tightly regulated balance between proliferation and lineage choice that can be subverted in cancer [132].

For the experimental work in this thesis, Notch1 (NICD1) was selected over Notch3 based on several considerations. First, while Guest *et al.* (2016) demonstrated that Notch3 is robustly upregulated in established cholangiocarcinoma and drives tumour survival through non-canonical pathways, Notch1 and Notch2 are the primary receptors mediating canonical Notch signalling during developmental lineage specification [15,25]. Second, the Fan *et al*. (2012) seminal study establishing hepatocyte-derived iCC used NICD (likely Notch1) with AKT, providing a validated experimental precedent. Third, Notch1 expression is more broadly distributed across liver cell types during regeneration, making it suitable for studying initial hepatocyte plasticity and reprogramming, whereas Notch3 appears more specialised for BEC expansion and tumour maintenance phases. Thus, NICD1 was chosen as the driver to model the early hepatocyte-to-biliary transition.

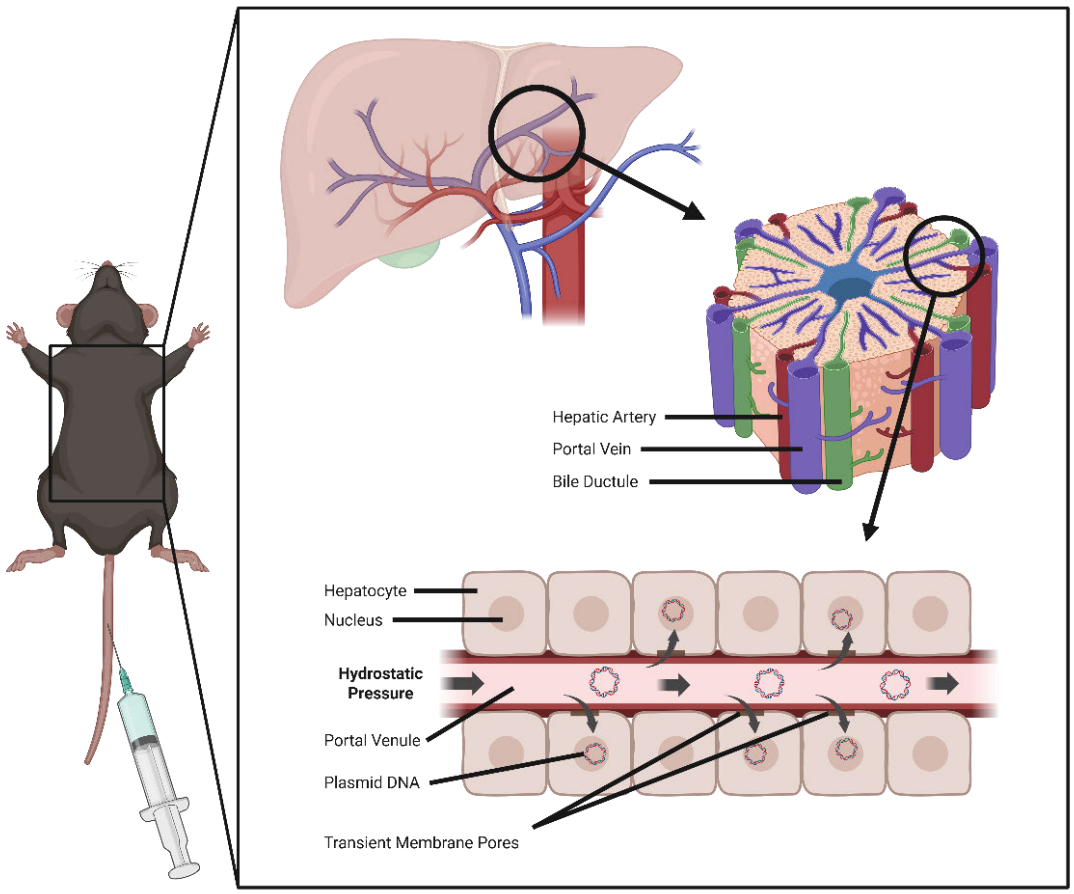

Figure 1.6: Hydrodynamic Tail Vein Injection Facilitates Efficient Delivery of Plasmid DNA into Murine Hepatocytes. *Through pressurised injection of a bolus of naked plasmid DNA containing the transgene of interest into the tail vein, transient right-sided congestive heart failure is induced, inducing hydrostatic pressure within the hepatic vessels. The capillary endothelium is permeabilised, and transient pores open in the plasma membranes of hepatocytes through which the plasmid DNA passes and transposes the gene of interest (Created in BioRender).*

Building upon this mechanistic framework, Hu *et al*. (2022) further delineated the key molecular axis governing hepatocyte-to-biliary/ICC conversion by identifying a novel NOTCH-YAP1/TEAD-DNMT1 circuit as also being essential for this lineage change [133]. Using an HTVI transposon system to express AKT and the NICD in murine hepatocytes, they confirmed rapid development of iCC directly from transfected hepatocytes. This expression profile recapitulated the signature of a subset of human iCC, which demonstrated the clinical relevance of this model. Through sophisticated loss- and gain-of-function experiments, they also established that whilst both Sox9 and Yap1 were regulated independently downstream of NICD and were required for efficient iCC formation, it is the YAP1-TEAD-mediated induction of DNA methyltransferase 1 (DNMT1) that is vital for the actual reprogramming step. DNMT1 was shown to epigenetically silence hepatocyte-identity genes (including Hnf4α, Hnf1α,

and C/EBPα/β), thereby permitting the acquisition of biliary fate and supporting neoplastic transformation [133]. Notably, either genetic or pharmacologic inhibition of DNMT1 or TEAD activity completely blocked Akt-NICD-induced hepatocyte-to-biliary conversion and iCC formation, while re-expression of DNMT1 rescued iCC development even when TEAD activity was suppressed. Histological studies also revealed that DNMT1 was upregulated in human livers at risk for iCC, especially in primary sclerosing cholangitis, supporting the translational relevance of this pathway. These results confirm that the orchestration of epigenetic remodelling by the NOTCH-YAP1/TEAD-DNMT1 axis is a fundamental requirement for the cell fate change underpinning hepatocyte-derived iCC, and highlight the potential for targeting DNMT1 as a strategy to interrupt aberrant oncogenic plasticity in high-risk clinical settings [133].

Together, these findings cement a model in which Notch and PI3K/AKT signalling constitute an integrated regulatory system that orchestrates both normal liver regeneration and, under oncogenic conditions, neoplastic transformation from mature hepatocytes. While it is clear that Notch signalling is required for hepatocyte-to-BEC fate transition *in vivo*, detailed knowledge of the downstream transcriptional programmes governing this conversion remains limited and warrants further investigation.

1.3 *In Vitro* Models of Hepatocyte Culture

1.3.1. Primary Hepatocyte Isolation and Limitations of *In Vitro* Culture

Given the intricacies involved in hepatic repair following injury, the advent of *in vitro* primary hepatocyte culture models offers unique opportunities to study temporal changes in hepatocyte identity, transdifferentiation, and pathological mechanisms. Primary hepatocyte culture has undergone a substantial evolution over the past several decades, progressing from early two-dimensional (2D) monolayer systems that rapidly lost hepatic functionality to sophisticated three-dimensional (3D) models capable of faithfully recapitulating liver biology *in vitro* (Figure 1.7) [134-136].

The terms “organoid” and “spheroid” are often used inconsistently in this context, necessitating clear operational definitions for this thesis. Here, organoids are considered three-dimensional structures derived from pluripotent stem cells, progenitors, or differentiated cells that self-organise through cell–cell and cell–matrix interactions to recapitulate selected aspects of native tissue architecture and function in vitro, without any requirement for a specific number of constituent cell types. Many liver organoid systems are multicellular and contain multiple interacting lineages, but organoids can also be generated from a single cell type; both single-type and multi-type cultures are therefore

encompassed within this definition. In contrast, spheroids are defined as simpler 3D aggregates, usually of a single primary cell type, that self-assemble through cell–cell adhesion on non-adherent surfaces or in hanging drops. Spheroids generally lack the patterned lineage diversification and developmental potential characteristic of organoids, but they offer superior retention of primary cell phenotype and functionality compared with 2D monolayer cultures. For the purposes of this thesis, primary murine hepatocyte spheroids (PMHS) refer to aggregates of mature hepatocytes that form 3D structures without exogenous matrix or proliferative signals, maintaining hepatocyte-specific functions while avoiding the developmental plasticity inherent to progenitor-derived liver organoids. This distinction is critical for studying mature hepatocyte plasticity in response to defined signalling perturbations.

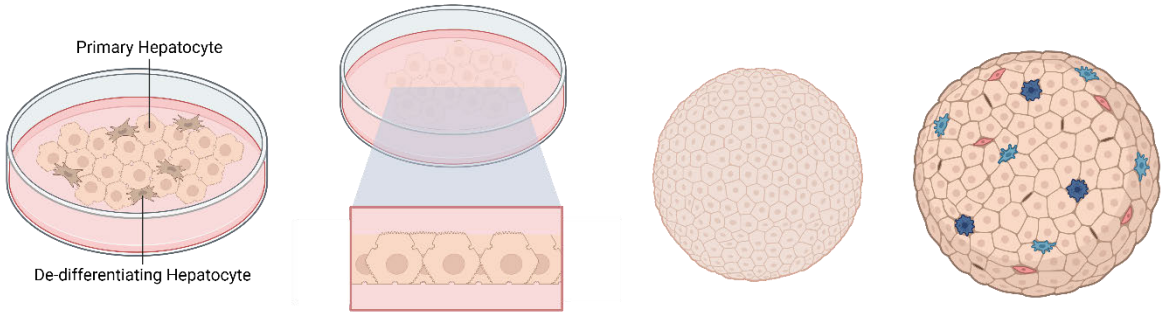

Feature	Standard 2D Culture	2D Sandwich Culture	Spheroid Culture	Organoid Culture
Structure	Monolayer[134]	Monolayer, ECM sandwich[134]	3D cell aggregate[134]	3D cell aggregate[154]
Cell Composition	Hepatocytes[134]	Hepatocytes[134]	Hepatocytes[134]	Single cell or Multiple cell types[154]
Polarity & Canaliculi	Minimal polarity No canaliculi[145]	Polarity present Transient canaliculi[144]	Polarity present Canaliculi present[134]	Polarity present Canaliculi present[154]
Function Retention	Rapid loss of function[134]	Functionality prolonged[134]	Maintained long-term function[154]	Maintained long-term function[154]
Complexity	Low[134]	Moderate[134]	Moderate[134]	High[134]
Documented Usages	Basic short-term studies[134]	Transport & Toxicity[145]	Metabolism & Toxicity[134]	Modeling Complex Disease & Development[154]

Figure 1.7: Key Differences Between Standard 2D, 2D Sandwich, Spheroid, and Organoid Hepatocyte Culture Systems. *Comparison of primary hepatocyte culture formats illustrating distinct structural organisation, cell composition, polarity and bile canaliculi formation, functional retention, system complexity, and typical applications. Standard 2D cultures consist of monolayers with rapid function loss and no canaliculi, while 2D sandwich cultures incorporate extracellular matrix to promote polarity and transient canaliculi formation. Spheroid cultures comprise 3D primary hepatocyte aggregates, supporting the maintenance of long-term function and canaliculi formation, whilst organoid cultures exhibit high complexity, multilineage composition, and advanced tissue architecture suitable for disease modelling and development studies (Created with BioRender).*

The initial reliance on 2D monolayer cultures – where hepatocytes are seeded onto plastic or collagen-coated substrates – revealed major drawbacks for drug metabolism and toxicity studies. In these cultures, hepatocytes exhibit rapid dedifferentiation marked by increased expression of mesenchymal genes such as vimentin (Vim), Col1A1, and Snail2 [134,136,137]. Alongside this shift in expression profile, the core functionality of the hepatocytes rapidly declined in 2D culture, with a decline in albumin secretion, urea production, cytochrome P450 (CYP) enzyme activity, and bile canalicular transport being described, thus significantly limiting their utility for experimental modelling [137]. Attempts to mitigate this loss of hepatocyte phenotype through optimisation of substrate stiffness or extracellular matrix (ECM) composition yielded only transient improvements, underscoring the inadequacy of conventional 2D approaches for long-term studies.

Recognising the importance of mimicking the hepatic microenvironment, researchers then introduced 2D sandwich cultures that enclose the hepatocytes between layers of ECM materials like Matrigel or collagen [134,135,138-143]. These arrangements improved the preservation of cell polarity and sustained functions such as transporter activity and bile canaliculi formation for more extended periods post-isolation [144-146]. Despite the improvements in maintenance of the hepatocyte phenotype, dedifferentiation continued to occur in these cultures over time. Even with repeated ECM overlays, proteomic analyses revealed extensive loss of metabolic protein expression and a decrease in the activity of enzymes and transporters involved in drug absorption, distribution, metabolism, and excretion by the two-week mark [134]. Simultaneous increases in the detection of lysosomal proteins and proteins engaged in the complement system – which encompasses proteins involved in opsonisation, inflammation, and cell lysis – in the sandwich cultures also suggested heightened degradation and stress responses that further eroded physiological relevance [134,135,141]. Consequently, whilst 2D sandwich cultures proved useful for short- and medium-term experiments – such as those studying bile canalicular transport and screening for cholestatic toxicity – they are ill-suited for studying chronic hepatic processes or maintaining hepatocyte function over extended periods.

1.3.2. Three-Dimensional (3D) Spheroid and Organoid Hepatocyte Culture

A breakthrough occurred with the emergence of 3D spheroid culture systems wherein hepatocytes self-aggregate into spherical clusters when plated onto low-adhesion surfaces or in hanging drop arrays [134,147-155]. Spheroid culture dramatically improves retention of liver-specific gene and protein expression because it enables primary hepatocytes to regain and maintain crucial cell–cell and cell–matrix interactions that are lost in 2D culture, thereby more closely mimicking the microarchitecture of liver tissue [134,147,148,156]. Proteomic and transcriptomic analyses have confirmed that spheroid-

cultured cells express higher and more stable levels of hepatocyte markers such as albumin (ALB), arginase 1 (ARG1), CYP enzymes, and bile transporters compared to 2D-cultured cells [134]. The 3D environment also reduced the occurrence of oxidative and metabolic stress that was observed in 2D monolayers, further preserving hepatocyte differentiation and metabolic competence [134,147]. Importantly, the pharmacological performance of spheroids surpassed previous models; these cultures were capable of accurately detecting hepatotoxicity at clinically relevant concentrations of compounds like acetaminophen, troglitazone, and fialuridine [150,155,157].

In terms of the utility of these model systems for studying liver disease *ex vivo*, Bell *et al*. (2018) demonstrated that primary human hepatocyte (PHH) spheroids maintain high functional stability for several weeks [134]. Importantly, these spheroids can reproduce clinically relevant features of steatosis, cholestasis, and drug-induced liver injury when exposed to specific compounds [134]. For example, treating spheroids with chlorpromazine induces cholestasis and recapitulates bile acid retention, while cyclosporine A drives lipid accumulation, modelling aspects of hepatic steatosis [134]. Additional work has shown that PHH spheroids infected with hepatitis viruses can be used to study viral pathogenesis and inflammation-driven drug toxicity responses [147]. Primary murine hepatocyte spheroids (PMHS) have also reliably detected acetaminophen- and fialuridine-induced toxicity, providing key insights into injury mechanisms [157]. More recently, protocols have enabled modelling of non-alcoholic fatty liver disease (NAFLD), oxidative stress, and fibrogenic progression in spheroid formats, supporting studies of metabolic liver diseases and fibrosis [158].

Despite these strengths, spheroid cultures have a few notable limitations. In larger spheroids (greater than 200μm), diffusion barriers can develop, resulting in hypoxia or even necrosis at the centre of the cell aggregate [148]. Additionally, the ECM used *in vitro* lacks the complexity of liver-specific structural proteins, glycoproteins, and dynamic signalling cues present in the native hepatic environment, resulting in less accurate support for hepatocyte function and organisation [148]. Achieving uniform spheroid size can also be challenging, particularly for high-throughput screening where spheroids are simultaneously plated in U-bottom low-adhesion plates or in drop cultures. Finally, while co-culture approaches are possible, spheroid models still fall short of replicating the true tissue architecture, multicellular diversity, and vascularisation found in intact liver tissue [148]. Nonetheless, spheroid models remain a scalable and physiologically relevant platform for liver disease modelling and preclinical research.

Increasing the complexity of 3D hepatocyte cultures, organoids offer new opportunities to reproduce the multicellular architecture of the liver. The term “organoid” has been defined as an *in vitro* 3D

cellular cluster derived from tissue-resident progenitor cells, embryonic stem cells, or induced pluripotent stem cells capable of self-renewal and self-organisation that recapitulates the functionality of the tissue of origin [159-161]. Unlike spheroids, these structures typically comprise multiple liver cell types – for example, albumin-positive hepatocytes, K19-positive BECs, hepatic stellate cells, and Kupffer cells – and can be sustained for many months *in vitro* [162-165]. Importantly, however, organoids do not have to be multicellular; depending on their source and method of derivation, organoids can be generated from a single lineage yet still self-organise into 3D tissue-like structures. These cells are then typically aggregated through centrifugation and embedded within ECM-rich hydrogels such as Matrigel to support three-dimensional growth and organisation [165-169]. Recent protocols, such as those established by Peng *et al.* (2018), have developed organoid culture protocols based on the observation that mature hepatocytes proliferate and undergo hyperplasia in response to injury-induced regenerative signals, in particular tumour necrosis factor-alpha (TNFα) [170]. By incorporating TNFα into the culture media, they succeeded in establishing 3D primary hepatocyte organoids that not only maintained hepatocyte transcriptional activity and function *ex vivo*, but also enabled serial passaging and long-term culture for more than six months [170]. Organoid systems thus recapitulate tissue architecture, support genetic manipulation, and demonstrate a broad array of physiological activities, including bile acid synthesis, albumin and urea production, and CYP3A4 activity [169].

Liver organoids have also been successfully used to model a range of diseases. For steatosis and NAFLD, human liver organoids have been engineered to accumulate lipids either through exposure to free fatty acids or genetic editing – facilitating drug and genetic screening for anti-steatosis targets and reflecting the mechanisms underlying NAFLD and metabolic dysfunction–associated steatotic liver disease (MASLD) [171-173]. In the context of fibrosis, organoid systems have been developed that reproduce fibrotic processes, including collagen deposition and activation of myofibroblasts as seen in congenital and acquired liver fibrosis [174]. Guan *et al*. (2021) recapitulated the abnormal bile duct formation and fibrosis, which is characteristic of Autosomal Recessive Polycystic Kidney Disease (ARPKD) organoids, within 21 days of culture [174]. Cancer modelling is also becoming more common, with patient-derived liver cancer organoids retaining the morphology, genetic heterogeneity, and drug response characteristics of the primary tumours, allowing for personalised drug testing and the study of tumour evolution and resistance mechanisms [175-177].

In addition to supporting hepatocyte function, studies have made use of hepatic organoids to explore hepatocyte plasticity *in vitro*. A study by Hu *et al.* (2018), for example, established primary human and murine organoids which were considered to exhibit transcriptional profiles resembling those of

proliferating hepatocytes after partial hepatectomy [178]. The group went on to describe a short-term experiment in which the hepatocyte organoids were cultured in BEC organoid media to assess the cell plasticity. The results of this experiment indicated that biliary marker expression was strongly induced in hepatocyte organoids whilst hepatocyte markers (ALB and Hnf4α) gradually decreased; however, it should be noted that these results were produced using cells derived from a single donor (n=1) and no further investigation into the signalling pathways involved in the fate change was pursued [178]. Similarly, Akbari *et al*. (2019) demonstrated that enrichment for EpCAM-positive cells derived from human induced pluripotent stem cells (iPSCs) enables the efficient generation of hepatic organoids with remarkable lineage versatility [179]. These EpCAM-positive endodermal progenitors were able to self-organise into organoids that could be expanded for over a year without losing their capacity to differentiate into mature hepatocyte-like cells. Functional analysis showed that these organoids displayed key hepatocyte features, including albumin secretion and expression of mature hepatic markers, but could also recapitulate disease-specific phenotypes – having modelled the urea cycle disorder citrullinemia type 1 – illustrating their potential for personalised disease modelling [179]. Notably, EpCAM-positive populations enabled the formation of both hepatocyte and BEC lineages within the organoids, further evidencing their potential for generating multiple hepatic compartments and highlighting the plasticity inherent in organoid cultures derived from human stem and progenitor cells.

Despite these advances, limitations remain that make organoids less than ideal for studying hepatocyte plasticity directly. Organoid growth often depends on sustained exposure to proliferative or injury-mimicking signals such as TNFα or Wnt agonists. These conditions are not reflective of the quiescent state characteristic of hepatocyte biology in a healthy liver. Moreover, organoids frequently contain mixed or progenitor-like populations rather than mature, stable hepatocytes, making it difficult to identify true hepatocyte fate transitions from the developmental plasticity intrinsic to immature or heterogeneous cultures. By contrast, primary hepatocyte spheroid cultures – which are capable of maintaining the quiescent, differentiated state – provide a more physiologically relevant baseline for assessing hepatocyte plasticity, since fate changes observed in spheroids can be attributed to stable mature hepatocytes rather than to mixed or progenitor-derived cell populations.

Regarding hepatocyte zonation, the recreation of *in vivo*-like zonation patterns in 3D cultures such as spheroids or organoids remains challenging but is an area of active investigation. In a study by Ramli *et al*. (2020), a human pluripotent stem cell–derived hepatic organoid system was developed that was shown to effectively model multiple aspects of human liver biology, including cellular heterogeneity and functional architecture [180]. Notably, the authors demonstrated that their hepatic organoids contain

both hepatocytes and BECs, and express a wide range of hepatic functional genes and liver-specific transcription factors, including those linked to metabolic zonation. Specifically, high-resolution RNA sequencing and gene expression analysis revealed that the organoids sustain robust expression of zone-defining markers such as CPS1 (a periportal marker) and GS (a pericentral marker), indicating that at least partial metabolic heterogeneity, reminiscent of *in vivo* liver zonation, is preserved in the 3D organoid culture [180]. However, despite these robust models, achieving the full complement of spatial cues and metabolic gradients seen in the liver sinusoid – driven by gradients in oxygen, nutrients, and hormone concentrations – remains a significant limitation for *in vitro* systems [181].

While liver organoids may present notable limitations as models for *in vitro* liver biology, they still offer distinct promise as therapeutic vehicles for tissue repair through transplantation and engraftment. Some studies have achieved *in vivo* engraftment of hepatic organoids and demonstrated functional benefits, such as reduced fibrosis and formation of bile ducts, following transplantation into animal models. For example, the fusion and transplantation of hiPSC-derived liver organoids onto mouse livers produced functional connections with host vasculature and contributed to disease amelioration, yet these grafts still faced issues of limited maturation, incomplete integration, and an immune response even in immunodeficient hosts [182]. Similarly, direct orthotopic implantation of 3D-cultured hepatic organoids in mice resulted in local engraftment, but survival remained constrained by early apoptosis, chronic inflammation, and the formation of foreign-body giant cells rather than true integration with host parenchyma [183]. These findings illustrate persistent barriers such as insufficient vascularisation, lack of robust maturation, and immune barriers that limit the complete integration of the implanted organoids.

It is also worth noting that in contrast to the widespread use of intestinal organoids, liver organoid models have seen slower adoption, with many groups reporting difficulty in consistently replicating and maintaining mature, multicellular liver tissue *in vitro*. Recurring challenges include the inability to stably preserve diverse hepatic cell types, restricted development of biliary and vascular structures, and unstable long-term culture, all of which compromise the utility of liver organoids as models for adult liver function and repair [136,178,184,185]. Thus, despite the promise of organoid models, sustaining long-term growth typically requires persistent exposure to proliferative or injury-mimicking signals such as TNFα or Wnt agonists – conditions not reflective of healthy liver tissue. For this reason, spheroid cultures have been selected as the preferred model for the studies of plasticity set out in this thesis.

1.4 Overarching Study Hypothesis and Aims

The present study aims to establish how the zonal identity of hepatocytes influences their plasticity and response to oncogenic signals. As discussed, Notch and Akt pathways play pivotal roles in directing hepatocyte and biliary lineage decisions, and when activated, have the capacity to reprogramme hepatocytes towards a biliary phenotype [100,133]. Evidence from studies of hepatic development suggests that the liver cell identity response to Notch/Akt varies across the liver lobule; however, whether the spatial origin of hepatocytes modulates this during adult homeostasis or in response to pathology remains poorly understood. It is exciting to speculate whether this response might be modulated to reduce the susceptibility of liver cells to disease-causing stimuli, in particular factors known to drive cholangiocarcinoma. Furthermore, while *in vitro* hepatocyte culture systems, including 3D spheroids, have provided valuable insights into cell plasticity, faithfully reproducing zonation patterns in such models remains a significant challenge. On the basis of these identified gaps, it is hypothesised that the zonal origin of hepatocytes dictates their susceptibility to lineage reprogramming through NICD1/Akt-signalling upregulation. Accordingly, the present study was designed with three principal aims:

1) To establish whether hepatocyte zonation can be preserved *in vitro* and/or whether re-programming of liver cells can be modelled in *ex vivo* cultures.
2) To characterise the intrinsic transcriptional differences between periportal (Gls2+) and pericentral (GS+) hepatocytes affecting cell identity and susceptibility to drivers of re-programming.
3) To define the transcriptional changes occurring in these zonally distinct populations during NICD1/Akt-induced reprogramming *in vivo*.

2.1 Ethical Approval and Mouse Strains

All animal work was performed under the UK Home Office project license held by Dr Luke Boulter (PP5208647). Animals were maintained in individually ventilated HEPA-filtered cages of 2-6 mice in 12-hour light-dark cycles and were allowed access to food and water ad libitum.

This study used the C57BL/6J mouse strain from Charles River, UK, as the background control strain for all hepatocyte characterisation in 2D and 3D culture. The other mouse strains used in this study, Gls2CreER (*Gls2*$^{em1(cre/ERT2)Hzhu}$*/J,* Strain # 036247) and GSCreER (*Glul*$^{em1(cre/ERT2)Hzhu}$*/J,* Strain # 036248), were purchased from the Jackson Laboratory [66,186,187]. Both use a tamoxifen-induced Cre-loxP system, which stimulates Cre recombination in Glutaminase 2 (Gls2) and Glutamine Synthetase (GS) expressing cells, respectively. These mouse strains were generated using CRISPR/Cas9 endonuclease-mediated genome editing to introduce an IRES enhancer sequence and CreER(T2) fusion gene into the 3' untranslated region (UTR) immediately downstream of either the Gls2 or GS gene locus, thereby enabling inducible and cell-type specific recombination upon tamoxifen administration in Gls2-expressing cells. The background mouse line of both strains is C57BL/6J.

These lines were both cross-bred with a membranous Tomato / membranous GFP (mT/mG) reporter mouse line (Gt(ROSA)26Sor$^{tm4(ACTB-tdTomato,-EGFP)Luo/J}$), which was received from the Pleasantine Mill Research Group at the University of Edinburgh, Institute of Genetics and Cancer (Figure 2.1a) [188]. The mT/mG reporter construct constitutively expresses a conditional membrane-targeted tdTomato (mTomato) transgene that converts to membrane-targeted green fluorescent protein (mGFP) expression upon exposure to Cre recombinase (Figure 2.1b) [188]. This mouse line was initially developed by inserting the mT/mG construct into the ROSA26 locus in mouse embryonic stem cells, with the resulting mT/mG-positive cells being used to create chimeric mice [188]. By crossing these with the Gls2CreER and GSCreER mouse lines, Gls2-expressing and GS-expressing hepatocytes were able to be lineage traced via the mGFP expression.

All experimental animals were between 4 and 8 weeks of age, included both sexes with approximately equal male-to-female ratios where possible, and the treatment and control cohorts consisted of littermates to mitigate potential confounding variables.

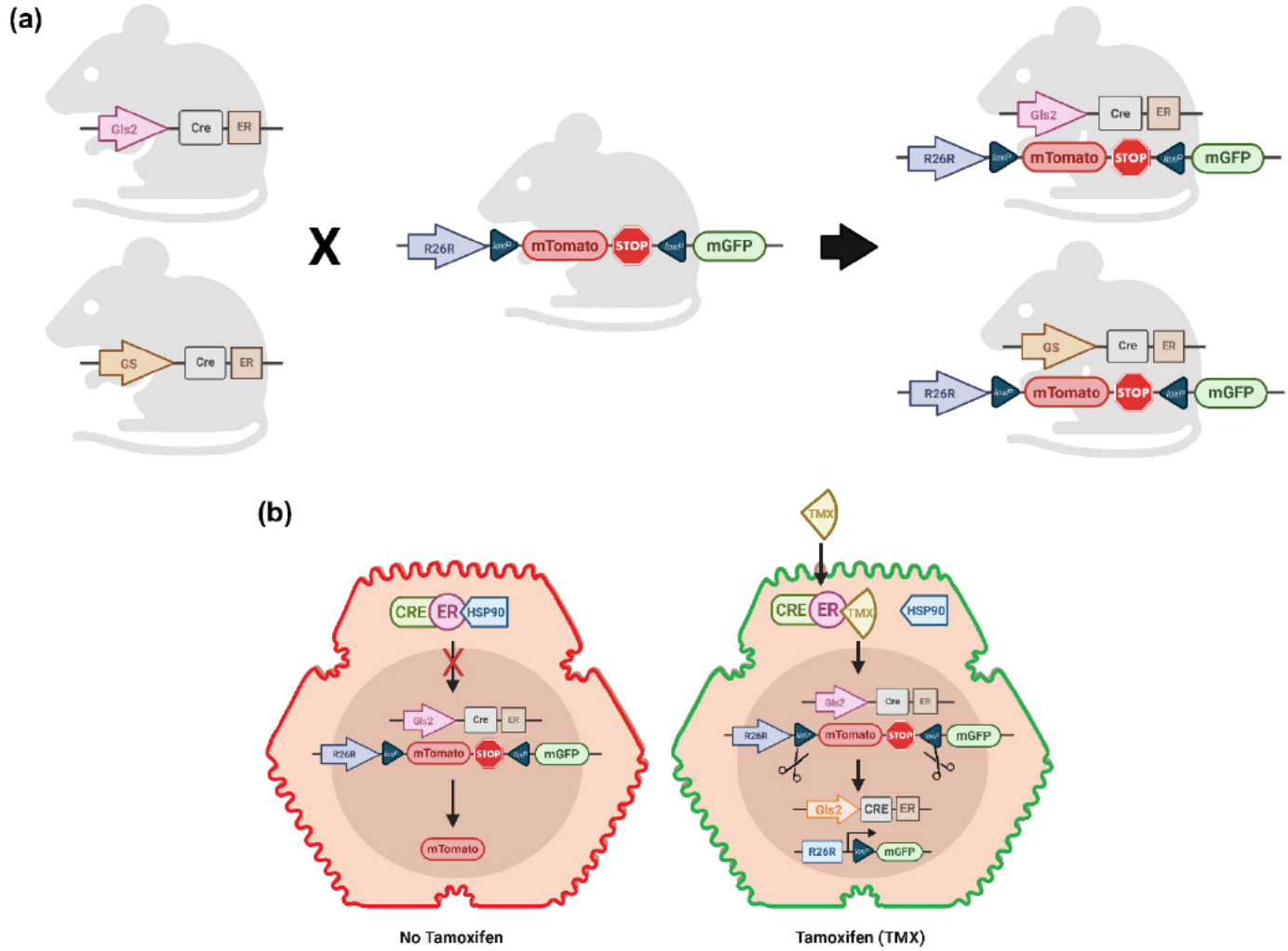

Figure 2.1: Schematic Representation of Cre/ERT2 Driver and mT/mG Reporter Mouse Lines. ***(a)*** *Breeding strategy showing Gls2$^{em1(cre/ERT2)\ Hzhu/J}$ and Glul$^{em1(cre/ERT)\ Hzhu/J}$ mice crossed with the Gt(ROSA)26Sor$^{tm4(ACTB-tdTomato,-EGFP)Luo/J\ (mT/mG)}$ reporter to generate double transgenic animals.* ***(b)*** *Mechanism of CreERT2-mediated reporter activation in the Gls2CreER-mT/mG mouse, depicting labelling states before and after Tamoxifen (TMX) exposure (Created with BioRender.com).*

2.1.1 Genotyping

Genotyping of experimental mice was performed by the commercial provider TransnetYX using ear snip samples. TransnetYX conducts genotyping by extracting DNA from the samples and performing automated, high-throughput PCR analysis to detect specific genetic modifications. Each Gls2CreER-mT/mG and GSCreER-mT/mG mouse was assessed for the presence of either the wild-type or modified Gls2 or GS alleles, respectively, as well as for wild-type or modified (mT/mG) ROSA alleles. The probe sequences used for this genotyping are shown in Table 2.1. This approach ensured accurate and reproducible identification of genotype for all individuals included in the study.

Table 2.1: TransnetYX Genotyping Probe Sequences.

Probe Name	Forward Primer	Reverse Primer	Reporter Sequence
ROSA Wild-Type	TTCCCTCGTGATCTGCAACTC	CTTTAAGCCTGCCCAGAAGACT	CCGCCCATCTTCTAGAAAG
mT/mG	CGAAGTTATATTAAGGGTTCCGGATCA	CCTTCGCTGCGGTCTTG	ATGGGTTGCTGTTTCTC
Gls2 Wild-Type	CTCAATGGATACCTGAGCAGAGCT	CTCACCCATTTCTCTTACTCTGCG	TCGAGCTGTATCTGGAGGT
Gls2 Knock-Out	CATGTTTTACTAGCCAGATTTTTCCTCC	CAAGGAAGTTGCTTGTTGGCAT	CCTGACTACTCCCAGTCAT
GS Wild-Type	CCAGTGATCCCTCTCCCAGC	TTGGTGTGTAGAGATTAAGAACCTGACC	TCCATCCTTTTGAGTTACAGT
GS Knock-Out	CAGGCGACGAACCCTTCC	CCTTATTCCAAGCGGCTTCG	CTTCCAGTGATCCCTCTC

2.2 Primary Murine Hepatocyte Isolation, Culture, and Characterisation

2.2.1 Isolation of Hepatocytes from Murine Livers

The hepatocyte isolation protocol used throughout this study has been adapted from published protocols and previously optimised by members of our laboratory [189-193]. Briefly, the process of murine hepatocyte isolation was initiated with a two-step enzymatic digestion of the liver *in situ* (Figure 2.2). By first perfusing the liver with a buffered, physiological saline perfusion medium (Gibco Liver Perfusion Medium (1X) (Gibco, Cat no. 17701038) via the inferior vena cava under general anaesthesia, blood was flushed from the liver. A Liver Digest Medium (Gibco, Cat no. 17703034) of proteolytic enzymes was subsequently perfused through the liver. By exploiting the *in situ* vasculature of the liver for this perfusion process, direct action of the enzymes on the intercellular attachments is facilitated, enabling efficient disaggregation of the tissue [189,193].

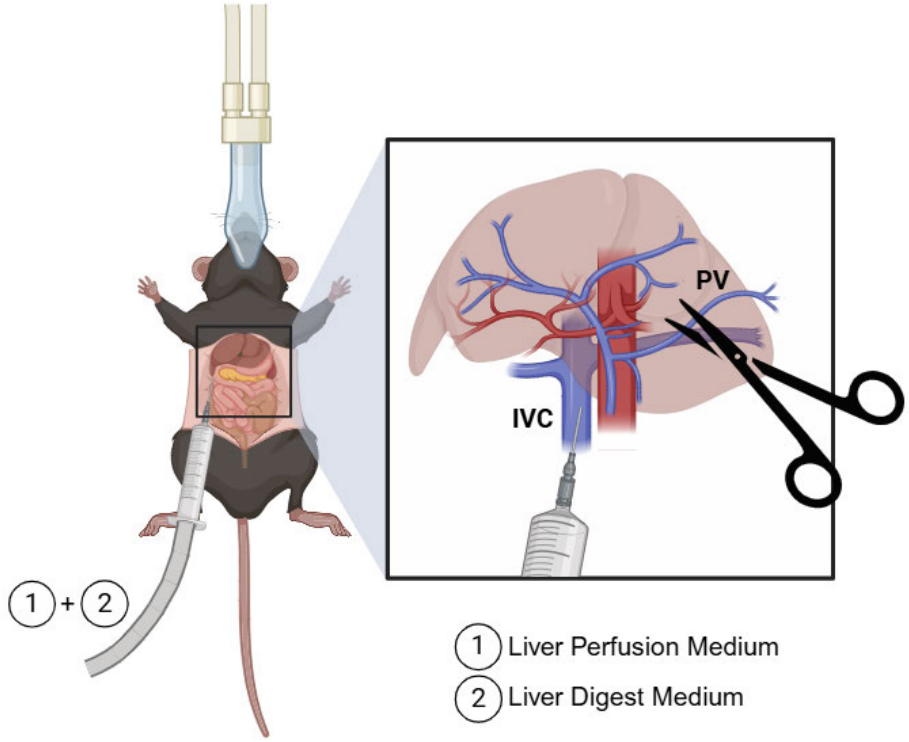

Figure 2.2: Schematic Overview of the Two-Step Murine Hepatocyte Isolation Procedure. *The process begins with in situ liver perfusion via the inferior vena cava under general anaesthesia to flush blood from the liver, followed by the proteolytic digestion of the liver (Created with BioRender.com).*

Upon completion of perfusion, the liver was dissected and transported in standard hepatocyte culture media (Williams E medium supplemented with 10% Foetal Calf Serum, 1% Antibiotic-Antimycotic, 1% Glutamax, 1% Insulin-Transferrin-Selenium) on ice to a laminar-flow biosafety cabinet for further processing. The murine livers were gently agitated under sterile conditions to liberate the component cells from the extracellular matrix. The resultant suspension was then passed through a 70µm cell strainer to filter out larger structures such as bile ductules, vasculature, and remnants of the ECM. The cell suspension was then pelleted at 50 *x g* for 3 minutes with low acceleration and deceleration speeds to avoid lysing the cells. Once pelleted, the supernatant was discarded, and hepatocytes were further purified by passing them through a 65% Percoll gradient, effectively separating any cell aggregates, debris, and non-parenchymal cells from the viable hepatocytes [194]. The cell pellet was washed twice with basic hepatocyte media via resuspension and centrifugation at 50 *x g* for 3 minutes, ensuring removal of excess Percoll and cell debris.

2.2.2 Maintenance of Primary Murine Hepatocytes in 2D Culture

To ensure hepatocytes preserve their *in vivo* functionality, rapid establishment of polarity in culture is essential following isolation. Thus, to assess which substrate best sustains the polarity of hepatocytes

over time, the cells were seeded into culture dishes which had either been plasma treated to increase their hydrophilicity – referred to as being tissue culture (TC) treated - or were seeded onto plates coated in rat tail collagen type I at a density of $1x10^6$ cells/cm^2 [144,195]. Hepatocytes in 2-dimensional (2D) culture typically lose polarity and dedifferentiate within 7 to 10 days [195,196]. The hepatocytes used in the immunofluorescence staining and CYP3A4 activity assays were seeded at a concentration of $1x10^5$ cells per cm^2 in duplicate wells of 8-well Nunc™ Lab-Tek™ II Chamber Slides™.

All 2D cultures were maintained in standard hepatocyte media and incubated at 37°C in a New Brunswick™ Galaxy® 170 S CO_2 incubator with 95% humidity and 5% CO_2. The culture media was changed daily. The spent conditioned medium – containing the hepatocyte secretome – was collected at 24-, 48-, 72-, and 96- hours post-isolation and stored at -80°C for further analyses.

2.2.3 Establishing and Maintaining Primary Murine Hepatocyte Spheroids

To establish three-dimensional (3D) spheroid cultures of the hepatocytes, the cells were isolated and processed as described in Section 2.2.1 and were then counted and seeded at 4000 cells per well into Nunclon™ Sphera™ 96-Well U-Shaped-Bottom Microplates (Cat No. 174925). After seeding, the plates were centrifuged at 50 *x g* for ~3 minutes to force the cells to aggregate at the bottom of the wells. These cultures were maintained in either standard hepatocyte culture media, standard hepatocyte culture media supplemented with 100nM Dexamethasone, or standard hepatocyte culture media supplemented with 3μM CHIR99021. The spheroids were left undisturbed for 3 days before the first media change, and the media was then changed every 3 days after that.

2.2.4 Quantitative PCR (qPCR) and Analysis

i. RNA Isolation

The RNeasy Mini kit® RNA isolation kit (QIAGEN, Cat no. 74104) was used per the manufacturer's instructions to extract the total RNA from the cultured hepatocytes at various time points post-isolation [197]. To establish RNA yields, the optical density of each sample was measured at 260nm (A260) using a Nanodrop 2000c Spectrophotometer (Thermo Scientific, DE, USA).

Despite repeated attempts at optimisation, it proved impossible to achieve adequate RNA yields and quality from spheroid-cultured hepatocytes using the above system. Satisfactory results were achieved, however, using the Invitrogen SYBR™ Green Fast Advanced Cells-to-CT™ Kit as per the manufacturer's instructions (Thermo Fischer Scientific Cat no. A35381) [198].

ii. Reverse Transcription

Following isolation, the QuantiTect Reverse Transcription kit (QIAGEN, Cat no. 205311) was used per the manufacturer's instructions to synthesise cDNA from the samples. Each RNA sample was diluted with RNase-free water to a final concentration of 1µg. A volume of 2µl QuantiTect gDNA Wipeout Buffer (7x) was incubated with the samples at 42°C for 2 minutes to minimise contamination with genomic DNA. A reverse-transcription master mix comprising Quantiscript Reverse Transcriptase, Quantiscript RT Buffer, and RT Primer Mix was added before incubation at 42°C for 20 minutes to facilitate primer binding and cDNA synthesis. A 3-minute incubation at 95°C inactivated the Quantiscript Reverse Transcriptase. The synthesised cDNA was stored at -20°C until analysis via quantitative polymerase chain reaction (qPCR).

iii. Quantitative Polymerase Chain Reaction (qPCR)

To measure expression of cell lineage and zone marker genes in 2D-cultured primary murine hepatocyte cultures, gene-specific primers were either designed in-house and ordered or validated Quantitect Primer assays were purchased (Table 2.2). cDNA samples were amplified using the Roche LightCycler® 480 SYBR Green I Master dye-based qPCR system (Fischer Scientific Cat no. 04887352001) [199]. The Applied Biosystems QuantStudio 12K Flex 384 Real-Time qPCR System was used to amplify samples. cDNA samples were diluted with nuclease-free H_2O to a final concentration of 1ng/µl.

Table 2.2: Sequences of Hepatocyte-, Cholangiocyte-, Mesenchymal-, Hepatic Zone-, and Notch Signalling Primers.

Gene Target	Primer Symbol	Sequence	Length	GC%	Tm (°C)
Housekeeping Gene					
Glyceraldehyde-3-phosphate dehydrogenase	Gapdh	Quantitect primer assay purchased from QIAGEN			
Hepatocyte Marker Genes					
Albumin	Alb	F: CAGATGACAGGGCGGAACTT	20	55	60.04
		R: AGGTGCTTTCTGGGTGTAGC	20	55	59.96
Hepatocyte nuclear factor 4 alpha	Hnf4α	F: GGCATGGATATGGCCGACTA	20	55	59.39
		R: TGTGGTTCTTCCTCACGCTC	20	55	59.97
Cytochrome P450, family 3, subfamily a	Cyp3a11	F: AAGCATTGAGGAGGATCACACA	22	45.45	59.69
		R: GACAGCAAGGAGAGGCGTTT	20	55	60.6
Cholangiocyte Marker Genes					

Epithelial cell adhesion molecule	EpCAM	F: GAAAGCCCCTACGACCATCA	20	55	59.46
		R: GACACCACCACAATGACAGC	20	55	59.41
SRY-Box Transcription Factor 9	Sox9	Quantitect primer assay purchased from QIAGEN			
Keratin 19	K19	F: GGG GGT TCA GTA CGC ATT GG	20	60	58.5
		R: GAG GAC GAG GTC ACG AAG C	19	60	57.8
Hepatocyte nuclear factor 4 beta	Hnf1β	F: GAGCCTCAACACCTCCCAAG	20	60	60.32
		R: AGGGCAGGGGTAGATAACGTG	21	57.14	61.31
Mesenchymal Marker Genes					
Snail	Snail	F: AAGCCCAACTATAGCGAGCT	20	50	56.1
		R: TTTTGCCACTGTCCTCATCG	20	50	55.5
Zinc Finger E-Box Binding Homeobox 2	ZEB2	F: CCGAGTCCATGCGAACTG	18	61.11	56.1
		R: TCCTGGGATTGGCTTTG	17	52.94	55.6
Vimentin	Vim	F: CAGTATGAAAGCGTGGCTGC	20	55	59.9
		R: AAGGGCATCCACTTCACAGG	20	55	59.96
Fibronectin 1	Fn1	F: CCCTATCTCTGATACCGTTGTCC	23	52.17	59.17
		R: TGCCGCAACTACTGTGATTCGG	22	54.55	63.41
Hepatic Zone Markers					
Glutaminase 2 (Zone 1)	Gls2	Quantitect primer assay purchased from QIAGEN			
Arginase-1 (Zone 1)	Arg1	F: CTCCAAGCCAAAGTCCTTAGAG	22	11	55.1
		R: AGGAGCTGTCATTAGGGACATC	22	50	56.2
Glutamine Synthetase (Zone 3)	Glul	Quantitect primer assay purchased from QIAGEN			
Axin2 (Zone 3)	Axin2	Quantitect primer assay purchased from QIAGEN			
Notch Signally Pathway Markers					
Hairy and enhancer of split-1	Hes1	Quantitect primer assay purchased from QIAGEN			
Hairy/enhancer-of-split related with YRPW motif-like protein	HeyL	Quantitect primer assay purchased from QIAGEN			
Notch-regulated ankyrin repeat protein	Nrarp	Quantitect primer assay purchased from QIAGEN			

iv. Standard Curve

In order to quantify the relative expression of the marker genes in cultures over time, the efficiency of the primer pairs was taken into consideration when analysing the results of the qPCRs. Standard curves were produced using the Roche LightCycler® 480 SYBR Green I master mix using cDNA from the H69 BEC cell line as template for all primers. Serial dilutions of cDNA template (ranging from 10 µg/ml to

100,000 µg/ml) were generated, and dilutions with two negative controls (no-template control; RNA without reverse transcription) were amplified with equal amounts of qPCR primers [199]. Ct values were plotted against the logarithm of initial template concentrations to generate standard curves. qPCR efficiency and linearity were calculated from the standard curve's slope and R^2 value. These values were then used in the analysis of the qPCR results using the Pfaffl method (Equation 2), where *E* represents the primer efficiency calculated using Equation 1 for the gene of interest (GOI) and housekeeping gene (HKG) – GAPDH in this study [200].

Equation 1: Calculating Primer Efficiency using the Standard Curve Slope Value (R^2).

$$Primer\ Efficicency\ (E) = \left(\frac{-1}{10^{R^2}}\right) \times 100$$

Equation 2: Pfaffl Mathematical Model of Relative Gene Expression Ratio in Quantitative PCR.

$$Gene\ expression\ ratio = \frac{(E_{GOI})^{\Delta Ct\ GOI}}{(E_{HKG})^{\Delta Ct\ HKG}}$$

When assessing the difference in marker gene expression between treated versus non-treated spheroid cultures, the delta delta Ct (ΔΔCt) method of analysis was used. This method differs from the Pfaffl method in that it involves first normalising the cycle threshold (Ct) values of your gene of interest to a housekeeping gene (ΔCt), and then comparing this normalised value between the treated and non-treated groups (ΔΔCt). The relative expression is then calculated as $2^{-\Delta\Delta Ct}$, providing a fold-change in expression between the groups being compared.

2.2.5 Quantifying CYP3A4 (Cyp3A11) Activity

Functionality of hepatocytes in 2D and 3D culture was assessed over time by measurement of Cyp3A11 activity, a cytochrome P450 enzyme (the murine homolog of human CYP3A4) [201]. The Promega Lytic CYP3A4/Luciferin-IPA P450-Glo™ assay was used as per manufacturer instructions. Briefly, cells were incubated for 15 minutes at 37˚C with 5% CO_2 in serum-free hepatocyte media containing 2X Luciferin-IPA. An equal amount of Luciferin Detection Reagent was added, incubating at room temperature for a further 15 minutes and cell lysate luminescence was read in triplicate using the Promega GloMax® Navigator Microplate Luminometer using an integration time of 1 second per well [202]. Mean background luminescence of a negative control containing no cell lysate was subtracted from the mean of the sample readings prior to analysis.

2.2.6 Measuring Glycogen Production and Storage

Periodic Acid Schiff (PAS) staining of fixed hepatocytes was undertaken using the Periodic Acid Schiff (PAS) Stain Kit (Mucin Stain) as per the manufacturer's instructions (Abcam, ab150680). Prior to staining, 4000-cell hepatocyte spheroids were cultured in 9 x 9 MicroTissues® 3D Petri Dish® micro-moulds (Merck, Z764019), and fixed for 1 hour at room temperature in 10% neutral-buffered formalin (NBF) before washing with phosphate-buffered saline (PBS) and incubation with 0.5% Periodic Acid solution for 5 minutes. The spheroids were rinsed with distilled water and immersed in Schiff's Solution for 15 minutes. Following further rinsing, hepatocytes were counterstained with Mayer's Haematoxylin solution for 1 minute, rinsed under running water for 2 minutes and treated with Bluing Reagent for 10 seconds. PAS staining was quantified using the Colour Thresholding plugin in Fiji ImageJ (Version 2.16.0, National Institute of Health, US). Thresholding of images was set according to hue, saturation, and brightness the region of interest was selected. Resulting measurements were expressed as a percentage of PAS-stained surface area of each spheroid.

2.2.7 Albumin ELISA

2D- and 3D-cultured hepatocytes were washed with PBS and incubated in serum-free hepatocyte media for 72 hours, with conditioned media collected on days 3, 6, 9, and 12. The supernatant was analysed using a Mouse Albumin ELISA Kit as described by the manufacturer (Abcam, ab108792) and the absorbances of the samples were read using the Tecan Spark® 20M multimode plate reader at 450nm with a 570nm wavelength correction. The mean of triplicate sample readings was calculated and compared to a standard curve generated simultaneously using samples of pre-determined concentrations to determine the quantity of secreted albumin in the conditioned media. A negative control of media collected from wells containing no cells or spheroids was used in this assay so that the background luminescence could be subtracted from the sample readings prior to analysis.

2.3 Immunohistochemical and Immunofluorescent Staining

Liver tissues undergoing immunohistochemical (IHC) or immunofluorescent (IF) staining were fixed in 4% paraformaldehyde (PFA) overnight before being transferred to 70% ethanol, before being embedded in paraffin (Tissue-Tek VIP 5 Jr.) and microtomed at a 4 µm thickness onto positively charged glass slides (Thermo Scientific SuperFrost Plus Adhesion: 10149970). Spheroids intended for IHC or IF were cultured in 9 x 9 MicroTissues® 3D Petri Dish® micro-moulds (Merck, Z764019) at 4000 cells per well and fixed using 10% NBF for 1 hour at room temperature, before being encased in agarose (Figure 2.3), before being embedded in paraffin and sectioned.

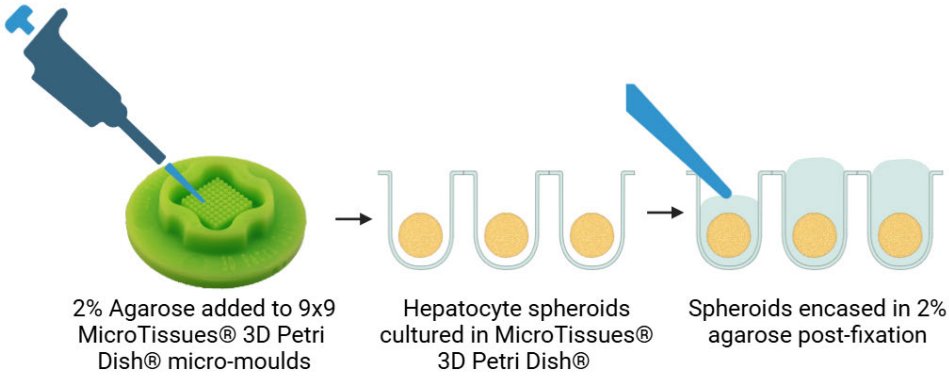

Figure 2.3: Workflow for Embedding Hepatocyte Spheroids using Micro-Moulds. *Spheroids are generated and cultured in 9×9 MicroTissues® 3D Petri Dish® micro-moulds with 2% agarose, then harvested and encased in 2% agarose post-fixation to facilitate subsequent paraffin wax embedding (Created with BioRender.com).*

Prior to IHC and IF, the paraffin wax was removed from the tissues and spheroids with three 5-minute xylene immersions, and the samples were rehydrated through a series of decreasing ethanol concentrations (100%, 75%, 50%, and 25%) before being washed in distilled water for 5 minutes. For antigen retrieval, slides were immersed in either a preheated Tris-EDTA (pH 9.0) or Tri-Sodium Citrate buffer (pH 6.0) and placed into a pressure cooker for 10 minutes (Table 2.4). Slides were rinsed in cold running water for 5 minutes and mounted into Epredia™ Shandon™ Sequenza™ Slide Racks (Thermo Fischer Scientific, Cat no. 10098889).

2.3.1 Immunohistochemical Staining

When staining for proteins of interest using 3,3'-diaminobenzidine (DAB), the Sequenza™-mounted slides underwent blockade of endogenous peroxidase activity with 3% hydrogen peroxide for 15 minutes at room temperature. The following steps involved further PBS rinses and sequential blocking with avidin and biotin (Vector Labs Avidin/Biotin Blocking Kit, Cat no. SP-2001) for 15 minutes each at room temperature, followed by three further PBS rinses. Protein block (Abcam, ab64226) was applied for 30 minutes at room temperature, followed immediately by overnight incubation at 4˚C with relevant primary antibody (Table 2.4) diluted in antibody diluent (OriGene, E09-500).

Slides were rinsed three times in PBS, after which a biotinylated secondary antibody (Table 2.5) diluted in antibody diluent was applied and incubated for 30 minutes at room temperature. After three additional PBS rinses, Vector RTU ABC reagent (Vector Laboratories, SK-4100) was added to each slide and left for 30 minutes at room temperature for DAB detection. The DAB reagent was prepared as per the manufacturer's instructions (Vector Laboratories, SK-4100), applied to the slides, and left in the dark for between 1 and 5 minutes. Once the DAB had developed, the slides were rinsed in PBS and

counterstained in Harris haematoxylin for 3 minutes before being briefly dipped in Scott's Tap Water (Table 2.3) until the sections turned blue, then washed again in tap water. Finally, the slides were dehydrated through a graded series of alcohols (50% to 100%) and cleared in xylene before being mounted in DPX mountant (Sigma-Aldrich, Cat no. 06522) and dried overnight. Whole-slide scans were acquired using the Hamamatsu NanoZoomer 2.0-HT slide scanner and NDP Scan software (Hamamatsu).

i. Quantification of DAB Staining in Tissue Sections

When quantifying the recombination efficiency in the mouse models, the percentage of positively stained area in the DAB-stained liver sections was analysed using QuPath v0.5.1 [203]. Five random regions, each with an area of 6306225 μm^2, were selected on each slide (n=5), and thresholding was applied to detect the DAB-stained areas. The thresholding parameters were optimised, with a smoothing sigma of 1 to reduce background noise and improve detection accuracy. A threshold value of 0.1 was used to distinguish between positively stained areas and the background. This method allowed for consistent and reproducible quantification of the DAB-stained regions across all samples, providing a reliable measure of the percentage of positively stained area in each selected region.

2.3.2 Immunofluorescent Staining

When dual staining for proteins via IF, the Sequenza™-mounted slides were permeabilised by incubation in PBS with 0.1% Triton X-100 for 5 minutes at room temperature. The tissues were treated with Protein Block for 60 minutes at room temperature, and the primary antibodies, mixed with the Antibody Diluent at an appropriate dilution (Table 2.2), were added to the slides and left to incubate at 4˚C overnight. Approximately 12 hours later, the slides were rinsed with PBS, and a solution of Antibody Diluent containing a combination of fluorescent secondary antibodies of the appropriate host species was added to each slide and allowed to incubate at room temperature for 60 minutes (Table 2.4). Following a final PBS rinse, slides were mounted in VECTASHIELD® Antifade Mounting Medium with DAPI and imaged using the Nikon ECLIPSE Ti-U inverted epifluorescence microscope.

Table 2.3: Primary Antibodies for Immunohistochemical- and Immunofluorescent Staining.

Protein Target and Symbol	Host Species	Company	Catalogue No.	Antibody Dilution	Antigen Retrieval (TE or SC) ***
Albumin (Alb)	Rabbit	Abcam	ab20737	1/500	TE
Blue Fluorescent Protein (BFP)	Rabbit	Bioassay Technology Laboratory	BT-AP06749	1/200	SC
Cyp2E1	Mouse	Abcam	MA5-25001	1/100	SC
Cytokeratin 19 (K19)	Rat	DSHB	TROMA-III	2 - 5µg/mL	TE
E-cadherin (24E10)	Rabbit	Cell Signalling Technology	3195S	1/500	SC
Green Fluorescent Protein (GFP)	Chicken	Abcam	ab13970	1/1000	SC
Glutaminase 2 (Gls2)	Rabbit	Abcam	ab113509	20µg/mL	SC
Glutamine Synthetase (Glul/GS)	Rabbit	Abcam	ab73593	1/1000	SC
HA-Tag (6E2)	Mouse	Cell Signalling Technology	2367S	1/1000	SC
Hepatocyte nuclear factor 4 alpha (Hnf4α)	Mouse	Abcam	MA1-199	10 - 20µg/mL	TE
IgG monoclonal Isotype Control [EPR25A]	Rabbit	Abcam	ab172730	*	**
Myc-Tag (71D10)	Rabbit	Cell Signalling Technology	2278S	1/1000	SC
Ornithine aminotransferase (Oat)	Rabbit	Abcam	ab137679	1/100	SC
SRY-box transcription factor 9 (Sox9)	Rabbit	Sigma-Aldrich	HPA001758	0.25 - 2µg/mL	TE

** Used at same concentration as the antibody used at the time; **Used the same antigen retrieval buffer as the antibodies used to stain the tissues for at the time; *** Antigen retrieval buffer compositions (Tris EDTA [TE] and Sodium Citrate [SC]) can be found in Table 2.5.*

Table 2.4: Secondary Antibodies for Immunohistochemical- and Immunofluorescent Staining.

Antibody	Company	Catalogue No.	Dilution
Biotinylated Secondary Antibodies - IHC			
Biotinylated rat anti-mouse	Vector Laboratory	BA-2001	1/500
DSB-X™ biotin goat anti-chicken	Life Technologies	D20701	1/500
Biotinylated goat anti-rat IgG (H+L)	Vector Laboratory	BA-1000	1/500
Fluorescent Secondary Antibodies- IF			
Alexa Fluor™ 647 donkey anti-mouse IgG (H+L)	Invitrogen	A31571	1/500
Alexa Fluor™ 647 donkey pAb to Rat	Abcam	ab150155	1/500
Alexa Fluor™ 594 donkey anti-rat IgG (H+L)	Invitrogen	A21209	1/500
Alexa Fluor™ 555 goat anti-rabbit IgG (H+L)	Invitrogen	A21430	1/500
Alexa Fluor™ 488 donkey anti-chicken IgG (H+L)	Invitrogen	A78948	1/500
Alexa Fluor™ 488 goat anti-rabbit IgG (H+L)	Life Technologies	A11034	1/500

2.4 Gibson Cloning, Preparation, and Transfection of Plasmid DNA

The plasmids used in this study (pSBbi-BH, pT3-EF1α-*myr*-Akt-HA, pT3-EF1α-Myc-NICD1, and pCMV(CAT)T7-SB100) were a gift from the Luke Boulter laboratory at the Institute for Genetics and Cancer, University of Edinburgh, originally purchased from Addgene.

Gibson assembly was used to clone the *myr*-AKT-HA sequence into a pSBbi-BH (Addgene, Cat No. 60515) plasmid backbone (Figure 2.4). Specific primers were designed to isolate and amplify the *myr*-AKT-HA sequence within the pT3-EF1α-*myr*-Akt-HA plasmid (Addgene, Cat No. 31789) using the NEBuilder Assembly Tool. Primers (FWD: 5'-tcgaggctgatcagcgagctTCAAGCGTAGTCTGGGAC-3' and REV: 5'-ttcgaaggcctgtcaggccaATGGGGAGCAGCAAGAGC-3') were designed with specific overlap and spacer sequences related to the intended cloned backbone (pSBbi-BH) to ensure correct orientation of the *myr*-AKT-HA sequence relative to the bidirectional promoter of the backbone. Using these primers, the gene of interest was amplified via standard PCR using the pT3-*myr*-AKT-HA plasmid as a template. The PCR product was then confirmed to be of the correct size and yield by conducting a 2%

agarose gel electrophoresis and was then gel extracted using the QIAquick Gel Extraction Kit (QIAGEN, Cat No. 28704).

Concurrently, the plasmid backbone was digested with HindIII-HF and Xba1 enzymes, as digesting at these sites would generate "sticky" ends required for primer annealing (Figure 2.4). The digested backbone was run on a 2% agarose gel to confirm complete digestion and linearisation, followed by gel extraction using the QIAquick Gel Extraction Kit (QIAGEN, Cat No. 28704).

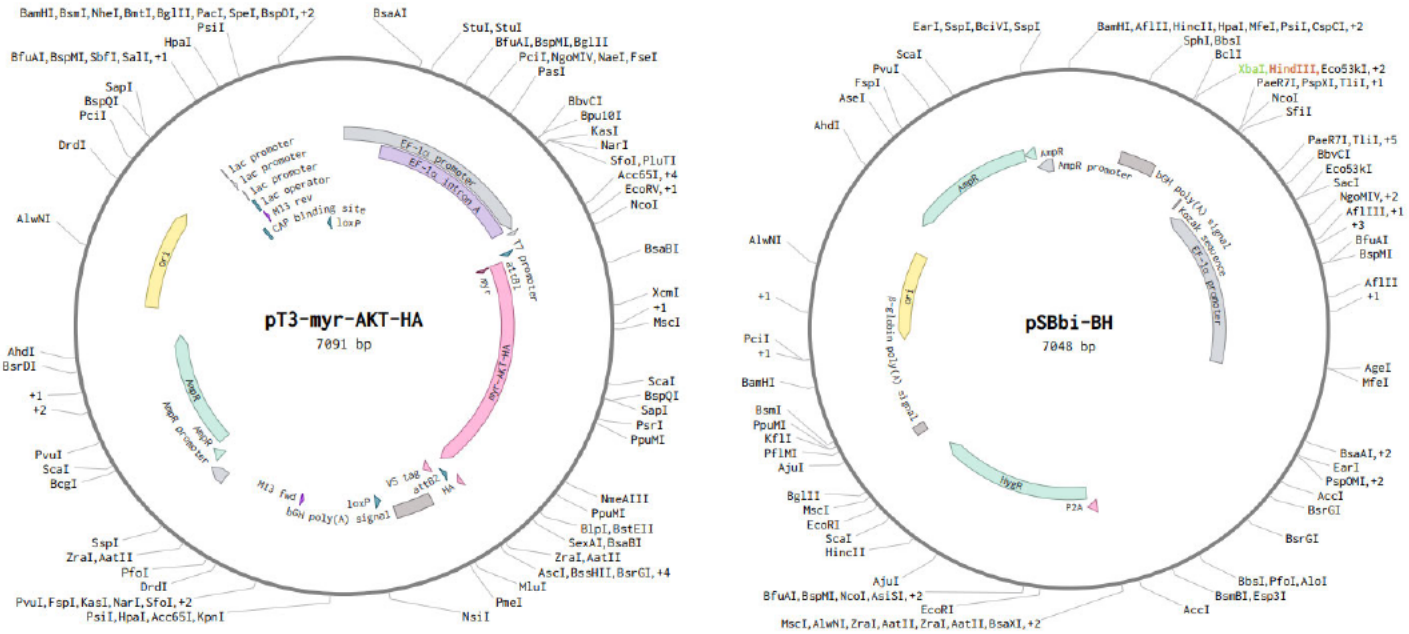

Figure 2.4: pT3-myr-AKT-HA and pSBbi-BH Plasmid Maps. *XbaI and HindIII digestion sites are highlighted in green and orange, respectively, on the pSBbi-BH map (Created in Benchling).*

For the assembly process, the NEBuilder® HiFi DNA Assembly Master Mix and Assembly Reaction protocol were utilised to combine the digested pSBbi-BH backbone and the *myr*-AKT-HA PCR-amplified fragment. The resulting product (~1µg) was transformed into 50µl of NEB® 5-alpha Competent *E. coli* (New England Biolabs, Cat No. C2987I). This was achieved by adding the plasmid DNA solution to the bacteria, which were incubated for 30 minutes on ice, subjected to heat shock in a 42°C water bath for 30 seconds, and inoculated onto pre-poured agar plates supplemented with ampicillin (100µg/ml).

The plates containing transformed bacteria were cultured for 24 hours, after which positive colonies (colonies which had grown on the ampicillin selection plates) were picked, and the plasmid DNA was isolated using a QIAGEN Plasmid Mini Kit (QIAGEN, Cat no. 12123) as per the manufacturer's instructions. Briefly, a single bacterial colony was inoculated into a Lysogeny broth (LB) supplemented

with 100µg/ml ampicillin for approximately 8 hours at 37°C with vigorous shaking (~300rpm). This provided the starting material for subsequent centrifugation and wash steps through the QIAGEN-tip columns to purify the plasmid DNA. Once the plasmid DNA had been precipitated, the yield was measured through Nanodrop UV spectrophotometry at a wavelength of 260nm. Sanger sequencing (Applied Biosystems™ 3730xl DNA Analyser, Cat No. A41046) was conducted by the in-house DNA Sequencing Facility at the Institute of Genetics and Cancer, University of Edinburgh, to verify the presence and correct orientation of the insert. Subsequently, the plasmid quantity was amplified using the QIAGEN Plasmid Maxi Kit (QIAGEN, Cat no. 12162), and glycerol stocks were prepared and stored for future use at -80˚C.

As a tertiary test to ensure the BFP was detectable, the pSBbi-BH-*myr*-AKT-HA plasmid (Figure 2.5) was transfected into HEK293T cells using the jetOPTIMUS® DNA Transfection Reagent (Polyplus, Cat No. 101000025). The transfection procedure briefly involved the removal of the culture media (Dulbecco's Modified Eagle's Medium (DMEM) supplemented with 10% foetal bovine serum (FBS)) rinsing the cells gently with PBS, and then adding the transfection solution (0.13µg plasmid DNA + 12.5µl jetOPTIMUS® buffer + 0.13µl jetOPTIMUS® reagent + 125µl culture media per well in 96-well plate) to the cultures and incubating them for 24 or 48 hours at 37˚°C. The cells were live imaged on the Nikon ECLIPSE Ti-U inverted epifluorescence microscope. This same lipofectamine-based transfection protocol was used to introduce the pCMV(CAT)T7-SB100, pT3-EF1α-Myc-NICD1, and pSBbi-BH-*myr*-AKT-HA plasmids into the primary murine hepatocyte spheroids. Finally, whole plasmid sequencing was arranged through Plasmidsaurus (https://plasmidsaurus.com/) using Oxford Nanopore Technology with custom analysis and annotation to ensure the sequence map was recorded for archival purposes.

The pCMV(CAT)T7-SB100 transposon-transposase system (Addgene, Cat No. 34879) and the pT3-EF1a-Myc-NICD1 plasmid were amplified with the QIAGEN Plasmid Maxi Kit (QIAGEN, Cat No. 12123) as per the manufacturer's instructions before use. The protocol for the amplification and purification of the plasmid DNA using this kit is as described above; however, the starter ampicillin-supplemented lysogeny broth (LB) culture was initiated with the inoculation of the bacteria directly from the glycerol stocks previously stored at -80˚C, and LB media cultures were prepared in a 400ml LB media volume.

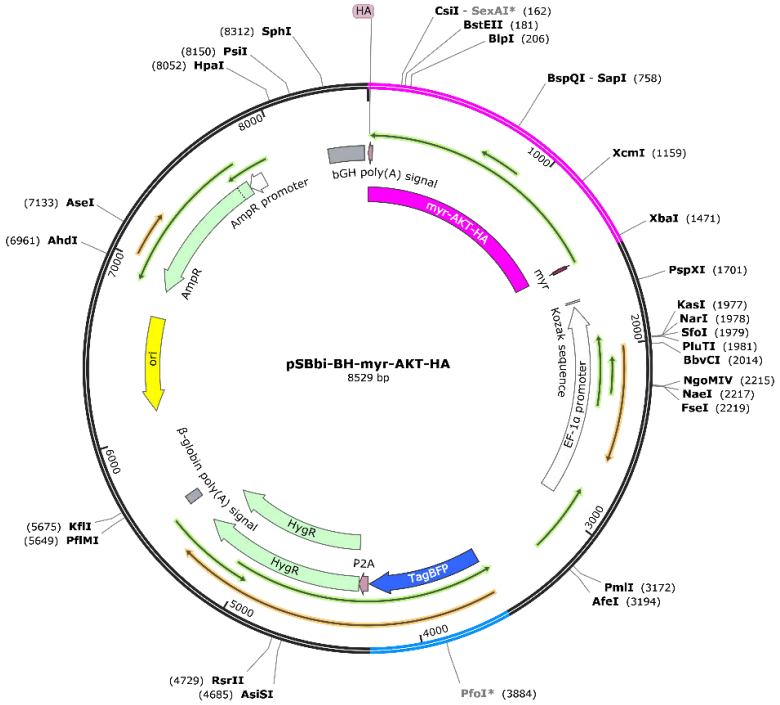

Figure 2.5: Cloned pSBbi-BH-myr-AKT-HA plasmid map. *The myr-AKT-HA sequence is highlighted in magenta, and the blue fluorescent protein (TagBFP) reporter sequence is highlighted in blue (Created in SnapGene).*

2.5 Tamoxifen Treatment for Cre-Recombination Induction

Cre-recombination was induced by dosing the mice with a single dose of tamoxifen at a concentration of 100mg/kg from a working solution of 4mg of tamoxifen solubilised in 0.2ml corn oil (Sigma-Aldrich, C8267-500mL) and 10% ethanol. The GSCreER-mT/mG mice received an oral gavage of a vehicle control corn oil + 10% ethanol solution rather than the tamoxifen-containing mixture. Mice were left to recover for 7 days prior to commencing the experimental procedure.

2.6 Hydrodynamic Tail Vein Injection (HTVI) for Tumour Model Induction

The pT3-EF1α-Myc-NICD1 (20µg, Addgene, Cat No. 86500) and pSBbi-BH-*myr*-AKT-HA (10µg) plasmids were diluted in physiological saline (Scientific Laboratory Supplies, 52455-100TABF) together with a pCMV(CAT)T7-SB100 (6µg, Addgene, Cat No. 34879) transposase-transposon system for dosing. The Sleeping Beauty (SB) system consists of the SB transposase enzyme, which is able to recognise inverted repeat/direct repeat (IR/DR) sequences which flank the genes of interest (the transposon) on the pT3-EF1α-Myc-NICD1 and pSBbi-BH-myr-AKT-HA plasmids [204]. When the plasmid DNA enters the hepatocytes, the SB transposase binds to the IR/DR sequences, which initiates a cut-and-paste mechanism where the transposase excises the transposon from the plasmid and integrates it into the hepatocyte's genome at a TA dinucleotide base pair insertion site (Figure 2.6).

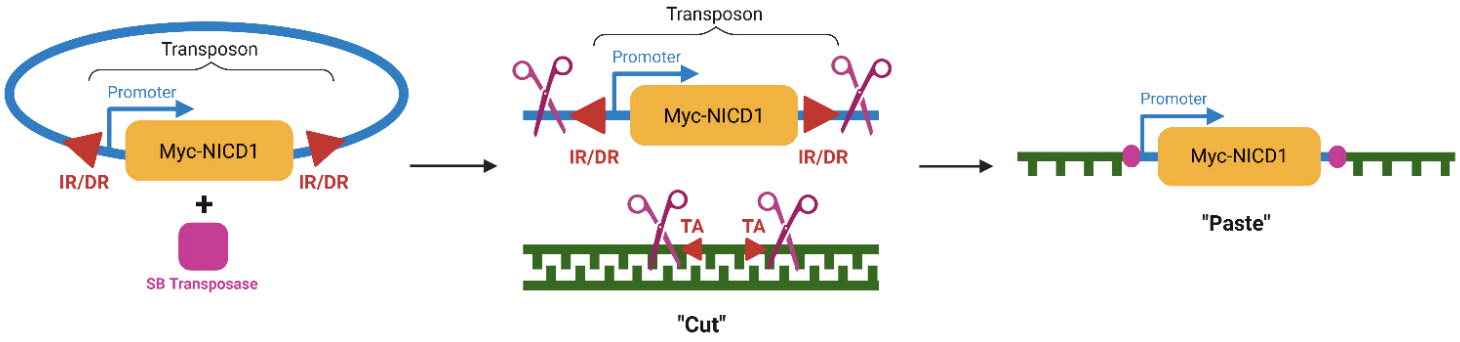

Figure 2.6: Basic Representation of the Mechanism of Action of the Sleeping Beauty (SB) Transposon System. *The SB transposase system recognises the gene of interest (Myc-tagged Notch Intracellular Domain 1 [NICD1]) in the accompanying plasmid DNA sequence by the flanking inverted repeat and direct repeat (IR/DR) sequences. Once defined, the transposase is able to excise the Myc-NICD1 with its promoter and integrate it into the host cell genome within Thymine/Adenine (TA) dinucleotide integration sites (Created with BioRender.com).*

The plasmid solutions were transported to the Western General Hospital Animal Unit at room temperature and were incubated at 37°C before injection. C57Bl6/J, Gls2CreER-mT/mG, and GSCreER-mT/mG mice were warmed in an oxygenated incubator at 26-30˚C to induce vasodilation, specifically in their tails, to prepare them for the hydrodynamic tail vein injection (HTVI) [205,206]. Once the tail veins were judged to be adequately vasodilated, physiological saline and plasmid solution were injected into the lateral tail vein in under 10 seconds, with the volume equivalent to 2mL of solution per 20g of the mouse's body weight.

Mice were observed for 30 minutes post-HTVI for tachycardia. Once assessed as satisfactory, they were monitored daily for 4 weeks [133]. At 4 weeks post-treatment, mice were culled via CO_2 overdose if the livers were intended for immunostaining analysis (Section 2.3) or by terminal perfusion (Section 2.2.1) if intended for cell isolation. In all animal experiments conducted in this study, it was ensured that the mice were of the same age at the time of dosing and sample collection, were littermates, and were processed together as much as possible to minimise batch effects.

2.7 Fluorescent-Activated Cell Sorting (FACS)

Livers were perfused, removed, dissociated, and filtered as described in Section 2.2.1. Cells were centrifuged at 50 *x g* for 3 minutes with low acceleration and deceleration speeds for pelleting. Once pelleted, the supernatant was discarded, and the cells were rinsed once more with hepatocyte culture media and re-centrifuged to remove as much digestion buffer from the sample as possible. The sample

was resuspended in ~5mL PBS supplemented with 10% FBS (Gibco, Cat No. A5256701) and the samples were transferred to the Flow Cytometry Facility on ice.

Immediately preceding the analysis of the liver samples on the BD FACSAria™ II Cell Sorter with a 100µM nozzle, the cells were centrifuged again at 50 *x g* for 3 minutes, resuspended in PBS supplemented with 1% FBS and approximately 3mL of the suspension was filtered through the 35µm cell strainer cap of the Falcon™ Round-Bottom Polystyrene Tube (Fischer Scientific, Cat no. 10585801).

Cells were sequentially gated as follows: (i) FSC-A vs SSC-A to exclude sub-cellular debris, (ii) FSC-H vs FSC-A to select single cells, and (iii) exclusion of Draq7+ events to define the live population (Appendix Figure 1). Fluorescent reporter gates for mTomato and mGFP were set using reporter-negative and single-colour control samples to minimise spectral spill-over, and only events within the live, singlet gate were sorted.

2.8 Bulk RNA Sequencing and Analysis

2.8.1 Library Preparation and 3' mRNA Sequencing

Before sequencing, the integrity of the RNA samples isolated using the QIAGEN RNeasy Mini Kit from the FACS-sorted mGFP expressing cells was assessed using the Agilent 2100 Electrophoresis Bioanalyser (Agilent Technologies Inc., #G2939AA) and RNA 6000 Nano chip (#5067-1511) in-house at the Wellcome Trust, Edinburgh Clinical Research Facility. RNA was quantified with the Qubit RNA broad-range assay kit (#Q10210) and Qubit 2.0 Fluorometer (ThermoFisher Scientific, #Q32866). To evaluate DNA contamination, the Qubit dsDNA HS assay kit (#Q32854) was used.

Once RNA yield and quality were confirmed, library preparation was undertaken using the QuantSeq 3' mRNA-Seq V2 Library Prep Kit (FWD) for Illumina with UDI 12nt (Lexogen GmbH, A2 – 194.96) according to the manufacturer's protocol. First-strand synthesis generated one fragment per transcript, initiated by oligo-dT priming. Following successful first-strand synthesis, the RNA was removed from the reaction mixture, and second-strand synthesis was initiated by random priming and addition of a DNA polymerase, after which a magnetic bead-based purification was performed. The cDNA libraries underwent 18 cycles of amplification to incorporate sequences necessary for cluster generation and index sequences for multiplexing. A final bead purification step removed excess primers and adapter dimers, ensuring the libraries were clean and ready for sequencing. The final step of the library preparation involved fluorometric quantification and quality checking of the cDNA using the Qubit dsDNA High Sensitivity assay and Agilent Bioanalyser with the DNA High Sensitivity Kit (#5067-4626), respectively.

3’ mRNA sequencing was performed on the NextSeq 2000 platform (Illumina Inc., #20038897) using NextSeq 1000/2000 P1 XLEAP-SBS Reagent Kit (100 cycles) (#20100983). The sequencing outputs were provided in the form of FASTQ files ready for further processing.

2.8.2 3’ mRNA Sequencing Analysis

Bulk RNA-seq analysis was performed using the Galaxy web-based genome analysis platform (https://usegalaxy.org/) [207]. Raw sequencing data in FastQ format were uploaded, and quality trimming was conducted using Trimmomatic to remove adapter sequences and low-quality reads. The quality of the trimmed reads was assessed using FastQC, which generated read quality reports. High-quality reads were aligned to the Mus musculus GRCm39 reference genome using HISAT2, an efficient alignment tool optimised for RNA-seq data. Gene expression levels were quantified using the featureCounts tool by counting the number of reads mapped to annotated genes. Differential gene expression analysis was performed with DESeq2, which calculated fold changes and adjusted p-values for genes across experimental conditions. To enhance interpretability, annotations from the Mus Musculus GRCm39 (version M36, Ensembl 113) GFF3 file were appended to the DESeq2 output tables using the "Annotate DESeq2 Output Tables" tool. Finally, -log10 of the adjusted p-values were calculated and plotted against log2 fold change values to visualise significantly differentially expressed genes.

When analysing the paired-end bulk RNA sequencing data published by Ben-Moshe *et al.* [51], the Galaxy platform was used similarly to above, with the following exceptions. The data (NextSeq 500 analysed C57BL/6 hepatocytes) were retrieved from the NCBI sequence read archive (SRA) Run Selector library (BioProject No. PRJNA556572) and downloaded as an SRA file directly to Galaxy (Table 2.5). The “Download and extract reads in FASTQ format from NCBI SRA” tool was then used to extract the files, after which the same pathway as above was used to trim, align, and count reads. Once the featureCounts files had been produced, they were extracted, and the rest of the analysis was performed manually in R Studio (Version 2024.12.1).

A pairwise Pearson’s correlation analysis was performed on the data to identify the genes significantly associated with the expression of Gls2 and GS. Using a custom threshold (absolute correlation > 0.5), genes with strong correlations to either Gls2 or GS were filtered from the dataset. The top 20 genes most strongly correlated with each target gene were selected, and duplicates were removed to highlight the most relevant candidates. Data visualisation was conducted using the ggplot2 package. A scatter plot was generated to display the correlation values of each gene with Gls2 (x-axis) and GS (y-axis), with point colour indicating the combined correlation strength. The top correlated genes were

labelled directly on the plot for clarity. This approach facilitated the identification of genes most closely associated with Gls2 and GS expression patterns.

Table 2.5: Ben-Moshe SRA Bulk RNA-Seq Data Downloaded from NCBI (Accession: PRJNA556572).

ID	BioSample	Sex	Birthdate	Age	Bases
SRR9831244	SAMN12360372	Male	05-Nov-2017	3 months	2.89 G
SRR9831245	SAMN12360373	Male	05-Nov-2017	3 months	6.97 G
SRR9831246	SAMN12360374	Male	05-Nov-2017	3 months	2.56 G
SRR9831247	SAMN12360375	Male	05-Nov-2017	3 months	1.57 G
SRR9831248	SAMN12360376	Male	05-Nov-2017	3 months	1.60 G
SRR9831249	SAMN12360377	Male	05-Nov-2017	3 months	5.73 G
SRR9831250	SAMN12360378	Male	05-Nov-2017	3 months	3.03 G
SRR9831251	SAMN12360379	Male	05-Nov-2017	3 months	2.93 G
SRR9831252	SAMN12360380	Male	05-Nov-2017	3 months	2.45 G
SRR9831253	SAMN12360381	Male	10-Nov-2017	3 months	1.92 G
SRR9831254	SAMN12360382	Male	05-Nov-2017	3 months	1.55 G

In both the 3' bulk RNA sequencing data produced from the FACS-sorted cells in the present study and in the Ben-Moshe dataset, Gene Ontology (GO) Enrichment analyses were conducted through the Galaxy genome analysis platform. This analysis identified biological processes, molecular functions, and cellular components that were significantly overrepresented in the gene sets. GO term definitions were provided by the go-basic.obo ontology file, and the gene-to-GO term annotations for Mus musculus were sourced from the mgi.gaf.gz file (Gene Ontology release 2025-03-16). The software assessed the statistical significance of enrichment using a hypergeometric test, and the p-values were adjusted for multiple testing using the Benjamini-Hochberg false discovery rate (FDR) method. GO terms with an adjusted p-value below 0.05 were considered significantly enriched.

2.9 Statistical Analysis

GraphPad Prism software (v10.4.1) was used to perform statistical analyses. All data were assessed for normal distribution by the Shapiro-Wilk test ($p \leq 0.05$) and are expressed as mean ± standard deviation unless otherwise stated. Parametric data spanning three or more timepoints were analysed by repeated measures one-way ANOVA with Tukey's HSD multiple comparisons test. Parametric data from three or more timepoints across two or more groups were evaluated by two-way ANOVA with Bonferroni multiple comparisons. For non-parametric data – whether gene expression comparisons or quantification of size or staining over three or more timepoints – a Kruskal-Wallis or Friedman test with Dunn's multiple comparisons was employed. All data are graphed as mean ± standard deviation unless noted otherwise and are presented in the text as mean ± standard error of the mean (SEM).

2.10 Reagents, Media, and Buffer Compositions

Table 2.6: Reagents used throughout the Present Study.

Product	Supplier	Product Code
Liver Perfusion Medium (1X)	Life Technologies	17701-038
Liver Digest Medium	Life Technologies	17703-034
Percoll	Sigma-Aldrich	P1644-500mL
HBSS with calcium, magnesium	Life Technologies	24020117
William's E Medium, no phenol red	Life Technologies Ltd. (Invitrogen)	A1217601
Antibiotic-Antimycotic (100X)	Life Technologies	15240062
Foetal Bovine Serum (FBS)	Sigma-Aldrich	F9665-500mL
Glutamax Supplement	Thermo Scientific	35050038
Insulin, Transferrin, Selenium (ITS) Liquid Media Supplement 100X	Sigma-Aldrich	I3146-5mL
Tween® 20	Sigma-Aldrich	P1379-100mL
Dexamethasone	Sigma-Aldrich	D4902
CHIR99021	Scientific Laboratory Supplies Ltd	SML1046-25MG
Hydrogen peroxide 30%	Merck	H1009-500mL

Vectastain ABC-HRP Reagent, Peroxidase RTU	Vector laboratories	PK-7100
Triton X-100	Sigma-Aldrich	H5141
Protein Block	Abcam	ab64226
Antibody diluent	Life Technologies	00-3218
VECTASHIELD® Antifade Mounting Medium with DAPI	Vector laboratories	H-1200-10
DPX (Phthalate Free) Mounting Medium	CellPath	03822524
Corn Oil	Sigma-Aldrich	C8267-500mL

Table 2.7: Media and Buffers used throughout the Present Study.

Media/Buffer	**Composition**
Hepatocyte Culture Media	Williams E medium supplemented with 10% Foetal Calf Serum, 1% Antibiotic-Antimycotic, 1% Glutamax, 1% Insulin-Transferrin-Selenium (ITS)
Tris-EDTA Buffer (pH 9.0)	1.21g Tris, 0.37g EDTA, 0.5mL Tween20, 1L distilled H_2O
Sodium Citrate Buffer (pH 6.0)	2.94g Tri-Sodium Citrate (Dihydrate), 0.5mL Tween20, 1L distilled H_2O
Scott's Tap Water	10.0g $MgSO_4$, 2.0g Sodium bicarbonate, 3L Tap water

CHAPTER 3

Characterisation of Primary Murine Hepatocytes in 2D and 3D Culture

3.1 Introduction

The culture of primary hepatocytes is a highly desirable tool in the study of drug metabolism, toxicology, and the spectrum of hepatic pathologies. Traditional 2D monoculture of the hepatocytes, however, has been limited by the tendency of the cells to lose polarity and rapidly dedifferentiate [134,157]. Some studies have suggested that dedifferentiation can be slowed by culturing on an extracellular matrix or overlaying the cells with a secondary layer of collagen (2D 'sandwich' culture); however, dedifferentiation still occurs, as evidenced by the appearance of mesenchymal markers and reductions in functionality after 2 weeks in culture [134,135,138,139,208-210]. Thus, as discussed in Chapter 1, the use of 3D primary hepatocyte spheroid cultures offers several significant advantages, including the preservation of hepatic phenotype and functionality, recapitulating *in vivo* cell states. Moreover, 3D cultures demonstrate enhanced viability in hepatocytes when compared to 2D cultures over time, thus enabling longer-term studies and repeat dosing experiments [134,150,153,155,211].

3.1.1 Aims and Hypothesis

This study sought to better understand the behaviour of hepatocytes *ex vivo* through a comprehensive characterisation of both 2D and 3D cultures of primary murine hepatocytes (PMH). It was hypothesised that PMH would rapidly dedifferentiate in 2D culture as described in the published literature, but might potentially maintain phenotype and functionality longer-term when cultured as spheroids.

Once the optimal culture method for PMH had been established, the effects of *in vitro* culture on zone-specific markers and functions were studied, specifically whether alterations to culture media can influence zone-specific phenotypes. The hypothesis being that zonal characteristics would be lost over time in culture due to the loss of proximity to the anatomical zone-defining structures and their associated signalling cues, as well as loss of oxygen and nutrient concentration gradients.

3.2 Characterisation of Two-Dimensional (2D) Hepatocyte Cultures

3.2.1 Phenotypic Characterisation

To investigate the morphology and behaviour of PMH *ex vivo*, hepatocytes were isolated from ~6-week-old male and female C57Bl6/J mice using the two-step enzymatic perfusion method. An average of $1.09x10^8$ hepatocytes were obtained per whole perfused mouse liver, with an average viability of 87.63% (Figure 3.1a, n=70).

Primary hepatocytes have been used in studies of drug metabolism and disease for many years and are known to exhibit specific morphological and functional characteristics *in vitro* under specific culture conditions that closely resemble those *in vivo* [212]. In terms of gross morphology, hepatocytes are typically cuboidal with well-defined, refractile borders and exhibit prominent, round nuclei with cells containing either one large nucleus or being multinucleated with nuclei occurring in multiples of 2 [213,214]. Polyploidy is a distinctive feature of mature hepatocytes and is observed in about 20-30% of the cells in a healthy liver [215,216].

Hepatocytes form confluent monolayers when seeded at the correct density and often arrange in cord-like structures reminiscent of hepatic trabeculae *in vivo*. Notably, primary hepatocytes do not proliferate *in vitro,* and when seeded at suboptimal densities, these cells fail to establish the necessary cell-cell contacts crucial for attachment and preserve their phenotype. An optimal seeding density of ~$1x10^6$ cells/cm^2, determined through a series of seeding density dilution studies, results in preservation of the characteristic polygonal morphology in culture.

Once the hepatocyte monocultures were established on either hydrophilic tissue-culture (TC) plastic culture plates or on collagen-1-coated culture dishes, confocal micrographs were taken of the live cells daily for the first 96 hours (4 days) (Figure 3.1b). A progressive change in cell appearance was observed under both conditions, with the most apparent changes occurring between 46 and 96 hours. Specifically, cells appeared to undergo a reduction in cell size, a shift from a polygonal to a spindle-like shape, and an increase in the granularity of the cytoplasm. By 96 hours, cells appeared more spindle-shaped and granular. Hepatocytes cultured on collagen-1-coated plates appeared to establish visible focal adhesions (magenta arrows in the 2-hour timepoint in Figure 3.1b), attaching the cells to the extracellular matrix rapidly within 2 hours post-isolation. These cells maintained a more cuboidal shape with well-defined cell membranes for up to 72 hours. Despite this initial maintenance, collagen-cultured hepatocytes accumulated more debris over time, making observation difficult at later time points, and they also began to exhibit more spindle-like morphology after 96 hours.

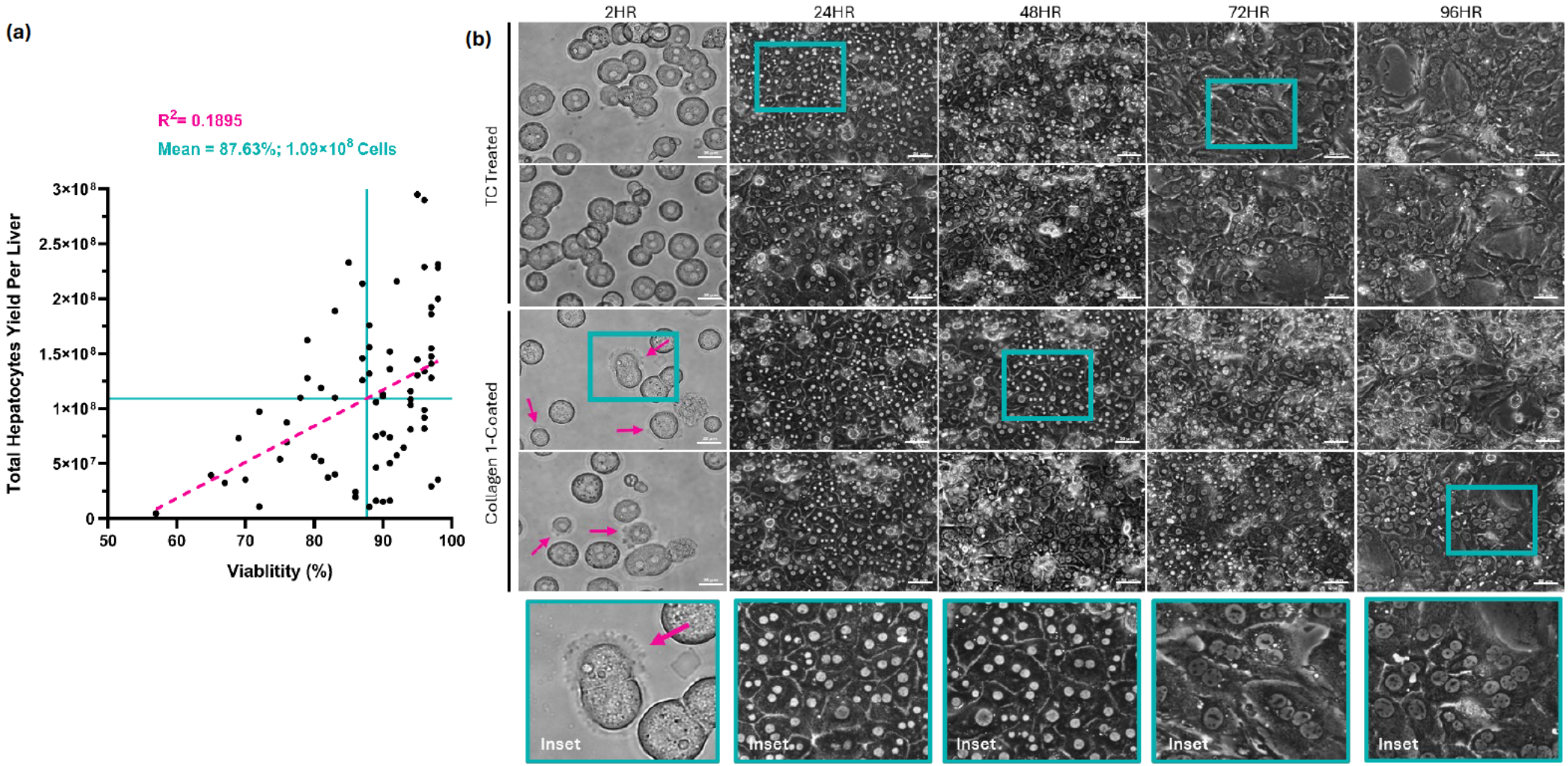

Figure 3.1: Hepatocyte Yield per Mouse Liver and Time-Dependent Loss of Hepatocyte Polarity in Two-Dimensional Culture. ***(a)*** *Yield of viable hepatocytes isolated per whole perfused C57Bl6/J mouse liver plotted against the percentage viability of the hepatocytes in each isolation. Mean hepatocyte yield (1.09x10^8 cells) and viability (87.63%) shown in cyan (n=70)* ***(b)*** *Representative confocal micrographs of hepatocytes cultured on tissue-culture (TC)-treated plastic and collagen I-coated plastic dishes over a 96-hour (HR) period. Cells were plated immediately following isolation. Magenta arrows indicate focal adhesions attaching cells to the extracellular matrix (Scale bars = 25 - 50µm).*

3.2.2 Characterisation of Gene Expression Profiles

After demonstration of the progressive loss of morphological features of hepatocytes over time in 2D culture, this loss of phenotype was further explored through characterisation of the gene expression profiles using quantitative PCR (qPCR). A panel of hepatocyte, biliary, and mesenchymal lineage marker genes was selected based on genes widely accepted as cell identity markers in the published literature [100,133,159,217]. Cholangiocyte organoids derived from C57Bl6/J control mice were included as a reference population for all hepatocyte, biliary, and mesenchymal lineage markers, with RNA collected at passages 8, 9, and 10 (Appendix Figure 2 and Appendix Table 1). Across this time frame, these control organoids did not exhibit substantial variation in expression of any genes within the panel, consistent with their maintenance in a defined 3D culture system supplemented with stem cell and mitogenic growth factors (including RSPO1, EGF, FGF10, HGF, nicotinamide, forskolin, A83-01, and CHIR99021). This relative stability is in keeping with the capacity of organoid cultures to undergo long-term expansion in an artificial niche that supports self-renewal while preserving a cholangiocyte-like identity.

The gene expression profiles of the primary hepatocytes cultured in 2D closely mirrored the observed morphological changes. The relative gene expression results in Table 3.1 and Figure 3.2 show that as the culture period progressed, hepatocytes on both TC-treated and collagen-1 coated plates demonstrated a significant down-regulation in expression of hepatocyte genes Albumin (Col1 0-48 hours p=0.0238), Cyp3a11 (TC 0-48 hours p=0.0329; TC 48-96 hours p=0.0171), and Hnf4α (TC 0-48 hours p=0.0120).

Expression of biliary genes EpCAM (TC 48-96 hours p=0.0155), K19 (TC 0-48 hours p=0.0099; TC 48-96 hours p=0.0282; 48-96 hours p=0.0322), Hnf1β (TC 0-48 hours p=0.0244; 48-96 hours p=0.0466; Col 0-48 hours p=0.0146; 48-96 hours p=0.0217), and Sox9 (TC 48-96 hours p=0.0221) significantly increased in expression in both culture conditions over time. Expression of all biliary genes included in this panel increased; however, the upregulated expression of K19 was the most notable in both culture conditions, with a total mean fold change difference of 1126 ± 131.1 in cells cultured on plastic and 1490 ± 199.5 in collagen-1 cultured cells between 0 and 96 hours.

Expression of a majority of the mesenchymal genes were also increased over time, with Vim (TC 48-96 hours p=0.0089; Col 0-48 hours p=0.0066; Col 48-96 hours p=0.0088), Fn1 (TC 0-48 hours p=0.0068; TC 48-96 hours p=0.0131; Col 0-48 hours p=0.0006; 48-96 hours p=0.0419), and Snail (0-48 hours p=0.0434) all showing upregulation. Vim and Fn1 exhibited the highest increases in expression, with Vim expression showing a mean fold change difference of 540.4 ± 37.94 in TC-cultured cells and 6172

± 431.3 in Collagen-1 cultured cells between 0 and 96 hours, while Fn1 demonstrated a total mean fold change difference of 45.41 ± 3.874 in TC-cultured cells and 631.7 ± 97.81 in Collagen-1 cultured cells over the same period.

Table 3.1: Expression of Hepatocyte, Biliary, and Mesenchymal Gene Markers in Hepatocytes Cultured on (a) Tissue Culture-Treated and (b) Collagen-1 Coated Plates over 96 Hours. *Mean differences (Mean Diff.), standard error of the mean (Std. Error), and adjusted p-value all calculated through a repeated-measures one-way ANOVA and Tukey HSD multiple comparisons test (*p ≤ 0.05; **p ≤ 0.01).*

(a)	Tissue Culture-Treated					
	O-48 Hours			48-96 Hours		
	Mean Diff.	Std. Error	p.adj	Mean Diff.	Std. Error	p.adj
Alb	-0.5767	0.1617	0.1255	-0.08	0.1274	0.8216
Cyp3A11	-0.99	0.1352	0.0329*	-0.0247	0.0024	0.0171*
Hnf4α	-0.9507	0.0775	0.0120*	0.1687	0.0969	0.3755
EpCAM	-0.6598	0.2386	0.1927	-39.64	3.681	0.0155*
K19	-101.8	7.533	0.0099**	-1024	129	0.0282*
Hnf1β	1.013	0.1186	0.0244*	-0.0617	0.0101	0.0466*
Sox9	0.5821	0.1377	0.0927	-6.578	0.7309	0.0221*
Vim	31.37	6.3	0.0686	540.4	37.94	0.0089**
Fn1	20.52	1.257	0.0068**	45.41	3.874	0.0131*
Snail	-0.8896	0.1403	0.0434	1.004	0.2059	0.0713
Slug	1.130	1.206	0.6743	8.831	4.963	0.3652

(b)

	Collagen-1 Coated					
	O-48 Hours			48-96 Hours		
	Mean Diff.	Std. Error	p.adj	Mean Diff.	Std. Error	p.adj
Alb	-0.54	0.0625	0.0238*	-0.0167	0.1099	0.9875
Cyp3A11	-0.9987	0.2055	0.0718	-0.0393	0.0071	0.0566
Hnf4α	-0.9303	0.1594	0.0509	-0.0397	0.0572	0.7909
EpCAM	13.03	3.056	0.0913	44.94	8.671	0.0637
K19	62.54	12.48	0.0678	1427	192.7	0.0322*
Hnf1β	10.43	0.94	0.0146*	-9.675	1.067	0.0217*
Sox9	0.9890	0.5496	0.3601	4.937	1.845	0.2031
Vim	114	6.886	0.0066**	6172	431.3	0.0088**
Fn1	48.86	1.504	0.0006***	631.7	97.81	0.0419*
Snail	-0.9674	0.5833	0.3984	0.9483	0.3820	0.2283
Slug	-1.017	0.4184	0.2359	11.48	1.827	0.0443*

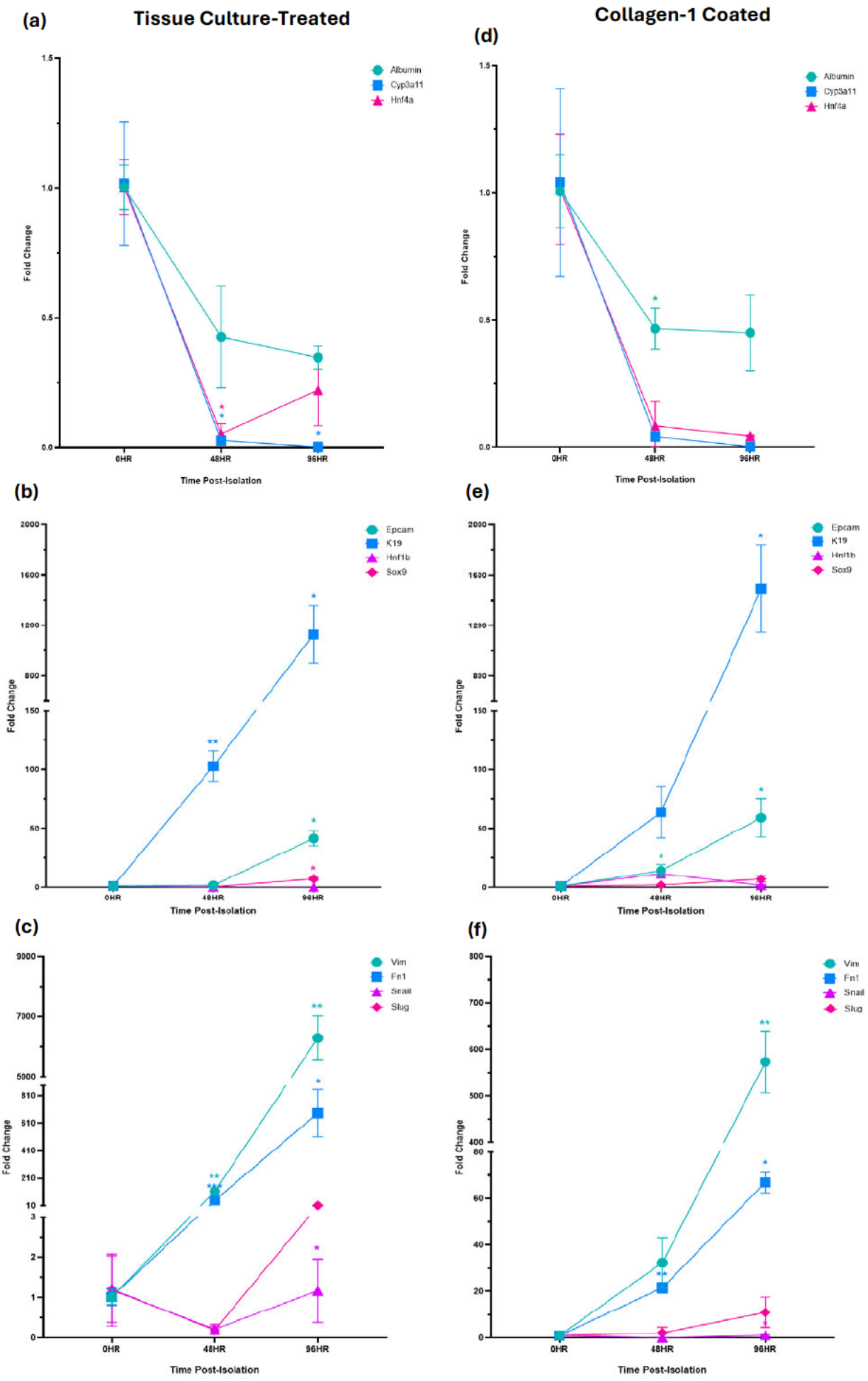
(a)
Tissue Culture-Treated
(d)
Collagen-1 Coated
Albumin
Cyp3a11
Hnf4a
Fold Change
Time Post-Isolation
0HR
48HR
96HR
(b)
(e)
Epcam
K19
Hnf1b
Sox9
(c)
(f)
Vim
Fn1
Snail
Slug

Figure 3.2: Gene Expression Profiles of Hepatocytes Cultured on Tissue Culture-Treated and Collagen-1 Coated Plates over 96 Hours (HR), Determined via qPCR Analysis. *Relative expression levels of hepatocyte-specific (Alb, Cyp3a11, Hnf4α), biliary-specific (EpCAM, K19, Hnf1b, Sox9), and mesenchymal genes (Cdh1, Cdh2, Vim, Fn1) in murine hepatocytes at 0-, 48-, and 96-hours post-isolation when cultured on different substrates.* ***(a-c) Tissue culture-treated plates: (a)*** *Hepatocyte gene markers,* ***(b)*** *Biliary gene markers,* ***(c)*** *Mesenchymal gene markers.* ***(d-f) Collagen-1 coated plates: (d)*** *Hepatocyte gene markers,* ***(e)*** *Biliary gene markers,* ***(f)*** *Mesenchymal gene markers. Data were analysed using a repeated-measures one-way ANOVA and Tukey HSD multiple comparisons test. Data shown as mean ± SD from n = 3 biological replicates measured in triplicate (*p ≤ 0.05; **p ≤ 0.01).*

To validate these findings and visualise the changes in hepatocyte-specific protein expression, immunofluorescent staining was performed in the 2D hepatocyte cultures over time (Figure 3.3). The presence of two of the key hepatocyte markers, Hnf4α, a master regulator of hepatocyte differentiation and function, and Albumin, the most abundant protein synthesised by hepatocytes, was examined [217,218]. The results revealed a reduction in nuclear Hnf4α expression over the culture period, with staining intensity diminishing to almost undetectable levels by 96 hours. Interestingly, while Hnf4α expression was reduced, Albumin protein levels were largely maintained throughout the experimental period.

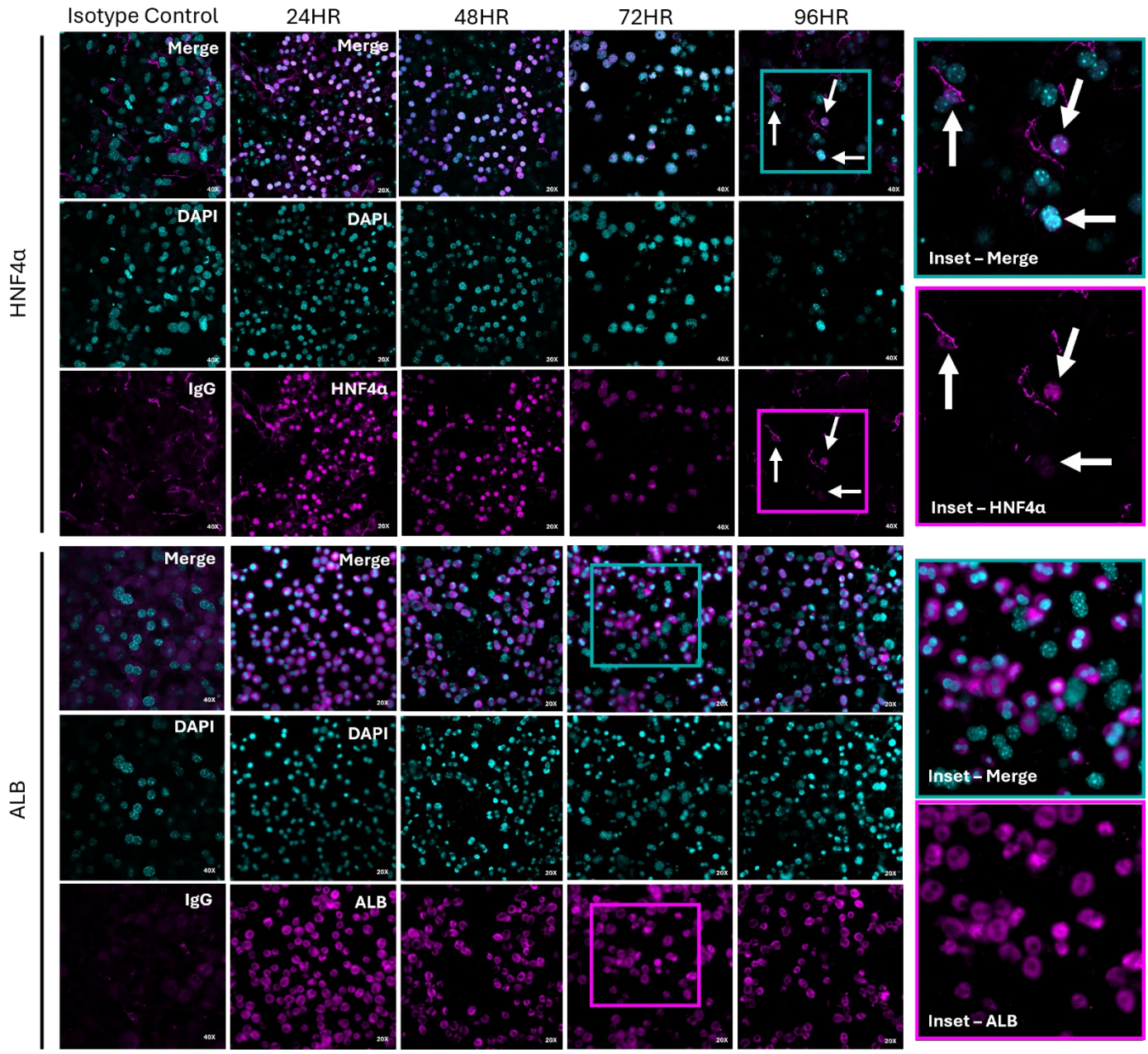

Figure 3.3: Temporal Expression of Hepatocyte Gene Markers in Hepatocytes Cultured on Collagen-1 Coated Plates over 96 Hours. *Immunofluorescent images of hepatocytes cultured on collagen I-coated plates at 24-, 48-, 72-, and 96-hours, stained for hepatocyte markers Hnf4α and Albumin. White arrows indicate positive Hnf4α staining. Images taken at 20X magnification.*

The expression levels of Glutaminase 2 (Gls2) and Glutamine Synthetase (GS) were quantified in the PMH cultured on collagen-1-coated plates over time (Figure 3.4a). Whilst the levels of both Gls2 and GS decreased over time in culture, the fold change in GS was most significant between 48 and 96 hours (mean difference = 0.3805 ± 0.0363, p=0.0164).

Changes in Hes1 and HeyL expression downstream of Notch intracellular domain activation were assessed to ascertain the basal expression levels in hepatocytes after isolation from the liver (Figure 3.4b). Whilst no significant differences in expression of HeyL were observed, the expression of Hes1 increased significantly in the first 48 hours of culture (2.094 ± 0.3016, p=0.0365) as well as between the 48- and 96-hour timepoints (6.103 ± 0.7935, p=0.0300).

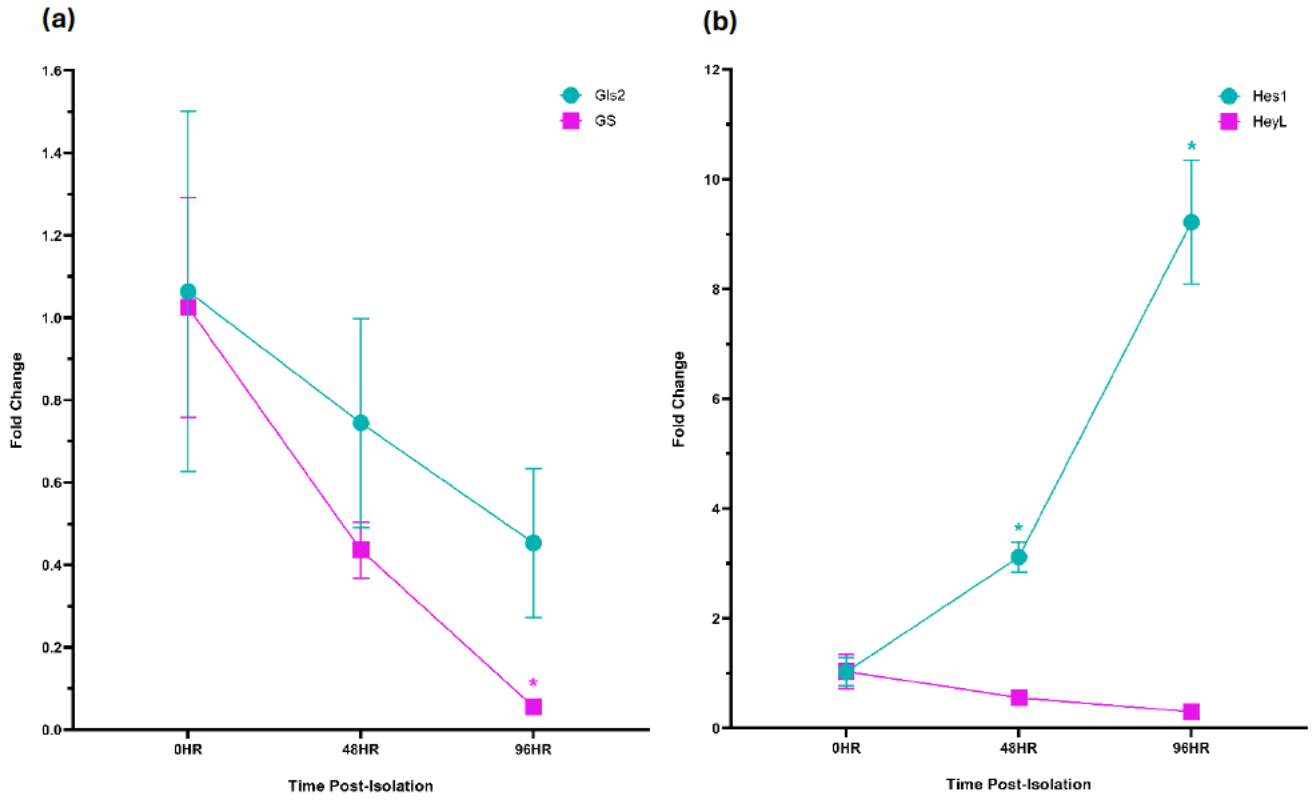

Figure 3.4: Temporal Expression of Zonated Genes and Notch Signalling in Collagen-1 Cultured Hepatocyte Monolayers. *Relative expression levels of* ***(a)*** *Zone markers Glutaminase 2 (Gls2 – Zone 1) and Glutamine Synthetase (GS – Zone 3), and* ***(b)*** *Notch downstream genes Hes1 and Heyl in murine hepatocytes 0 - 96 hours post-isolation following culture on collagen-1 coated plates. Data were analysed using a repeated-measures two-way ANOVA and Tukey HSD multiple comparisons test. Data shown as mean ± SD (*p ≤ 0.05).*

3.2.3 Functional Characterisation

The most widely accepted *in vitro* measures of hepatocyte functionality include Albumin secretion and cytochrome P450 enzyme activity [134,148-153,157,211,219]. Over the 96-hour culture period, a progressive significant decrease in both characteristics was observed in collagen-1 cultured cells (Figure 3.5). Albumin secretion showed a substantial decline in cultures over time, with a significant reduction observed between 24 and 72 hours of culture (Figure 3.5a, mean change of 1.371 ± 0.032ng/ml, p=0.0001). Cyp3a11 enzyme activity diminished substantially over time, decreasing by an average RLU of 0.045 ± 0.005 (p=0.0084), 0.047 ± 0.005 (p=0.0078), and 0.0497 ± 0.005 (p=0.0070) from 24 hours to 48, 72, and 96 hours, respectively (Figure 3.5b).

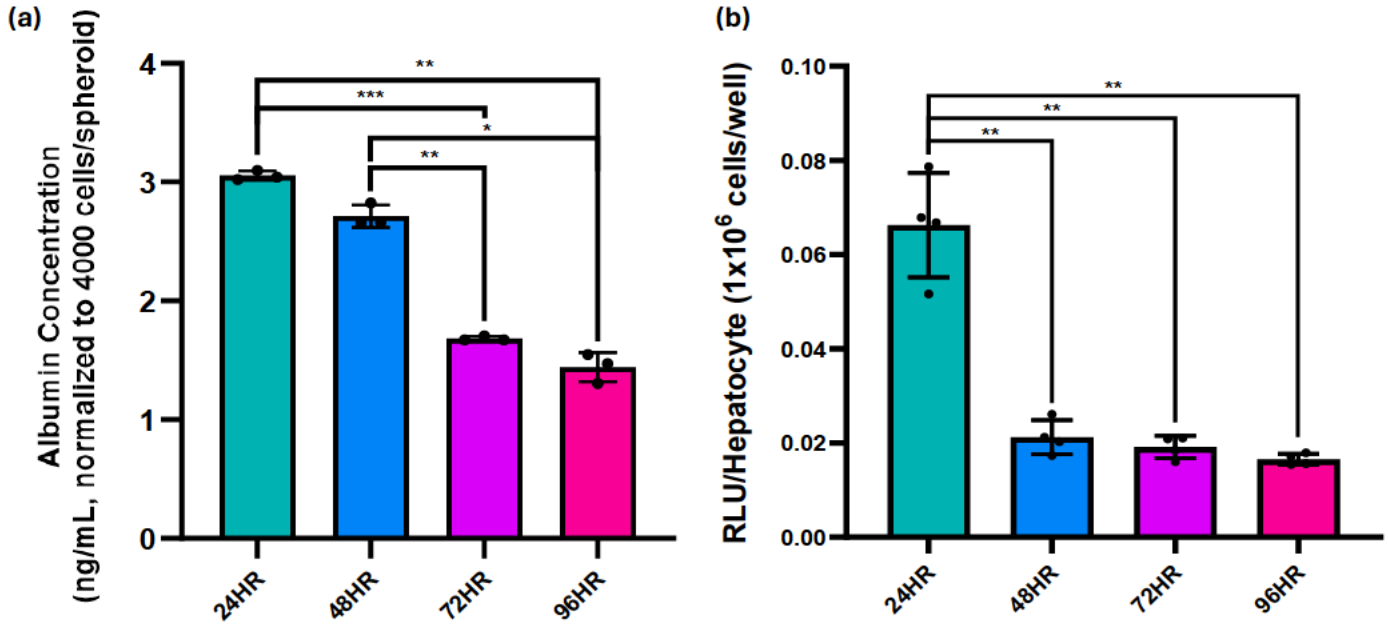

Figure 3.5: Functional Characterisation of Murine Hepatocytes Cultured on Collagen-1 Coated Plates Through Measurement of Albumin Secretion and Cyp3a11 Activity. ***(a)*** *Albumin concentration in conditioned media collected from collagen-1 cultured hepatocytes measured by ELISA at 24-, 48-, 72-, and 96-hours post-isolation (n=3). Data presented as ng of Albumin per mL of conditioned media.* ***(b)*** *Cyp3a11 activity in lysed murine hepatocytes cultured in 2D on collagen-1 coated plates expressed in Relative Light Units (RLU) of detected luciferin per hepatocyte (n=4). Data were analysed using a repeated-measures one-way ANOVA and Tukey HSD multiple comparisons test. Data shown as mean ± SD (*p ≤ 0.05; **p ≤ 0.01; ***p ≤ 0.001).*

3.3 Characterisation of Three-Dimensional (3D) Hepatocyte Cultures

3.3.1 Phenotypic Characterisation

Having demonstrated rapid loss of hepatocyte phenotype under 2D culture conditions, 3D culture models were explored as a superior model to recapitulate the complex 3D microenvironment of the liver. Primary murine hepatocyte spheroids (PMHS) exhibit a distinct morphology characterised by their spherical shape and non-proliferative nature (Figure 3.6) [134].

Spheroids were generated as per Section 2.2.3. Confocal imaging of whole 4000 cell PMHS was performed after 24 hours *in vitro*. Spheroids were observed to aggregate and form budding spherical structures after 24 hrs (Figure 3.6a). Whole-mount immunostaining for DAPI and the cytoskeletal protein Phalloidin highlights the proximity of the cells to one another and a honeycomb-like cytoskeletal arrangement of the cultures (Figure 3.6b). Haematoxylin and eosin (H&E) staining of 5µm spheroid sections demonstrates a densely packed cellular arrangement and lack of a central lumen [220].

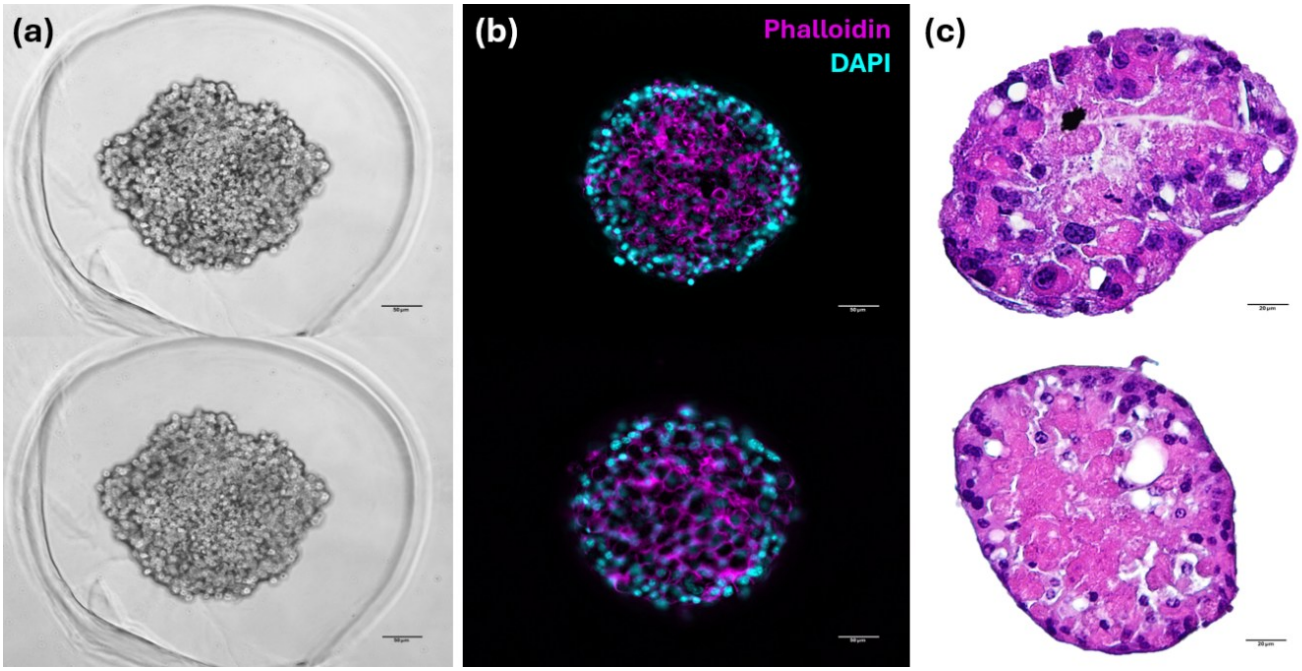

Figure 3.6: Morphological and Structural Characterisation of 4000-cell Primary Murine Hepatocyte Spheroids (PMHS) 24-hours Post-Isolation. ***(a)*** *Representative confocal micrographs of whole PMHS cultured for 24 hours post-isolation in MicroTissues® 3D Petri Dish® micro-moulds (Scale bar = 50µm).* ***(b)*** *Representative immunofluorescent micrographs of whole-mount PMHS fixed at 24 hours post-isolation and stained with phalloidin to demonstrate the filamentous actin structure (Scale bar = 50µm).* ***(c)*** *Representative haematoxylin and eosin stain of 5µm sections through PMHS fixed 24 hours post-isolation (Scale bar = 20µm).*

Hepatocyte spheroids were cultured and analysed at days 3, 6, 9, and 12 to assess morphological stability over time (Figure 3.7a). H&E staining revealed that the structure and cellular organisation remained consistent throughout the culture period. Whilst culturing the spheroids, the structures appeared to become smaller over time and therefore quantitative analysis of spheroid volumes was undertaken (n=25, measured in QuPath). A statistically significant decrease in spheroid area was seen between day 3 (mean area = 21956μm²) to day 12 (mean area = 16940μm²; p=0.0264) (Figure 3.7b).

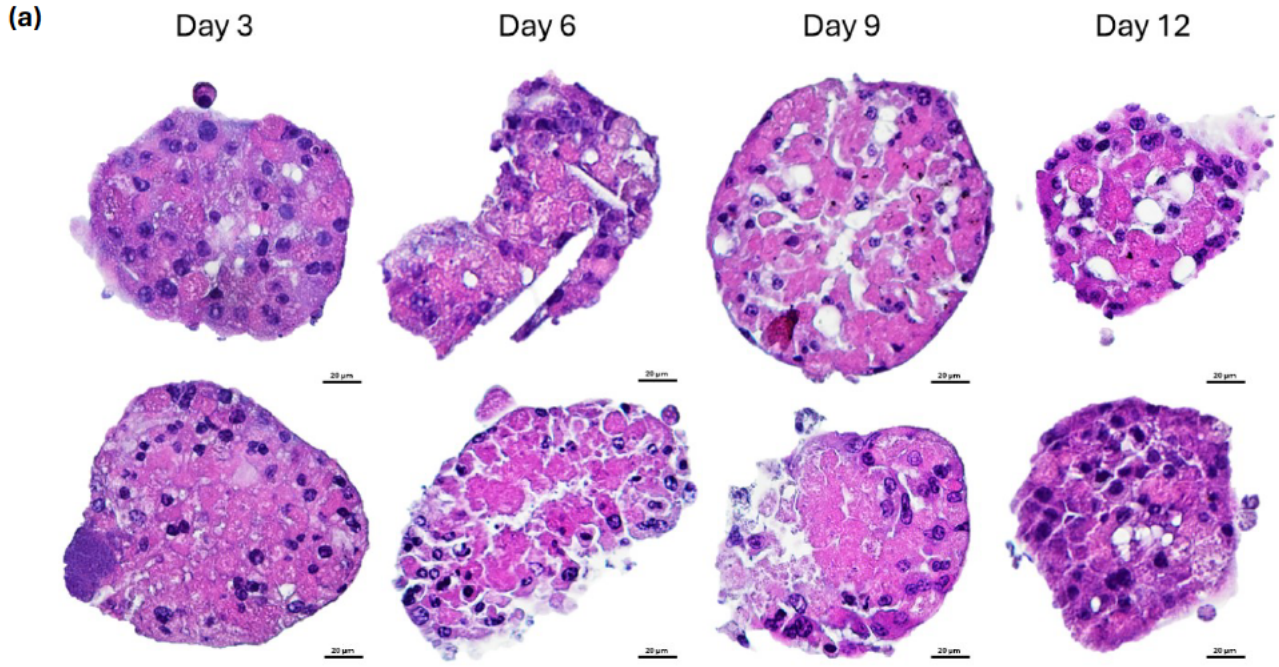

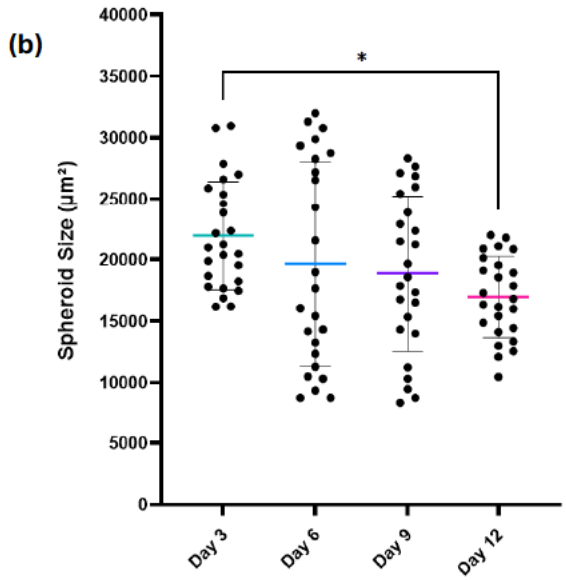

Figure 3.7: Structure of 4000-cell Primary Murine Hepatocyte Spheroids (PMHS) Over a 12-day Culture Period. (a) *Representative haematoxylin and eosin staining of 5μm sections through PMHS fixed on days 3, 6, 9, and 12 post-isolation (Scale bar = 20μm)* ***(b)*** *Quantification of spheroid size over time in culture. Data were analysed using a Friedman test (non-parametric) and Dunn's multiple comparisons test. Data shown as mean ± SD from N = 25 spheroids (**p ≤ 0.01).*

3.3.2 Characterisation of Spheroid Gene Expression

After it was established that hepatocytes had the ability to form spheroids within 24 hours under favourable culture conditions and to maintain these structures until at least day 12, an evaluation was undertaken to determine whether hepatocyte identity gene transcription would be sustained *in vitro*. Relative gene expression analysis (Table 3.2 and Figure 3.8) indicated that throughout the culture period, only one hepatocyte gene, Albumin, showed significant down-regulation between days 9 and 12 (Fold change of 0.7233 ± 0.0754; p=0.0194).

Biliary genes, including EpCAM (Day 3-9 p<0.0001; Day 9-12 p=0.0072), Hnf1β (Day 3-9 p=0.0344), and Sox9 (Day 3-9 p=0.0056), significantly increased in expression over time. Unlike in 2D-cultured hepatocytes, the most up-regulated biliary genes in spheroids are early markers of the biliary lineage, potentially suggestive of a true lineage change in the cells. Similarly, the expression of mesenchymal genes such as Vim (Day 9-12 p=0.0112), Fn1 (Day 3-9 p=0.0258; Day 9-12 p=0.0036), Snail (Day 3-9 p=0.0071; Day 9-12 p=0.0044), and Slug (Day 3-9 p=0.0021) also rose significantly over time. In this case, Fn1 had the largest increase over the time course (60732 ± 3097, p=0.0045), as well as Snail, being the other mesenchymal marker, which had a steady increase in expression over the time course (436 ± 22.39, p=0.0046).

Table 3.2: Expression of Hepatocyte, Biliary, and Mesenchymal Gene Markers Cultured as Primary Murine Hepatocyte Spheroids (PMHS) Measured at Days 3, 9, and 12. *Mean differences (Mean Diff.), standard error of the mean (Std. Error), and adjusted p-value all calculated through a repeated-measures one-way ANOVA and Tukey HSD multiple comparisons test (*p ≤ 0.05; **p ≤ 0.01; ****p<0.0001).*

	Day 3 - 9			**Day 9 - 12**		
	Mean Diff.	**Std. Error**	**p.adj**	**Mean Diff.**	**Std. Error**	**p.adj**
Alb	-0.1033	0.1017	0.6379	-0.7233	0.0754	0.0194*
Cyp3A11	-0.6547	0.1874	0.1302	-0.2267	0.0467	0.0718
Hnf4α	-0.3430	0.2786	0.5457	-0.3933	0.0921	0.0910
EpCAM	75.79	1.085	<0.0001****	5413	342.5	0.0072**
K19	-0.3806	0.1068	0.1257	0.3862	0.1217	0.1534
Hnf1β	3.348	0.4674	0.0344*	4202	943.9	0.0844
Sox9	8461	474.3	0.0056**	405017	133180	0.1648
Vim	-0.5992	0.1605	0.1158	31.49	2.482	0.0112*
Fn1	3559	428.5	0.0258*	57173	2668	0.0036**
Snail	25.23	1.579	0.0071**	410.8	20.82	0.0044**
Slug	-0.9361	0.0371	0.0021**	0.0708	0.0336	0.2917

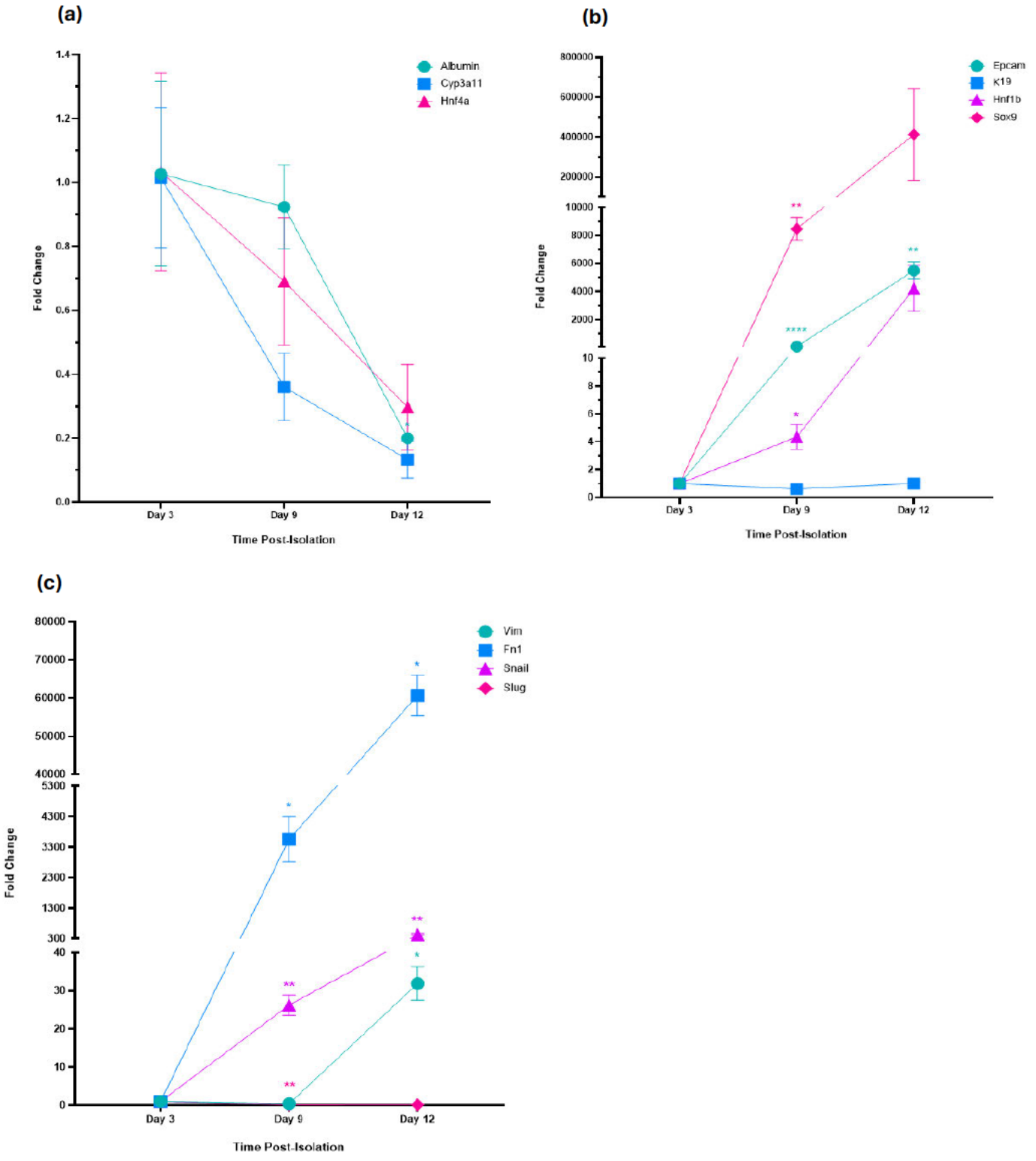

Figure 3.8: Gene Expression Profiles of Hepatocytes Cultured as Primary Murine Hepatocyte Spheroids (PMHS) Measured at Days 3, 9, and 12. *Relative expression levels of* ***(a)*** *Hepatocyte-specific (Alb, Cyp3a11, Hnf4α),* ***(b)*** *Biliary-specific (EpCAM, K19, Hnf1b, Sox9) and* ***(c)*** *Mesenchymal (Vim, Fn1, Slug, Snail) genes at days 3, 9, and 12 of culture. Data analysed using a repeated-measures one-way ANOVA and Tukey HSD multiple comparisons test. Data shown as mean ± SD from n=3 biological replicates measured in triplicate (*p ≤ 0.05; **p ≤ 0.01; ****p ≤ 0.0001).*

3.3.3 Functional Characterisation of Spheroids

As in the 2D cultures, Albumin secretion and Cytochrome P3a11 activity were selected as surrogate measures of hepatocyte function. Albumin secretion was maintained at a constant level throughout the experiment, with no detectable difference observed between 3 and 12 days of culture (Figure 3.9a). Cyp3a11 activity exhibited a significant reduction in activity from day 3 with a mean relative light unit (RLU) of 0.837 ± 0.021 to days 6 (0.216 ± 0.024; $p<0.0001$), 9 (0.041 ± 0.002; $p<0.0001$), and 12 (0.061 ± 0.034; $p<0.0001$) (Figure 3.9b). The reduction in Cyp3a11 activity between day 6, day 9 ($p=0.0006$) and day 12 ($p=0.0055$) also reached statistical significance but did not fall to zero, with low levels of enzyme activity remaining detectable through the time course.

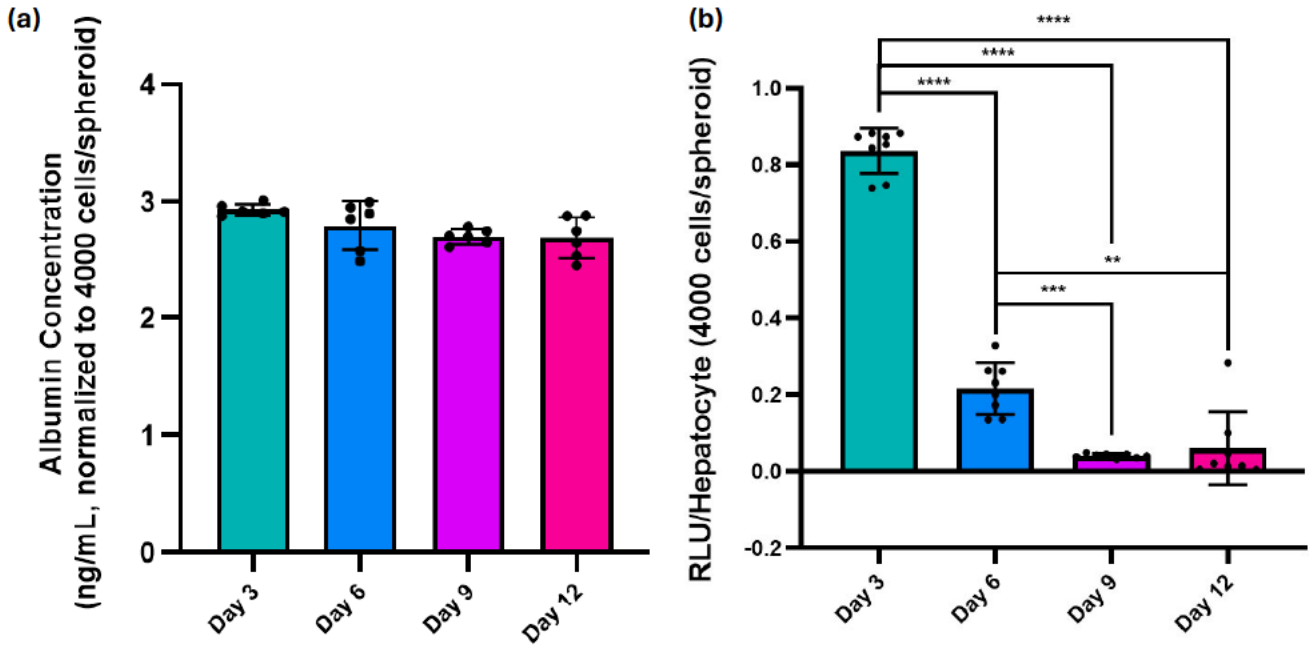

Figure 3.9: Functional Characterisation of Primary Murine Hepatocyte Spheroids (PMHS) Through the Measurement of Albumin Secretion and Cyp3a11 Activity. ***(a)*** *Albumin concentration in conditioned media collected from PMHS cultures and measured by ELISA at 24-, 48-, 72-, and 96-hours post-isolation (n=6). Data presented as ng per mL of conditioned media.* ***(b)*** *Cyp3a11 activity in lysed PMHS expressed in Relative Light Units (RLU) of detected luciferin per hepatocyte (n=8). Data analysed using a repeated-measures one-way ANOVA and Tukey HSD multiple comparisons test. Data shown as mean ± SD (*p ≤ 0.05; **p ≤ 0.01; ***p ≤ 0.001; ****p ≤ 0.0001).*

Hepatocytes play a critical role in the synthesis and storage of glycogen to maintain energy homeostasis *in vivo*. Cytoplasmic glycogen was therefore selected as a third measure of hepatocyte function and visualised through Periodic Acid Schiff (PAS) staining [117]. When PAS comes into contact with polysaccharides, the stain oxidises to produce a distinct purple-magenta colour (Figure 3.10a). Because spheroids vary in size and shape and distinguishing individual cells after sectioning is challenging, the quantity of PAS-staining within the spheroids is represented as a percentage of the overall spheroid area.

Negative control spheroid cultures using the biliary cell line H69 (RRID:CVCL_8121)[221] demonstrated very little PAS positivity (3.577 ± 0.611%), whilst the positive control cell line HEPG2 (a human hepatoblastoma cell line, RRID:CVCL_0027)[222] showed a high volume of glycogen storage in culture (85.014 ± 0.859%) (Figure 3.10b) [150,213]. In PMHS cultures, a significant reduction was observed in the amount of glycogen detected on day 3 (67.123 ± 1.498%) of culture as compared to days 9 (21.686 ± 1.271%; $p<0.0001$) and 12 (21.686 ± 1.271%; $p<0.0001$). At day 6, the spheroids (47.165 ± 2.003%) were storing significantly more glycogen than the spheroids at day 9 ($p<0.0001$) and day 12 ($p<0.0001$). Despite a decrease in PAS positivity, at day 12, there was still discernible glycogen presence detectable (20.848 ± 2.027%).

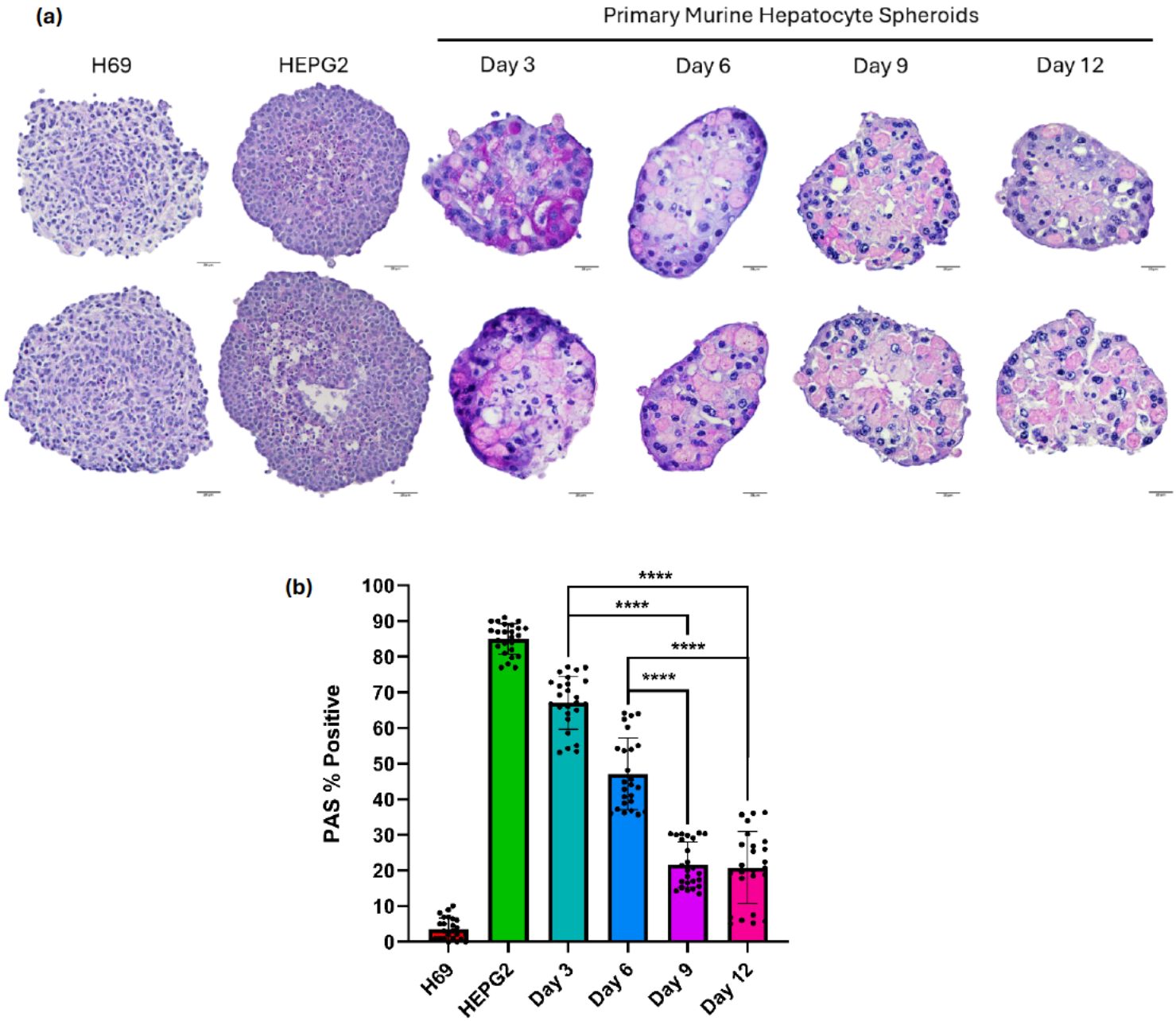

Figure 3.10: Functional Characterisation of Primary Murine Hepatocyte Spheroids (PMHS) Through the Staining and Quantification of Glycogen. ***(a)*** *Representative confocal micrographs of Periodic Acid-Schiff (PAS) stained negative control H69 biliary spheroids, positive control HEPG2 spheroids, and PMHS cultured for 3-, 6-, 9-, and 12 days post-isolation in Hepatocyte Culture Media (Scale bar = 20µm).* ***(b)*** *Quantification of PAS-positive staining (magenta) demonstrates the production and storage of glycogen over time, supporting maintained hepatocyte functionality in ex vivo culture. Data were analysed using a Friedman test (non-parametric) and Dunn's multiple comparisons test. Data shown as mean ± SD from n=25 (****p < 0.0001).*

Staining for dipeptidyl peptidase IV (DPPIV/CD26) to assess the presence of bile canaliculi was used as a further functional characterisation method in the PMHS model [144]. DPPIV is a key enzyme expressed on the apical surface of hepatocytes, specifically localised to bile canaliculi [223]. The presence of DPPIV-positive structures indicates the formation of these specialised channels between adjacent hepatocytes, required for bile secretion and transport (Figure 3.11) [144].

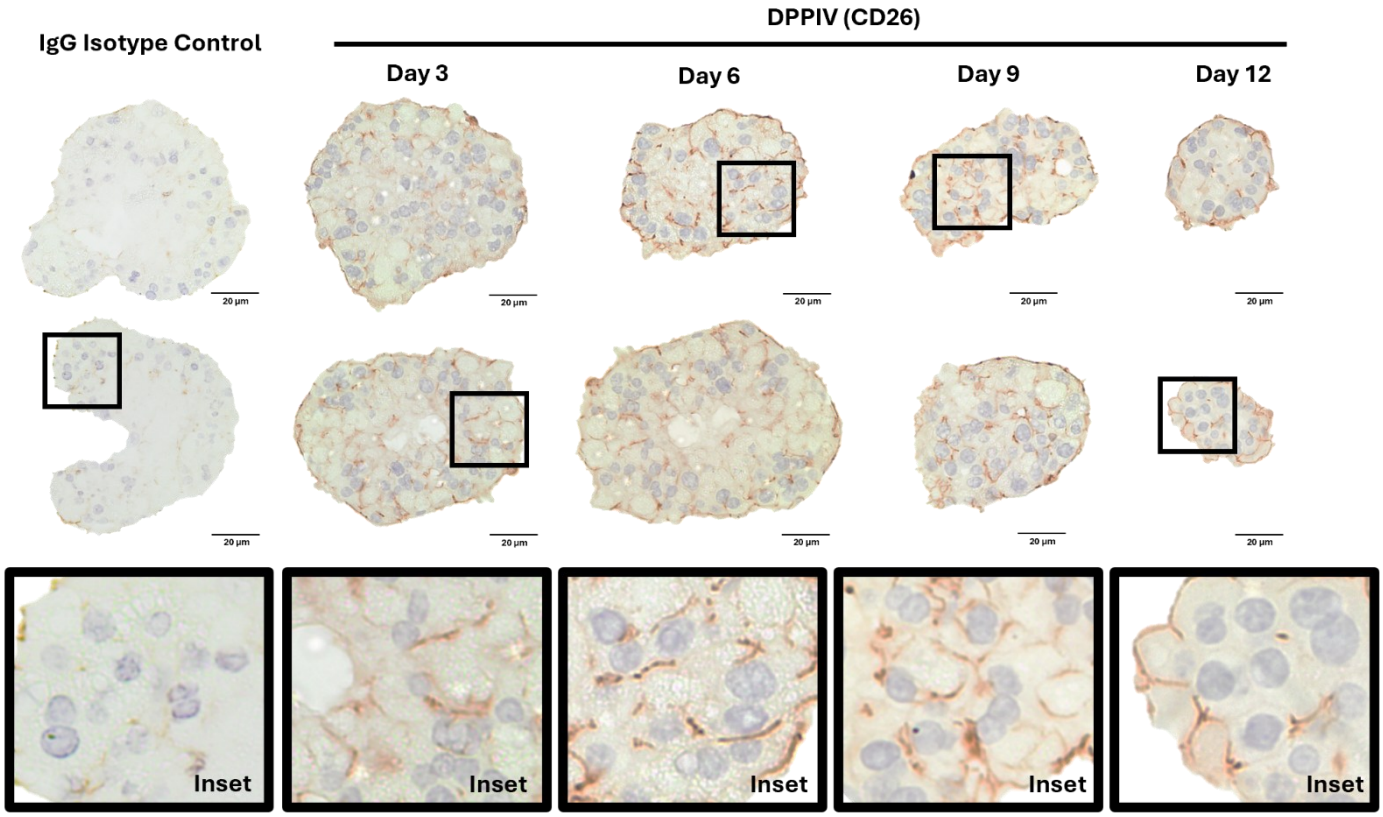

Figure 3.11: Development of Bile Canaliculi in Primary Murine Hepatocyte Spheroids Over Time Demonstrated by Immunostaining for Dipeptidyl peptidase IV (CD26). *DAB-stained PMHS cultured for 3-, 6-, 9-, and 12 days post-isolation in Hepatocyte Culture Media (Scale bar = 20µm).*

3.4 Maintenance of Zonation *In Vitro*

Once it was established that the PMHS were able to maintain hepatocyte functionality *in vitro*, the next goal was to investigate whether the distinct transcriptional patterns of lobular zonation were preserved in this model. To do this, expression of the two zonal markers, Gls2 and GS, was assessed. To interrogate how specific culture conditions affect the maintenance of zonated cell identities *ex vivo*, spheroids were cultured in 3 distinct media formulations: (1) standard hepatocyte culture medium containing 1% Glutamax, 1% Insulin-Transferrin-Selenium, and 1% Antibiotic-Antimycotic; (2) standard medium supplemented with 100nM dexamethasone, a synthetic glucocorticoid; and (3) standard medium with the addition of 3μM CHIR99021, a potent GSK3β inhibitor that modulates Wnt signalling (Figure 3.12).

Dexamethasone was specifically selected for this investigation to assess whether glucocorticoid signalling could promote a more physiologically realistic balance between periportal (Gls2+) and pericentral (GS+) hepatocyte identities in spheroids, while CHIR99021 was used as a complementary approach to enhance Wnt-dependent pericentral features.

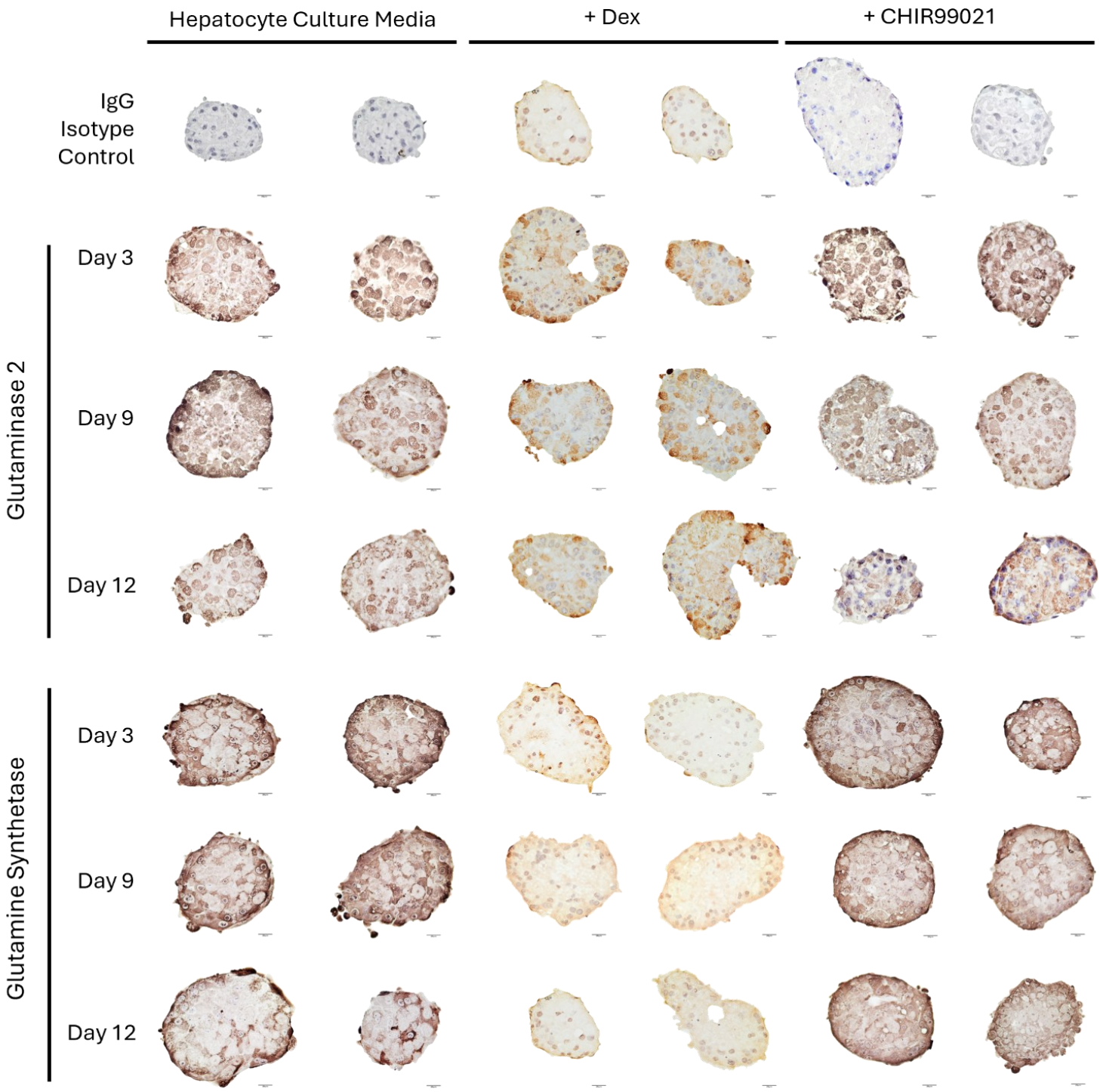

Figure 3.12: Immunohistochemical Staining of Gls2 (Zone 1) and GS (Zone 3) in Primary Murine Hepatocyte Spheroids Over Time when Cultured in Media with Varying Compositions. *Representative images of DAB-stained PMHS cultured for 3-, 6-, 9-, and 12 days post-isolation in Hepatocyte Culture Media (Williams E medium supplemented with 10% Fetal Calf Serum, 1% Antibiotic-Antimycotic, 1% Glutamax, 1% Insulin-Transferrin-Selenium), Hepatocyte Culture Media with 100nM Dexamethasone (Dex) and Hepatocyte Culture Media with 3μM CHIR99021 demonstrating Gls2 and GS expression (Scale bar = 20μm).*

When cultured in standard hepatocyte culture media, expression of Gls2 and GS was observed with no significant changes in immunoreactivity occurring throughout the time course (Figure 3.13a). In contrast, PMHS cultured in dexamethasone-supplemented media induced a difference in detectable expression between Gls2 and GS which reached statistical significance at days 3 (mean difference = 13.32%, p=0.0041), 6 (mean difference = 14.24%, p=0.0026), 9 (mean difference = 12.30%, p=0.0068), and 12 (mean difference = 14.24%, p=0.0276) (Figure 3.13b). This culture condition seemed to almost completely inhibit the expression of GS. Interestingly, whilst the supplementation of hepatocyte culture medium with the Wnt agonist CHIR99021 increased GS expression similar to the levels observed when cultured in standard hepatocyte culture media, overall, the expression levels of Gls2 remained significantly higher than GS throughout the time course (Figure 3.13c). The most significant difference between the expression of the two markers was seen at day 3 post-isolation (mean difference = 21.40%, p<0.0001), although days 6 (mean difference = 9.97%, p=0.0035), 9 (mean difference = 10.58%, p=0.0022), and 12 (mean difference = 7.81%, p=0.0164) also reached significance.

In summary:

- Hepatocyte culture media maintained similar levels of expression of both Gls2 and GS.
- Expression of Gls2 and GS decreased in response to the presence of dexamethasone.
- GS expression in the presence of CHIR99021 reduced from that observed in spheroids cultured in unsupplemented media, but this effect was not as profound as the decrease observed in the dexamethasone-exposed spheroids.

Retention of GS immunoreactivity in response to CHIR99021-supplemented media and the observation that the proportions of Gls2 and GS expression are closer to expected *in vivo* proportions (which is maintained at a ratio of approximately 1:4 in the mammalian liver based on the spatial distribution of Gls2+ hepatocytes being ~80-85% of the liver and GS+ hepatocytes being ~15-20% of the liver [51,66,224-227]) led to the decision to use CHIR99021-supplemented media for all further *in vitro* experiments of hepatocytes in this study.

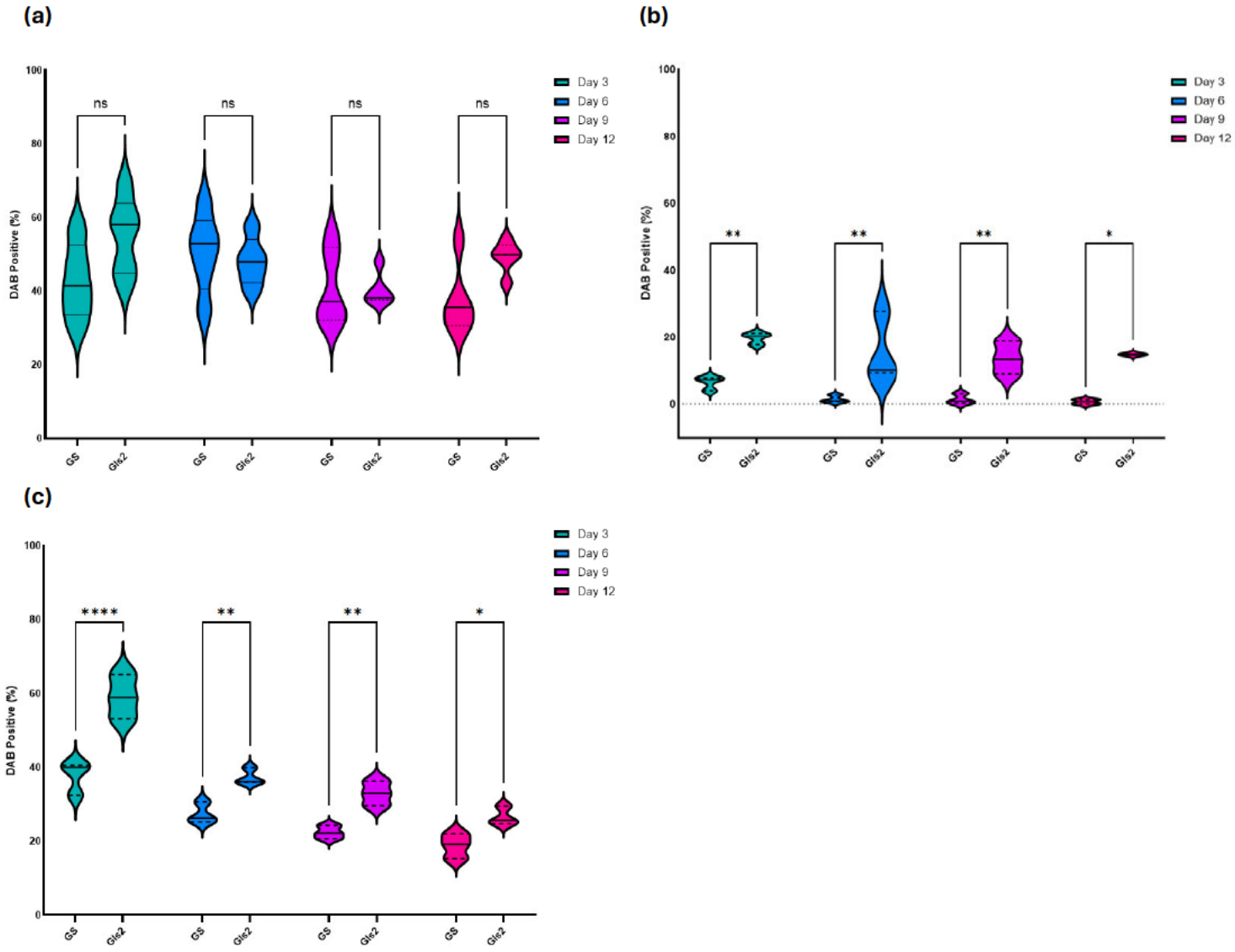

Figure 3.13: Quantification of the Percentage of Gls2 (Zone 1) and GS (Zone 3) Positivity in Primary Murine Hepatocyte Spheroids Cultured in Varying Media Compositions. *PMHS were cultured in (a) Hepatocyte Culture Media, (b) Hepatocyte Culture Media with Dex, and (c) Hepatocyte Culture Media with CHIR99021 for 3-, 6-, 9-, or 12-days prior to being fixed and immunostained. Data were analysed using a repeated-measures two-way ANOVA and a Bonferroni multiple comparisons test. Data shown as mean ± SD from n = 5 biological replicates, each with n=3 technical replicates (*p ≤ 0.05; **p ≤ 0.01; ****p ≤ 0.0001).*

In order to quantify the relative expression of zone 1 (periportal) markers Gls2 and Arginase 1 (Arg1), and zone 3 (pericentral) markers GS and axis inhibition protein 2 (Axin2) in the PMHS cultured in hepatocyte culture medium + 3μM CHIR99021, qPCR was conducted [66,89]. Whilst immunoreactivity of these markers was detectable at day 3 in the PMHS cultures, the expression of the majority of markers decreased over time *in vitro*. The most significant reduction in the expression of Gls2 (0.6252 ± 0.071; p=0.0229), Arg1 (0.2906 ± 0.0193; p=0.008), and GS (0.8234 ± 0.076; p=0.0155) was seen between

culture days 9 and 12. Axin2 was the only marker assessed that was upregulated in the PMHS over time, having increased by a total fold change of 44.83 ± 4.743 (p=0.0200) from days 3 to 12 (Figure 3.14a).

Next, expression of Notch pathway downstream genes, specifically Hes1 and HeyL, was investigated. While these genes are not typically expressed in mature primary hepatocytes, establishing basal expression levels was crucial for evaluating the potential of primary hepatocyte spheroid culture systems as models of Notch induction in later experiments. A gradual increase in the expression of Notch pathway components was observed over time, with Hes1 exhibiting an overall fold change of 15.74 ± 1.086 (p=0.0086), and HeyL an overall fold change of 73.30 ± 4.362 (p=0.0064) between days 3 and 12 (Figure 3.14b).

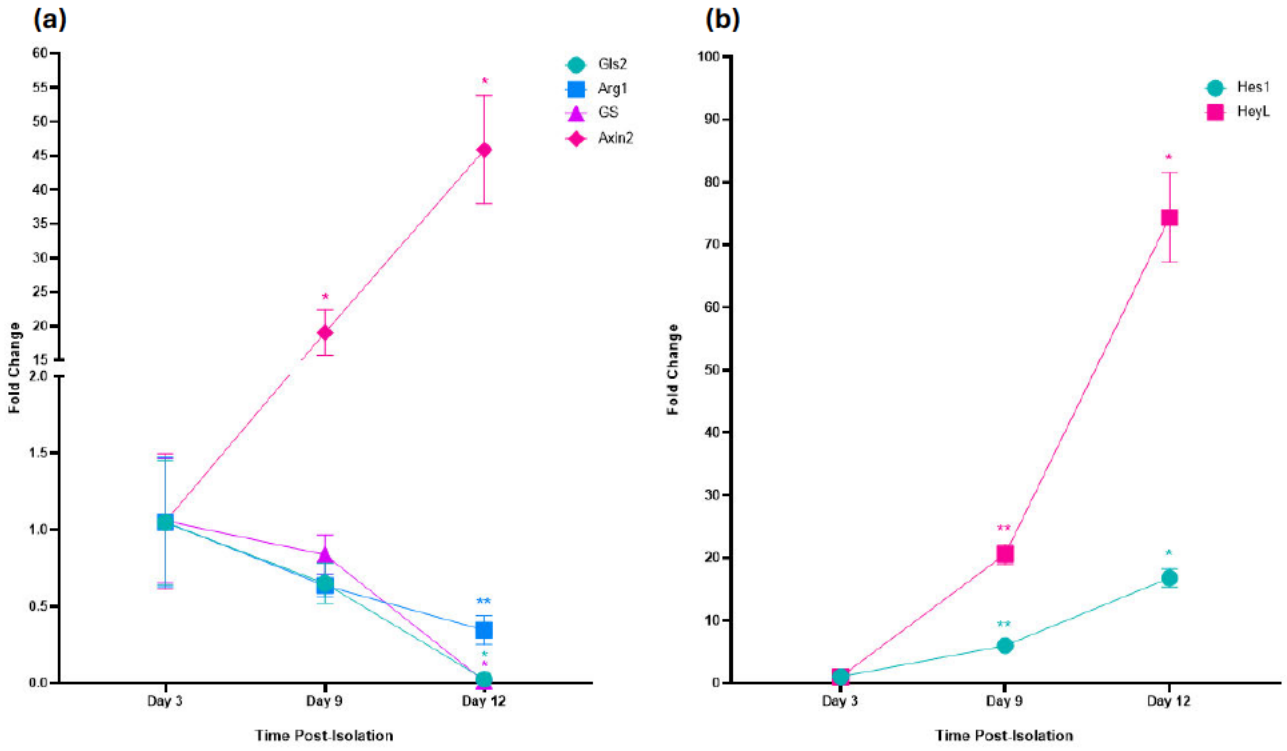

Figure 3.14: Temporal Expression of Zone and Notch Signalling Markers in Primary Murine Hepatocyte Spheroid Cultures Supplemented with CHIR99021. *Relative expression levels of* ***(a)*** *Zone markers Glutaminase 2 (Gls2 & Arg1 – Zone 1) and Glutamine Synthetase (GS & Axin2 – Zone 3), and* ***(b)*** *Notch downstream genes Hes1 and Heyl in murine hepatocytes 3-, 6-, and 9-days post-isolation after being cultured in Hepatocyte Culture Media + CHIR99021. Data analysed using a repeated-measures one-way ANOVA and Tukey HSD multiple comparisons test. Data shown as mean ± SD from n = 3 biological replicates measured in triplicate (*p ≤ 0.05; **p ≤ 0.01; ****p ≤ 0.0001).*

To further investigate the maintenance of liver zonation *in vitro*, PMHS cultured in hepatocyte culture medium supplemented with CHIR99021 for 3 days were stained for E-cadherin and Ornithine Aminotransferase (Oat) (Figure 3.15). E-cadherin, a key cell adhesion protein, exhibits a distinct zonation pattern in the liver, being highly expressed in the periportal hepatocytes [60,228]. In the PMHS system, E-cadherin positivity was noted in the membranes of the majority of the cells. Oat is accepted as a reproducible marker of pericentral hepatocytes, being a zonated transaminase enzyme which catalyses amino acid metabolism and the urea cycle [28,229]. In the PMHS, Oat staining was evident and, upon qualitative assessment, appeared to be less frequent than E-cadherin staining. This observation aligns with the patterns of Gls2 and GS expression shown in Figure 3.13.

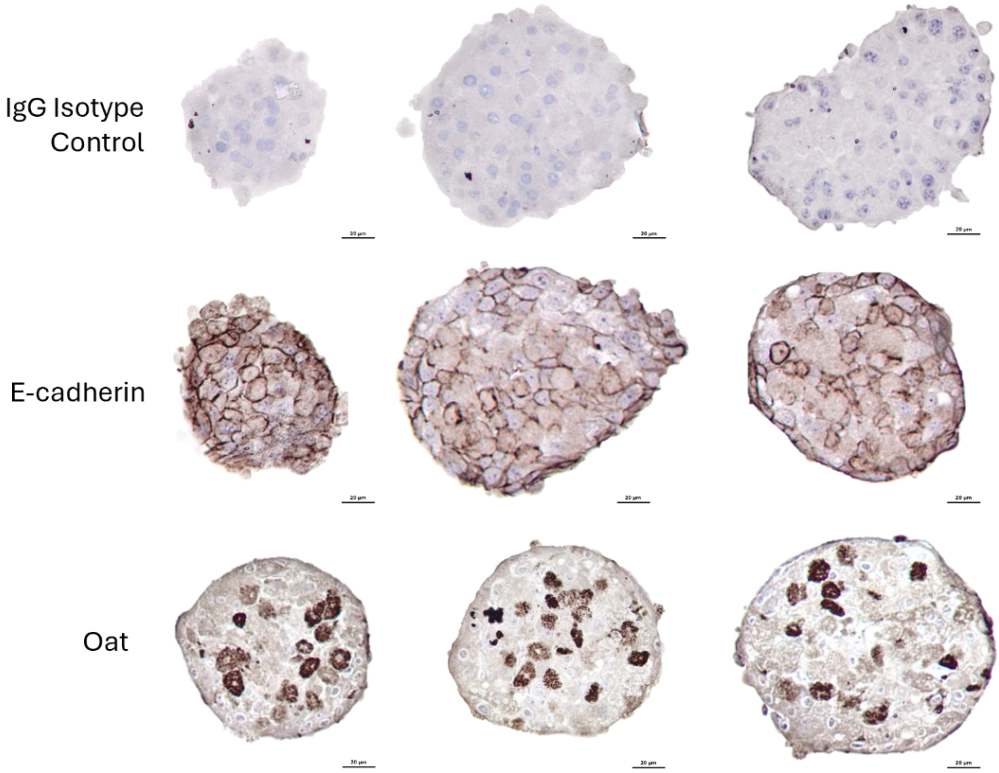

Figure 3.15: Expression of Periportal Marker E-cadherin and Pericentral Marker Ornithine Aminotransferase (Oat) in Primary Murine Hepatocyte Spheroids Cultured in CHIR99021-Supplemented Hepatocyte Culture Media for 3 Days. *Representative micrographs of DAB-stained PMHS cultured for 3 days post-isolation in Hepatocyte Culture Media (n=3, Scale bar = 20μm).*

3.5 Discussion

Primary hepatocyte culture has been a much sought-after goal for preclinical researchers for many years; however, achieving high yields of viable hepatocytes has been a challenge. Early attempts to isolate hepatocytes relied on methods such as shaking the liver with glass beads followed by filtration; however, this led to extensive cell membrane damage, resulting in low yields of viable hepatocytes (5-10%) [136,189,230]. Other techniques were explored, such as collagenase digestion, which did produce viable intact hepatocytes [136,192], but has generally been overshadowed by the two-step perfusion technique pioneered by Seglen *et al.* [193]. This protocol exploits the liver's vasculature to allow the digestive enzymes to interact with a larger quantity of the parenchymal cells, thus significantly improving the hepatocyte yield and integrity of the cells [136,193].

Making use of the well-established two-step *in situ* digestion technique, high yields of viable hepatocytes were successfully isolated from the murine livers. Whilst the isolation of high-quality hepatocytes is an essential step, the next challenge was to maintain these cells *in vitro*. The culture of primary hepatocytes is notoriously challenging due to the cells' propensity to rapidly lose polarity and the hepatocyte phenotype once removed from the liver [134,143,209,231-233]. Following seeding of isolated hepatocytes onto hydrophilic tissue-culture-treated and collagen-1-coated culture dishes, hepatocyte monocultures mimicked the behaviour predicted by the existing literature. The cells rapidly lost polarity and appeared less polygonal as time progressed, deviating from their characteristic hepatocyte morphology.

De-differentiation of hepatocytes was corroborated when expression of lineage marker genes was assessed using qPCR and IF staining. The selection of BEC and mesenchymal gene markers is particularly relevant, as hepatocytes and BECs are known to derive from a common bipotential progenitor cell type [92,100,234-237]. The plasticity demonstrated during development suggests that hepatocytes may revert to a more primitive mesenchymal state or potentially transdifferentiate towards a BEC lineage under specific culture conditions [238]. Notably, when examining the expression patterns of two key hepatocyte markers, Hnf4α and Albumin, an intriguing observation emerged. While Hnf4α expression declined as expected, Albumin expression persisted to some degree throughout the time course. This persistence may suggest that either specific aspects of hepatocyte function are more resistant to de-differentiation or that the Albumin protein has a longer half-life under these culture conditions (known to be approximately 19-21 days in human systems [218,239,240]) and can thus be detected after active expression has ceased. These results were mirrored in the data on cell functionality, with an observed parallel decline in Albumin secretion and Cyp3a11 activity. These

results suggest that there may be differential loss of hepatocyte-specific proteins during the de-differentiation process, highlighting the complexity and challenges of maintaining the hepatic phenotype *in vitro*.

When assessing gene expression of 2D cultured hepatocytes, the most striking observation was the significant upregulation of K19 expression. Results recently published by Miura *et al*. (2024) reported a similar trajectory of K19 expression in primary murine hepatocytes over time in 2D culture [238]. This trend may be attributable to several factors; the first being that K19 is a well-established marker for BECs as well as hepatic progenitor cells (HPCs) [241,242]. Thus, upregulation of K19 in hepatocyte cultures in this study could suggest a shift towards a more primitive or de-differentiated cell state [241,243]. This increase may reflect the potential plasticity of hepatocytes and capacity for transdifferentiation towards a biliary-like phenotype, given specific culture conditions. Additionally, K19 expression has been associated with increased invasiveness and metastatic potential in hepatocellular carcinoma (HCC), indicating that K19 upregulation, combined with the shift to a more fibroblastic phenotype, could reflect changes towards increased motility and proliferation [241,244]. To add further complexity, some studies identify K19 as a potential marker for cell death and apoptosis [245,246]. Therefore, increased expression of K19 in hepatocyte cultures may also indicate elevated levels of cellular stress and apoptosis occurring over time in the 2D culture system, which would seem likely given the apparent reduction in cell density and accumulation of debris observed in the 2D cultures.

This loss of phenotype, coupled with signs of apoptosis and cellular stress in the 2D cultures, highlights the need for alternative approaches, such as 3D spheroid cultures, to better preserve hepatocyte functionality and phenotype over extended periods *in vitro*. Initial efforts in this project aimed to produce primary hepatocyte organoids utilising the technique reported by Peng *et al*. (2018), which involved culturing hepatocytes with the inflammatory cytokine TNFα to replicate an inflammatory *in vitro* environment, thereby promoting the proliferation of primary hepatocytes [169,170]. However, attempts at these cultures were unsuccessful in reproducing the published phenotype, with observation of lipid accumulation, lack of proliferation, and cell death throughout the culture period (from 24 hours post-isolation, data not shown). Consequently, the decision was made to focus on 3D primary murine hepatocyte spheroid (PMHS) cultures, as they are described to consistently preserve hepatocyte-specific characteristics with little required manipulation of culture conditions [134,152,157,247]. PMHS cultures are a tool that has repeatedly demonstrated preservation of hepatocyte-specific gene expression and phenotype *in vitro* [134,149-151,157,219]. This might be attributed to several factors inherent to the 3D spheroid microenvironment, such as enhanced cell-cell interactions and a more physiologically relevant ECM composition, which better mimics the *in vivo* liver architecture [148]. The positive

honeycomb-like phalloidin staining and DPPIV (CD26) staining indicate well-organised cytoskeletal structures and bile canaliculi formation, which are supported by a more physiologically relevant microenvironment compared to 2D cultured cells. Bile canaliculi are microscopic channels, approximately 0.5-2 μm in diameter, which develop between adjacent hepatocytes and function as conduits for bile secretion [144,248,249]. *In vitro* these structures can only form in the presence of tight cell-cell contacts and correct cellular polarity, as they emanate from the cells' apical surfaces [196,250,251]. Therefore, the apparent formation in the PMHS, coupled with expression of E-cadherin, a transmembrane protein crucial for cell-cell adhesion, suggests this model is a significant improvement over 2-dimensional cultures at recapitulating the *in vivo* environment of the hepatocytes [147]. The development of tight cell-cell adhesions, as evidenced by E-cadherin expression, is likely also associated with the observed compaction of PMHS over time.

Having established that PMHS exhibit evidence of cell polarity and organised cellular structures such as bile canaliculi formation, it was crucial to assess whether these structural advantages translated into improved longevity and functionality compared to 2D hepatocytes. Transcriptionally, whilst there was still a progressive loss of hepatocyte gene expression and concurrent upregulation in expression of BEC and mesenchymal marker genes, changes occurred significantly slower than in the 2D cultures. All significant changes in the 2D cultures occurred within 4 days (96 hours) of *ex vivo* isolation from the livers; however, the spheroids maintained some degree of hepatocyte gene expression throughout the time course. The differences in the expression patterns of the BEC markers Sox9, Hnf1β, EpCAM, and K19 highlight the varied responses of hepatocytes to different culture environments. In spheroids, upregulation of these markers suggests a partial shift towards a progenitor-like state, whereas in 2D cultures, a more rapid phenotypic change occurs, including increased expression of mature BEC markers like K19. In PMHS cultures, the significant upregulation of Sox9, Hnf1β, and EpCAM over the time course not only suggests a shift towards a progenitor-like state but is widely used in studies as an early marker of a BEC lineage [108,133,235,252]. However, the lack of K19 upregulation in spheroids indicates that either the cells are not fully transitioning to a biliary phenotype (K19 being a mature BEC marker) or are not undergoing as much programmed cell death as seen in 2D cultures [246]. While apoptosis markers (such as Caspase-3) were not successfully stained for in this study due to technical challenges with staining the 2D cultures, the observed gene expression changes suggest potential differences in levels of cell death between the two models. Future studies could focus on optimising staining techniques to verify apoptosis levels more effectively.

Despite a progressive decrease in Albumin expression over time, consistent levels of Albumin secretion were maintained by the PMHS model over 12 days, reflecting functional stability. Caution

must be exercised in interpreting these results, however, since Albumin can persist in the media long after its production [218,239,240]. To account for this, conditioned media were collected sequentially from the same cultures at regular intervals from day 3 to day 12. By employing continuous sequential sampling, any Albumin detected in each sample was ensured to have been produced within the three-day interval between collections. Consequently, although the exact amount of Albumin produced on day 12 cannot be definitively stated, it can be inferred that spheroids were actively secreting Albumin between days 10 and 12.

Cyp3A11 activity (murine homologue of human CYP3A4) is a widely used marker of hepatocyte functionality *in vitro* [253,254]. Despite a marked decrease in Cyp3A11 activity observed over time, there was still detectable activity by day 12. Importantly for my study, Cyp3A11 expression is zonated in the liver, with higher levels typically observed in zone 3 hepatocytes [255,256], inferring some degree of functionality of zone 3 hepatocytes *in vitro*. A decrease in activity might not only reflect overall hepatocyte health but could also suggest a selective loss or dedifferentiation of zone 3 hepatocytes in the culture system. This zonation aspect adds another layer of complexity to interpreting the Cyp3A11 activity data and highlights the importance of taking hepatic zonation into consideration when using *in vitro* hepatocyte models in drug metabolism and disease studies.

Glycogen is a polysaccharide that plays a crucial role in maintaining glucose homeostasis and provides a readily available energy source when needed [257]. Thus, the levels of glycogen present in hepatocytes reflect both the metabolic status of the cells and their response to various stimuli, such as hormones, nutrients, or drugs [258]. PMHS cultures were observed to synthesise and store glycogen throughout the 12-day time course, indicating that the culture conditions maintain this function.

Overall, these experiments suggest that whilst PMHS may be progressively undergoing dedifferentiation as observed in 2D culture hepatocytes, the process is significantly slowed by a 3-dimensional microenvironment. Collectively, these observations underscore the superiority of spheroid cultures in recapitulating the intricate cellular arrangements and functions of the liver, offering a valuable platform to study the complex processes involved in liver cell differentiation and function.

Given the importance of maintaining hepatocyte function, it was crucial to determine if metabolic zonation, indicated by markers Gls2 and GS, was preserved in PMHS. These markers have been used in several studies to identify hepatocyte zones 1 and 3; thus, by staining for these genes, insights can be gained into whether zonation patterns are maintained to some degree in spheroids. [55,71,259,260]. Initially, 4000-cell PMHS were cultured in the standard hepatocyte culture media (formulated on media

published in prior studies [134,147,151]) and were formalin-fixed and stained for Gls2 and GS every 3 days over the 12-day time course. The results indicate that not only do the PMHS express both markers Gls2 and GS, but unexpectedly, they appeared to be expressed at similar levels. This observation was interesting, as fewer GS+ cells would be expected to be present in the spheroids due to the significantly smaller proportion that GS+ hepatocytes represent in the liver (~7-10%), whereas Gls2+ hepatocytes typically make up approximately 40-50% of the liver lobule [260,261].

Recognising that standard media will not fully recapitulate the complex signalling environment of the liver, and to see whether the proportion of GS and Gls2 positive cells could be manipulated, the effects of media supplementation were then explored. Some studies use Dexamethasone, a synthetic glucocorticoid, as a standard supplement in hepatocyte spheroid culture media due to its support of liver-specific genes such as Albumin and various CYP enzymes, while also preventing dedifferentiation. [262,263]. The addition of Dexamethasone differentially modulates zonal marker expression; specifically, it suppresses GS expression whilst maintaining expression of Gls2. This selective regulation by Dexamethasone aligns the proportions of GS- and Gls2-positive cells more closely with physiological *in vivo* patterns. A study conducted by Wallace *et al*. (2010) demonstrated that Dexamethasone induces hepatocyte-like transdifferentiation in pancreatic progenitor cells by transiently suppressing constitutively active Wnt signalling, evidenced by decreases in Wnt3a expression, β-catenin phosphorylation, and nuclear localisation, and a concurrent fall in Tcf/Lef transcriptional activity [42]. Given that canonical Wnt/β-catenin signalling preferentially supports pericentral hepatocyte identity and GS expression, the glucocorticoid-mediated suppression of this pathway likely underlies the reduction of GS in culture [29,30,35,53,60,63,64,264]. Thus, it appears that Dexamethasone is able to fine-tune the hepatocyte zonal marker distribution *in vitro* by modulating Wnt signalling activity, offering a more physiologically relevant model of hepatic zonation.

It was hypothesised that supplementing the media with CHIR99021, a potent GSK3β inhibitor which modulates Wnt signalling by stabilising β-catenin activity, would amplify GS expression (GS is a well-described Wnt/β-catenin target), potentially shifting the balance toward increased pericentral marker representation [265]. The expression of GS did not increase significantly in the presence of the Wnt agonist as compared to the standard hepatocyte media without supplementation. The consistently elevated expression of Gls2 observed across all timepoints and media compositions suggests that the PMHS, under the culture conditions employed in this study, demonstrate a tendency to adopt a periportal hepatocyte phenotype. Supplementation with CHIR99021, however, appeared to more effectively balance the proportions of Gls2 to GS, resulting in a distribution that more closely resembled the expected *in vivo* ratios. Evidence for the maintenance of zonation *in vitro* is supported by the presence

of E-cadherin (a zone 1 marker) and ornithine aminotransferase (a zone 3 marker) positivity in the respective PMHS derived from Gls2CreER-mT/mG and GSCreER-mT/mG mouse models. It is possible that the lack of a significant increase in the expression of GS in response to CHIR99021 could be due to the PMHS already exhibiting characteristics of a zone 3 phenotype before supplementation. This could result from the inherent tendencies of the culture conditions favouring a periportal phenotype, potentially affecting the responsiveness to further zone 3-inducing signals. These results highlight the complexity of recreating liver zonation *in vitro* and underscore the importance of carefully considering media composition when developing hepatocyte models for research and drug testing purposes.

While the expression patterns of Gls2 and GS provide insights into the potential for PMHS to model liver zonation, further markers must, of course, be considered. Arginase 1 (Arg1), a key enzyme catalysing the final step of the urea cycle, is often used as a marker for zone 1, whilst Axin2, a direct target and negative regulator of the Wnt signalling pathway, is often used as a marker for zone 3 hepatocytes, as its expression marks cells actively responding to Wnt signals [88,89]. When quantifying the expression of these markers together with Gls2 and GS in the CHIR99021-supplemented PMHS cultures, a divergent trend in gene expression over time was observed, with the expression of GS, Gls2, and Arg1 decreasing and Axin2 expression significantly increasing over time. While this could potentially demonstrate that some zone 3 phenotype is maintained in the PMHS, in adult mouse liver, pericentral Axin2+ hepatocytes have been observed to exhibit a higher proliferative capacity than their Axin2- counterparts [89]. Long-term lineage tracing studies have also shown that Axin2+ hepatocytes can self-renew and repopulate the entire liver lobule over time, suggesting stem cell-like properties [88]. Interestingly, while most mature hepatocytes in the adult liver are polyploid, the majority of pericentral Axin2+ hepatocytes are diploid, though they can differentiate into mature polyploid hepatocytes [90]. The expression of Axin2 is not limited to mouse models; in human hepatocellular carcinoma (HCC) cell lines, AXIN2 is expressed at higher levels than AXIN1, particularly in β-catenin mutant lines [266]. These findings collectively indicate that the significant upregulation of Axin2 in the PMHS over the time course could suggest that the hepatocytes are transdifferentiating into a hepatic progenitor cell type. These results, coupled with the upregulation of Hes1 and HeyL, genes not typically expressed in hepatocytes, provide evidence for cellular plasticity in the PMHS.

In conclusion, this study provided valuable insights into the behaviour of primary murine hepatocytes *ex vivo*, addressing essential questions about their phenotypic stability and zonation characteristics. The results largely confirmed the initial hypotheses, demonstrating the rapid dedifferentiation of hepatocytes in 2D culture within 96 hours, whilst the 3D spheroid cultures maintained their hepatocyte functionality for at least 12 days. This finding underscores the superiority of spheroids in preserving

hepatocyte phenotype and function, albeit with some evidence of cellular plasticity in these cultures over time.

The investigation into the maintenance of zonation yielded contrasting results that have partially supported the hypothesis. Contrary to the initial hypothesis that zonal characteristics would be lost, the assays conducted suggest that some aspects of zonation can be maintained *in vitro* in 3-dimensional spheroid cultures. Furthermore, it was demonstrated that the zonation patterns can be influenced using media supplementation, highlighting the plasticity of these cells and the importance of the culture microenvironment. The ability to maintain functional hepatocytes in medium-term cultures, coupled with the potential to modulate zonation patterns, opens new avenues for studying liver physiology, disease mechanisms, and drug metabolism in more physiologically relevant models.

Defining Periportal and Pericentral Hepatocytes

4.1 Introduction

Hepatocytes are separated into distinct metabolic compartments along the portal-central axis of the lobule, with the functional separation of cells being critical to the maintenance of metabolic homeostasis and detoxification [54,60,225,255,260]. This metabolic zonation is maintained by an oxygen and nutrient gradient as well as molecular signals that spatially segregate hepatocytes in the oxygen-rich periportal zones (zone 1/2), marked by Gls2 expression in the present study, from those in the relatively hypoxic pericentral (zone 3) regions, marked by the expression of GS.

Gls2-expressing hepatocytes play a pivotal role in gluconeogenesis, β-oxidation, and ammonia detoxification [225,227,237,267]. Gls2 catalyses the hydrolysis of glutamine into glutamate and ammonia, enabling the carbon skeleton of glutamine to fuel the tricarboxylic acid (TCA) cycle for energy production and gluconeogenic pathways, particularly under glucagon stimulation [267,268]. This activity is influenced by pathways that are known to integrate cellular energy demands with metabolic fluxes, such as AMPK (AMP-activated protein kinase) and mTOR (mechanistic target of rapamycin) [269-272]. Beyond its metabolic role, Gls2 has been implicated in antioxidant defence and energy metabolism, with emerging evidence suggesting its regulation by p53 and involvement in tumour suppression [267].

In contrast, GS-expressing hepatocytes drive glycolysis, lipogenesis, and xenobiotic metabolism while maintaining ammonia clearance through the urea cycle, catalysing ATP-dependent synthesis of glutamine from ammonia and glutamate [225,273-276]. This activity effectively detoxifies residual ammonia that escapes processing by the urea cycle in periportal hepatocytes, preventing toxic accumulation and maintaining nitrogen homeostasis [277-279]. GS expression and its zonal restriction are tightly regulated by Wnt/β-catenin signalling [29,61,63]. Transgenic models demonstrate this mechanistically: hepatocyte-specific β-catenin knockout mice exhibit loss of perivenous markers like GS and Cyp1a2, while ectopic β-catenin activation expands GS+ hepatocytes into periportal regions, disrupting metabolic zonation [34,280]. Lineage-tracing studies using Axin2-LacZ mice further confirm that Wnt-responsive hepatocytes are confined to the perivenous zone, where they sustain GS activity and glutamine synthesis [88,100]. Dysregulation of GS expression has been observed in liver pathologies such as cirrhosis, chronic hepatitis, and hepatocellular neoplasms, highlighting its importance in hepatic regeneration and disease states.

To investigate potential differences in cellular plasticity across the lobule, two lineage-tracing systems were developed through cross-breeding previously published Gls2CreER and GSCreER lines with a

mouse model of the mT/mG dual-fluorescent reporter system (Section 2.1). These models enable tamoxifen-inducible, zone-specific labelling of hepatocytes, converting membrane-targeted tdTomato (mTom) to membrane-targeted Green Fluorescent Protein (mGFP) in either Gls2+ or GS+ populations. Fluorescence-activated cell sorting (FACS) of mGFP+ cells from these models permits isolation of zonally restricted hepatocytes for bulk RNA sequencing, offering a platform to systematically compare their basal transcriptomes and uncover molecular drivers of metabolic specialisation. It was hypothesised that this approach might elucidate how spatially encoded gene expression programmes coordinate the liver's functional compartmentalisation and adaptive responses.

4.1.1 Aims and Hypothesis

The experiments described in this chapter are designed to characterise the Gls2CreER-mT/mG and GSCreER-mT/mG mouse models, with a particular focus on comparing the transcriptional differences between Gls2+ (zone 1 and 2) and GS+ (zone 3) hepatocytes. By utilising these models, it is possible to selectively target and analyse hepatocytes from opposite poles of the liver lobule, to investigate their distinct molecular profiles and establish a platform to investigate cellular plasticity of liver cell populations. It is hypothesised that, in addition to the well-established differences in gene expression and function, hepatocytes across the liver lobule will exhibit variable responses to defined stimuli known to specify liver cell identity, such as Notch signalling. This variability may reflect the liver's need to mobilise different cell populations in response to specific types of injury, for example, the activation of hepatic progenitor or biliary cells in the periportal regions following biliary damage, or the recruitment of hepatocytes in zone 3 in response to pericentral injury.

4.2 Glutaminase 2- and Glutamine Synthetase-Expressing Hepatocytes

4.2.1 Zonation of Gls2- and GS-Expressing Hepatocytes

As expected, liver tissues of wild-type C57Bl6/J mice exhibit restricted expression of Gls2 and GS in hepatocytes (Figure 4.1). Gls2-expressing hepatocytes were seen to be predominantly localised in the periportal region (zone 1) surrounding the portal vein and extending outward into zone 2. This zonation pattern supports its role in glutamine hydrolysis, contributing to amino acid and nitrogen metabolism in the periportal area [53,55,71,225,260]. In contrast, GS expression is highly restricted to one to three cell layers of hepatocytes immediately adjacent to the central vein, reflecting their role in ammonia detoxification and glutamine synthesis [53,55,71,225,260].

(a)

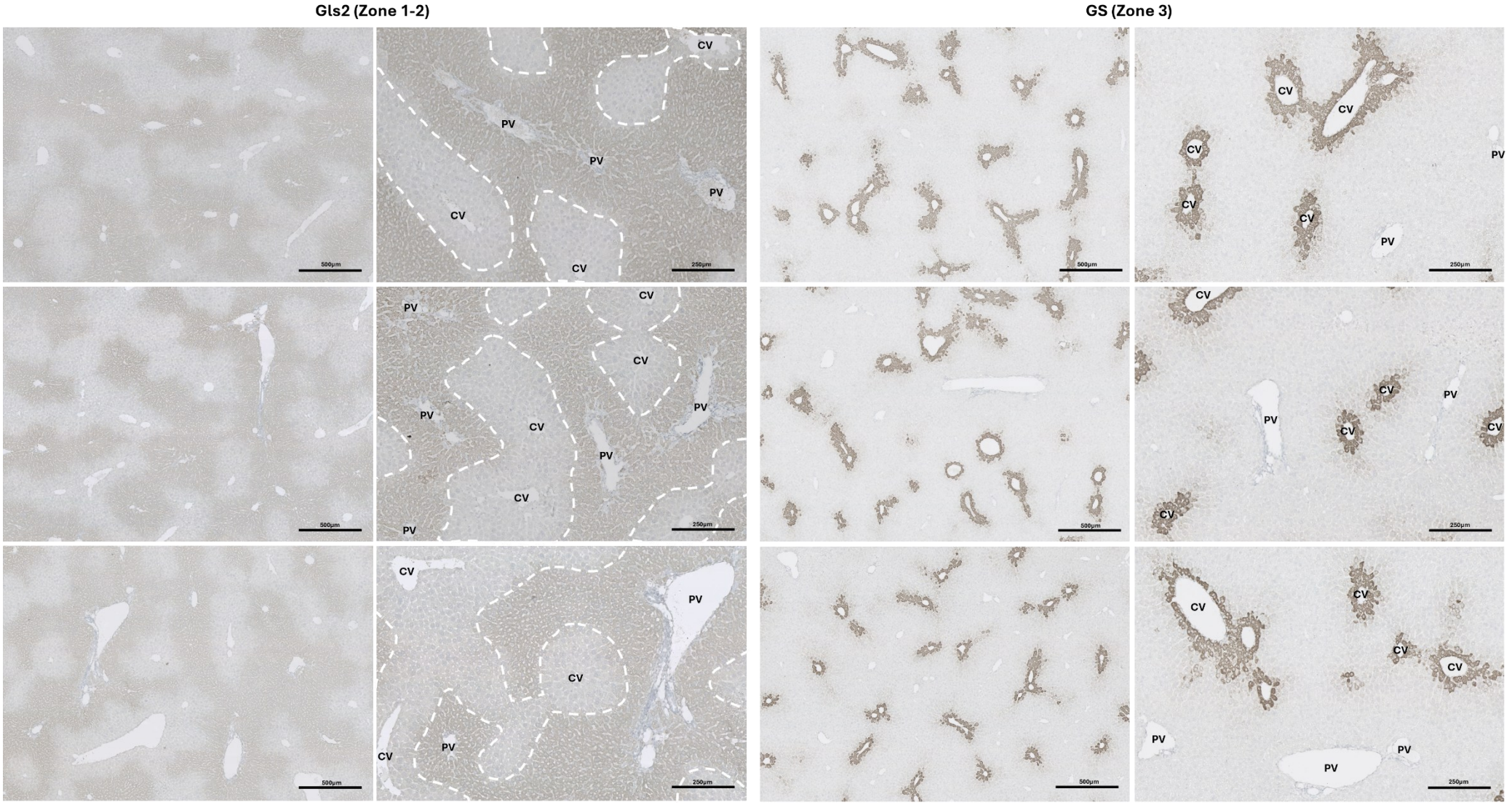

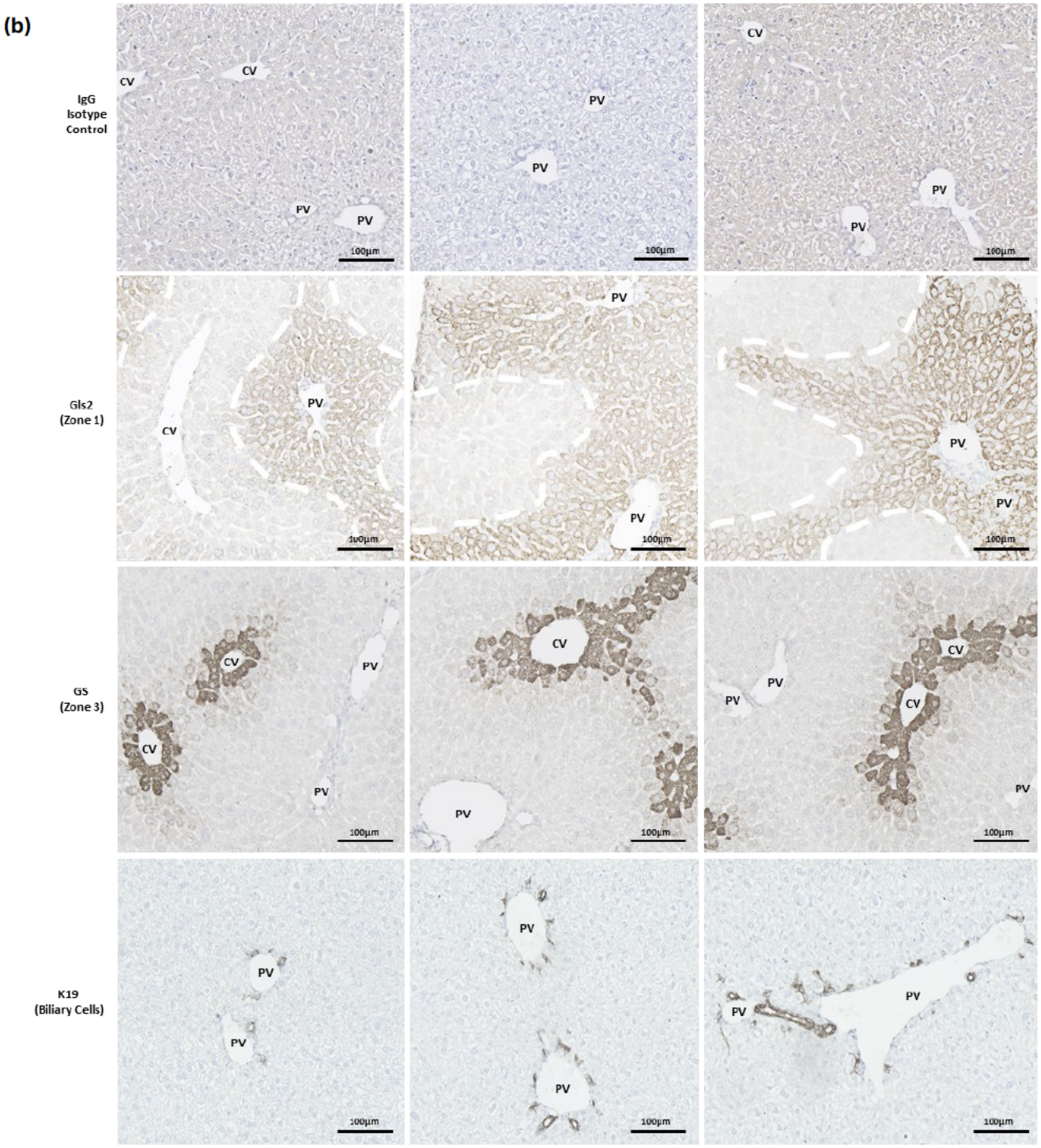

Figure 4.1: Immunohistochemical Staining of Glutaminase 2, Glutamine Synthetase, and Cytokeratin 19 in C57Bl6/J Liver Tissue. (a) *Representative DAB (3,3'-diaminobenzidine) staining of Gls2 and GS in C57Bl6/J livers demonstrates the higher expression of Gls2 in hepatocytes closer to the portal vein (PV), with diminishing levels towards the central vein (CV), and the highly restricted expression of GS within one to two cell layers around the central vein (Scale bars = 250µm / 500µm)* ***(b)*** *Representative higher magnification images of DAB-stained C57Bl6/J livers showing hepatocyte-specific staining of Gls2 and GS and biliary epithelial cell-specific staining of cytokeratin 19 (K19) (Scale bars = 100µm).*

4.3 Characterisation of Gls2CreER-mT/mG and GSCreER-mT/mG Mouse Models

To assess Cre recombinase efficiency in Gls2CreER-mT/mG and GSCreER-mT/mG mouse models, mice received a single dose of tamoxifen (100mg/kg tamoxifen solubilised in corn oil + 10% ethanol) or vehicle control (corn oil + 10% ethanol) (Figure 4.2a). This tamoxifen dose was selected based on Wei *et al*. (2021), who demonstrated optimal recombination efficiency in these CreER mouse models with minimal hepatotoxicity. Seven days post-administration, tamoxifen-treated mice exhibited cre-recombination-induced mGFP expression in the liver (Figure 4.2b). No mGFP was observed in vehicle-treated Gls2CreER-mT/mG mice. In contrast, vehicle-treated GSCreER-mT/mG mice showed mGFP staining restricted to a 2- to 3-cell-wide pericentral band (zone 3), aligning with endogenous GS zonation (Figure 4.2b). In tamoxifen-induced Gls2CreER-mT/mG mice, mGFP expression coincided with the reported zonation pattern of Gls2 (zones 1–2), whereas GSCreER-mT/mG mice displayed diffuse mGFP across all three zones, diverging from wild-type GS's pericentral restriction.

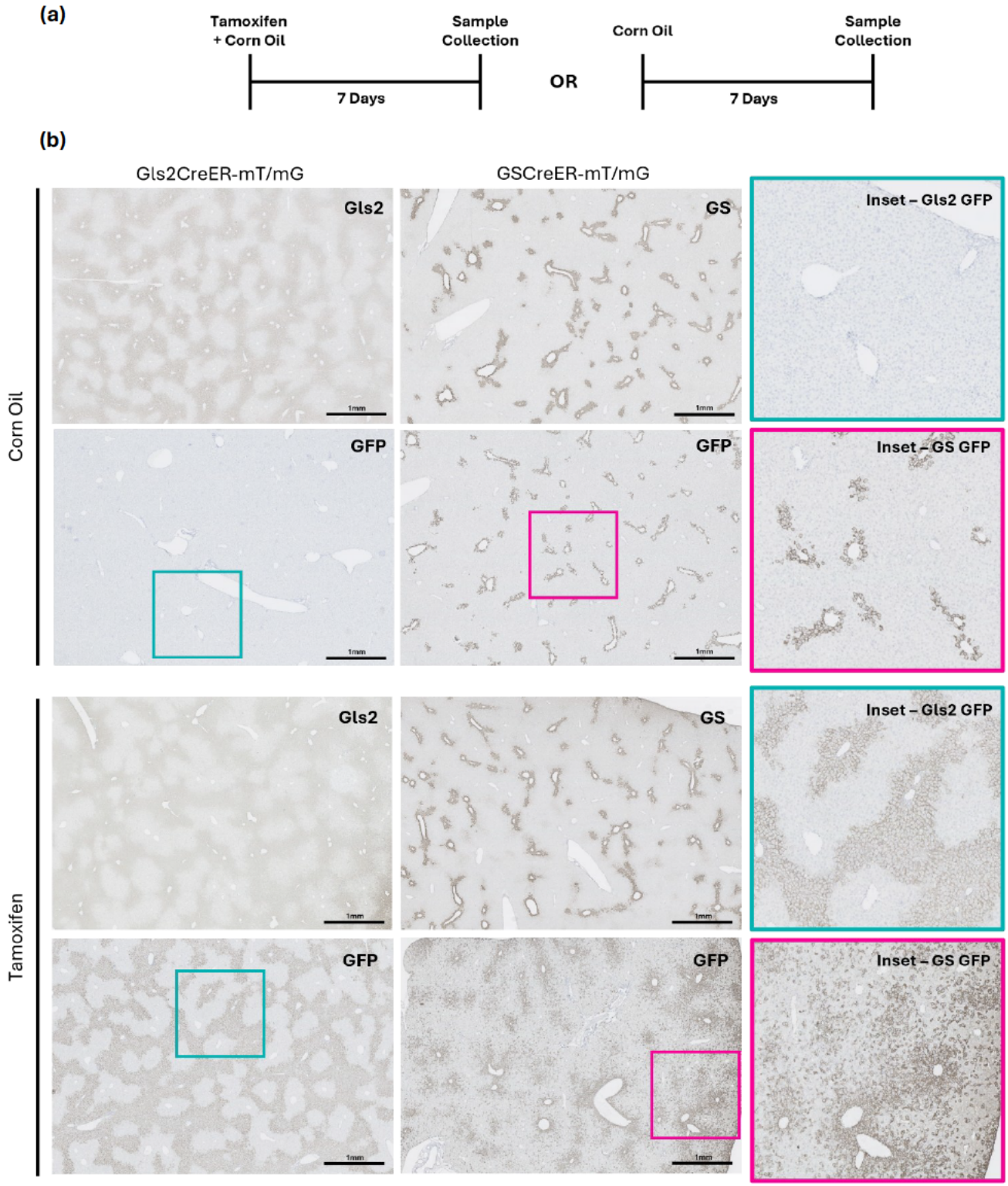

Figure 4.2: Immunostaining of Glutaminase 2, Glutamine Synthetase, and Cre-Recombination-Induced Expression of Membranous Green Fluorescent Protein in the Gls2CreER-mT/mG and GSCreER-mT/mG Mouse Models. ***(a)*** *Schematic demonstrating the tamoxifen and/or corn oil dosing 7 days before tissue collection for each mouse model* ***(b)*** *Representative DAB-stained livers demonstrating the pattern of Cre-recombination in the Gls2CreER-mT/mG and GSCreER-mT/mG models 7 days after gavage with a single dose of either 4mg Tamoxifen + Corn Oil or a Corn Oil vehicle control (Scale bars = 1mm).*

In liver tissues from Gls2CreER-mT/mG and GSCreER-mT/mG mice, co-staining for mGFP and the corresponding zonal markers (Gls2 or GS) demonstrated dual expression of the Cre reporter and the zone-specific proteins. The distribution of mGFP expression appeared to overlap with the zonated expression of Gls2 (mean Gls2+ staining = 32.31% of total liver cells) and GS (mean GS+ staining = 17.02%) in both mouse models (Figure 4.3b). Quantification showed that 96.38% of Gls2+ cells were mGFP+ in the Gls2Cre-mTmG model, while 86.37% of GS+ cells in the GSCre-mTmG model were mGFP+. Thus, the percentages reported in Figure 4.3b refer to the proportion of marker-positive cells that were also mGFP+. No significant differences were observed in the number of mGFP+ cells co-localising with Gls2 or GS between animals of the same genotype, suggesting little variability in tamoxifen dosing in the models.

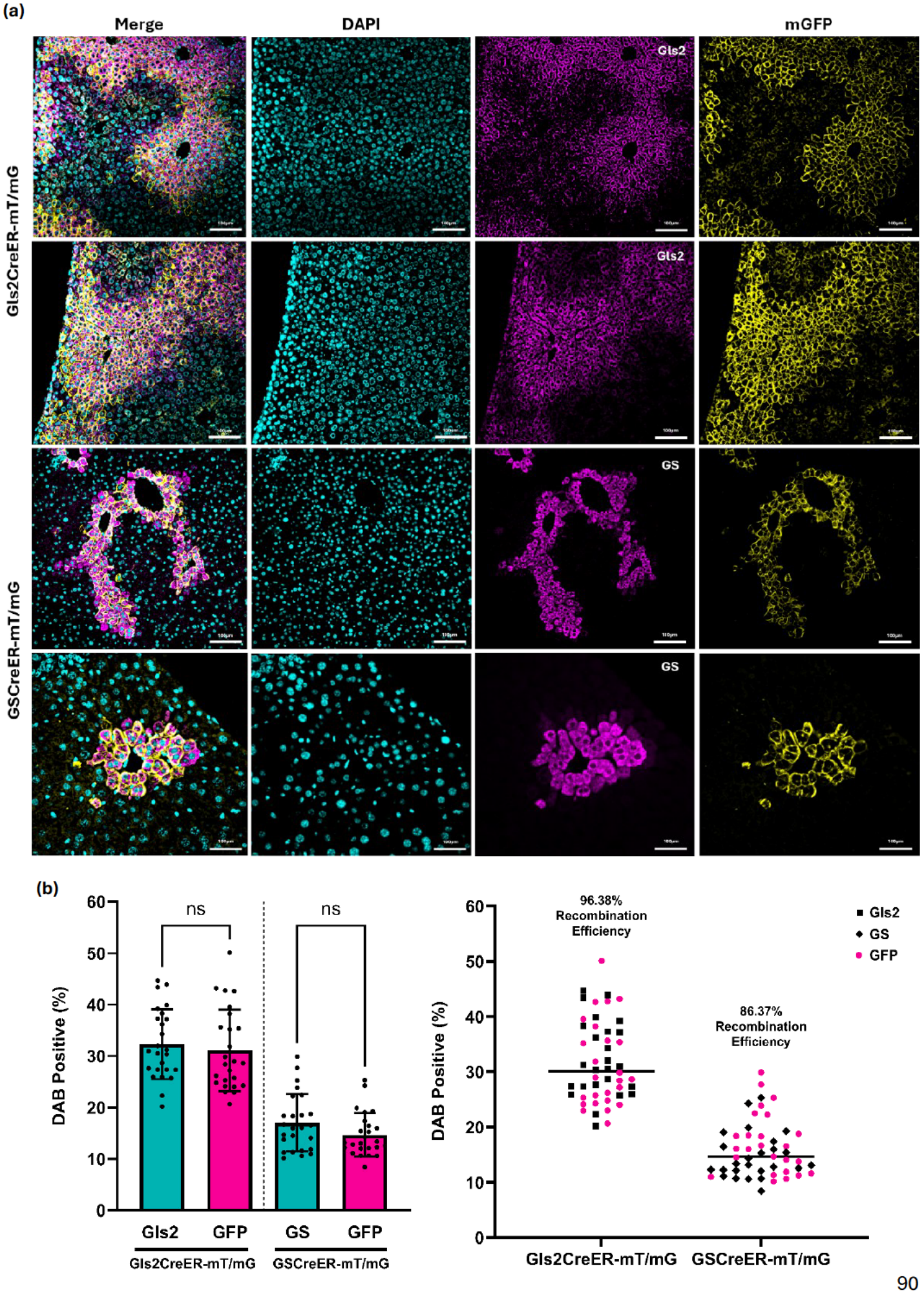
(a)
Merge
DAPI
mGFP
Gls2
GS
Gls2CreER-mT/mG
GSCreER-mT/mG
(b)
DAB Positive (%)
ns
ns
Gls2
GFP
GS
GFP
Gls2CreER-mT/mG
GSCreER-mT/mG
96.38%
Recombination
Efficiency
86.37%
Recombination
Efficiency
Gls2
GS
GFP

Figure 4.3: Cre-recombination Efficiency of Membranous Green Fluorescent Protein in Gls2CreER-mT/mG and GSCreER-mT/mG Mouse Models 7 Days Post-Tamoxifen or Corn Oil Gavage. ***(a)*** *Representative immunofluorescent staining demonstrating the co-expression of Gls2 + mGFP in the Gls2CreER-mT/mG and GS + mGFP in the GSCreER-mT/mG mouse models after 7 days following treatment with tamoxifen or corn oil (Scale bars = 100μm)* ***(b)*** *Quantification of DAB positive area per measured sample (n=5 per strain with 25 technical repeats) in livers 7 days post-tamoxifen or corn oil gavage, respectively. Recombination efficiency calculated as mean mGFP+ area ÷ mean Gls2+/GS+ area × 100. Data were analysed using one-way ANOVA with Bonferroni multiple comparisons test. Results are presented as mean ± SD (ns = not significant).*

Staining with E-cadherin, an accepted zone 1 and 2 marker, demonstrated significant overlap with mGFP expression in the Gls2CreER-mT/mG mouse strain, which supports the use of this model as a tool for lineage tracing hepatocytes originating from these zones (Figure 4.4) [228]. In the GSCreER-mT/mG model, mGFP expression is restricted to a narrow band of hepatocytes surrounding the central vein (zone 3), aligning with the expression pattern of Ornithine Aminotransferase (Oat), a pericentral hepatocyte marker [229,281]. These findings confirm that cre-recombination-induced mGFP expression identifies the functional zones of interest, further supporting the utility of these mouse models for studying liver metabolic zonation.

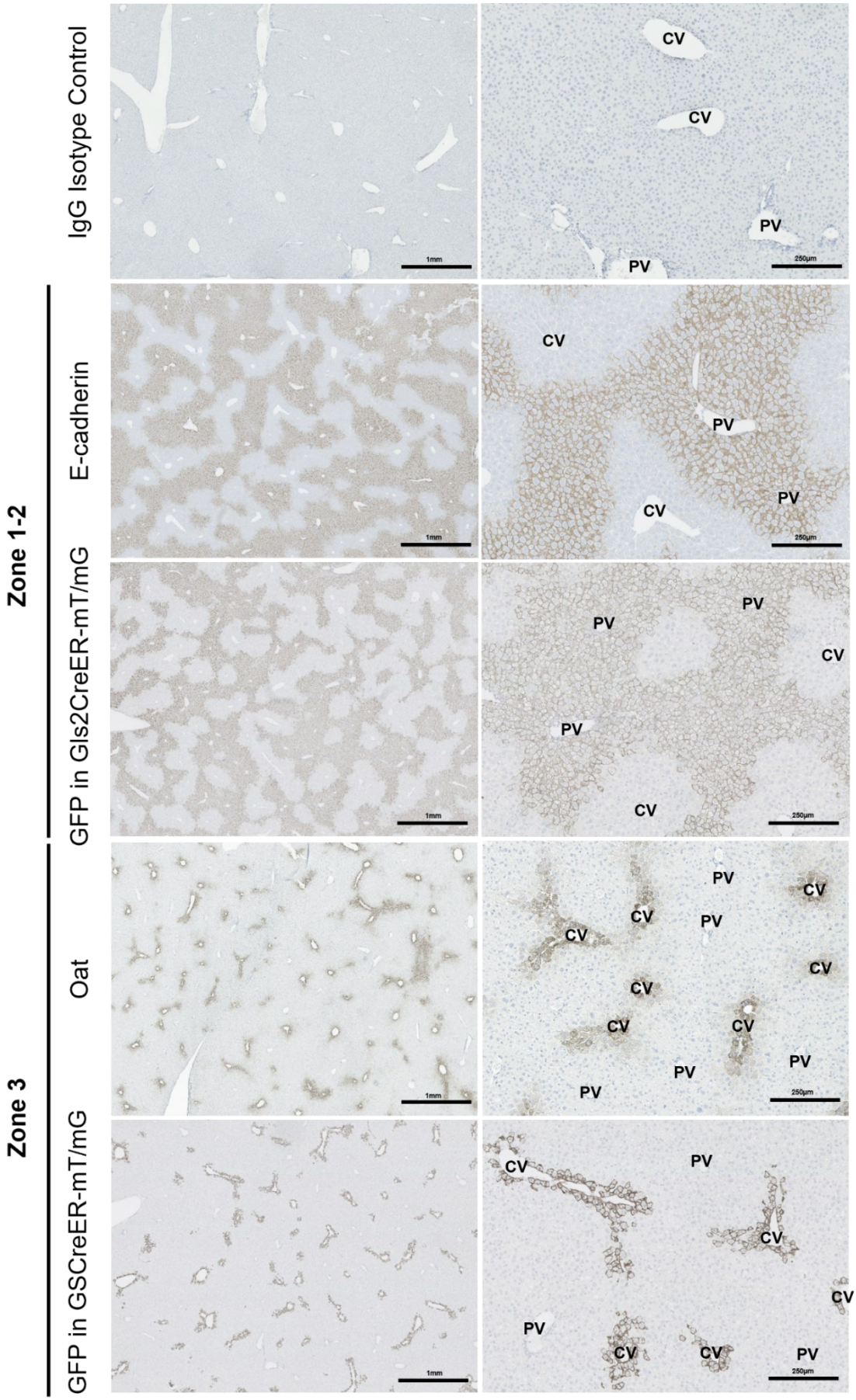

Figure 4.4: Immunohistochemical Staining of Glutaminase 2, Glutamine Synthetase, E-cadherin, and Ornithine Aminotransferase (Oat) in the Gls2CreER-mT/mG and GSCreER-mT/mG Mouse Models. *(Scale bars = 1mm / 250µm).*

4.4 Comparative Gene Expression Analysis of Gls2- and GS-Expressing Pericentral Hepatocytes

4.4.1 Isolation, FACS, and Bulk RNA-Sequencing of Primary Murine Hepatocytes Reveals Differences Between Gls2+ and GS+ Populations

To establish the differences in the gene expression profiles of Gls2+ and GS+ hepatocytes, Gls2CreER-mT/mG and GSCreER-mT/mG mice were dosed with tamoxifen or corn oil, respectively (Figure 4.5a). Seven days later, the livers were subject to perfusion, enzymatic digestion, and hepatocyte isolation (Section 2.2) to separate hepatocytes from other hepatic cell types. Cell isolations were then sorted via fluorescent-activated cell sorting (FACS). The perfusions yielded an average of 1.09×10^8 cells per liver, with 99.56% live, single, unstained hepatocytes remaining before FACS analysis on average. Both models were gated to define the single, live cells that were expressing mTom (non-cre-recombined cells) and mGFP (cre-recombined cells) (Figure 4.5b). The live/dead gate was not drawn in an ultra-stringent manner (i.e. a small proportion of low-Draq intermediate events may have been retained), but the majority of sorted cells (>80-90% of singlet events in most sorts) fell well within the Draq7-negative peak, and any residual inclusion of Draq7-low or borderline events would be expected to dilute, rather than artificially enrich, reporter-positive populations, thereby making the observations conservative.

To validate gating and fluorophore detection, the following controls were included:

Negative controls:

1) Wild-type (mT/mG-negative) mice treated with tamoxifen.
2) Gls2CreER- and GSCreER-negative littermates carrying the mT/mG allele treated with tamoxifen.

Positive controls:

1) Gls2CreER-mT/mG and GSCreER-mT/mG mice treated with tamoxifen and corn oil, respectively.
2) Gls2CreER-mT/mG mice treated with corn oil instead of tamoxifen.

Thus, due to the mGFP+ and mTomato+ fractions being defined relative to appropriate negative controls (Appendix Figure 1), they represent clearly separated positive populations, which supports the validity of the lineage-tracing conclusions despite this conservative gating.

Once defined and sorted (100,000 mGFP+ and 100,000 mTom+ cells per mouse), hepatocytes were prepared for bulk RNA sequencing. Across n=3 independent liver samples per strain, 28.50% of hepatocytes isolated from Gls2CreER-mT/mG mice were mGFP+, whereas 2.43% of hepatocytes isolated from GSCreER-mT/mG mice were mGFP+ (Figure 4.5c). The corresponding proportions of mTom+ hepatocytes were 28.77% in Gls2CreER-mT/mG mice and 43.83% in GSCreER-mT/mG mice (Figure 4.6c).

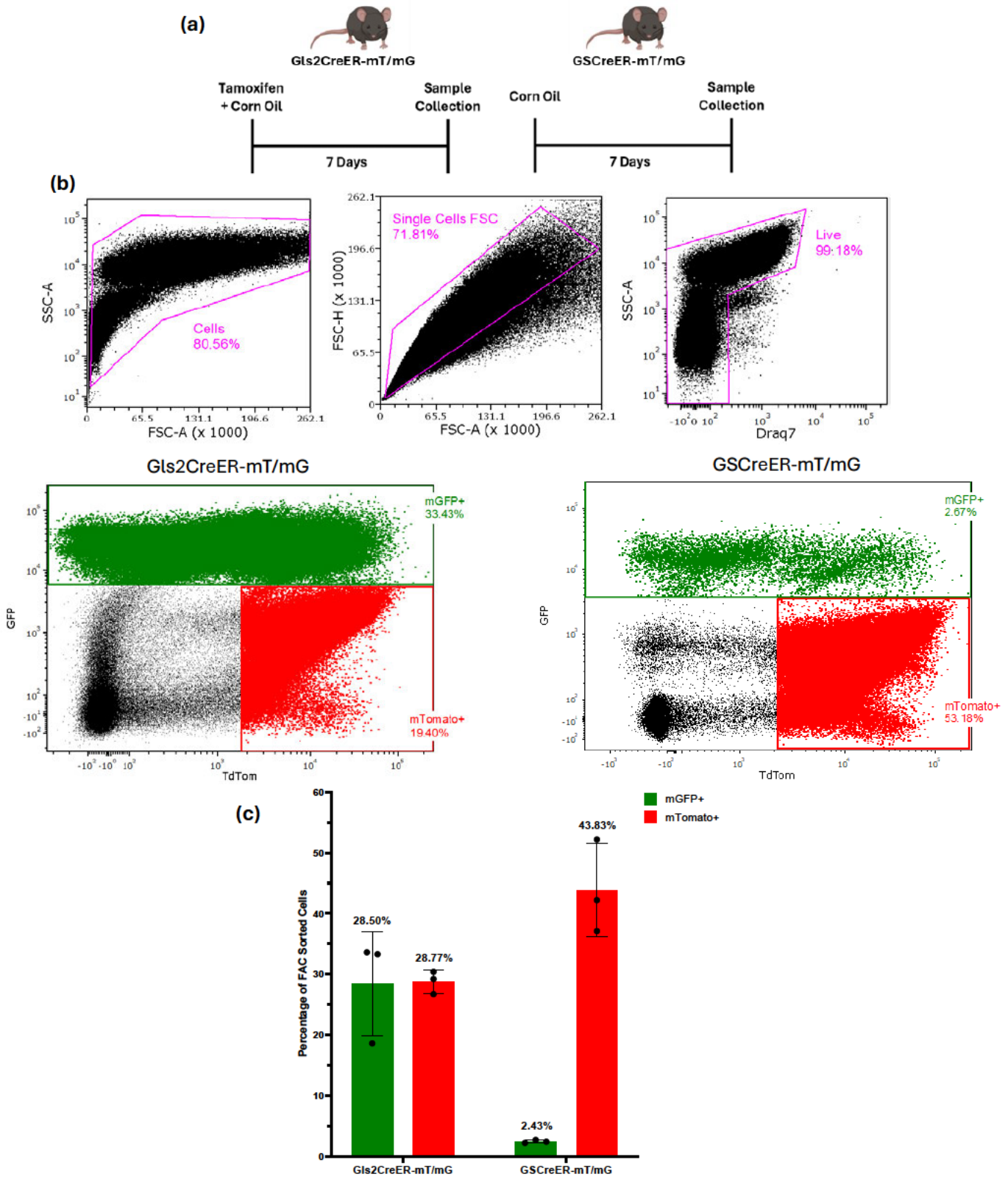

Figure 4.5: Dosing Strategies and FACS Quantification of Cre-Recombined and Non-Recombined Hepatocytes. ***(a)*** *Schematic showing the dosing timeline of the Gls2CreER-mT/MG and GSCreER-mT/mG mice prior to sample collection and fluorescent activated cell sorting of cells* ***(b)*** *Representative FACS plots showing the gating parameters used to identify single, live, mGFP+, and mTom+ hepatocytes in both Gls2CreER-mT/mG and GSCreER-mT/mG mice (100,000 mGFP+ hepatocytes and 100,000 mTom+ hepatocytes sorted per mouse for sequencing, n-3 mice/strain)* ***(c)*** *Bar plot demonstrating the mean percentage ± standard deviation of mTom and mGFP positive cells sorted from Gls2CreER-mT/mG and GSCreER-mT/mG mice (n=3).*

DESeq2 analysis was conducted on the bulk RNA output data, wherein the mGFP+ hepatocytes were compared between the two mouse models to compare cre-recombined periportal and pericentral hepatocytes. Several genes associated with metabolic processing were observed to be differentially expressed. These included cytochrome P450 family members (Cyp1a2, Cyp2a5, Cyp2c29, Cyp2c50, Cyp2e1, Cyp4a12a), multiple Major Urinary Proteins (Mup7, Mup9, Mup11, Mup15–18, Mup21), Oat, Slc1a2, and Elovl3 (Figure 4.6a).

To account for potential confounding effects of tamoxifen on gene expression – given its function as a selective estrogen receptor modulator capable of influencing transcriptional activity – an additional control analysis was conducted (Figure 4.6b). In this comparison, mGFP+ hepatocytes isolated from tamoxifen-treated Gls2CreER-mT/mG mice were compared to mTom+ hepatocytes obtained from corn oil–treated GSCreER-mT/mG mice. Importantly, both sets of samples were processed identically, except that the GSCreER-mT/mG mTom+ cells were not exposed to tamoxifen. Moreover, since these mTom+ samples should not contain mGFP+ GS-expressing hepatocytes, this analysis served as an appropriate reference for distinguishing tamoxifen-dependent transcriptional effects from differences attributable to zonal identity.

Cross-referencing the results of this control analysis with the initial periportal versus pericentral dataset revealed a subset of transcripts likely influenced by tamoxifen exposure (Figure 4.6c; complete gene list in Appendix Table 2). These included several metabolic genes identified in the primary analysis, as well as additional transcripts associated with estrogen signalling (eg, Gas6, Lgr5), cell proliferation and differentiation (Tbx3), secretion and solute transport (Slc17a8), and immune modulation or signalling pathways (Sucnr1, RNase4).

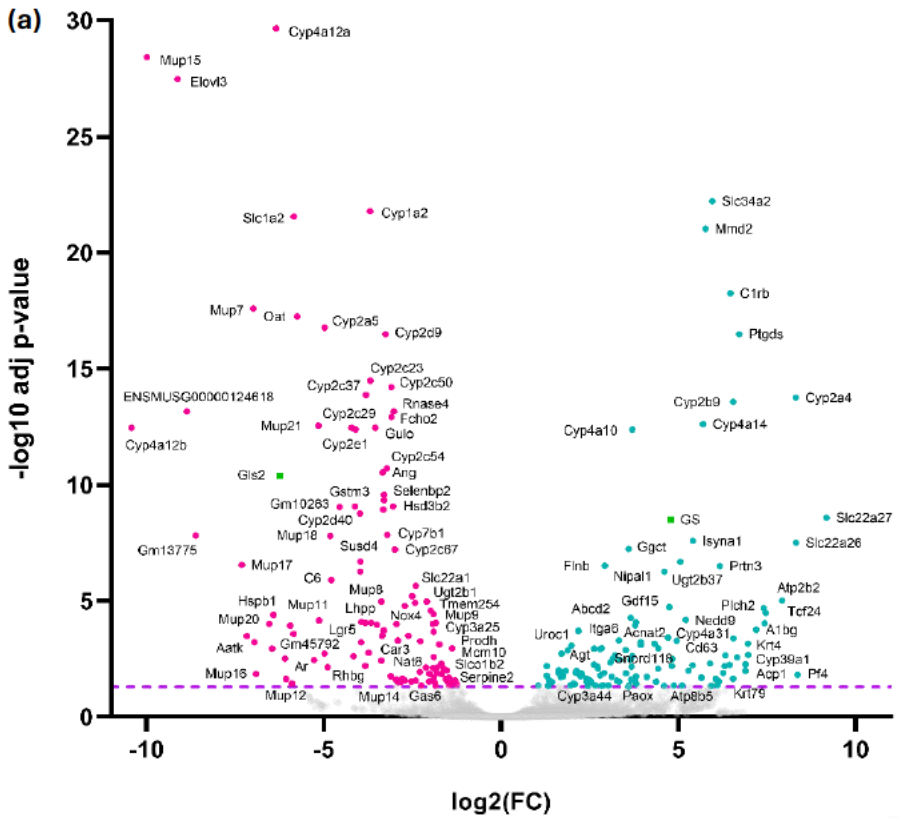

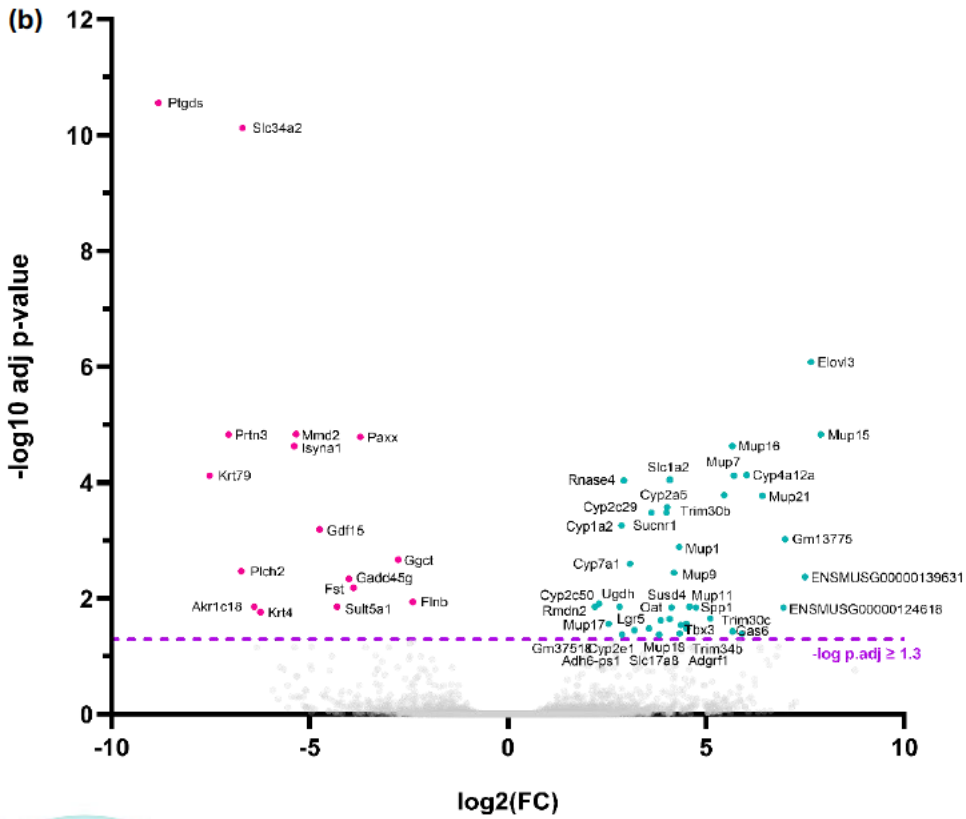

(c)

Significantly Downregulated Genes from Gls2 mGFP+ (Tamox) vs. GS mGFP+ (Corn Oil) Dataset (Genes upregulated in the tamoxifen-treated Gls2+ cells)

Significantly Upregulated Genes from Gls2 mGFP+ (Tamox) vs. GS mTomato+ (Corn Oil) Dataset

Including:

Cyp1a2, Cyp2a5, Cyp2c29, Cyp2c50, Cyp2e1, Cyp4a12a, ENSMUSG00000124618, Elovl3, Gas6, Gm13775, Lgr5, Mup11, Mup15, Mup16, Mup17, Mup18, Mup21, Mup7, Mup9, Oat, Rmdn2, Rnase4, Slc17a8, Slc1a2, Sucnr1, Susd4, Tbx3

Figure 4.6: Defining the Effects of Tamoxifen on Hepatic Gene Expression in Gls2CreER-mT/mG Mice. (a) *Volcano plot comparing mGFP+ hepatocytes in the Gls2CreER-mTmG model (7 days post-tamoxifen gavage, magenta) vs mGFP+ hepatocytes from the GSCreER-mTmG model (7 days post-corn oil gavage, cyan)* ***(b)*** *Volcano plot comparing corn-oil treated non-recombined mTom+ hepatocytes (no tamoxifen control, magenta) vs mGFP+ hepatocytes in the Gls2CreER-mTMG model (tamoxifen treated, cyan)* ***(c)*** *Venn diagram showing genes upregulated in both the mGFP+ hepatocytes sorted from the tamoxifen-dosed Gls2CreER-mT/mG mice and the non-recombined mTom+ hepatocytes isolated from corn oil-dosed GSCreER-mT/mG mice. Data derived from bulk RNA-seq of FACS-sorted hepatocytes (n=4 mice/group). Highlighted genes include top up- and downregulated genes which passed the DESeq2 analysis (Benjamini-Hochberg) cut off of adjusted p<0.05 (-log10 adjusted p<1.3) and log2 fold change > 1 (upregulated, cyan) or log2 fold change < -1 (downregulated, magenta).*

Genes identified as having been influenced by the presence of tamoxifen were excluded from the Gls2CreER-mT/mG mGFP+ dataset, and DESeq2 analysis was repeated. DESeq2 analysis revealed 84 significantly DEGs in Gls2+ cells, and 103 DEGs with significant fold change alterations in GS+ cells (Figure 4.7a, complete gene list can be found in Appendix Table 3). The genes that were significantly upregulated ($p < 0.05$; log2FC > -1) in the Gls2+ hepatocytes included those involved in glutamine metabolism (including Gls2 itself), antioxidant defence, and energy metabolism. Genes associated with detoxification pathways, including Cyp2c37, Cyp2c23, Cyp2c54, and Gstm3 (a glutathione S-transferase), and transporters such as Slc13a3 (dicarboxylate transporter) and Rhbg (ammonium transporter), were elevated. Additionally, Gulo (vitamin C synthesis) and Selenbp2 (selenium metabolism) were significantly upregulated, with both having functions in antioxidant defence mechanisms, whilst Cyp7b1 contributes towards bile acid metabolism [282,283].

Genes enriched in GS-expressing hepatocytes frequently corresponded to pathways related to xenobiotic metabolism, glycolysis, cholesterol synthesis, lipid metabolism, and glutamine synthesis. Significant genes ($p < 0.05$; log2FC > 1) include the pericentral marker used to define the hepatocyte population of interest, GS, apoptosis regulator Mmd2, sodium-phosphate cotransporter Slc34a2, detoxification enzyme Ugt2b37, and Ggct (γ-glutamylcyclotransferase) which functions in glutathione metabolism. Cytochrome P450 enzymes Cyp2b9, Cyp3a44, Cyp4a10, and Cyp4a14 were also significantly upregulated.

The heatmap in Figure 4.7b displays the expression profiles of the genes that are significantly up- or down-regulated ($p < 0.05$, log2FC > -1/1) in Gls2+ or GS+ hepatocytes, as identified by DESeq2 analysis (also shown in Figure 4.7a). The samples can be seen to cluster according to their respective groups,

indicating consistent gene expression patterns within each population. Notably, one Gls2+ sample stands out due to markedly higher expression of Pf4, Gm19705, Gng5c, Gm56807, Igf1os, ENSMUSG00000143648, GM42047, GM49417, and Mob3a compared to the other samples.

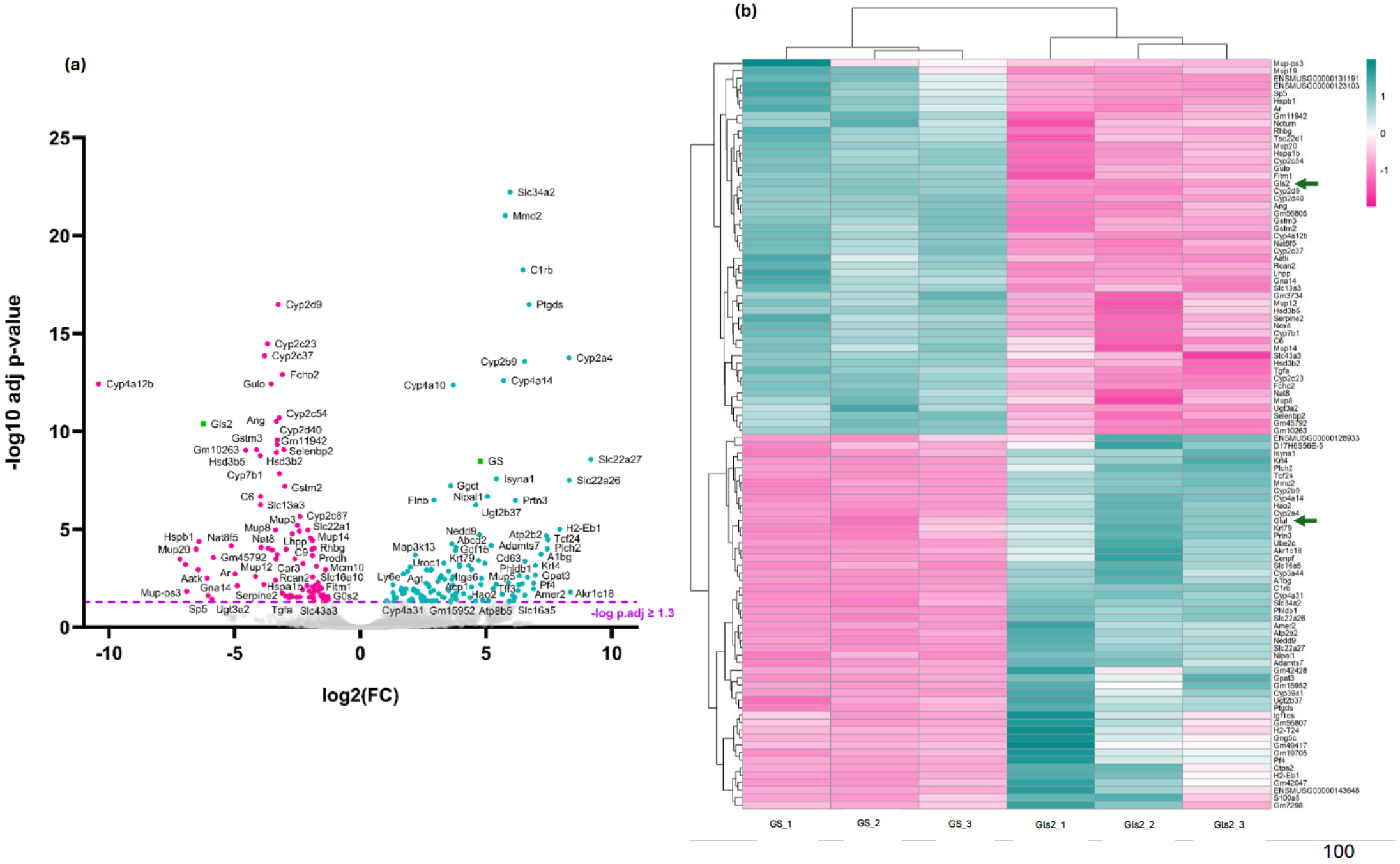
(a)
-log10 adj p-value
log2(FC)
-log p.adj ≥ 1.3
(b)
GS_1
GS_2
GS_3
Gls2_1
Gls2_2
Gls2_3
100

Figure 4.7: Differentially Expressed Genes in Gls2+ and GS+ Hepatocyte Populations. (a) *Volcano plot comparing mGFP+ Gls2+ hepatocytes (7 days post-tamoxifen gavage - with tamoxifen-associated genes removed) vs mGFP+ GS+ hepatocytes (7 days post-corn oil gavage) (n=3 mice/strain). Highlighted genes include those upregulated in the Gls2+ population (magenta) and those upregulated in the GS+ population (cyan) which passed the DESeq2 analysis (Benjamini-Hochberg) cutoff of adjusted p<0.05 (-log10 adjusted p<1.3) and log2 fold change > 1/-1* ***(b)*** *Expression heatmap of the top 50 genes upregulated in the Gls2+ hepatocyte population (magenta) and 50 genes upregulated in the GS+ hepatocyte population (cyan) across the 6 samples (3 Gls2CreER-mT/mG and 3 GSCreER/mT/mG). Each row represents a gene, and each column corresponds to an individual mouse (n=3 per group).*

To gain an understanding of the functional specialisations of the genes reaching significance thresholds in both the Gls2-expressing (periportal) and GS-expressing (pericentral) hepatocyte populations, a Gene Ontology (GO) enrichment analysis was conducted using the Galaxy genome analysis platform (Figure 4.8). The Gls2+ hepatocyte population demonstrated strong enrichment for GO terms predominantly related to metabolic and catalytic processes (Figure 4.8). Among the most highly represented terms were ‘metabolic process’, ‘cellular process’, and ‘regulation of signal transduction’, together indicating active participation in key cellular and metabolic pathways. In the molecular function category, top enriched terms included ‘catalytic activity’, ‘oxidoreductase activity’, ‘heme binding’, ‘small molecule binding’, and ‘glutathione transferase activity’, highlighting extensive involvement in enzymatic reactions and substrate transformations. Additional frequent terms such as ‘modified amino acid binding’, ‘lipid binding’, ‘hydrolase activity’, ‘enzyme binding’, and ‘transmembrane transporter activity’ further emphasise the broad biochemical capabilities of Gls2+ hepatocytes. Collectively, these enrichment patterns suggest that the Gls2+ population is functionally versatile, with significant roles in numerous metabolic, detoxification, and regulatory pathways within the liver.

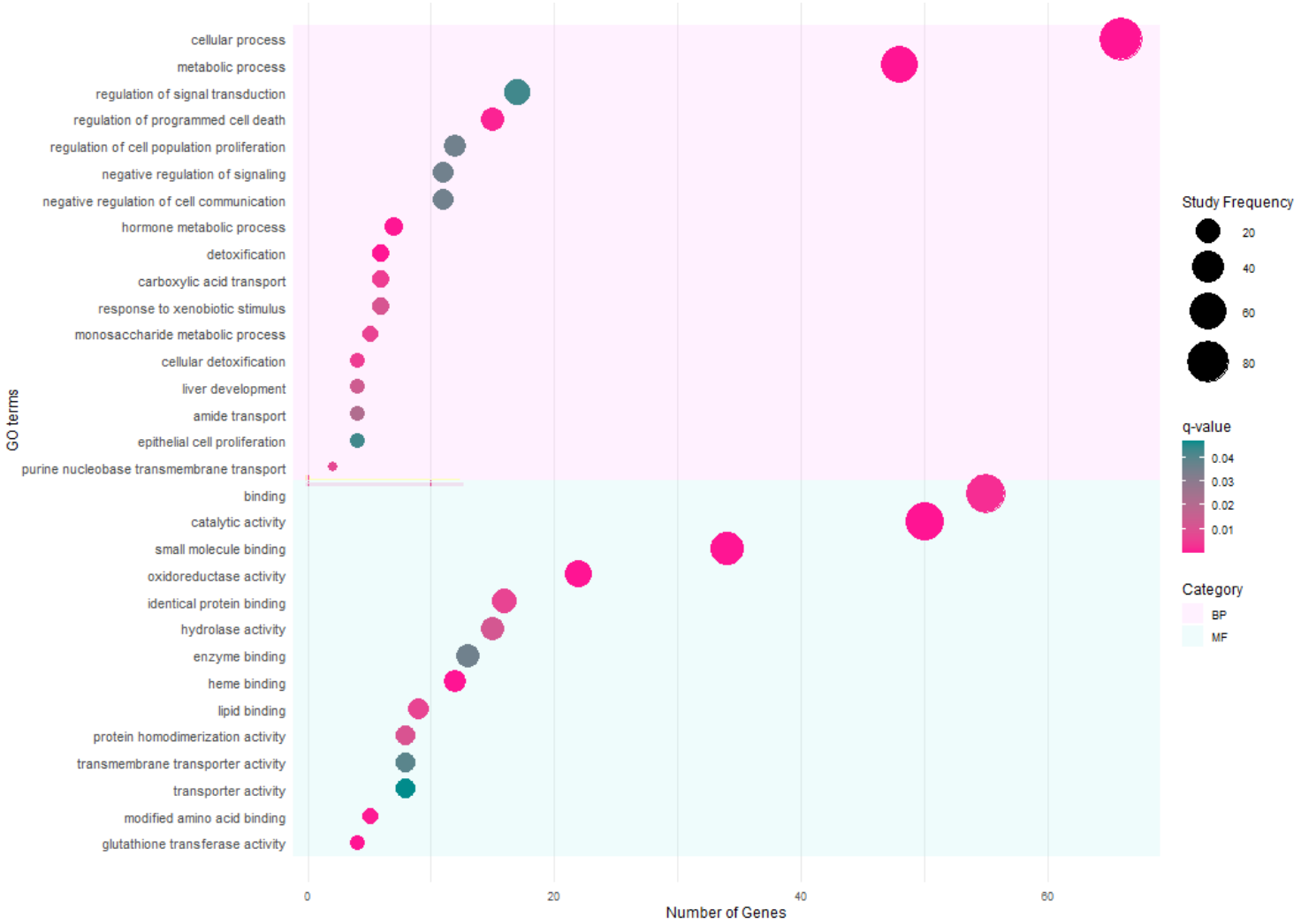

Figure 4.8: Gene Ontology (GO) Enrichment Analysis of mGFP+ Gls2+ Hepatocytes. *Differentially expressed genes were identified through DESeq2 analysis, following which GO Enrichment analysis was conducted on the Gls2+ datasets in Galaxy using a Benjamini-Hochberg multiple test correction (adjusted $p < 0.05$). GO terms were further filtered to show only those occurring at a frequency of >5% within the dataset. The GO terms are rank-ordered within each category by their frequency of occurrence within the study, with larger bubbles indicating higher frequencies and colours (cyan-magenta) reflecting q-values. BP – Biological Processes; MF – Molecular Functions.*

The mGFP+ GS+ hepatocyte population demonstrated enrichment for GO terms including ‘cellular process’, ‘biological regulation’, ‘regulation of biological process’, ‘metabolic process’, and ‘positive regulation of biological process’, as well as molecular function terms such as ‘binding’, ‘protein binding’, ‘catalytic activity’, ‘small molecule binding’, ‘ion binding’, ‘hydrolase activity’, ‘protein-containing complex binding’, ‘oxidoreductase activity’, and ‘monooxygenase activity’ (Figure 4.9). Additional enriched terms reflected regulation and cellular response, including ‘regulation of small molecule metabolic processes’, ‘regulation of reactive oxygen species metabolic processes’, ‘cell migration’, ‘positive regulation of catalytic activity’, ‘protein kinase activity’, ‘response to stimulus’, ‘response to chemical’, and ‘regulation of lipid metabolic processes’. These results highlight that the GS+ hepatocyte population is actively engaged in diverse metabolic, regulatory, and signalling pathways, underscoring its functional heterogeneity within the liver.

Figure 4.9: Gene Ontology (GO) Enrichment Analysis of mGFP+ GS+ Hepatocytes. *Differentially expressed genes were identified through DESeq2 analysis, following which GO Enrichment analysis was conducted on the GS+ dataset in Galaxy using a Benjamini-Hochberg multiple test correction (adjusted $p < 0.05$). GO terms were further filtered to show only those occurring at a frequency of >5% within the dataset. The GO terms are rank-ordered within each category by their frequency of occurrence within the study, with larger bubbles indicating higher frequencies and colours (cyan-magenta) reflecting q-values. BP – Biological Processes; MF – Molecular Functions.*

4.2.2 Validation of Gls2+ and GS+ Hepatocyte Gene Expression Results with Published RNA-sequencing Dataset

To provide greater context to the above results, a previously published dataset of bulk RNA sequencing data by Ben-Moshe *et al*. (2019) was analysed and then compared to those obtained in the present study [51]. The Ben-Moshe dataset comprises spatially resolved hepatocyte transcriptomes, obtained through sorting based on two zonated cell surface markers, CD73 and E-cadherin, which are inversely expressed in periportal and pericentral regions. This study systematically reconstructed the transcriptional, miRNA, and proteomic gradients across the liver lobule, thereby establishing one of the most comprehensive references for hepatocyte zonation. As such, it provides an ideal framework to assess how closely the present dataset of isolated murine hepatocytes recapitulates established zonal gene-expression signatures and metabolic compartmentalisation patterns described in physiologically normal liver tissue.

Pearson correlation analysis was used to identify genes most highly correlated with the expression of Gls2 and GS (Figure 4.10). The dataset was filtered to display only genes achieving significant correlation (adjusted $p < 0.05$) with the expression of Gls2, GS, or both. Genes such as Odad3, Pcca, Cyp2f2, Otc, Uox, Gsap, Itm2c, Hsd17b6, Keg1, Nab2, 2810408I11Rik, Got1, Eif4h, Csnk1g2, Hal, Las1l, As3mt, Fahd1, and Aldob were identified as strongly associated with Gls2.

Genes most strongly correlated with GS included Cldn2, Rcan2, Slc13a3, Slc1a2, Gm57349, Pdss2, Slc22a26, Slc43a3, Rpl22l1, Enpp1, Gm17087, Slc38a10, Vdac1, Gm57094, Nanp, Serpina7, Gm15502, Cpne8, and Gm3734 (Figure 4.10, see Appendix Table 4 for the top 50 most correlated genes).

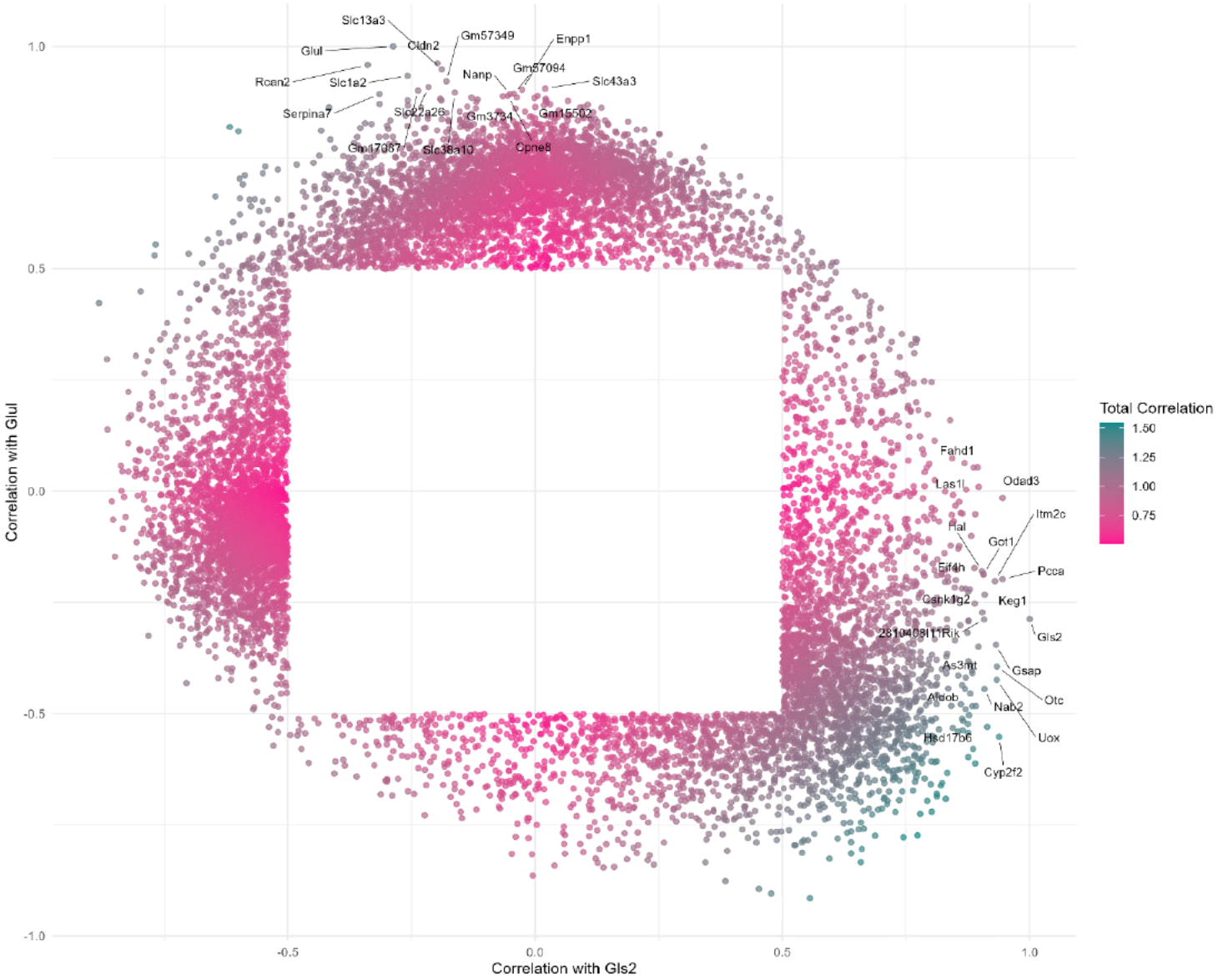

Figure 4.10: Genes Significantly Correlated with the Expression of Glutaminase 2 (Gls2) and/or Glutamine Synthetase (Glul/GS) in Hepatocytes Identified through RNA Sequencing Data Published by Ben-Moshe et al. [51]. *Scatter plot illustrating genes significantly correlated with the expression of Gls2 or GS (Pearson Correlation). Genes with absolute correlations exceeding a threshold of 0.5 were selected, and their overall correlation strength was calculated as the sum of the absolute correlations with Gls2 and GS. Points are coloured by total correlation strength, with a gradient from magenta (low correlation) to cyan (high correlation) (n=5 C57Bl6/J mice).*

GO enrichment analysis was performed on all genes identified to be highly correlated with Gls2 (107091 genes) or GS (103094 genes) in the Ben-Moshe *et al*. bulk RNA-seq dataset (Figure 4.11). The most enriched GO terms in the Gls2-correlated dataset related to cellular component organisation or biogenesis, primary metabolic process, and regulation of metabolism (Figure 4.11). Significant upregulation was also observed in genes involved in 'positive and negative regulation of cellular and biological processes' (with a frequency in the dataset (study freq.) of 29%-58%, respectively), 'localisation' (study freq. = 24%), 'developmental process' (study freq. = 28%), 'response to stimulus' (study freq. = 29%), 'binding proteins' (study freq. = 51%), 'binding small molecules' (study freq. = 32%), as well as 'catalytic activities' (study freq. = 32%).

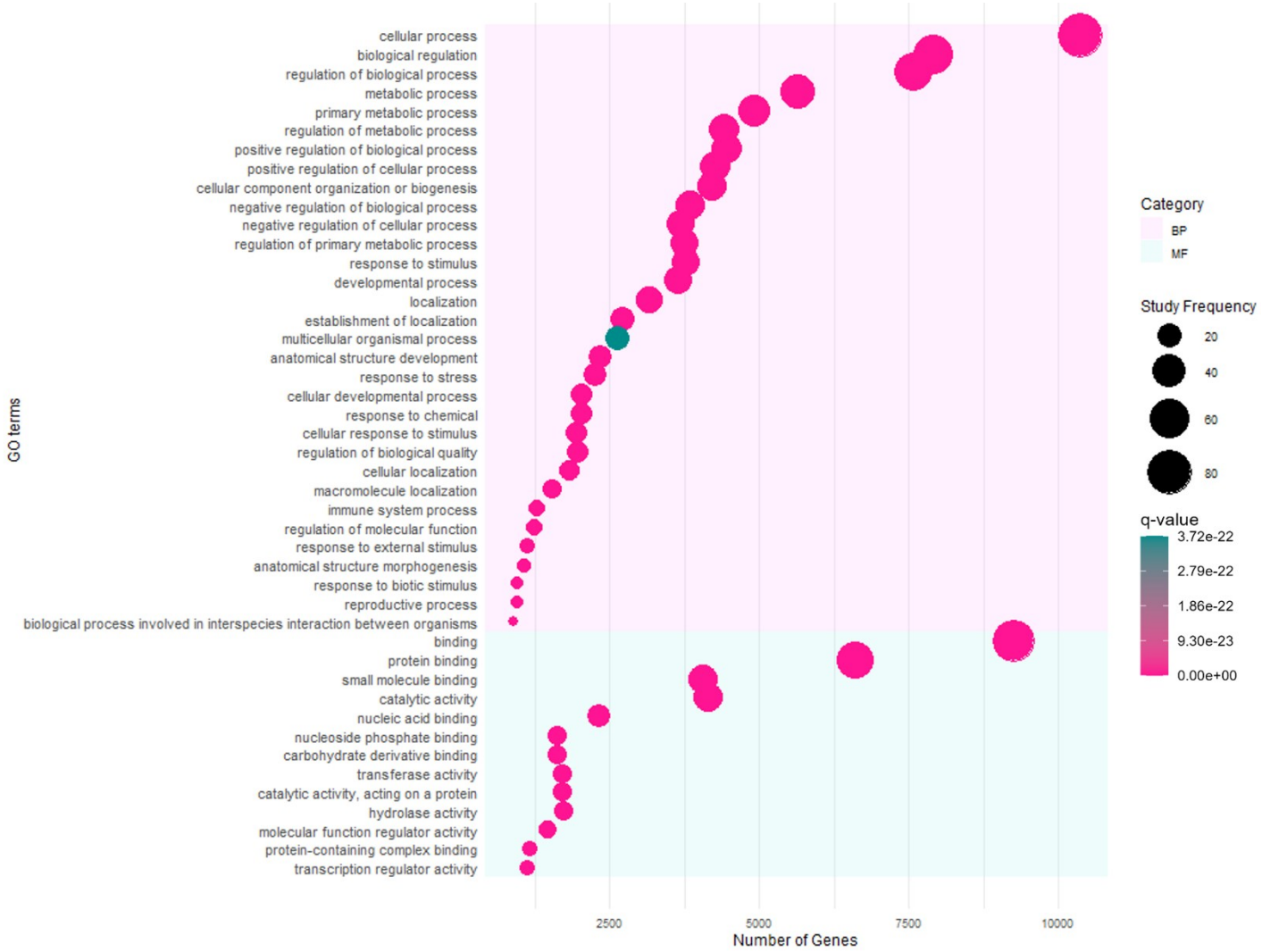

Figure 4.11: Gene Ontology (GO) Enrichment Analysis of Ben-Moshe et al.'s C57Bl6/J Dataset Demonstrating the Biological Processes and Molecular Functions Associated with Gls2-Expression in Hepatocytes [51]**.** *GO Enrichment analysis was conducted on the genes identified to be most highly correlated with Gls2 expression. Data were filtered using Benjamini-Hochberg multiple test correction (adjusted $p < 0.05$), and only GO terms occurring at a frequency of >5% within the dataset are shown. The GO terms are rank-ordered within each category by their frequency of occurrence within the study, with larger bubbles indicating higher frequencies and colours (cyan-magenta) reflecting q-values. BP – Biological Processes; MF – Molecular Functions.*

Similarly, the GO enriched terms in the GS-correlated dataset also included those related to broad cellular functions such as ‘metabolic processes’, ‘biological regulation’, ‘cellular processes’, ‘localisation’, ‘developmental processes’, ‘responses to stress’, ‘responses to stimuli’, ‘cell cycle processes’, ‘homeostatic processes’, ‘small molecule binding’, and ‘protein binding’ (Figure 4.12).

However, compared to the Gls2-correlated dataset, the GS-correlated gene set appeared to be more weighted towards ‘cellular component organisation’ or ‘biogenesis’ (study freq. = 33%), ‘primary metabolic process’ (study freq. = 39%), ‘regulation of metabolic process’ (study freq. = 35%), ‘positive regulation of cellular processes’ (study freq. = 32%), ‘regulation of primary metabolic processes’ (study freq. = 30%), ‘metabolic processes’ (study freq. = 44%), and ‘catalytic activity’ (study freq. = 33%).

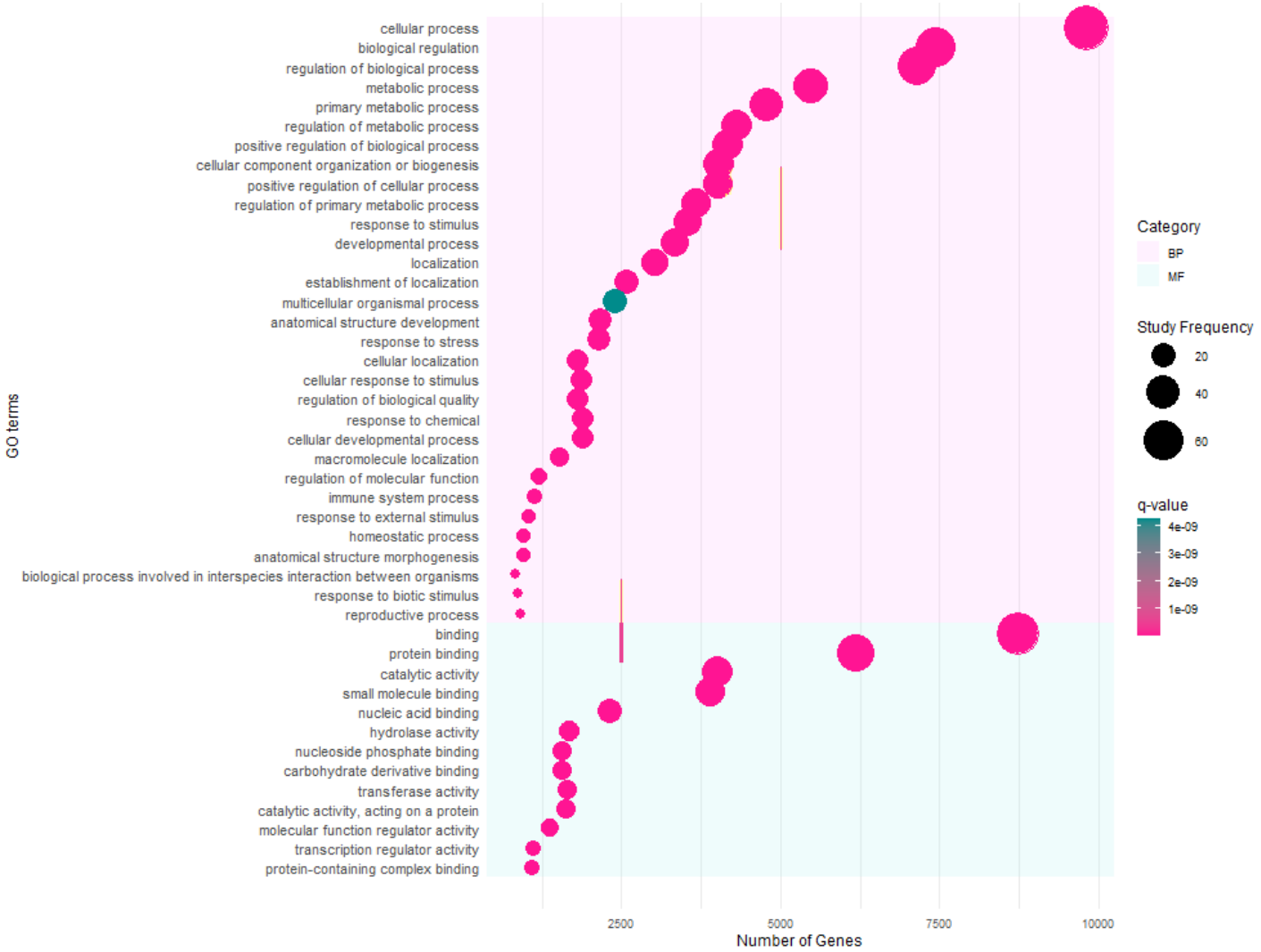

Figure 4.12: Gene Ontology (GO) Enrichment Analysis of Ben-Moshe et al.'s C57Bl6/J Dataset Demonstrating the Biological Processes and Molecular Functions Most Often Occurring in GS+ Pericentral Hepatocytes [51]. *GO Enrichment analysis was conducted on the genes identified to be most highly correlated with Gls2 or GS expression. Data were filtered using Benjamini-Hochberg multiple test correction (adjusted $p < 0.05$) and only GO terms occurring at a frequency of >5% within the dataset are shown. The GO terms are rank-ordered within each category by their frequency of occurrence within the study, with larger bubbles indicating higher frequencies and colours (cyan-magenta) reflecting q-values. BP – Biological Processes; MF – Molecular Functions.*

The GO term lists derived from bulk RNA-sequencing data of mGFP+ hepatocytes isolated from Gls2CreER-mT/mG and GSCreER-mT/mG mice were compared with those generated from the analysis of Gls2- and GS-correlated genes from the dataset published by Ben-Moshe *et al*. (Figure 4.10). From these comparisons, GO terms shared or uniquely occurring in each dataset were identified.

Shared GO terms in the data generated from Gls2-expressing hepatocytes and the Gls2+ cells identified in the Ben-Moshe data include catalytic activity, hydrolase activity, metabolic process, small molecule binding, and transmembrane transporter activity (Figure 4.13a). Terms uniquely enriched in the recombined mGFP+ hepatocytes from Gls2CreER-mT/mG mice include 'oxidoreductase activity', 'heme binding', 'glutathione transferase activity', 'hormone metabolic process', 'regulation of programmed cell death', 'cellular detoxification', 'carboxylic acid transport', 'monosaccharide metabolic process', 'response to xenobiotic stimulus', and 'liver development'. Contrastingly, the Ben-Moshe dataset exhibited enrichment for broader terms including 'primary metabolic process', 'regulation of metabolic process', 'chemical homeostasis', 'response to abiotic and external stimuli', and various categories of 'molecular function regulation', suggesting a more generalised, systemic metabolic and regulatory signature.

GO terms shared between the mGFP+ GS-expressing hepatocytes and the GS+ cells identified in the Ben-Moshe *et al*. data include terms referring to responses to chemical, endogenous, and other stimuli, as well as transferase activity (Figure 4.13b, a complete list of significant GO terms used in the comparisons can be found in Appendix Table 5). As in the Gls2 comparison, the Ben-Moshe data, filtered for GS-correlated GO words, demonstrated enrichment for more general categories, including 'primary metabolic processes' and 'regulation of metabolic processes', among others. However, the GS dataset generated in the present study encompassed terms such as 'chemical homeostasis', 'response to abiotic and external stimuli', and 'enzyme regulatory activity'.

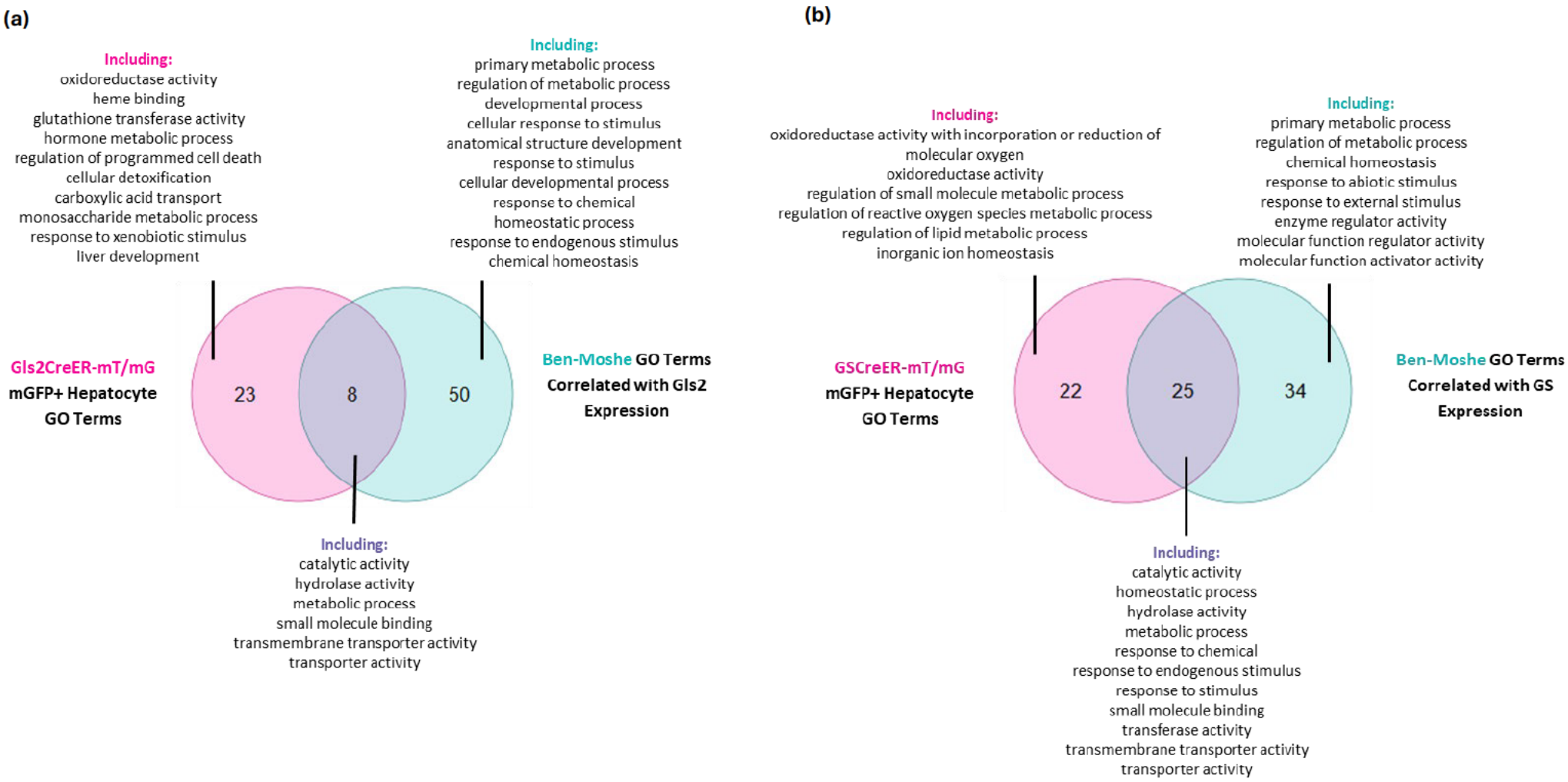

Figure 4.13: Venn Diagrams Illustrating Overlap and Distinction Between Gene Ontology (GO) Enrichment Terms from Bulk RNA-Sequencing of mGFP+ Hepatocytes from (a) Gls2CreER-mT/mG and (b) GSCreER-mT/mG Mice in This Study and Published Data by Ben-Moshe et al. [51]***.*** *The representative GO terms listed were selected due to their known correlation with the functional specialisation of (a) periportal or (b) pericentral hepatocytes, respectively.*

4.5 Discussion

Having confirmed the restricted expression of Gls2 and GS in hepatocytes at opposing poles of the lobule, two mouse models were developed to facilitate lineage tracing of the periportal and pericentral hepatocyte populations through Cre-recombination-induced membrane-bound GFP (mGFP) expression. To assess Cre efficiency, both models were treated with tamoxifen. Notably, Wei *et al*. (2021) demonstrated that the GSCreER mice could undergo recombination in GS-expressing hepatocytes even in the absence of tamoxifen, a phenomenon attributed to "leaky" Cre activity, in which the Cre recombinase exhibits unintended basal activity without ligand induction [66]. This may reflect unusually high levels of GS promoter activity leading to sporadic nuclear entry of the CreERT2 fusion protein without ligand activation. In addition to tamoxifen-independent recombination, widespread mGFP labelling was observed in the GSCreER-mT/mG mice following tamoxifen treatment, extending beyond the expected GS-expressing pericentral domain. Such recombination events may be explained by off-target Cre activity at pseudo-loxP sites upon tamoxifen activation, or by tamoxifen-induced alterations in CreERT2 dynamics that increase recombination efficiency in unintended hepatocyte subpopulations [284-286]. These observations highlight the potential caveats of tamoxifen-inducible Cre models and underscore the importance of validating recombination specificity in each experimental context [66,287-291].

Despite these limitations, the administration of the tamoxifen (solubilised in corn oil and 10% ethanol) to Gls2CreER-mT/mG mice and the vehicle control (corn oil and 10% ethanol) to GSCreER-mT/mG mice resulted in high recombination efficiency in both models, with rates of 96.38% for Gls2CreER-mT/mG and 86.37% for GSCreER-mT/mG. Having established this efficiency in both models, it was essential to assess whether recombination accurately reflected the expected zonal gene expression patterns. Specifically, GS expression was noted to overlap with a further restricted zone 3 marker, Ornithine Aminotransferase (Oat) [229,261], and Gls2 expression corresponded with the zone 1/2 marker Epithelial cadherin (E-cadherin) [228,292]. This finding confirmed that the Gls2CreER-mT/mG and GSCreER-mT/mG mouse lines are capable of accurately identifying hepatocytes within the target zones.

Once satisfied that the fluorescent reporting was restricted to the hepatocyte populations of interest, cre-recombination was induced, the livers were dissociated, and single-cell suspensions were prepared for fluorescence-activated cell sorting (FACS). The discrepancies between the higher percentages of mGFP+ cells observed in the IHC as compared to the percentages of mGFP+ cells in the FACS analysis could be explained by immunostaining being able to detect low-level mGFP

expression in partially recombined cells. In contrast, FACS requires a minimum fluorescence intensity threshold to register as mGFP+ [293,294]. It is also possible that the perfusion and *in situ* digestion of the livers prior to FACS may have damaged or killed some of the mGFP+ hepatocytes; thus, they would not have been identified in the live cell population following gating. Nevertheless, the mouse models facilitated the successful FACS isolation of 100,000 recombined and 100,000 non-recombined cells from each liver, which were then processed and sent for sequencing (Section 2.7).

As hepatocytes are notoriously fragile, single-nuclear RNA sequencing has become the preferred technique for hepatic transcriptomics, as the isolation of the nuclei from frozen or mechanically dissociated tissues is able to preserve transcriptional signatures without requiring intact cells and reducing the potential for enzymatic-dissociation-induced stress responses [295-297]. snRNA-seq is unsuitable for the models used in this study because the mT/mG reporter system relies upon membrane-bound fluorescent proteins, which are eliminated during nuclear isolation [296-298]. Thus, bulk RNA-seq offered a robust alternative for this study to facilitate the comparison between the transcriptional profiles of the Gls2-expressing and GS-expressing hepatocyte populations. Future studies requiring a higher sequencing resolution could try to adopt a whole single-cell sequencing (scRNA-seq) protocol; however, previous studies have found that the large sizes of the hepatocytes can induce cell sorting inefficiencies in these protocols, making cell barcoding for downstream analysis challenging [295,299]. Prior studies have also reported that enzymatic dissociation of liver tissue can introduce artefacts and alter the results to some extent [295,299]**.** Therefore, to enable more reliable investigation of hepatocytes using scRNA-seq, optimised approaches such as mechanical tissue dissociation or microfluidic devices to address size-related challenges could be explored, although these methods remain technically demanding because of hepatocytes' sensitivity to stress-induced transcriptional changes during isolation [297-300].

When transcriptionally profiling hepatocytes, even after reducing cell stress as much as possible through optimised dissociation protocols, caution is needed when interpreting results because exogenous factors can inherently alter gene expression. One such factor in this study is tamoxifen, which has been shown to modulate hepatic transcriptomes significantly [288,301-304]. Tamoxifen is a selective oestrogen receptor modulator known to competitively bind to oestrogen receptors (ERs) and modulate transcriptional programmes involved in drug metabolism, lipid homeostasis, and stress responses [305,306]. To avoid confounding effects, genes whose expression may have been influenced by tamoxifen administration were excluded before comparing periportal and pericentral hepatocyte populations. By contrasting non-recombined (mTom+) cells isolated from corn-oil vehicle–treated

GSCreER-mT/mG mice with recombined (mGFP+) tamoxifen-treated Gls2CreER-mT/mG mice, the genes affected by tamoxifen metabolism could be identified.

What resulted from this comparison was a list of genes which included members of the cytochrome P450 enzyme (Cyp) and major urinary protein (Mup) families, as well as other proteins involved in xenobiotic detoxification, fatty acid elongation, and urea cycle function. The lipophilic nature of the tamoxifen is hypothesised to have induced expression of the xenobiotic metabolising enzymes including Cyp1A2, Cyp2A5, Cyp2A29, Cyp2A50, Cyp2E1, and Cyp4E12α through activation of the nuclear pregnane X receptor (PXR) [255,307-311]. Although no direct mechanistic links between PXR and Slc17a8 (vesicular glutamate transporter 3) appear in published literature, PXR's role in altering neurotransmitter-related transporters seems plausible considering its cross-talk with other nuclear receptors (eg, constitutive androstane receptor) affecting hepatic stress reactions [307,308,312]. Similarly, Tbx3, a transcription factor critical for hepatocyte differentiation and zonation, and Lgr5, a stem/progenitor cell marker, may also be indirectly regulated through some interaction between PXR and Wnt/β-catenin signalling, though there is little evidence for this in published literature [308,310,313].

Tamoxifen has also been shown to influence the activity of SREBP-1c, a principal regulator of lipid synthesis, with studies demonstrating downregulation [314] or upregulation [315] of activity depending on experimental parameters. In this case, the activation of SREBP-1c by the drug could explain the transcription of genes associated with fatty acid metabolism, such as Elovl3 (involved in fatty acid elongation) and Slc1a2 (a glutamate transporter) [316,317]. Activation of SREBP-1c could be a potential explanation for the observation of Gas6 expression (a protein involved in inflammation, regeneration and tissue repair), as an increase in lipid synthesis might be expected to trigger a compensatory response through activation of the Axl receptor in response to cellular damage that may occur [318]. Gas6 has been shown to be oestrogen responsive in human osteoblasts, so tamoxifen's oestrogen receptor agonist activity of tamoxifen in hepatocytes might activate Gas6 expression through oestrogen-responsive elements in its promoter [319]. The presence of ornithine aminotransferase (Oat), a urea cycle enzyme which has been used earlier in the present study as a stringent marker for pericentral hepatocytes, could be attributed to the hormonal regulation of urea cycle enzymes, with activity being reportedly induced by ER-mediated transcriptional programmes [320]. Similarly, the tamoxifen-induced upregulation of Mup11, Mup15, Mup16, Mup17, Mup18, Mup21, Mup7, and Mup9 may occur through oestrogen receptor-mediated mechanisms involving putative oestrogen-responsive elements in their promoter regions, particularly since Mup gene expression is normally sexually dimorphic (with males expressing 2-8 times higher levels than females) and is regulated by hormonal signalling pathways [321,322].

After identifying tamoxifen-induced genes in the Gls2CreER-mT/mG mGFP+ FACS sorted cells, they were systematically excluded from the differential gene expression analysis in order to better reveal the zonation-specific transcriptional signatures. This method of filtering the dataset does have its limitations, as it creates a blind spot where genes that are both tamoxifen-responsive and genuinely zone-specific cannot be adequately evaluated. Consequently, it is now not possible to measure the differences in the expression of genes which are characteristically zone 3 specific, such as Oat, Cyp2E1, and Cyp1A2. To mitigate this in future experiments, constitutive Cre drivers or knock-in reporter lines for both Gls2 could be used to isolate the populations of interest, thus eliminating the need for tamoxifen. Alternatively, surface marker-based spatial sorting or single-cell spatial transcriptomics could offer unbiased isolation and characterisation of zonated hepatocyte populations without reliance on genetic manipulation or exogenous compounds [51,70,295]. Surface marker approaches utilise endogenous proteins like CD73 for zone 3 and E-cadherin for zone 1 to physically sort hepatocytes by FACS based on their spatial origin, providing high resolution without genetic manipulation [51]. Meanwhile, spatial transcriptomic technologies such as MERFISH or Visium can profile gene expression while preserving spatial information, allowing simultaneous characterisation of all hepatocyte populations without the necessity for pre-labelling [323-325]. These alternative approaches would enable comprehensive analysis of hepatocyte zonation patterns while avoiding the technical confounding effects that can mask zone-specific transcriptional signatures [324,325].

After filtering, a differential gene expression analysis (DESeq2) was conducted comparing the refined Gls2 mGFP+ dataset to GS mGFP+ FACS-sorted hepatocytes. This analysis revealed the DEGs enriched in the cells of the periportal and pericentral zones, respectively. As anticipated, in Gls2+ hepatocytes, there is an upregulation of genes involved in glutamine metabolism, antioxidant defence, and energy metabolism. This validates the data presented in this study, given the known role of Gls2 as a catalyst in the conversion of glutamine to glutamate and ammonia, which supports the urea cycle to facilitate ammonia detoxification [225,267,268,279]. These observations are mirrored in metabolic tracing experiments, which show periportal hepatocytes preferentially uptake glutamine and secrete glutamate, supporting the intercellular glutamine cycle essential for ammonia and acid-base homeostasis. Furthermore, the upregulation of genes related to antioxidant defence (such as Gulo and Selenbp2) and detoxification (including Cyp2C37, Cyp2C23, Cyp2C54, and Gstm3) in Gls2+ hepatocytes aligns with the environment of the periportal region in the context of elevated levels of oxygen and nutrients entering the liver from the hepatic artery [282,283]. The presence of transporters like Slc13a3 and Rhbg further supports the periportal zone's specialisation in nutrient uptake and ammonia handling [326,327].

In contrast, the genes observed as upregulated in pericentral hepatocytes are predominantly involved in xenobiotic metabolism, glycolysis, cholesterol and lipid synthesis, as well as glutamine synthesis. Notably, GS – the canonical marker used to define pericentral cells in this study – plays a key role in capturing residual ammonia that escapes periportal ureagenesis and synthesising glutamine for systemic release [279]. This specialisation is complemented by expression of the drug, endo- and xenobiotic detoxifying cytochrome P450 enzymes (such as Cyp2B9, Cyp3A44, Cyp4A10, Cyp4A14) [255,256]. Further highlighting this specialisation, genes such as Ugt2b37 (involved in glucuronidation) and Ggct (supporting glutathione metabolism and oxidative stress defence) are upregulated in the pericentral hepatocytes, again emphasising their role in processing metabolic end-products and protecting against toxic insults [274,328,329]. The distinct gene expression profile of GS+ cells is known to be tightly regulated by Wnt/β-catenin signalling, as it sustains high GS expression and maintains the pericentral phenotype, but establishes and maintains lobular zonation as a whole [70,330,331]. These results appear consistent with the well-established concept of metabolic zonation within the liver lobule, where periportal hepatocytes are optimised for nutrient processing, ammonia detoxification, and oxidative metabolism, while pericentral hepatocytes are specialised for xenobiotic metabolism, glycolysis, and glutamine synthesis [71,103,225,259,260].

Once the DEGs between the Gls2+ and GS+ hepatocyte populations had been identified, Gene Ontology (GO) enrichment analysis was conducted on significant DEGs to provide a broad functional overview of the divergent pathways of the hepatocyte populations. This method does not have the resolution to capture more nuanced regulatory interactions. Still, it can effectively highlight systemic differences in metabolic, signalling, and homeostatic processes, which aligns well with the goal of characterising the zonal hepatocyte identities.

The Gls2CreER-mT/mG mGFP+ dataset showed enrichment in GO terms associated with catalytic activity, oxidoreductase activity, and glutathione transferase activity, reflecting roles in detoxification, redox balancing, and metabolite processing. These functional enrichments are consistent with the classical roles of periportal hepatocytes, where fatty acid β-oxidation, amino acid catabolism, and ammonia detoxification predominate, consistent with previous reports demonstrating enriched expression of metabolic enzymes in this zone [51,53,101]. Interestingly, the enrichment of glutathione transferase activity correlates with periportal hepatocyte engagement in xenobiotic detoxification, as substances absorbed from the portal circulation are primarily metabolised in this oxygen-rich region. The dataset also displayed enrichment for heme binding activity, a function often linked to Cyp enzymes predominantly expressed in pericentral hepatocytes [201,254-256,309]. This seemingly hybrid phenotype may arise from the Gls2+ cells spanning both the periportal and midlobular regions. This

spatial heterogeneity is supported by recent spatial transcriptomic and single-cell studies identifying zone 2 hepatocyte subpopulations with mixed metabolic features [66,103]. For example, IGFBP2+ hepatocytes, which mainly reside in midlobular zone 2, exhibit dual characteristics enabling participation in both periportal and pericentral metabolic pathways, highlighting the dynamic and adaptable nature of hepatocyte zonation [332].

While the Gls2CreER line effectively labels periportal hepatocytes, using Gls2 as a zone 1 marker carries some limitations because its expression extends slightly into the midlobular (zone 2) region, producing a gradient rather than a discrete boundary around the portal vein. Alternative periportal markers could include genes such as Hal (histidine ammonia-lyase), Cps1 (carbamoyl phosphate synthase 1), Sds (serine dehydratase), or Cdh1 (E-cadherin), as they are known to exhibit periportal enrichment. However, among all zone markers experimentally evaluated in the Wei *et al*. (2021) paper, Gls2 remained the most spatially restricted and robust zone 1 marker suitable for genetic targeting, balancing expression strength with positional fidelity [66]. Consequently, while Gls2-based labelling adequately captures the periportal metabolic program, it may also encompass adjacent midlobular hepatocytes, introducing mild heterogeneity into zone 1 lineage and transcriptomic analyses.

In contrast, the GSCreER-mT/mG mGFP+ hepatocyte population demonstrated enrichment for monooxygenase activity, iron ion binding, and regulation of reactive oxygen species (ROS) metabolic processes, aligning with their role in xenobiotic detoxification and redox homeostasis [51,53,63,333]. The transmembrane transporter activity likely reflects bile acid handling and ammonia detoxification, with pericentral hepatocytes converting residual ammonia to glutamine via the action of GS as described above [273-277,279,330]. Notably, the regulation of lipid metabolic processes and protein kinase activity terms suggests that the cells are performing broader roles in lipogenesis and Wnt/β-catenin signalling, which are critical for maintaining pericentral identity [28,61,63].

The functional profiles of cells sorted from the Gls2CreER-mT/mG and GSCreER-mT/mG mice appear to fit with the established periportal and pericentral hepatocyte identities; however, these analyses and interpretations could be strengthened by validating them against large spatially resolved published datasets such as that published by Ben-Moshe *et al*. (2019) [51]. In their study, the researchers spatially sorted C57Bl6/J hepatocytes based on zonated surface markers (CD73 for pericentral and E-cadherin for periportal) in order to reconstruct spatial atlases of multiple zonated features using transcriptomics, miRNA array measurements and mass spectrometry proteomics (n=5) [51].

The results of these correlation analyses support existing evidence for the spatial specialisation of hepatocyte populations in the liver. Genes such as Pcca, Otc, Hal, and Aldob, which show strong

positive correlation with Gls2, are representative of the canonical functions of the periportal hepatocyte population in ammonia detoxification, amino acid catabolism, and gluconeogenesis [281,334,335]. Both Pcca and Otc are central to the urea cycle, a pathway spatially restricted to the periportal zone to efficiently convert toxic ammonia into urea – a phenomenon validated by spatial transcriptomics and single-cell RNA-seq studies that consistently demonstrate periportal enrichment of urea cycle genes like Cps1 and Ass1 [49,51]. The identification of Got1 (glutamic-oxaloacetic transaminase 1) further highlights the periportal compartment's role in nitrogen shuttling and transamination, while Uox (urate oxidase) aligns with the region's responsibility for purine catabolism and prevention of uric acid-induced oxidative stress [336,337]. Detecting the expression of As3mt (arsenic methyltransferase) also reiterates the periportal zone's role in neutralising absorbed xenobiotics, which have entered the liver through the portal vein [338].

In contrast, genes correlated with GS expression, such as Slc1a2 (a glutamate transporter), Cldn2 (a tight junction protein), and Vdac1 (a mitochondrial metabolite channel), correspond with the pericentral hepatocyte's specialisation in glutamine synthesis, paracellular transport, and mitochondrial metabolism [77,339-341]. The enrichment of additional solute carriers (Slc13a3, Slc38a10) and mitochondrial regulators (Pdss2) in this region supports the pericentral emphasis on metabolite exchange and redox balancing – adaptations consistent with the lower oxygen environment near the central vein as well as with the prominent occurrence of glycolytic and reductive pathways [51,103,225,330]. These findings strongly concur with the spatial atlas generated by the Ben-Moshe *et al.* (2019) study, which confirms Otc as a marker of the periportal regions, and Slc1a2 as a pericentral marker [51].

Several key pathways are notably absent from the GO enrichment analysis that would be expected in these hepatocyte populations. The most significant omissions in the Gls2+ hepatocyte dataset include: gluconeogenesis and glucose homeostasis pathways, urea metabolic process and nitrogen cycle metabolic process, amino acid catabolic process pathways that feed gluconeogenesis, cholesterol biosynthetic process and bile acid biosynthetic process machinery, and insulin receptor signalling pathway that regulates gluconeogenic gene expression. In the GS+ hepatocyte dataset, notable absences include glycolytic process, fatty acid biosynthetic process and *de novo* lipogenesis pathways, hypoxia-inducible factor (HIF) signalling pathways, comprehensive Wnt signalling pathway and canonical Wnt signalling pathway target gene networks beyond basic signalling components, and drug metabolic process, including xenobiotic metabolic process and phase II detoxification pathways that complement cytochrome P450 metabolism. The absence of these expected pathways may arise from metabolic plasticity, where hepatocytes rapidly alter their gene expression profiles during isolation and processing in response to changing nutritional conditions, thereby masking their original

zone-specific signatures. Alternatively, this could reflect post-transcriptional regulation of zonation-dependent functions that are primarily controlled at the protein and enzymatic levels rather than through transcriptional changes, making these pathways undetectable in RNA-based analyses. These factors may collectively explain the observed "hybrid phenotype" displaying mixed metabolic characteristics that blur traditional zonal boundaries.

The liver's compartmentalised metabolism is reinforced by the detected correlations between Gls2 and transporters (Slc22a26, Slc43a3) and GS and metabolic enzymes (Aldob, Fahd1) in the published dataset. This dichotomy is maintained by a combination of factors, including the Wnt/β-catenin signalling gradient through the lobule, which originates from endothelial cells and hepatic stellate cell-derived R-spondin 3 (RSPO3), which stabilises the pericentral identity [3]. Conversely, increased hormone levels (glucagon, insulin) and decreased WNT/β-catenin signalling in the periportal area promote the activation of genes involved in gluconeogenesis and amino acid metabolism [51,53,103]. At the molecular level, this is further supported by the prevalence of the Hnf4α/TCF transcriptional complex in periportal hepatocytes [52,64,342]. This complex actively promotes genes expressed in the periportal region while simultaneously suppressing expression of pericentral programmes dependent on β-catenin/TCF complexes [52,64,342]. Additionally, periportal identity is further stabilised by Hedgehog signalling, which counteracts WNT/β-catenin activity in the liver and helps define the spatial boundaries of metabolic gene expression [54,343-345].

The comparative GO enrichment analysis between the bulk RNA-seq dataset of Gls2+ hepatocytes and the published Gls2-correlated gene set reveals both shared and distinct functional characteristics of Gls2-expressing hepatocytes. The shared GO terms include functions such as catalytic activity, hydrolase activity, metabolic processes, small molecule binding, and transporter activity, which collectively reflect fundamental metabolic and enzymatic functions standard in Gls2+ hepatocytes. These functions are consistent with roles that periportal hepatocytes play in glutamine metabolism, mitochondrial function, and substrate transport [51,53,101]. Among the Gls2-linked GO terms that were found to be uniquely enriched in the bulk RNA-seq dataset from the present study were ‘oxidoreductase activity’, ‘heme binding’, ‘glutathione transferase activity’, ‘hormone metabolic process’, ‘regulation of programmed cell death’, ‘cellular detoxification’, ‘carboxylic acid transport’, ‘monosaccharide metabolic process’, ‘response to xenobiotic stimulus’, and ‘liver development’. These terms suggest that cells FACS sorted from the Gls2CreER-mT/mG mice were more specialised in redox balancing, detoxification, and metabolic adaptation, which are critical for processing xenobiotics, managing oxidative stress, and supporting tissue-specific development and homeostasis

[2,53,71,103]. Notably, enrichment of glutathione transferase and oxidoreductase activities implies a powerful potential for oxidative damage mitigation and detoxification in this region [346,347].

The published dataset demonstrates a distinct enrichment for more general biological processes, such as the fundamental metabolic processes, developmental processes, cellular response to stimulation, and homeostatic processes. This pattern may reflect differences in cell population specificity or the broader correlation-based gene selection method, capturing genes co-expressed with Gls2 across diverse cellular states and responses rather than being restricted to Gls2+ cells. Considering this dataset is derived from hepatocytes, not specifically sorted for Gls2 or GS, this is unsurprising.

The GO terms identified as shared between the results of the GSCreER-mT/mG mGFP+ cell analysis and the published dataset include some of those seen in the shared Gls2 results but also include terms which relate to responses to chemical, endogenous, and other stimuli, as well as transferase activity. Based on this enrichment, it infers that GS+ hepatocytes play a significant role not only in the process of ammonia detoxification but also in sensing and catabolising a wide variety of exogenous substances (including drugs, toxins, and nutrients) and endogenous signals (including hormones and metabolic intermediates) [279]. 'Transferase activity' as a GO term in both datasets aligns well with other published literature describing the particular enrichment of phase II conjugation enzymes, including glutathione S-transferases and UDP-glucuronosyltransferases, in pericentral hepatocytes, where they facilitate the detoxification and elimination of xenobiotics and metabolic by-products [142,279]. With regard to the terms enriched in the GS+ hepatocyte dataset from this study, the enrichment of oxidoreductase and reactive oxygen species (ROS)-related activities highlights their enhanced capacity for managing oxidative stress and maintaining redox balance. This is a function imperative to the pericentral zone due to the increased exposure to metabolic by-products and xenobiotics coming into contact with cells in this zone.

Overall, the results of these experiments reflect the anticipated zonated metabolism of the liver lobule well, whilst highlighting the importance of both the Gls2+ and GS+ hepatocyte populations in the maintenance of homeostasis. Despite my results closely mimicking those in the published literature, it is important to note that increasing the number of biological replicates from both mouse lines would strengthen the statistical power of these findings and allow for more definitive conclusions regarding the functional specialisation of the hepatocyte subpopulations.

CHAPTER 5

NICD1/Akt-Driven Reprogramming in Periportal and Pericentral Hepatocyte Populations

5.1 Introduction

The liver possesses a remarkable regenerative capacity in response to injury and disease – a property driven by several distinct cellular processes. Restoration of liver mass following partial hepatectomy or acute injury typically occurs via hepatocyte division and, when this response is impaired, through the activation of hepatic progenitor cell (HPC)-mediated regeneration. However, a third mechanism – hepatocyte metaplasia, where mature hepatocytes transdifferentiate to acquire biliary or progenitor-like features – remains less well defined. Recent lineage tracing and transcriptomic studies, including significant work by Pu *et al*. (2023), have revealed how hepatocytes can undergo metaplastic transitions under severe or chronic injury, driven by transcriptional reprogramming and plasticity [9].

Although the molecular pathways regulating hepatocyte proliferation and HPC-mediated repair are relatively well characterised, the signals and cellular interactions underlying hepatocyte metaplasia and its contribution to disease initiation – such as cholangiocarcinoma – are only beginning to be uncovered. This chapter focuses on the mechanisms governing hepatocyte plasticity, with special attention to transdifferentiation-driven oncogenesis as a potential initiating event in cholangiocarcinoma. Specifically, the experiments presented investigate hepatocyte-to-biliary cell reprogramming mediated by upregulation of Notch and Akt signalling – an experimentally validated strategy to induce hepatocyte-to-biliary conversion [133].

Recent studies, such as that by Hu *et al.* (2022), systematically interrogated the NOTCH-YAP1/TEAD-DNMT1 signalling axis in mouse models of intrahepatic cholangiocarcinoma (iCC) [15,21,131,133,348]. Through hydrodynamic tail vein injection (HTVI), Hu *et al*. introduced plasmids encoding a constitutively active form of Akt, the Notch intracellular domain (NICD), and a mutant of YAP1. This approach demonstrated that combined activation of Notch and Akt, in synergy with YAP1, induced hepatocyte-to-biliary reprogramming and epigenetic silencing of hepatocyte identity genes (Hnf4α, HNF1α, C/EBPα/β) via DNMT1-mediated promoter methylation [133]. Using lineage-tracing of hepatocytes, they were able to confirm the development of biphenotypic, tumorigenic biliary cells co-expressing hepatocytic (Hnf4α) and biliary cell markers (K19 and Sox9), which had originated from transfected hepatocytes, mirroring what is observed in preneoplastic human iCC.[78,349-353].

Collectively, these findings highlight that PI3K/Akt and Notch pathways collaborate to regulate cell fate transitions within the liver, priming cells susceptible to oncogenic transformation. As described in Chapter 1, Notch signalling is essential for determining cell fate by directing progenitor cells toward a biliary epithelial cell (BEC) lineage and orchestrating bile duct morphogenesis, whilst Akt signalling promotes protein synthesis, cell survival, and proliferation, and interacting with Notch at several molecular nodes, influencing cell fate through pathways such as DNMT1 upregulation and YAP/TEAD activation [15,17,21,22,236,343,354-356]. Dysregulation of the PI3K/Akt pathway has been implicated in both tumorigenesis and fibrogenesis, with evidence from mouse models and spatial transcriptomics confirming a role in tissue repair and cancer [236,354,355]. In cholangiocarcinoma, these molecular events seemingly converge to promote the reprogramming of hepatocytes, contributing to oncogenic transformation [122,124,133,354,355,357,358].

Building on this, it is increasingly important to consider how the spatial context of hepatocytes – determined by liver zonation – shapes plasticity and the regenerative response. Recent advances in single-cell and spatial transcriptomics have revolutionised the understanding of metabolic zonation in the liver, mapping not only the transcriptional and regulatory landscape of hepatocytes across lobular zones but also exposing the complex interplay between gene expression, chromatin structure, and injury susceptibility [49,64,89,100,103,225,252,359,360]. Bravo Gonzalez-Blas *et al.* (2024) leveraged single-cell and spatial multi-omics, together with deep learning, to dissect how enhancer-driven regulatory networks underpin hepatocyte zonation within the liver lobule [73]. By integrating transcriptomic and chromatin accessibility data, the study revealed that the hepatic zone of origin is a major determinant of hepatocyte gene expression and enhancer accessibility, establishing that periportal and pericentral hepatocyte identities are specified by distinct regulatory codes involving both enhancer elements and transcription factor networks [73].

A substantial body of evidence now demonstrates that the response to liver injury is profoundly affected by this zonal organisation. For instance, acetaminophen (APAP) and thioacetamide (TAA) toxicities have been observed to preferentially injure pericentral hepatocytes due to the high local expression of CYP2E1, resulting in zone-specific accumulation of toxic intermediates [76,361-363]. Conditions such as autoimmune hepatitis, iron overload, and primary biliary cholangitis (PBC) have also been shown to predominantly impact periportal hepatocytes, each through distinct but converging mechanisms. In autoimmune hepatitis, immune-mediated injury is centred around the portal tracts and extends into periportal hepatocytes, resulting in interface hepatitis and significant inflammation at the portal-parenchymal interface due to dense lymphoplasmacytic infiltrates and ongoing antigen presentation in this region [81,82,364]. Iron overload syndromes, such as hereditary

hemochromatosis, are marked by the initial accumulation of iron in periportal hepatocytes, reflecting portal delivery of iron-rich blood. This progressively leads to oxidative stress, periportal fibrosis, and cell death as injury advances [80]. In PBC, the autoimmune targeting of intrahepatic bile ducts within portal tracts causes chronic periportal inflammation and cholestasis, which then results in localised hepatocyte injury due to the proximity of the bile ducts to the periportal hepatocytes [365-367]. This is shown in histologically, where periportal inflammation and fibrosis are evident in PBC patients [365-367]. On the other hand, by implementing spatial transcriptomics in a murine hepatic ischemia-reperfusion (I/R) injury model, Xin *et al*. (2023) demonstrated that the pericentral hepatocytes are markedly more susceptible to I/R injury than cells in other lobular regions, exhibiting the most severe necrosis, inflammation, and cell loss [368]. Transcriptomic profiling revealed extensive zone 3-specific changes with upregulation of acute-phase, stress response, and inflammatory genes, while zone 1 maintained enrichment in metabolic and antioxidant pathways and showed greater resistance to injury [368]. While these studies have established clear patterns of zone-specific injury susceptibility, understanding the regenerative response following such damage has proven more complex.

Although significant progress has been made, a knowledge gap remains in terms of the potential differences in plasticity and regenerative capacity among hepatocyte populations from different zones. Classical lineage tracing and single-cell studies have previously implicated periportal, pericentral, or even midlobular hepatocytes as chief contributors to regeneration after injury or during homeostasis; however, these findings are often contradictory, and the molecular mechanisms that might underlie such zonal disparity remain only superficially resolved [66,89,101,264,369,370]. Several landmark studies have demonstrated that while midlobular hepatocytes display the highest proliferative activity and function as the principal source for new hepatocytes during both normal homeostasis and after injury, additional reports point to a remarkable plasticity within the hepatocyte compartment.

These contradictory findings have been addressed by Wei *et al*. (2021) through their systematic analysis using 14 different lineage tracing mouse strains [66]. Using CRISPR-engineered CreER knock-in models targeting genes with defined zonal expression patterns, they employed tamoxifen-inducible lineage tracing over 52 weeks to track hepatocyte repopulation dynamics. Their injury studies utilised two chronic damage models: DDC diet for 6 weeks to induce periportal cholangiopathies and 12 biweekly doses of CCl_4 to create chronic centrilobular necrosis. Additionally, they performed a partial hepatectomy and tested acute injuries, including acetaminophen toxicity. These experiments demonstrated that zone 2 hepatocytes were sheltered from toxic injuries affecting either lobular terminus and contributed to regeneration after various hepatotoxic insults, with the mechanistic basis identified as the IGFBP2-mTOR-CCND1 signalling axis through *in vivo* CRISPR knockout and activation

screens [66]. Beyond these zone-specific populations, specialised hepatocyte subsets with unique markers have also emerged as critical players in liver regeneration.

Hepatocyte subpopulations that are telomerase reverse transcriptase (TERT)-high, which are sparsely distributed across all zones, and Mfsd2a+, which are typically restricted to the periportal zone, have been shown to play a key role in liver repair, independent of their original lobular position [371-373]. The TERT-high hepatocytes can clonally expand and intermix throughout the lobule during regeneration, thus contributing to repopulation beyond zonal constraints [371,372]. Importantly, Wei *et al*. demonstrated that TERT-positive cells were not randomly distributed as previously reported, but instead were predominantly localised at the zone 2-3 junction, suggesting these cells may overlap with the highly regenerative Hamp2-positive zone 2 populations [66]. Similarly, Mfsd2a+ cells – typically periportal in the uninjured liver – can proliferate extensively to replace damaged cells in distant lobular regions, such as the pericentral area, following chronic or severe injury [373]. The remarkable regenerative capacity demonstrated by these specialised populations reflects a broader phenomenon observed in chronic liver disease, where traditional zonal boundaries become blurred through the development of bridging fibrosis.

Recent spatial transcriptomic studies have provided detailed evidence that chronic liver injury or advanced liver disease leads to a marked loss of precise hepatocyte zonal identity, as well as increased cellular plasticity throughout the liver's parenchyma. A study by Watson *et al*. (2025) applied spatial transcriptomics to fibrotic human liver tissue and observed that hepatocytes in diseased regions frequently co-express periportal and pericentral markers that are typically mutually exclusive in healthy lobules, indicating a blurring of traditional zonation boundaries [323]. Similarly, Hildebrandt *et al*. (2021) used spatial transcriptomics to map the distribution of zonation markers in mouse liver and identified that under certain disease conditions, an overlapping of periportal and pericentral expression patterns is induced, particularly in areas of fibrosis and inflammation [70]. Studies performed on chronic and advanced liver disease have further refined the understanding of hepatocyte plasticity and transdifferentiation. Gribben *et al*. (2024) performed single-nucleus RNA sequencing and advanced 3D imaging of human liver biopsies across a range of metabolic dysfunction-associated steatotic liver disease (MASLD) severity, revealing striking evidence of hepatocyte-to-biliary transdifferentiation *in situ* [374]. These hepatocytes appeared to express BEC markers such as K7, K19, Sox9, and NCAM1, in conjunction with hepatocyte markers and, in end-stage disease, were also noted to lose classical zonal gene expression and co-express formerly exclusive periportal and pericentral markers at both the transcriptional and protein levels. These biphenotypic cells are noted to be prominent in late-stage fibrosis and cirrhosis, which was further illustrated in the same study using 3D

imaging, which identified localisation of biphenotypic cells to remodelled regions of the biliary tree and ductular structures [374]. Using BEC organoid cultures, Gribben *et al*. provided functional evidence that manipulation of the PI3K-AKT-mTOR pathway (which is activated by insulin during MASLD progression) governs the efficiency of BEC-to-hepatocyte transdifferentiation, with inhibition of this pathway blocking the acquisition of hepatocyte features *in vitro* [374].

Complementing these human findings, Schaub *et al*. (2018) used genetic and lineage-tracing mouse models of severe bile duct deficiency (mimicking Alagille syndrome) to prove that hepatocyte transdifferentiation is not limited to adaptive, metaplastic responses, but can generate mature, functional BECs and form an entirely new biliary tree [375]. By fate-mapping hepatocytes in mice lacking intrahepatic bile ducts due to disrupted Notch signalling, they demonstrated that hepatocytes stably convert into BECs via transdifferentiation, driven primarily by high TGFβ signalling [26,375]. These newly generated BECs expressed mature markers such as K19 and formed functional ducts restoring bile drainage. The conversion did not appear to require progenitor activation, and clonal analysis showed that many hepatocytes contributed to the new ductal network with limited proliferation, which emphasises the plastic potential of these cells [375]. They went on to show that blocking TGFβ with pharmacologic or genetic approaches abolished the transdifferentiation and bile duct formation, cementing TGFβ as a key mechanistic driver.

Overall, while high-throughput and spatially resolved technologies have mapped the detailed baseline and injury-associated transcriptomic profiles of hepatic zones, the nuances of zonal differences in hepatocyte plasticity, lineage commitment, and reprogramming capacity remain incompletely addressed. Addressing this deficit will be critical for designing targeted regenerative therapies and for understanding the full spectrum of liver adaptation to injury and disease.

5.1.1 Hypothesis and Objectives

The hypothesis guiding this experiment is therefore that upregulation of NICD/Akt signalling in hepatocytes induces hepatocyte-to-biliary metaplasia, but crucially, that this response is not uniform across the hepatic lobule. Instead, it is anticipated that Gls2+ (periportal) and GS+ (pericentral) hepatocytes undergo phenotypic changes to varying extents in response to the stimuli, reflecting the intrinsic differences in their zonal microenvironments and baseline signalling cues. This distinction is particularly relevant given the established zonal gradient of Wnt/β-catenin signalling, which is highest in pericentral hepatocytes and is known to profoundly influence both hepatic function and cell fate plasticity [31,36,376,377].

The rationale for predicting a differential response draws from extensive evidence that Wnt signalling imparts spatial and functional heterogeneity within the liver and is further supported by examples from other organ systems where Wnt gradients are known to orchestrate lineage decisions. In tissues such as the gut [68,378-380], kidney [381,382], and skin [383], Wnt signalling determines the balance between stemness and differentiation, specifying tissue architecture and regional fate outcomes. In neural [377,384,385] and cardiac [386-388] development, Wnt activity governs spatial patterning and the allocation of progenitor cell fates, underlining its role in region-specific lineage specification. Drawing on this broader literature, it is reasonable to hypothesise that hepatocyte fate transitions upon NICD/Akt activation will be modulated by the zonal context, particularly by the distinct Wnt microenvironments occupied by Gls2+ and GS+ cells.

Thus, by integrating lineage tracing with transcriptomic profiling, the present study should be able to dissect the molecular and spatial determinants underlying hepatocyte plasticity, aiming to clarify how canonical signalling pathways, notably Notch, Akt, and Wnt, interact within defined liver zones to regulate hepatocyte-to-biliary reprogramming.

5.2 Hydrodynamic Tail Vein Injection Introduces Plasmids into Hepatocytes in a Specific and Unbiased Manner

The Sleeping Beauty (SB) transposon system was selected for its efficient, non-viral transgene delivery and stable genomic integration in hepatocytes following hydrodynamic tail vein injection (HTVI), offering a robust approach for widespread *in vivo* labelling and genetic modification of mouse liver cells. To map spatial plasmid uptake, a blue fluorescent protein (BFP)-tagged reporter plasmid (pSBbi-BH) was co-injected with the SB transposase (pCMV(CAT)T7-SB100) into C57Bl6/J mice by HTVI. This resulted in abundant and broadly distributed BFP+ hepatocytes throughout the liver lobules, as visualised by DAB immunostaining (Figure 5.1a).

To quantify the distribution, QuPath software was used to algorithmically divide each liver lobule into ten equal-width concentric deciles, numbered from the central vein (decile 1, pericentral/zone 3) to the portal triad (decile 10, periportal/zone 1) (Figure 5.1a-b). The number of BFP+ (DAB+) hepatocytes per decile was counted across multiple lobules (Figure 5.1b). A quadratic (second-order polynomial) regression was used to assess the linearity of the data and demonstrated a lack of a statistically significant difference in numbers of BFP+ cells across the lobule ($p < 0.0001$; $R^2 = 0.088$) (Figure 5.1c).

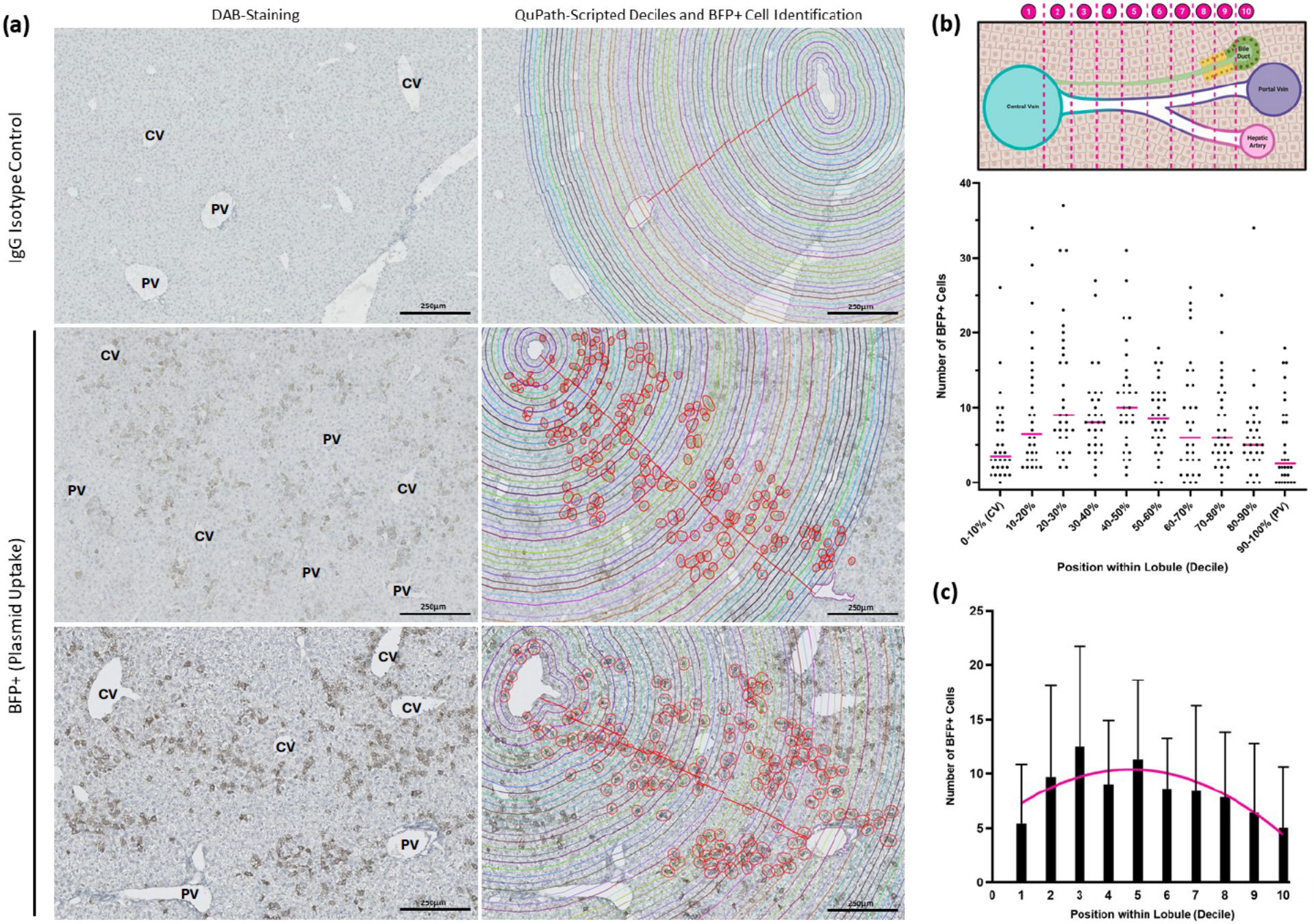
(a)
DAB-Staining
QuPath-Scripted Deciles and BFP+ Cell Identification
IgG Isotype Control
BFP+ (Plasmid Uptake)
CV
PV
250µm
(b)
1
2
3
4
5
6
7
8
9
10
Bile Duct
Portal Vein
Central Vein
Hepatic Artery
Number of BFP+ Cells
0
10
20
30
40
0-10% (CV)
10-20%
20-30%
30-40%
40-50%
50-60%
60-70%
70-80%
80-90%
90-100% (PV)
Position within Lobule (Decile)
(c)
Number of BFP+ Cells
0
5
10
15
20
25
0 1 2 3 4 5 6 7 8 9 10
Position within Lobule (Decile)

Figure 5.1: Anatomical Distribution of Plasmid Uptake Following Hydrodynamic Tail Vein Injection Delivery. (a) *Representative DAB-stained liver sections demonstrating uptake of Blue Fluorescent Protein (BFP)-tagged plasmids in hepatocytes throughout the lobule 24 hours post-injection. Representative images demonstrating quantification of BFP+ cells across the lobule by separating the central-to-portal vein axis into deciles, defined by 20μm rings radiating from the central venule.* ***(b)*** *Schematic showing the segmentation of deciles along the port-central axis (created with BioRender.com) and dot-plot illustrating the quantification of the number of BFP+ cells per decile.* ***(c)*** *A second-order polynomial (quadratic) regression analysis was conducted to assess for linearity (data shown as mean ± SD, n=7 with 5 central-to-portal axes quantified in each).*

5.3 Upregulation of NICD1/Akt in Hepatocytes Induces Biliary Neoplasms Throughout the Liver

Four weeks post-HTVI with NICD1/Akt, some hepatocytes exhibited marked morphological changes, becoming smaller in size, more cuboidal, and reorganising into duct-like structures forming lumens, as demonstrated by the haematoxylin and eosin (H&E) staining (Figure 5.2a-b). The proliferative activity of the cells within these lesions was established by Ki-67 immunohistochemistry, with nuclear positivity indicating mitotic activity in the cells comprising the neoplasms (Figure 5.2c).

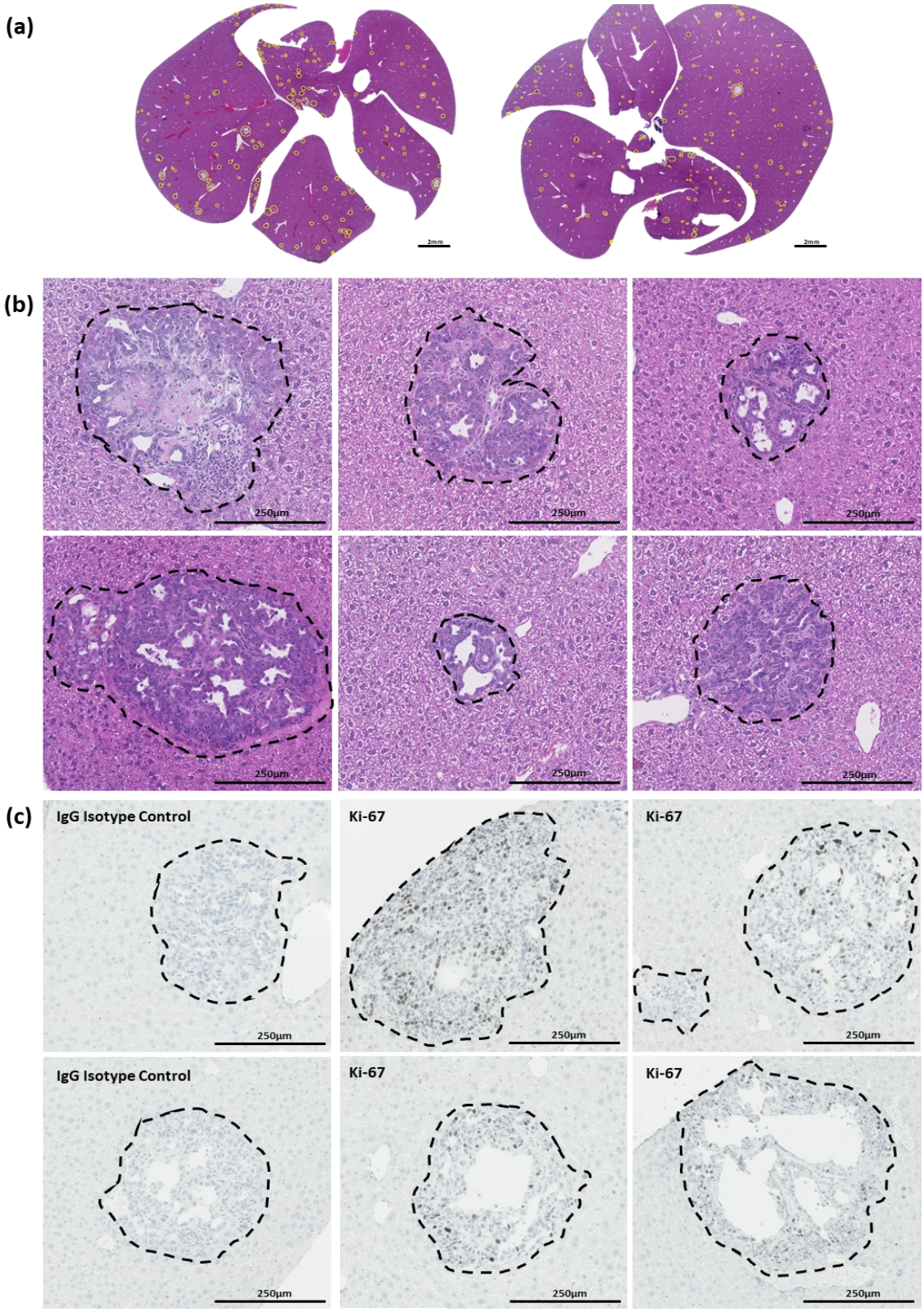

Figure 5.2: Hepatocyte-derived Biliary Neoplasms Following Upregulation of NICD1/Akt Signalling via HTVI. ***(a)*** *Representative H&E-stained whole sectioned (5µm) C57Bl6/J wild-type mouse livers 4 weeks post-NICD1/Akt HTVI. Biliary neoplasms were identified in H&E-stained sections as aggregations of cuboidal/columnar epithelial cells forming duct-like lumens (Highlighted in yellow, Scale bars = 2mm).* ***(b)*** *High magnification micrographs of H&E-stained biliary neoplasms (Scale bars = 250µm).* ***(c)*** *Representative DAB-stained images showing proliferation marker Ki-67 positivity (brown (Scale bars = 250µm).*

Both plasmids employed in this study – pT3-EF1a-Myc-NICD1 (20 µg) and pSBbi-BH-*myr*-AKT-HA (10 µg) – contained integrated epitope tags (Myc and HA, respectively), enabling detection by IHC and IF [357,358,389]. DAB staining of Myc- and HA-tags demonstrated the presence of both markers within the neoplasms, with co-expression of both tags also being consistently observed via IF, and no cells displaying HA-tag positivity in the absence of the Myc-tag (n=5) (Figure 5.3). Consequently, throughout this chapter, HA-tag-positive neoplasms are assumed to have also incorporated the NICD1-Myc-tagged plasmid, as the HA signal was more readily detectable by immunostaining.

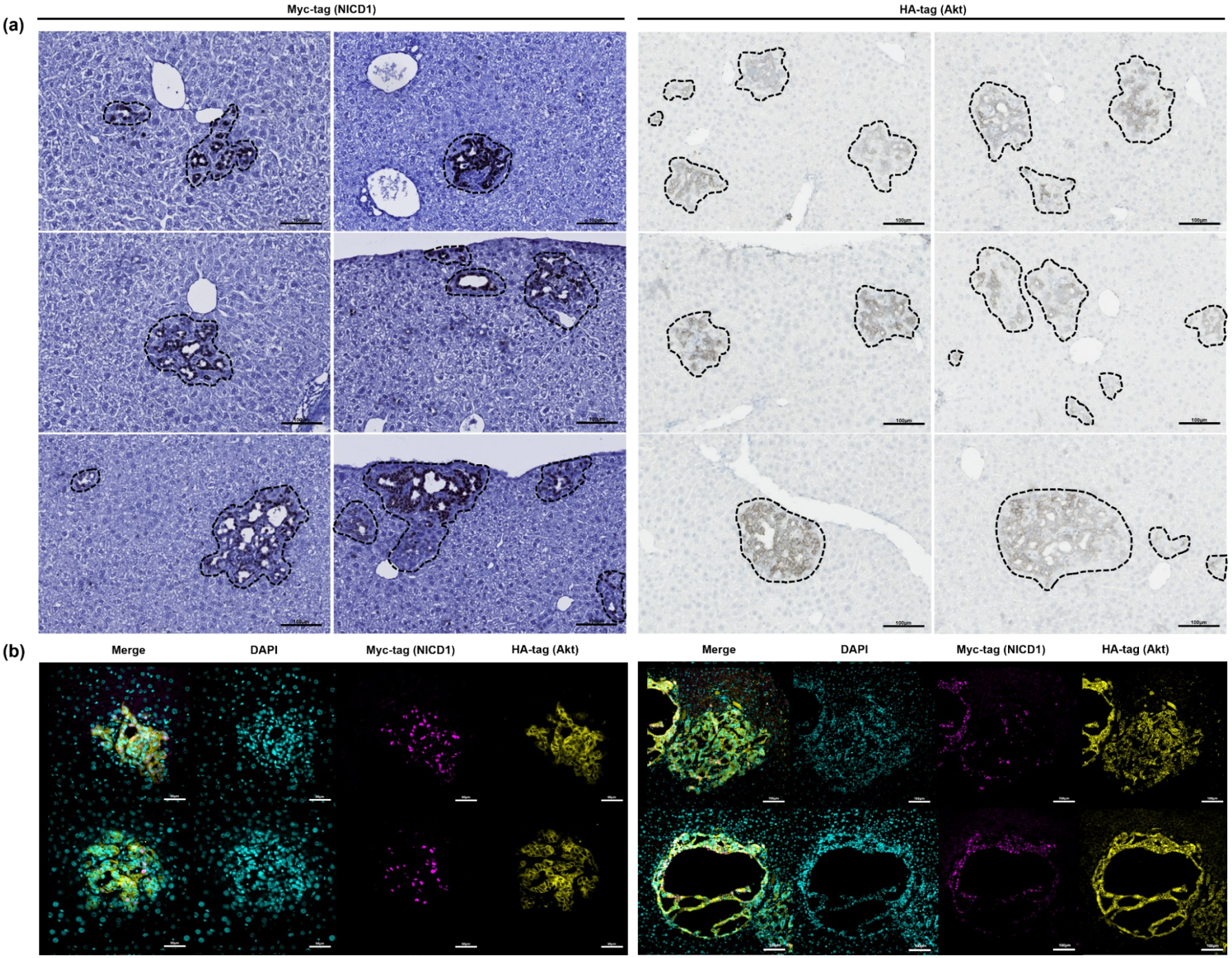
(a)
Myc-tag (NICD1)
HA-tag (Akt)
(b)
Merge
DAPI
Myc-tag (NICD1)
HA-tag (Akt)
Merge
DAPI
Myc-tag (NICD1)
HA-tag (Akt)

Figure 5.3: Hepatocyte-Derived Biliary Neoplasms Express Both Myc- and HA-Tags Indicating Concurrent Uptake of NICD1 and Akt Plasmids. ***(a)*** *Representative DAB-stained HA-tag (Akt) and Myc-tag (NICD1)-expressing biliary neoplasms (Scale bars = 100μm).* ***(b)*** *Representative immunofluorescent staining of Myc-tagged NICD1 and HA-tagged Akt in HTVI-induced neoplasms (Scale bars = 50μm/100μm).*

Immunohistochemical analysis revealed that upon formation of hepatocyte-derived neoplastic lesions, cells transfected with NICD1/Akt plasmids demonstrated nuclear positivity for the early BEC marker Sox9 and cytoplasmic expression of K19, a mature BEC marker; with expression of both markers absent from the surrounding non-transfected parenchyma (Figure 5.4a-b).

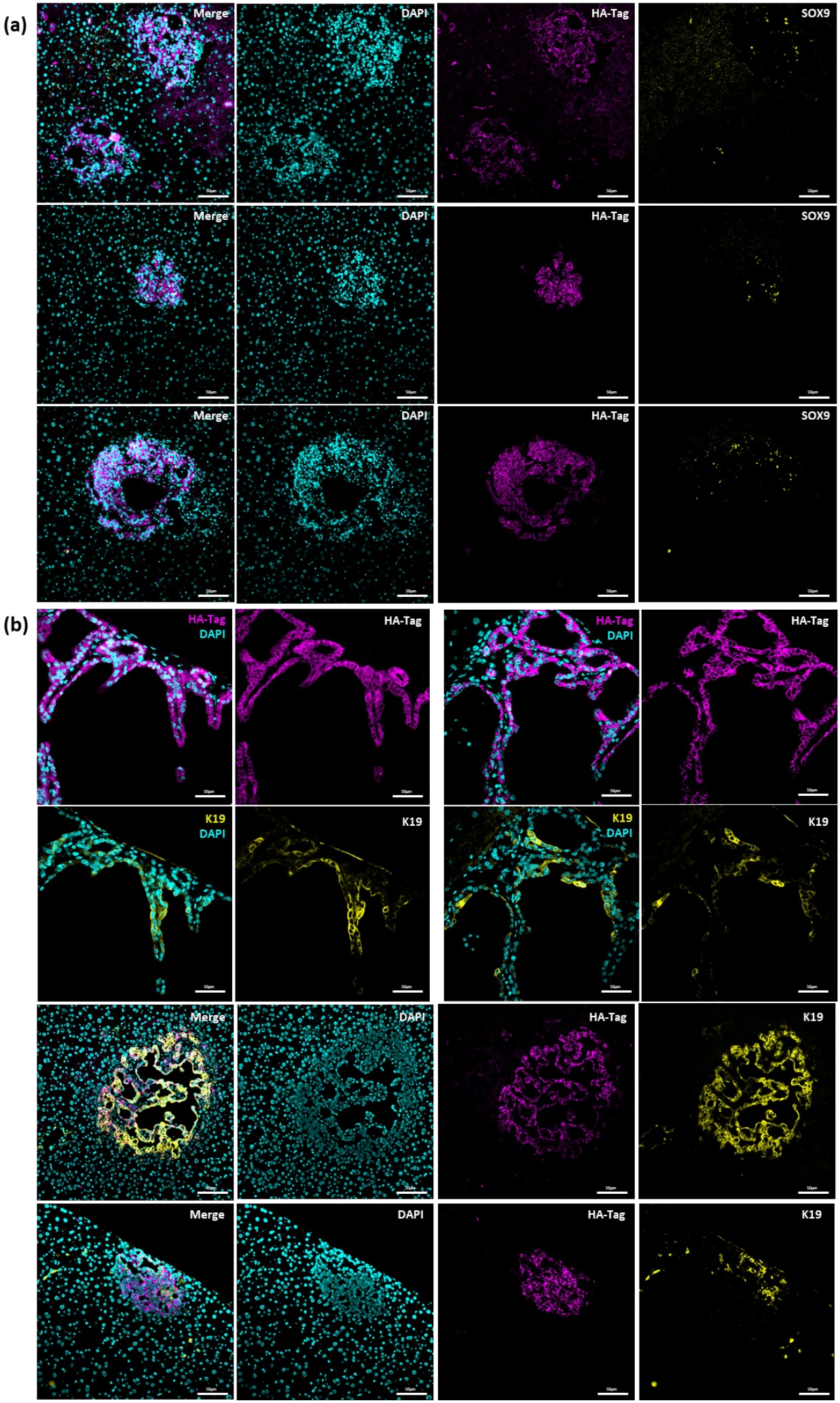
(a)
Merge
DAPI
HA-Tag
SOX9
Merge
DAPI
HA-Tag
SOX9
Merge
DAPI
HA-Tag
SOX9
(b)
HA-Tag
DAPI
HA-Tag
HA-Tag
DAPI
HA-Tag
K19
DAPI
K19
K19
DAPI
K19
Merge
DAPI
HA-Tag
K19
Merge
DAPI
HA-Tag
K19

Figure 5.4: Biliary Neoplasms Formed Following Upregulation of NICD1/Akt Signalling in Hepatocytes Express Biliary Epithelial Cell (BEC) Markers K19 and Sox9. (a) *Representative immunofluorescent staining of HA-tagged Akt and the early BEC marker Sox9 in HTVI-induced neoplasms (Scale bars = 50μm).* ***(b)*** *Representative immunofluorescent staining of HA-tagged Akt and the mature BEC marker Cytokeratin 19 (K19) in HTVI-induced neoplasms (Scale bars = 50μm).*

5.4 Phenotypic Changes in NICD1/Akt Upregulated Zone 1 and 3 Hepatocytes

Having demonstrated that the co-activation of NICD1/Akt results in the appearance of tagged biliary neoplasms, the study next sought to determine whether reprogramming was uniform across the liver lobule. To address this, Gls2CreER-mT/mG and GSCreER-mT/mG mice were administered tamoxifen seven days prior to HTVI of NICD1/Akt. This, resulted in mGFP expression, which facilitated the lineage tracing of the periportal (Gls2+) and pericentral (GS+) hepatocytes, respectively. Four weeks following HTVI, immunostaining for HA-tag (Akt) confirmed the induction of hepatocyte-derived biliary neoplasms in both models (Figure 5.5a-b). Individual counts of the HA-tag-positive neoplasms revealed no significant difference in the number of neoplasms between the Gls2CreER-mT/mG group (mean = 109.8, n=5) and the GSCreER-mT/mG group (mean = 93, n=5) (Two-tailed Mann-Whitney U test; U = 12, exact p>0.9999) (Figure 5.5c). This indicated a similar distribution and range in neoplasm burden between both groups.

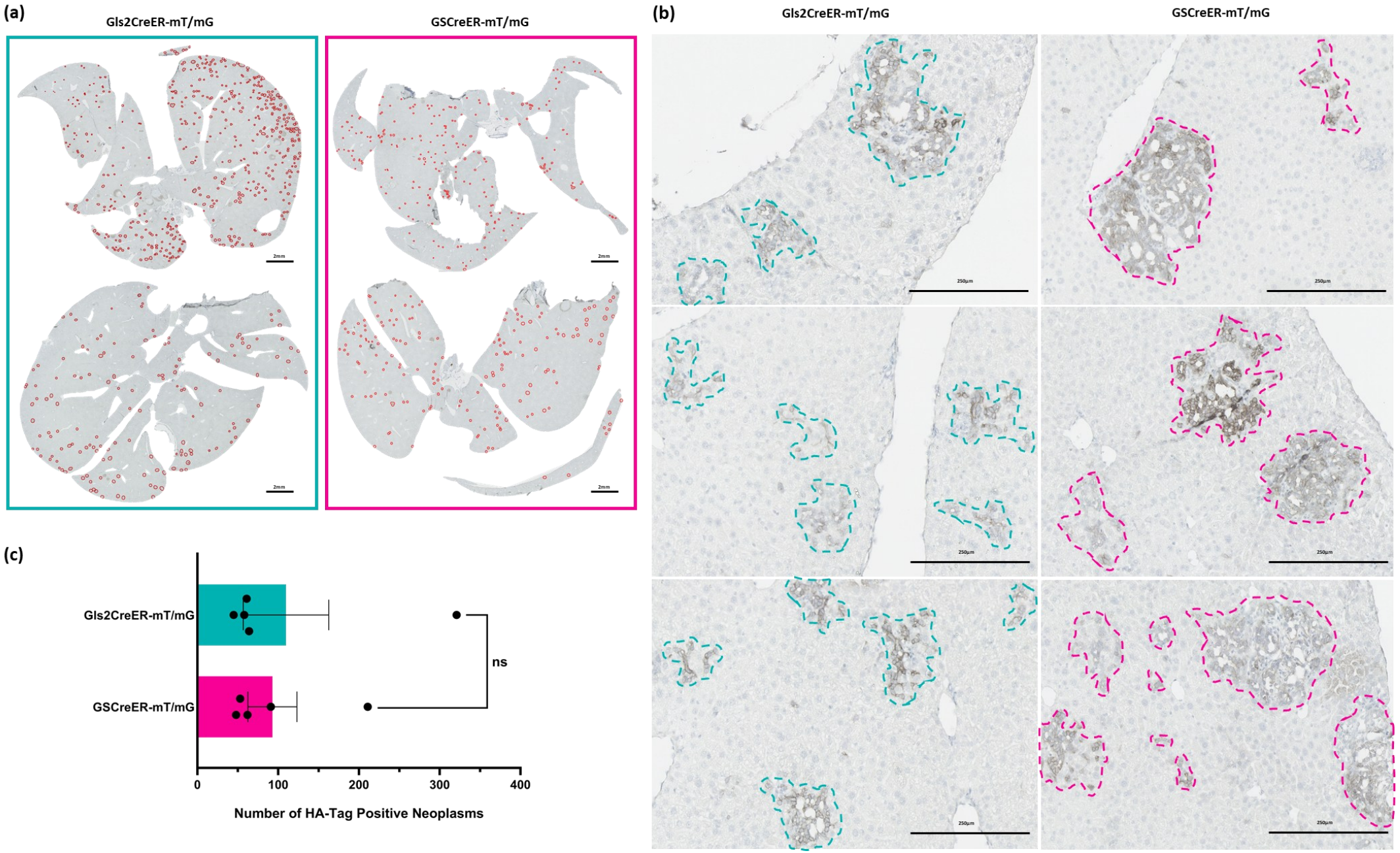
(a)
Gls2CreER-mT/mG
GSCreER-mT/mG
2mm
(b)
Gls2CreER-mT/mG
GSCreER-mT/mG
250μm
(c)
Gls2CreER-mT/mG
GSCreER-mT/mG
ns
0
100
200
300
400
Number of HA-Tag Positive Neoplasms

Figure 5.5: Biliary Neoplasms are Derived from NICD1/Akt-Transformed Hepatocytes. (a) *Representative DAB-stained whole sectioned (5µm) Gls2CreER-mT/mG and GSCreER-mT/mG mouse livers 7 days post-NICD1/Akt HTVI, demonstrating the number and distribution of biliary neoplasms (Neoplasms highlighted in red, Scale bars = 2mm).* ***(b)*** *Representative DAB-stained HA-tag positive biliary neoplasms formed in both the Gls2CreER-mT/mG (Cyan) and GSCreER-mT/mG (Magenta) mouse strains (Scale bars = 20µm).* ***(c)*** *Quantification of HA-tag positive neoplasms in Gls2CreER-mT/mG and GSCreER-mT/mG mice (Displayed as Mean ± SEM, n=5 per strain). No significant difference in neoplasm counts was observed between groups (Two-tailed Mann-Whitney U test, U=12, exact p > 0.9999).*

When immunostaining for mGFP to assess the contribution of the cre-recombined cells of interest in both mouse models, a clear zonal difference was noted in the cells' involvement in the formation of HA-tag-positive biliary neoplasms. In Gls2CreER-mT/mG mice (n=5), mGFP+ Gls2-expressing periportal hepatocytes displayed altered morphology and actively contributed to the formation of biliary neoplasms, demonstrating a marked reduction in cell size, adopting a cuboidal morphology, and frequently clustering together to form distinct lumen-like structures, actively contributing to biliary neoplasm formation (Figure 5.6a). Consistent with their transition towards a biliary phenotype, immunofluorescent staining demonstrated that mGFP+ cells in Gls2Cre-mT/mG livers also expressed the early biliary marker Sox9 (Figure 5.6b).

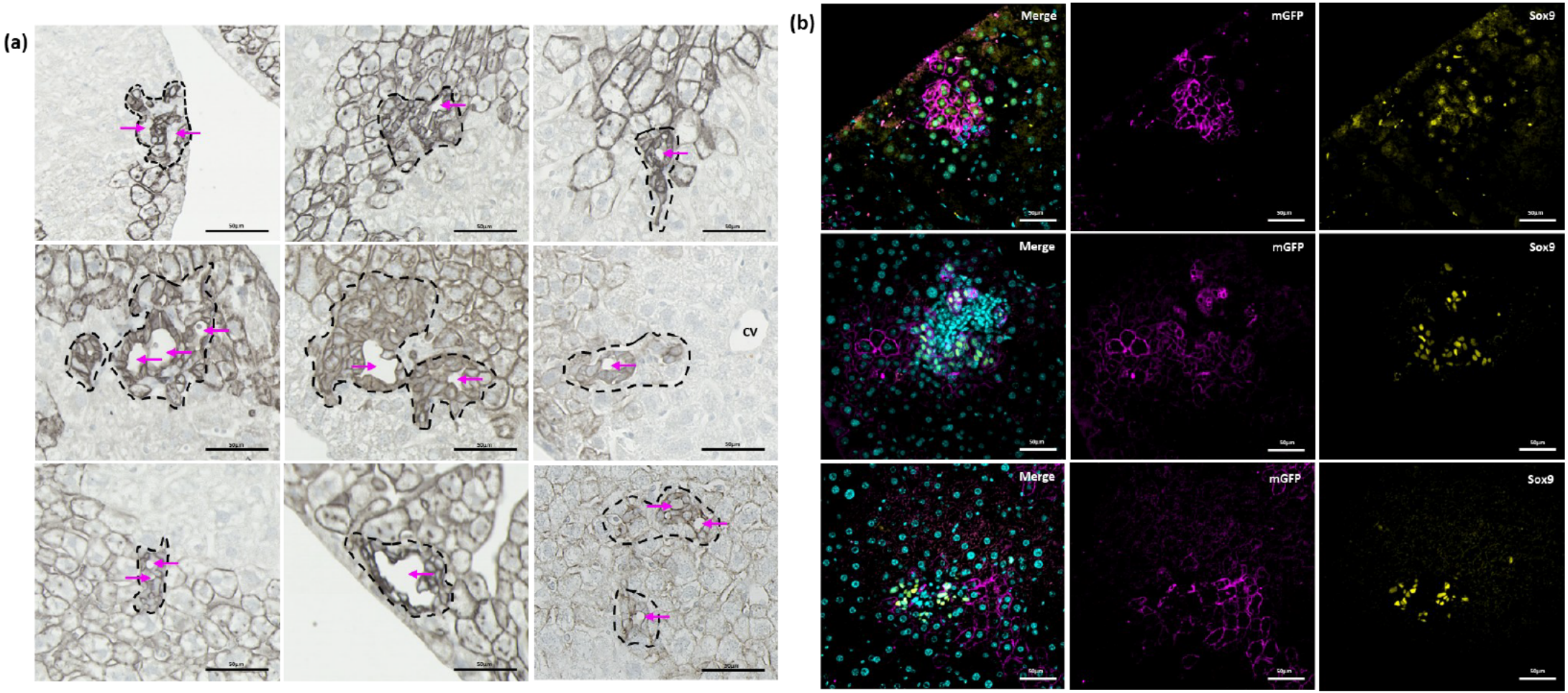

Figure 5.6: Gls2-expressing Hepatocytes Contribute to NICD1/Akt-Induced Neoplasms. ***(a)*** *Representative DAB-staining of mGFP in NICD1/Akt HTVI-treated Gls2CreER-mT/mG mice (n=5) demonstrating a change in cell morphology and formation of lumens (magenta arrows) in NICD1/Akt-upregulated cells 4 weeks post-treatment (Scale bars = 50μm).* ***(b)*** *Representative immunofluorescent staining of the mGFP+ recombined Gls2-expressing cells and biliary marker Sox9 in Gls2CreER-mT/mG mouse livers 4 weeks post-HTVI of the NICD1/Akt plasmids.*

Despite clear evidence that GS-expressing cells had efficiently taken up the NICD1/Akt plasmids (Figure 5.7a) and were frequently located adjacent to HA-tag-expressing neoplasms (Figure 5.7b), the mGFP+ GS-expressing pericentral hepatocytes in the GSCreER-mT/mG livers largely retained normal hepatocyte morphology. Notably, recombined GS-Cre-labelled cells showed no overt signs of morphological transition or direct contribution to neoplastic lesions (Figure 5.7c), suggesting a potential resistance to biliary reprogramming and tumorigenesis under these experimental conditions.

To address whether this lack of neoplasm formation reflects the much lower number of GS+ cells of interest in the GSCreER-T/mG system, a direct quantitative comparison was performed. In the Gls2CreER-mT/mG system, the average Gls2+ population made up 32.31% of the liver (n=5; as reported in Figure 4.4), which, when considering the average total number of hepatocytes isolated from murine livers in the present study was 1.09 x 10^8 hepatocytes (Figure 3.1), reflects an average total of 35,217,900 Gls2+ hepatocytes. Following upregulation of NICD1/Akt in the livers of both mouse models, an average of 101.4 neoplasms formed per liver (Figure 5.5c). This yields a hypothetical formation frequency of $\frac{101.4}{35{,}217{,}900} \approx 2.8\,x\,10^{-6}$ neoplasms per mGFP+ (Gls2+) cell. By contrast, the GSCreER-mT/mG system labels only 18,551,800 hepatocytes per animal (with a mean of only 17.02% of the hepatocytes being GS+; n=5; Figure 4.4). Applying the same calculated transformation efficiency, the average GSCreER-mTmG animal would be expected to generate $0.00000288 \times 18{,}551{,}800 \approx 53.43$ mGFP+ neoplasms, assuming equivalent susceptibility to the NICD1/Akt stimulus.

Statistically, to assert that the observed lack of GS+ neoplasms being formed is due to biological resistance rather than random sampling error, it is necessary to determine how many mGFP-negative neoplasms in GSCreER-mT/mG mice are required to confidently exclude that GS cells do not contribute towards neoplasm formation at the above calculated rate. By binomial probability, the chance of observing zero labelled neoplasms in n animals (each expected to form 53.43 neoplasms) is $(1 - 0.9999479)^n = (0.00000288)^n$. To achieve 95% confidence, this probability must fall below 0.05, so $(0.00000288)^n < 0.05$, giving $n > \frac{\log(0.05)}{\log(0.00000288)} \approx 0.23$. Thus, from these calculations, due to the high number of neoplasms formed per mouse, it appears as though at least one GSCreER-mT/mG animal must be analysed without a single labelled neoplasm observed to statistically exclude the possibility that pericentral hepatocytes are under-sampled rather than intrinsically resistant. Collectively, these calculations demonstrate that the absence of mGFP+ neoplasms in the statistically robust cohort of GSCreER-mT/mG animals (n=5) supports true pericentral resistance to reprogramming and neoplastic transformation, rather than a technical artefact due to limited labelling efficiency.

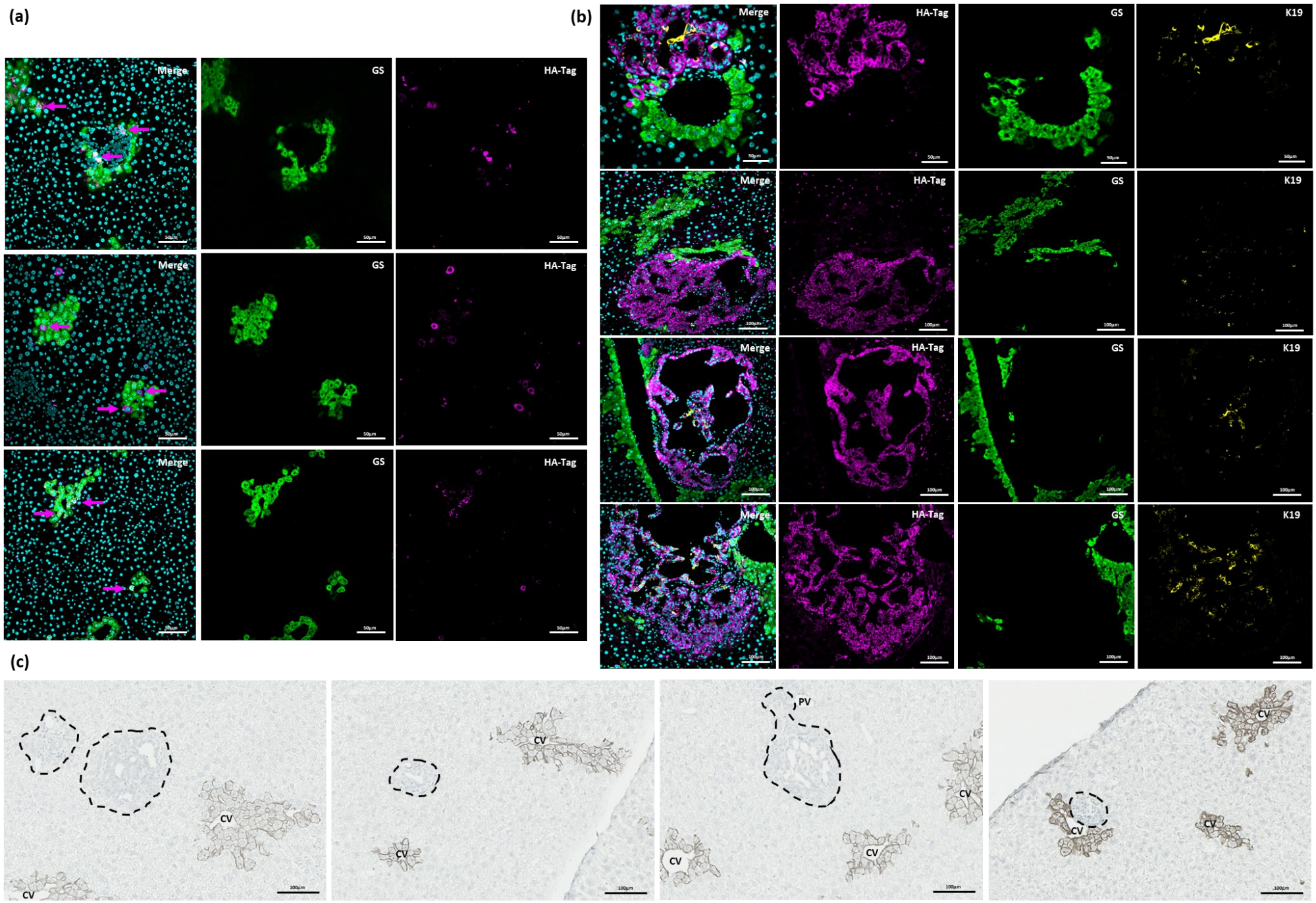
(a)
Merge
GS
HA-Tag
(b)
Merge
HA-Tag
GS
K19
(c)
CV
PV

Figure 5.7: GS-expressing Hepatocytes Exhibit No Morphological Change in Response to NICD1/Akt Upregulation. (a) *Representative immunofluorescent staining confirming plasmid uptake (HA-tag, Magenta) by GS-expressing cells (Green) (Scale bars = 50μm).* ***(b)*** *Representative immunofluorescent staining demonstrating GS expression (Green) in cells in proximity with HA-tag positive (Magenta) neoplastic lesions (Scale bars = 100μm/50μm). Expression of biliary marker K19 in neoplastic regions is demonstrated in yellow.* ***(c)*** *Representative DAB-immunostaining of mGFP in NICD1/Akt HTVI-treated GSCreER-mT/mG mice (n=5) demonstrating unchanged morphology of recombined DAB+ hepatocytes (Biliary neoplasms highlighted in black, Scale bars = 50μm). Tissue collection and staining were conducted 5 weeks post-tamoxifen gavage and 4 weeks post-HTVI of NICD1/Akt plasmids.*

5.4.1 Fluorescent Activated Cell Sorting of Recombined GFP+ Hepatocytes from Gls2CreER-mT/mG and GSCreER-mT/mG Models

Flow cytometry analysis (FACS) was performed to isolate mGFP+ (recombined) and mTom+ (non-recombined) cells in Gls2CreER-mT/mG and GSCreER-mT/mG mice for downstream RNA-sequencing (Figure 5.8a). Cells were isolated from Gls2CreER-mT/mG mice following treatment with each of three conditions: (a) tamoxifen gavage only, (b) tamoxifen gavage followed by HTVI with a BFP-tagged plasmid backbone, or (c) tamoxifen gavage followed by HTVI with BFP-tagged NICD1/Akt. Similarly, mGFP+ and mTom+ cells were isolated from the GSCreER-mT/mG mice following the three treatments, but instead of a gavage of tamoxifen, the mice were gavaged with corn oil vehicle control.

Although a distinct BFP^+ population could be detected in livers from mice that had received HTVI with either plasmid backbone or NICD1/Akt (0.97% BFP+ in Gls2; 0.19% BFP+ in GS), the frequency of these cells was too low to allow reliable gating and sorting of mGFP+/BFP+ double-positive hepatocytes as a discrete population (Figure 5.8a). Therefore, cells were segregated based only on Cre recombination status (mGFP+ vs mTom+), and the effect of NICD1/Akt expression was assessed post-sequencing. The fidelity of mGFP and mTom signals in the FACS-sorted cells was confirmed by immunofluorescent staining of cytospun cells (Figure 5.8b), which demonstrated bright mGFP in recombined hepatocytes and a weaker but still detectable mTom signal in non-recombined hepatocytes.

For all analyses, hepatocytes were pre-gated by forward/side scatter and doublet exclusion before quantifying the relative proportion of mGFP+ and mTom+ populations. Within this hepatocyte gate, there was a significant increase in the proportion of recombined (mGFP+) hepatocytes in Gls2CreER-mT/mG mice that received NICD1/Akt (51.267% ± 1.545%) compared to tamoxifen controls without HTVI (33.167% ± 0.296%; p=0.0002; Figure 5.8c). Likewise, the proportion of mGFP+ cells was

significantly higher in the NICD1/Akt group compared to the plasmid backbone control (33.4% ± 0.72%; p=0.0003), indicating enhanced expansion or survival of the recombined population following NICD1/Akt delivery.

Conversely, in GSCreER-mT/mG mice the non-recombined (mTom+) hepatocyte population was significantly increased in the NICD1/Akt-treated group (61.9% ± 5.06%) compared with both vehicle controls (43.8% ± 4.44%; p=0.0002) and plasmid backbone HTVI (46.1% ± 0.38%; p=0.0013) which indicates that NICD1/Akt expression promoted the expansion of unrecombined hepatocytes (Figure 5.8c).

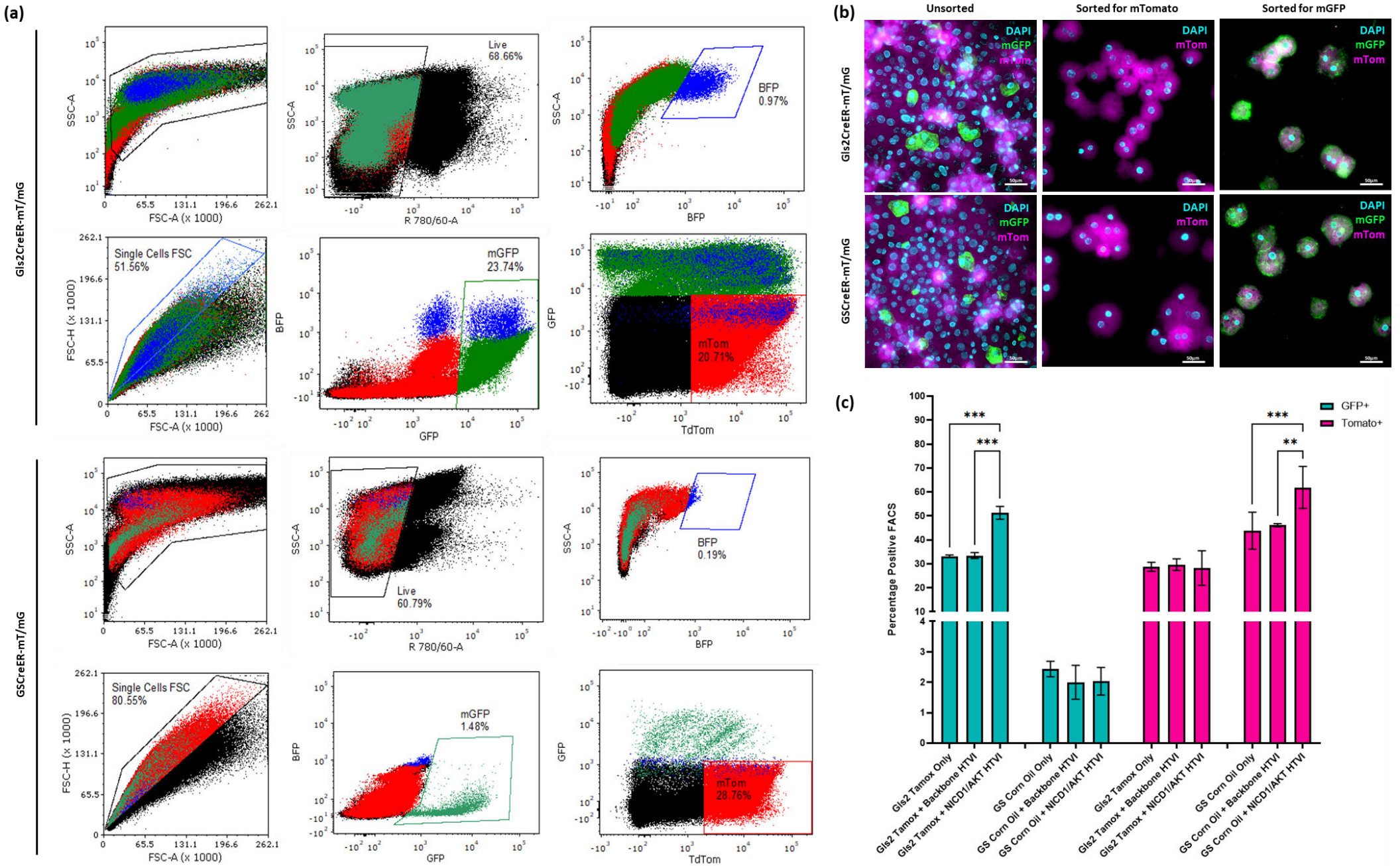
(a)
Gls2CreER-mT/mG
GSCreER-mT/mG
SSC-A
FSC-A (x 1000)
Live
68.66%
R 780/60-A
BFP
0.97%
Single Cells FSC
51.56%
FSC-H (x 1000)
mGFP
23.74%
GFP
mTom
20.71%
TdTom
Live
60.79%
BFP
0.19%
Single Cells FSC
80.55%
mGFP
1.48%
mTom
28.76%
(b)
Unsorted
Sorted for mTomato
Sorted for mGFP
DAPI
mGFP
mTom
(c)
Percentage Positive FACS
GFP+
Tomato+
***
**
Gls2 Tamox Only
Gls2 Tamox + Backbone HTVI
Gls2 Tamox + NICD1/AKT HTVI
GS Corn Oil Only
GS Corn Oil + Backbone HTVI
GS Corn Oil + NICD1/AKT HTVI

Figure 5.8: FACS Sorting and Characterisation of Membranous GFP (mGFP) and Tomato (mTomato) Positive Cells from Gls2CreER-mT/mG and GSCreER-mT/mG Livers. *Cells were isolated from mice treated with one of three conditions: (1) Tamoxifen (Gls2) or corn oil (GS) gavage only, (2) Tamoxifen (Gls2) or corn oil (GS) gavage followed by HTVI with a plasmid backbone, or (3) Tamoxifen gavage followed by HTVI with NICD1/Akt (Tagged with blue fluorescent protein [BFP] reporter).* ***(a)*** *Representative FACS gating plots showing BFP-tagged Akt expression in recombined mGFP+ and mTomato+ cells isolated from both mouse strains, 4 weeks post-NICD1/Akt HTVI (n=4 per strain).* ***(b)*** *Immunofluorescent staining of cytospin-prepared cells isolated from tamoxifen/corn oil-treated Gls2- and GSCreER-mT/mG mice post-NICD1/Akt HTVI, demonstrating expression of mGFP (Green) and/or mTomato (Magenta) in sorted and unsorted populations.* ***(c)*** *Bar chart depicting the percentage of mGFP+ and mTomato+ cells within each treatment group and mouse strain. Data are presented as mean ± SD, analysed by two-way ANOVA with Tukey HSD multiple comparisons (**p ≤ 0.01; ***p ≤ 0.001).*

5.5 Transcriptomic Changes Induced by NICD1/Akt Upregulation in Periportal and Pericentral Hepatocytes

To establish how the upregulation of NICD1/Akt affected the two hepatocyte populations of interest (Gls2- and GS-expressing) at the transcriptomic level, the mGFP+ cells isolated from both mouse lines post-NICD1/Akt and plasmid backbone HTVIs were prepared for QuantSeq 3' mRNA sequencing. Differential expression analysis focused first on mGFP+ hepatocytes from Gls2CreER-mT/mG mice, comparing those transfected with NICD1/Akt to those injected with the plasmid backbone control (Figure 5.9b). This comparison identified substantial transcriptional reprogramming in the NICD1/Akt group, with 328 genes identified as significantly upregulated and 5 genes significantly downregulated in the dataset (adjusted $p < 0.05$, $|\log_2 FC| > 1$). Upregulated transcripts included mitochondrial genes (eg. mt-Co3, mt-Nd3, mt-Atp8, mt-Co2, mt-Tp, mt-Tn, mt-Nd4l) and nuclear-encoded genes (Snord118, Gls2, Pnisr, Rsbn1, Ino80). The relatively few downregulated transcripts (Cyp2C23, Onecut1 (Hnf6), Bcl7c, Rnf138, Thoc6) represent potential markers of hepatocyte identity and transcriptional regulation.

In addition to the volcano plot (Figure 5.9b), global expression profiles of significant differentially expressed genes (DEGs) were assessed in FACS-sorted mGFP+ hepatocytes from Gls2CreER-mT/mG mice by heatmap visualisation (Figure 5.9c). This analysis compared NICD1/Akt-treated recombined hepatocytes with backbone-treated controls and highlighted apparent heterogeneity in the transcriptional responses of the treated samples to NICD1/Akt signalling upregulation.

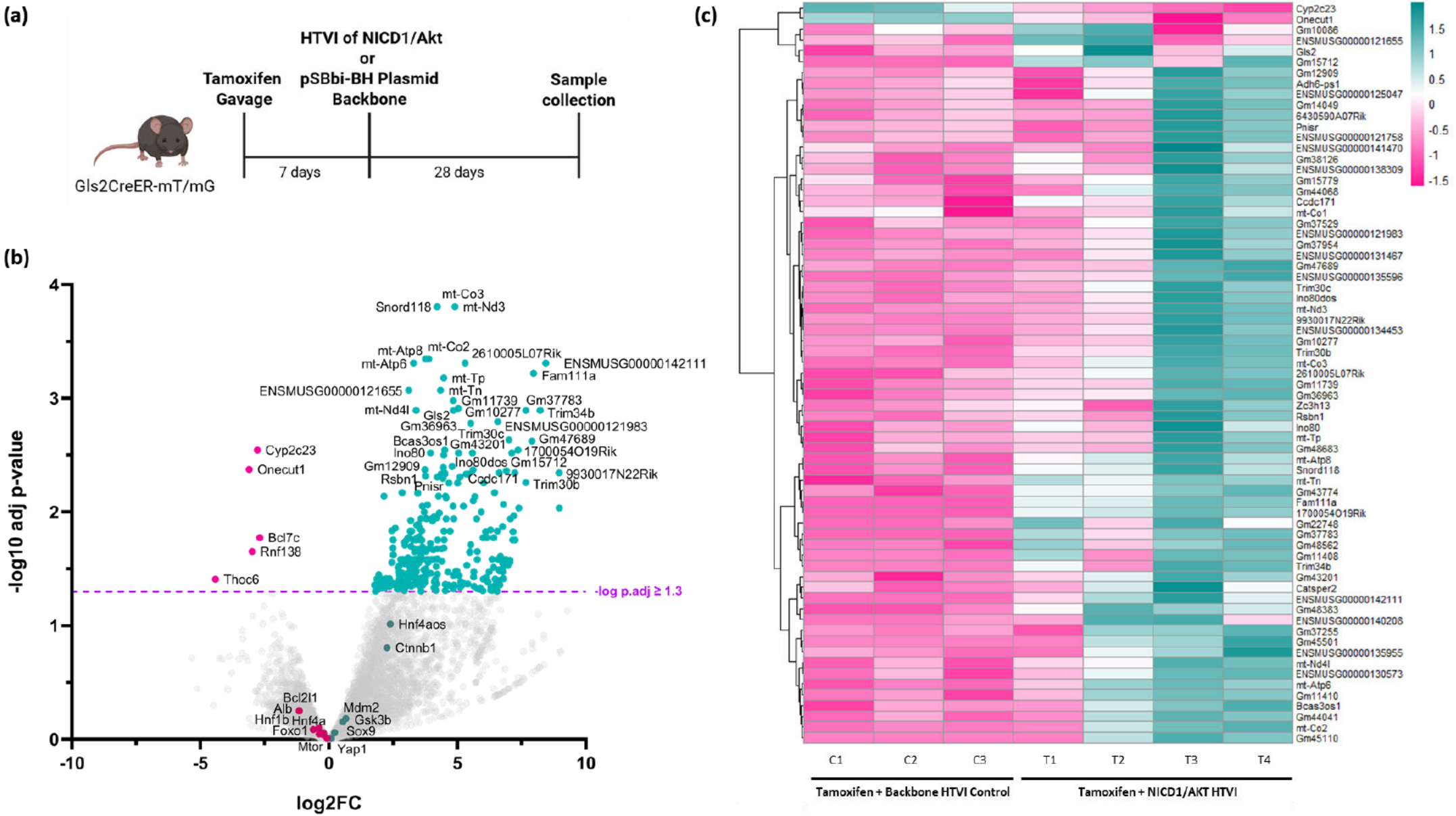
(a)
HTVI of NICD1/Akt
or
pSBbi-BH Plasmid
Backbone
Tamoxifen
Gavage
Sample
collection
7 days
28 days
Gls2CreER-mT/mG
(b)
-log10 adj p-value
log2FC
-log p.adj ≥ 1.3
mt-Co3
Snord118
mt-Nd3
mt-Atp8
mt-Co2
2610005L07Rik
mt-Atp6
ENSMUSG00000142111
Fam111a
mt-Tp
ENSMUSG00000121655
mt-Tn
Gm11739
Gm37783
mt-Nd4l
Gls2
Gm10277
Trim34b
Gm36963
ENSMUSG00000121983
Trim30c
Gm47689
Bcas3os1
Gm43201
Cyp2c23
Ino80
1700054O19Rik
Onecut1
Ino80dos
Gm15712
Gm12909
9930017N22Rik
Rsbn1
Cdc171
Pnisr
Trim30b
Bcl7c
Rnf138
Thoc6
Hnf4aos
Ctnnb1
Bcl2l1
Alb
Mdm2
Hnf1b
Hnf4a
Gsk3b
Foxo1
Sox9
Mtor
Yap1
(c)
C1
C2
C3
T1
T2
T3
T4
Tamoxifen + Backbone HTVI Control
Tamoxifen + NICD1/AKT HTVI

Figure 5.9: Differential Gene Expression in Gls2creER-mT/mG Mice Following Hydrodynamic Tail Vein Injection of NICD1/Akt. ***(a)*** *Schematic demonstrating timeline of tamoxifen gavage and NICD1/Akt HTVI treatment in the Gls2CreER-mT/mG mice (n=4).* ***(b)*** *Volcano plot comparing mGFP+ hepatocytes isolated from mice dosed with tamoxifen and HTVI of plasmid backbone vs mice dosed with tamoxifen and HTVI of NICD1/Akt. Highlighted genes include all up- (cyan) and downregulated (magenta) genes that passed the DESeq2 analysis (Benjamini-Hochberg) cutoff of adjusted p<0.05 (-log10 adjusted p<1.3) and log2 fold change > 1 (upregulated, cyan) or log2 fold change < -1 (downregulated, magenta).* ***(c)*** *Expression heatmap of significantly upregulated (p>0.05) and downregulated (p<0.05) differentially expressed genes. Each row represents a gene, and each column corresponds to an individual mouse (n = 3 control, n = 4 treated).*

Gene Ontology (GO) enrichment analysis was conducted on significantly altered DEGs (log2 fold change > 1 [upregulated] or log2 fold change < -1 [downregulated]) to identify what molecular functions (MF) and biological processes (BP) the NICD1/Akt upregulation may have influenced in mGFP+ cells isolated from Gls2CreER-mT/mG mice (n=4) (Figure 5.10). In the MF category (cyan section), enrichment in functions such as nucleic acid binding, oxidoreduction-driven active transmembrane transporter activity (including proton and electron transporters), cytochrome c oxidase activity, ATP-dependent helicase and transcription regulator activity, and NADH dehydrogenase activity are highlighted. These terms indicate elevated expression of genes involved in fundamental transcriptional control, mitochondrial respiratory chain activity, and energy-coupled molecular transport.

In the BP category (magenta section), the significantly enriched processes include metabolic process regulation, regulation of RNA biosynthetic process, chromatin remodelling, mitochondrial ATP synthesis, cell-cell signalling, immune modulation, embryonic organ morphogenesis, and cell division. These categories point to widespread transcriptomic reprogramming, impacting not only cellular metabolism and genetic regulation but also developmental pathways and immune-related functions (Full list of GO terms can be found in Appendix Table 6).

Figure 5.10: Gene Ontology Enrichment Analysis of mGFP+ Cells Fluorescently Sorted from Gls2CreER-mT/mG Mouse Livers. *Differentially expressed genes were identified through DESeq2 analysis, following which GO Enrichment analysis was conducted on the datasets in Galaxy using a Benjamini-Hochberg multiple test correction (adjusted $p < 0.05$). GO terms were further filtered to show only those occurring at a frequency of >5% within the dataset. The GO terms are rank-ordered within each category by their frequency of occurrence within the study, with larger bubbles indicating higher frequencies and colours (cyan-magenta) reflecting q-values. BP – Biological Processes; MF – Molecular Functions.*

To define the impact of NICD1/Akt upregulation in GS-expressing hepatocytes, FACS-sorted cells from GSCreER-mT/mG mice were compared between two cohorts: (1) corn oil gavage followed by HTVI with backbone control, and (2) corn oil gavage followed by HTVI with the NICD1/Akt plasmid (Figure 5.11a). Differential expression analysis revealed ten genes significantly upregulated in NICD1/Akt-treated hepatocytes versus backbone controls: Fosb, Trim30b, ENSMUSG00000121655, Agfg2, Atf3, Ccdc200, Rhpn2, Ugt2b37, Gm49260, and Gm17168 (Figure 5.11b, cyan). Conversely, seven genes showed significant downregulation: Onecut1 (Hnf6), Gadd45g, Aacs, Gm36220, Bhmt1b, 1810017P11Rik, and 1810019D21Rik (Figure 5.11b, magenta). Statistical thresholds were set as adjusted $p \leq 0.05$ and $|\log_2 FC| \geq 1$, corresponding to $-\log_{10}$ p.adj ≥ 1.3.

A subset of genes associated with the activation of Notch and AKT signalling – including Alb, Glul, Tbx3, Yap1, and Akt1 (upregulated), and Mdm2, Sox9, Mtor, Oat, Hes1, and Hnf4α (downregulated) – demonstrated directional but non-significant changes in NICD1/Akt-treated samples. These trends may nonetheless be relevant given the established roles of these genes in defining a hepatocyte or BEC lineage.

Heatmap analysis (Figure 5.11c) of the significant DEGs revealed robust clustering of samples according to treatment condition, with all control samples (C1–C3) tightly grouped and a clear separation from NICD1/Akt-treated samples (T1–T4). Genes upregulated in controls were consistently downregulated with NICD1/Akt treatment (eg., Bhmt1b, Gadd45g, Onecut1 (Hnf6), Aacs, Gm36220, 1810017P11Rik, 1810019021Rik), while Rhpn2, Atf3, Ccdc200, Trim30b, and Ugt2b37 displayed the opposite pattern.

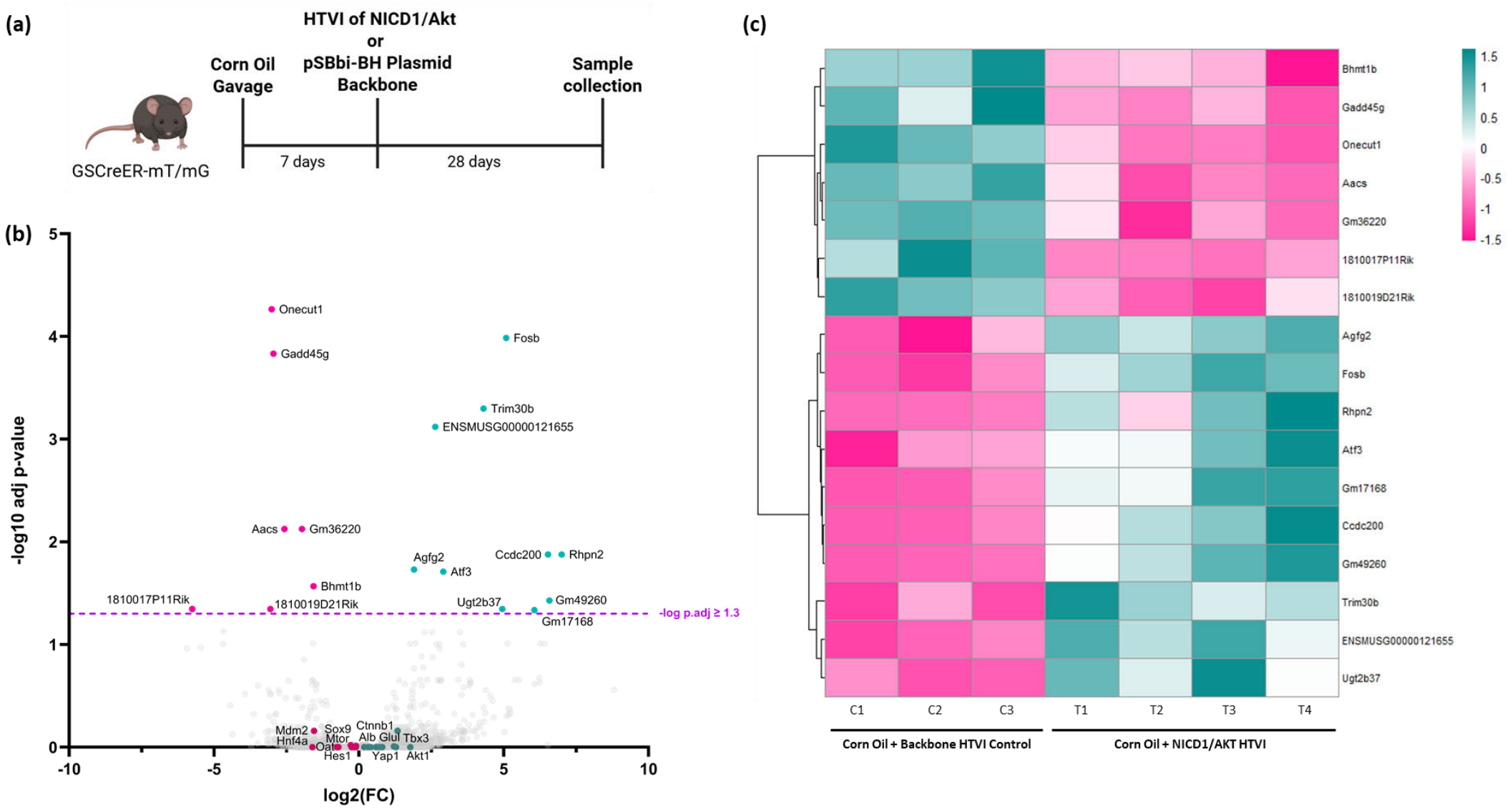
(a)
HTVI of NICD1/Akt
or
pSBbi-BH Plasmid
Backbone
Corn Oil
Gavage
Sample
collection
GSCreER-mT/mG
7 days
28 days
(b)
-log10 adj p-value
log2(FC)
Onecut1
Gadd45g
Fosb
Trim30b
ENSMUSG00000121655
Aacs
Gm36220
Agfg2
Ccdc200
Rhpn2
Atf3
Bhmt1b
1810017P11Rik
1810019D21Rik
Ugt2b37
Gm49260
Gm17168
-log p.adj ≥ 1.3
Mdm2
Hnf4a
Sox9
Mtor
Oat
Hes1
Ctnnb1
Alb
Glul
Yap1
Tbx3
Akt1
(c)
Bhmt1b
Gadd45g
Onecut1
Aacs
Gm36220
1810017P11Rik
1810019D21Rik
Agfg2
Fosb
Rhpn2
Atf3
Gm17168
Ccdc200
Gm49260
Trim30b
ENSMUSG00000121655
Ugt2b37
C1
C2
C3
T1
T2
T3
T4
Corn Oil + Backbone HTVI Control
Corn Oil + NICD1/AKT HTVI

Figure 5.11: Differential Gene Expression in GS2creER-mT/mG Mice Following Hydrodynamic Tail Vein Injection of NICD1/Akt. (a) *Schematic demonstrating timeline of corn oil gavage NICD1/Akt HTVI treatment in GSCreER-mT/mG mice (n=4).* ***(b)*** *Volcano plot comparing mGFP+ hepatocytes isolated from mice dosed with both tamoxifen and HTVI of plasmid backbone vs mice dosed with tamoxifen and HTVI of NICD1/Akt. Highlighted genes include all up- (cyan) and downregulated (magenta) genes that passed the DESeq2 analysis (Benjamini-Hochberg) cut-off of adjusted p<0.05 (-log10 adjusted p<1.3) and log2 fold change > 1 (upregulated, cyan) or log2 fold change < -1 (downregulated, magenta).* ***(b)*** *Expression heatmap of all significantly upregulated and downregulated differentially expressed genes. Each row represents a gene, and each column corresponds to an individual mouse (n = 3 control, n = 4 treated).*

The GO enrichment analysis of significant DEGs identified from bulk RNA-sequencing of mGFP+ GSCreER-mT/mG liver cells was limited by the small number of significantly altered genes, as well as by the fact that some of these genes were not directly associated with defined molecular functions or biological processes. Consequently, Figure 5.12a presents the GO term analysis restricted to the significant DEGs highlighted in Figure 5.12b, whereas a separate analysis of all DEGs with a q-value > 0 (as determined by DESeq2 with Benjamini–Hochberg multiple testing correction) is also shown for comparison (Figure 5.12b).

In the analysis focusing on significantly altered genes (adjusted -log p ≥ 1.3), enrichment was observed exclusively in the molecular functions of betaine-homocysteine S-methyltransferase activity, DNA-binding transcription activator activity (RNA polymerase II-specific), and acetoacetate-CoA ligase activity. These data thus indicate perturbation of one-carbon metabolism and methyl group flux within hepatocytes following NICD1/Akt upregulation, implicating changes in cellular methylation status – a process known to affect gene expression and liver function. The enrichment for transcriptional activator activity further reflects increased transcriptional stimulation downstream of NICD1/Akt signalling. In contrast, altered acetoacetate-CoA ligase activity suggests effects on lipid and energy metabolism, consistent with the broad metabolic roles of AKT in the liver.

A complementary GO analysis of all DEGs with q > 0 (Benjamini–Hochberg correction) revealed additional terms spanning protein binding, catalytic activity, nucleic acid binding, and enzyme regulator activity, as well as broader biological processes including cellular component organisation and metabolism (Full list of GO terms can be found in Appendix Table 6). This distribution demonstrates both the diversity of molecular functions influenced by NICD1/Akt and the central involvement of these pathways in maintaining hepatocyte identity and metabolic homeostasis.

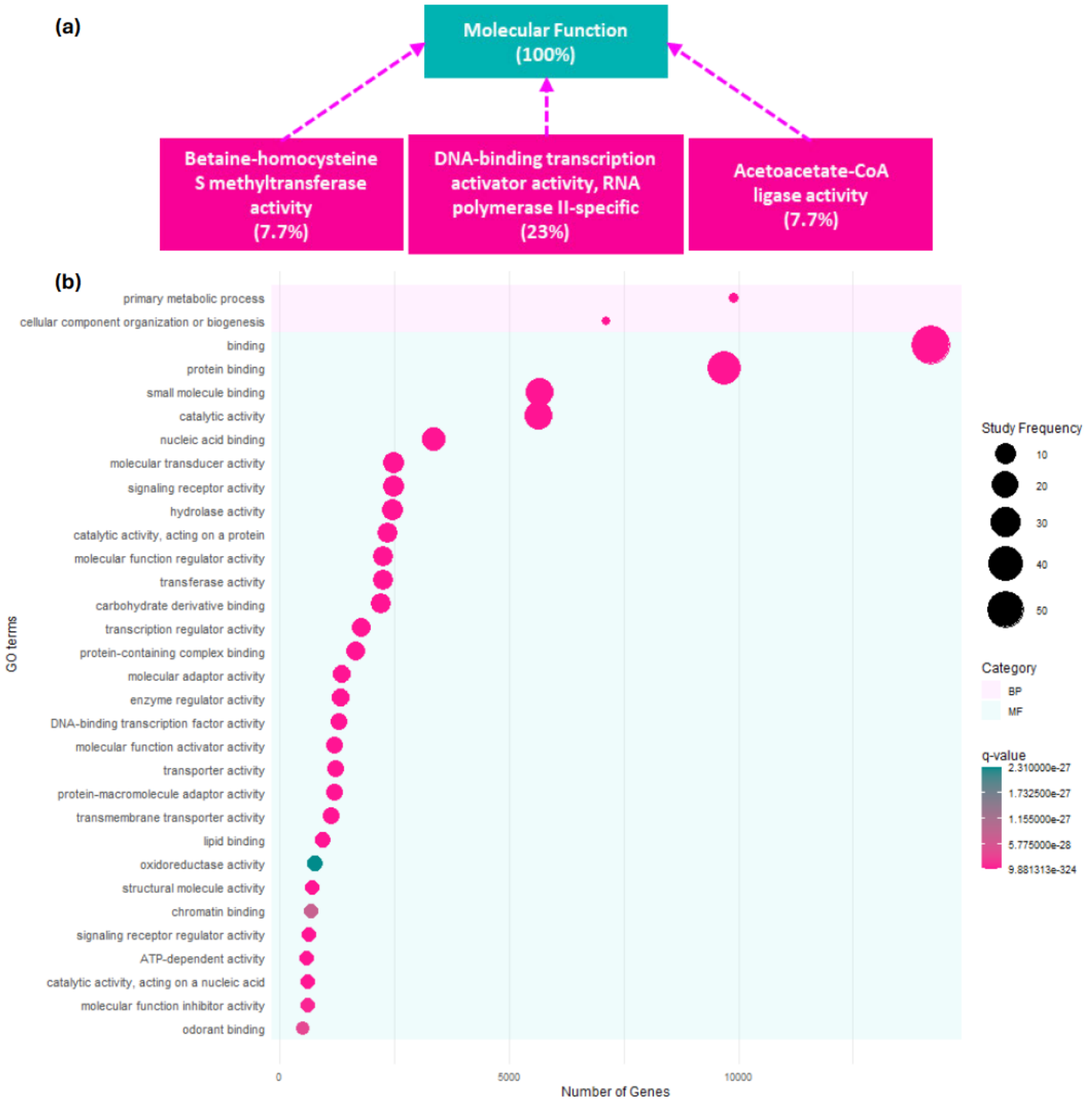

Figure 5.12: GO Enrichment Analysis of mGFP+ Cells Fluorescently Sorted from GSCreER-mT/mG Mouse Livers. *Differentially expressed genes were identified through DESeq2 analysis, following which GO enrichment analysis was conducted on the datasets in Galaxy using a Benjamini-Hochberg multiple test correction (adjusted $p < 0.05$).* ***(a)*** *Significant GO terms were filtered to show only those occurring at a frequency of >5% within the dataset, which resulted in genes in only the molecular function (MF) group being identified as significant.* ***(b)*** *Genes identified as having a q-value of >0 after DESeq2 and Benjamini-Hochberg analysis were plotted to visualise the broader functions occurring within the GSCreER-mT/mG dataset. The GO terms are rank-ordered within each category by their frequency of occurrence within the study, with larger bubbles indicating higher frequencies and colours (cyan-magenta) reflecting q-values. BP – Biological Processes; MF – Molecular Functions.*

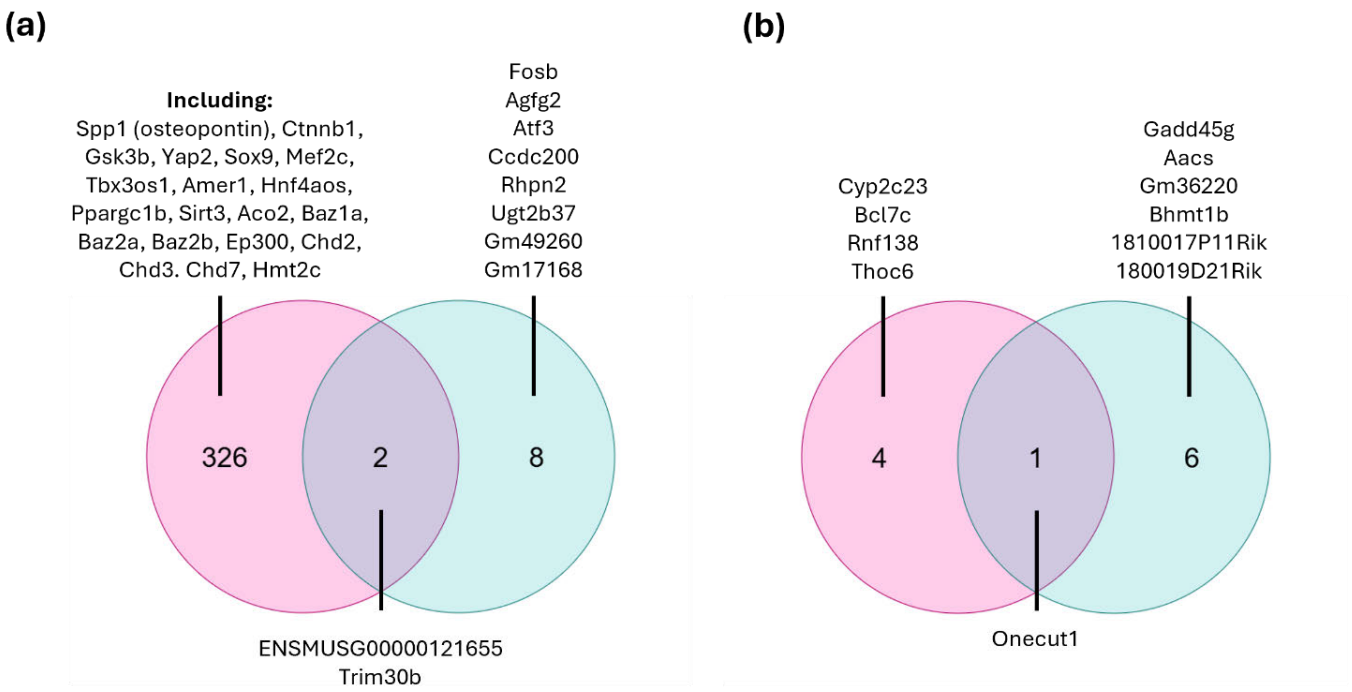

Figure 5.13: Overlap and Divergence of Differentially Expressed Genes in Gls2creER-mT/mG and GSCreER-mT/mG mice Following Hydrodynamic Tail Vein Injection of NICD1/Akt. (a) *Venn diagram showing overlap and divergence between genes significantly upregulated in Gls2creER-mT/mG (magenta) and GSCreER-mT/mG (cyan) livers.* ***(b)*** *Venn diagram showing overlap and divergence between genes significantly downregulated in Gls2creER-mT/mG (magenta) and GSCreER-mT/mG (cyan) livers.*

5.5.1 Exploration of Onecut1 (Hnf6) In Gls2CreER-mT/mG and GSCreER-mT/mG Livers Post-HTVI

With Onecut1 (Hnf6) having been identified as the only gene that was shown to be significantly downregulated in both the Gls2CreER-mTmG and GSCreER-mTmG RNA-sequencing analyses, immunostaining was performed to visually examine changes in the expression of this hepatocyte marker within tissues following HTVI of the NICD1 and Akt plasmids. Immunostaining revealed widespread nuclear localisation of Hnf6 in hepatocytes, confirming its role as a hepatocyte-enriched transcription factor essential for hepatocyte identity and function (Figure 5.13). Notably, there was an apparent absence of Hnf6 expression in mature BECs, underscoring its specificity. Furthermore, neoplastic lesions arising from the upregulated NICD1/Akt signalling showed heterogeneous Hnf6 expression, with cells immediately bordering the luminal structures exhibiting strong nuclear Hnf6 positivity, whilst other cells within the neoplasms lacked expression (Figure 5.13 insets). This differential staining pattern suggests variable retention or alteration of hepatocyte characteristics within neoplasm cells, reflecting the complex cellular heterogeneity and differentiation status in the neoplasms.

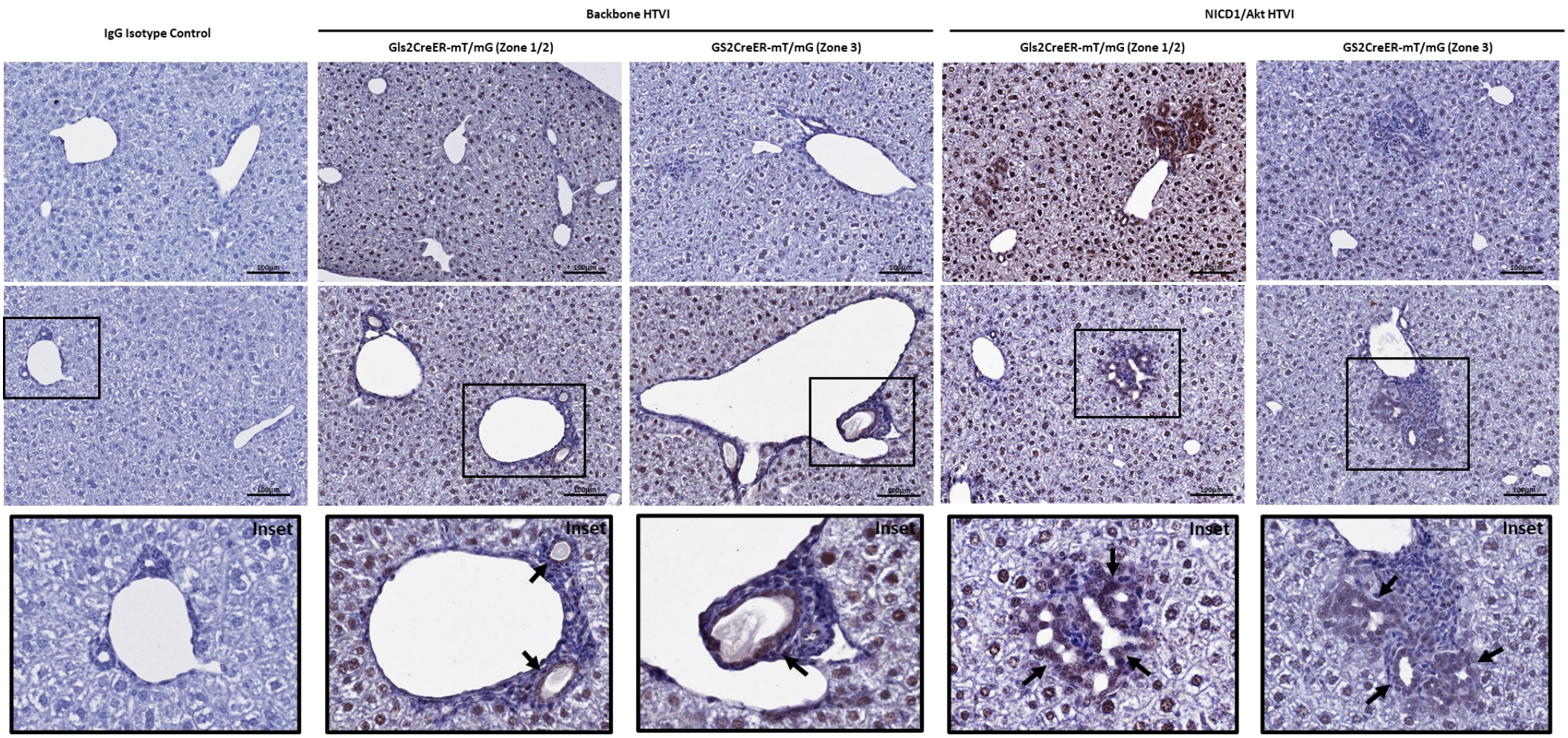

Figure 5.14: Onecut1 (Hnf6) Expression in Mature Hepatocytes and in NICD1/Akt-induced Biliary Neoplasms. *Representative DAB-stained sections from Gls2CreER-mT/mG and GSCreER-mT/mG mouse livers harvested 4 weeks post-HTVI with either NICD1/Akt or backbone (pSBbi-BH) plasmids are shown. Hnf6 expression is evident in mature hepatocytes across the liver parenchyma and in cells lining the lumens of NICD1/Akt-induced biliary neoplasms (black arrows in insets) (Scale bars = 100μm).*

5.6 *In Vitro* Transfection of NICD1/Akt in Primary Hepatocyte Spheroids Recapitulates *In Vivo* Lineage Changes

To assess whether the *in vivo* phenotypic changes could be reproduced *in vitro*, primary hepatocyte spheroids were generated from C57Bl6/J, Gls2CreER-mT/mG, and GSCreER-mT/mG mice and transfected with pT3-EF1α-Myc-NICD1 and pSBbi-BH-*myr*-AKT-HA plasmids for 24 or 48 hours (Section 2.4). Figure 5.14a shows mGFP positivity in spheroids from Gls2CreER-mT/mG and GSCreER-mT/mG mice, after 24 hours (HR) of exposure to 500nM 4-hydroxytamoxifen. Micrographs in Figure 5.14b confirm that C57Bl6/J PMHS successful transfection of HA-tagged Akt plasmids after 24 hours of lipofectamine-mediated delivery, as evidenced by immunoreactivity for HA in fixed spheroids.

qPCR analysis (Figure 5.14c) revealed a lineage shift in NICD1/Akt-transfected PMHS, characterised by significant downregulation of hepatocyte markers Albumin (Control vs 24HR, p.adj = 0.0211; Control vs 48HR, p.adj = 0.0211) and Hnf4α (Control vs 24HR, p.adj < 0.001; Control vs 48HR, p.adj < 0.001), with no significant change in Cyp3A4 expression. In parallel, biliary markers Sox9 (Control vs 48HR, p.adj = 0.0141; 24HR vs 48HR, p.adj = 0.0211), K19 (Control vs 24HR, p.adj = 0.0087; 24HR vs 48HR, p.adj = 0.0500) and EpCAM (Control vs 48HR, p = 0.0042; 24HR vs 48HR, p.adj = 0.0097), together with the Notch target gene Hes1 (Control vs 24 h, p.adj = 0.0190), were significantly upregulated, confirming successful reprogramming. The cre-recombination demonstrated in Figure 5.14a was further supported by mGFP expression changes observed between the spheroids treated with tamoxifen for 24 hours and the controls without tamoxifen treatment (Control vs 24HR, p.adj = 0.0192).

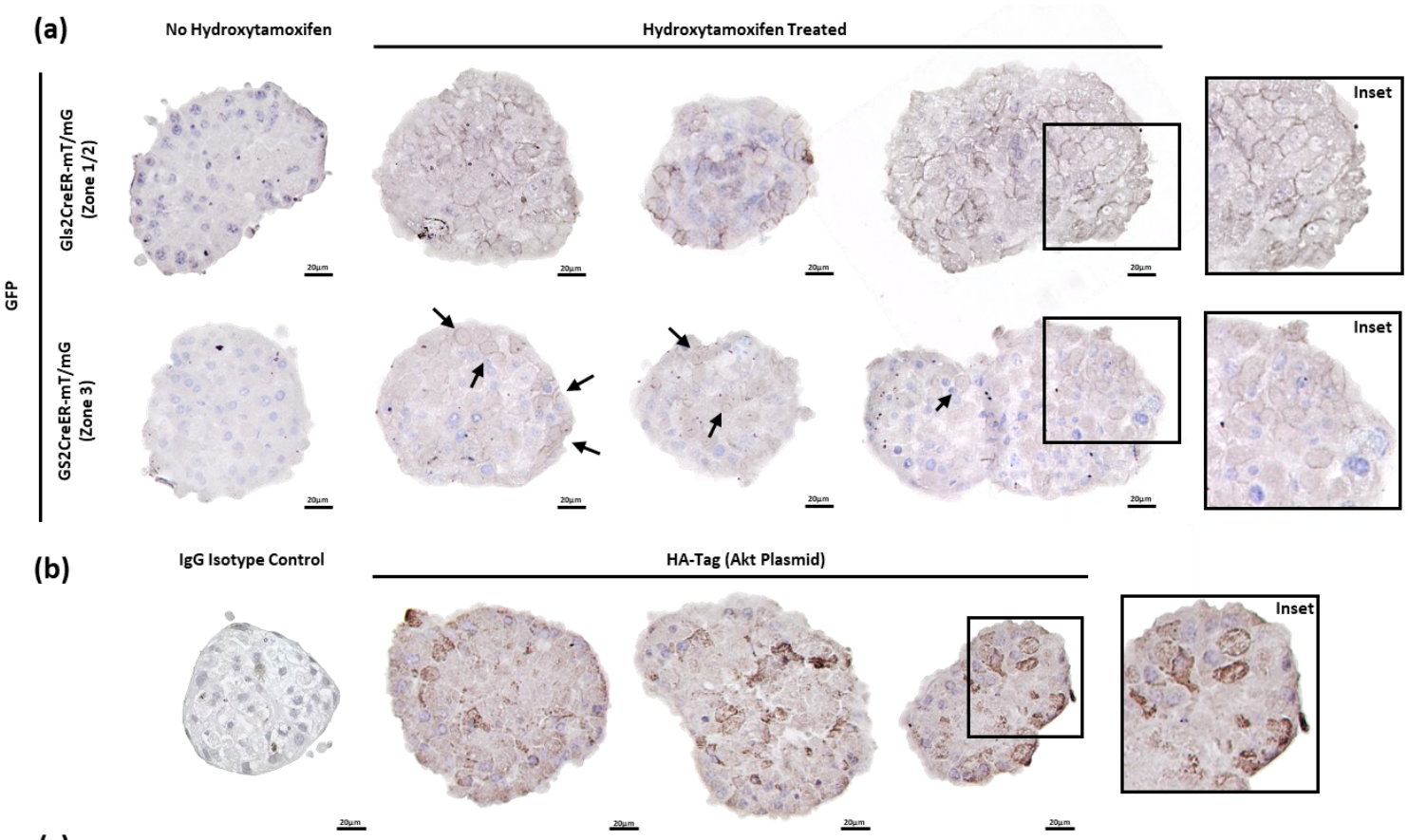
(a)
No Hydroxytamoxifen
Hydroxytamoxifen Treated
GFP
Gls2CreER-mT/mG (Zone 1/2)
GS2CreER-mT/mG (Zone 3)
Inset
Inset
20µm

(b)
IgG Isotype Control
HA-Tag (Akt Plasmid)
Inset
20µm

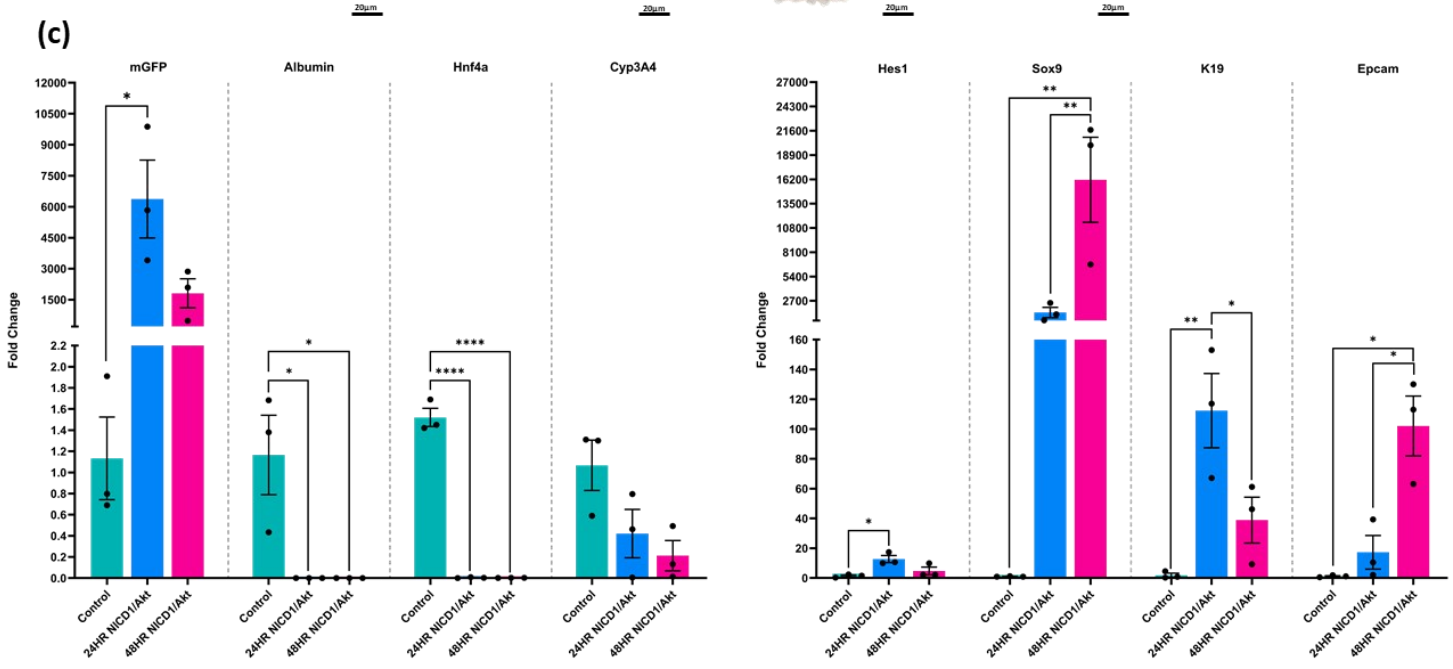
(c)
mGFP
Albumin
Hnf4a
Cyp3A4
Hes1
Sox9
K19
Epcam
Fold Change
Control
24HR NICD1/Akt
48HR NICD1/Akt

Figure 5.15: In vitro Tamoxifen-Induced Cre-Recombination and Lipofectamine-Mediated NICD1/Akt Transfection of Primary Murine Hepatocyte Spheroids. ***(a)*** *Representative DAB-stained PMHS demonstrating membranous GFP (mGFP) positivity following treatment with 500nM hydroxytamoxifen for 24 hours in both Gls2CreER-mT/mG and GSCreER-mT/mG derived PMHS (Scale bars = 20μm).* ***(b)*** *Representative DAB-stained C57Bl6/J PMHS showing cytoplasmic expression of HA-tagged Akt after 24 hours of NICD1/Akt transfection (Scale bars = 20μm).* ***(c)*** *qPCR analysis of cre-recombination-induced mGFP (24HR Hydroxytamoxifen treated), hepatocyte (Hnf4α, Alb, Cyp3A4) and biliary (Sox9, K19, EpCAM) lineage markers as well as Notch target gene Hes1 in PMHS derived from C57Bl6/J mouse livers transfected with NICD1/Akt for 24 hours (24HR) and 48 hours (48HR). Data analysed using a one-way ANOVA with Tukey multiple comparisons post-hoc and shown as mean ± SEM from n=3 biological replicates measured in duplicate (*p ≤ 0.05; **p ≤ 0.01; ****p ≤ 0.0001).*

5.7 Discussion

The synergistic activation of Notch (NICD1) and Akt signalling in hepatocytes represents a pivotal oncogenic axis in the initiation and progression of biliary tract cancers [15,17,22,124,131,133,390-393]. Multiple studies – including those by Fan *et al.* (2012), Tarlow *et al.* (2014), and Hu *et al.* (2022) – reproducibly demonstrate that simultaneous induction of these pathways precipitates loss of hepatocyte identity and acquisition of biliary epithelial characteristics, a process mediated by epigenetic remodelling and transcriptional reprogramming involving the Notch-YAP1/TEAD-DNMT1 axis [100,124,133].

Mechanistically, Notch signalling orchestrates lineage specification by suppressing hepatocyte identity genes such as Hnf4α and C/EBPα or C/EBPβ through DNMT1-mediated methylation and repressive chromatin remodelling [9,15,17-19,21,130,131,133,348,390,391]. This results in downregulation of key hepatocyte genes, including Cyp2C23, Alb, and Hnf4α, while upregulating biliary lineage markers such as Sox9, K19, and K8. The contribution of Akt signalling lies in promoting proliferation and survival, safeguarding tumorigenic expansion after lineage switch [354,355,357]. Akt further antagonises growth suppressors such as PTEN and supports chromatin accessibility, reinforcing the malignant transformation process [133,354,355,357].

As expected, having used this methodology based on that previously established by Fan *et al.* (2012) and Hu *et al.* (2022), co-delivery of two plasmids - pT3-EF1a-Myc-NICD1 and Gibson Cloned pSBbi-BH-*myr*-AKT-HA – together with a Sleeping Beauty (SB) transposon system (pCMV(Cat)T7-SB100) induced a phenotypic transformation of hepatocytes, characterised by the formation of biliary neoplasms with distinct luminal structures [124,133]. The simultaneous uptake and stable genomic incorporation of both plasmids was demonstrated by IHC of the Myc- and HA-tag expressing NICD1/Akt-induced neoplasms, as well as immunofluorescent co-staining showing that cells expressing the nuclear Myc-tag (the NICD1 plasmid) also expressed the cytoplasmic HA-tag (Akt plasmid). This co-integration has also been demonstrated clearly in a study by Sebestyen *et al.* (2006) through co-injection of an enhanced yellow fluorescent protein (pEYFP-Nuc) plasmid and a fluorescently labelled 200bp linear DNA fragment, with both fluorophores being expressed in 91% of the observed cells [394]. Other reviews and experimental reports describe the HTVI as delivering multiple plasmids with high efficiency to the liver, with most utilising this technique for co-delivery of oncogenic plasmids using the SB transposon system to induce combined expression of various genes, thus relying on the high likelihood of plasmids entering the same hepatocytes concurrently [78,130,133,349-353,357,394]. The experimental observations made in the present study, together with the support of the previous literature, strengthen the assumption that

the biliary neoplasms arising in this model have originated from hepatocytes that have been transfected with and modified by both the NICD1 and Akt oncogenic drivers.

Neoplasms arising in this NICD1/Akt model displayed robust proliferative activity, as evidenced by strong Ki-67 positivity – a clinical marker frequently associated with advanced tumour stage and poor prognosis in hepatobiliary cancers [128]. The increase in Ki-67 compared to surrounding cells indicates that these neoplasms circumvent typical hepatocyte growth controls, likely due to concomitant upregulation of oncogenic signalling pathways [395,396].

In the present study, the expression of BEC markers such as Sox9 and K19 within NICD1/Akt-induced neoplasms was evident, consistent with the transdifferentiation of hepatocytes toward a biliary phenotype. Cytokeratin 7 (CK7) is an established marker of immature biliary cells and biliary progenitors, with higher expression typically correlating with less differentiated, more aggressive cholangiocarcinoma subtypes. While K19 and Sox9 immunostaining confirmed biliary lineage identity in NICD1/Akt-induced neoplasms, CK7 status was not assessed in this study. Future characterisation of CK7 expression would help determine the maturation state of these neoplasms and whether the proportion of Cre+ cells differs between more differentiated (K19+/Sox9+/CK7−) versus less mature (K19+/Sox9+/CK7+) tumour regions; such heterogeneity in CK7 expression could reflect differences in the extent of hepatocyte-to-biliary reprogramming across different zones of the liver lobule. This recapitulates findings from previous reports, notably those by Hu *et al*. (2022) and Fan *et al*. (2012), which similarly observed expression of biliary lineage markers, including Sox9 and K8, in hepatocytes subject to NICD1/Akt upregulation [235,241,397-400]. These findings align with lineage-tracing evidence that mature hepatocytes, when exposed to potent oncogenic stimuli, can undergo transdifferentiation into bipotential progenitor-like cells capable of fuelling iCC development.

A study by Sekiya and Suzuki (2012) is of particular note, as it provided direct proof that hepatocyte-specific activation of Notch and Akt is sufficient to induce iCC from mature hepatocytes [401]. By labelling hepatocytes and BECs via inducible Cre/loxP systems – Alb-CreER for hepatocytes and K19-CreER for BECs – they lineage-traced the fates of these populations following Notch and Akt signalling activation in hepatocytes or following chronic thioacetamide (TAA) injury. Subsequent histological and immunofluorescent analyses revealed that the hepatocyte-derived tumours expressed biliary markers K8, K19, and Sox9 but had lost hepatocyte identity markers such as Hnf4α [401]. The authors confirmed transdifferentiation of cells at the molecular level through observation that the hepatocyte lineage-traced reporter signals (YFP or β-gal) co-localised with biliary, but not hepatocyte, marker expression within the tumours. Furthermore, spatial analyses reveal that pericentral hepatocytes were particularly

vulnerable to this reprogramming, as they are primarily responsible for metabolising TAA via Cyp2E1-mediated bioactivation [256,401]. Overall, the Suzuki *et al*. study firmly concluded that fully differentiated hepatocytes can be reprogrammed into biliary lineage cells through Notch (and Akt) activation, leading to iCC characterised by loss of Hnf4α and gain of K8, K19, and Sox9 expression, which effectively recapitulates human iCC pathogenesis [401].

The induction of BEC markers and acquisition of a proliferative, neoplastic phenotype in NICD1/Akt models closely mirror events underlying aggressive human iCC and strengthen the argument for a potential hepatocyte origin of these tumours [123,124,126,129,133,351,391]. A recent review by Pu & Zhou (2022) explored the cellular origins and regenerative potential of hepatocytes in the adult liver, emphasising that hepatocyte renewal is typically maintained by self-duplication rather than progenitor cell input [56]. Their review of previous lineage-tracing studies highlights that hepatocytes retain a remarkable degree of plasticity, which is revealed under conditions of chronic injury or induction of developmental pathways. In this context, the findings of the present study showing that NICD1/Akt co-activation drives mature hepatocytes to become highly proliferative, biliary marker-positive neoplastic cells – exhibiting the elevated Ki-67 expression characteristic of malignant cholangiocarcinoma – align well with this emerging view and further cement the concept that hepatocyte plasticity is a critical determinant of hepatobiliary tumorigenesis.

The present study made use of two in-house bred Gls2CreER-mT/mG and GSCreER-mT/mG mouse models to lineage-trace hepatocyte populations based on the expression of Gls2 and GS, respectively (Chapter 4). Upon treatment with the NICD1/Akt HTVI, both models formed biliary neoplasms at statistically equivalent rates after 4 weeks, with no significant difference in neoplasm number between models, indicating that the basal susceptibility to NICD1/Akt-driven transformation does not differ between mouse strains. However, lineage tracing revealed distinct differences in cellular behaviour: mGFP+ cre-recombined hepatocytes from the Gls2CreER-mT/mG model actively changed morphology, participated in neoplasm formation and expressed Sox9, thus directly contributing to biliary tumorigenesis. In contrast, mGFP+ cre-recombined cells from the GSCreER-mT/mG model, despite being in close physical proximity or direct contact with developing neoplasms, did not contribute to their formation.

Notably, Chen *et al.* (2023) identified that pericentral hepatocytes exhibit greater proliferative potential in response to chronic liver injury, such as long-term Carbon Tetrachloride (CCl_4) administration or fibrotic injury, while periportal hepatocytes were more inclined to initiate ductular reactions and biliary reprogramming [52]. This distinction provides essential context for the divergent plasticity observed in

Gls2+ versus GS+ hepatocytes in these experiments, implying that intrinsic differences in canonical Wnt/β-catenin signalling activity and the associated metabolic gene network modulate the hepatocyte's capacity for lineage conversion in response to NICD1/Akt stimulation [29,63,89,333,402]. GS+ (Wnt-high) hepatocytes, marked by robust expression of Wnt pathway targets such as Axin2 and Cyp2E1, are governed by persistent Wnt/β-catenin signalling, enforcing a highly differentiated, metabolically specialised state that involves the activation of cyclin-D family genes, c-Myc, and various drug-metabolising enzymes [3,28,29,53,54,58,63,264,280]. This transcriptional and metabolic stability, potentially reinforced by Wnt pathway agonists such as RSPO3, Wnt9b, and Wnt2 expressed in zone 3, is hypothesised to impose resistance to cellular plasticity and impede engagement with biliary reprogramming cues—mechanistically, such resistance may involve direct β-catenin-mediated antagonism of Notch-driven transcriptional programs and promoter occlusion at loci such as Hnf4α and Hnf6 [29-31,266,403].

In contrast, periportal Gls2+ hepatocytes display weaker Wnt/β-catenin signalling activity compared to pericentral hepatocytes, with a gene expression signature which is tailored for metabolic functions such as gluconeogenesis and amino acid catabolism, rather than the detoxification and synthetic processes dominant in zone 3 [51,65,103,264,330]. This periportal metabolic profile is coupled with greater sensitivity to alternative signalling pathways, making these cells more adaptable and responsive to signals that promote cellular plasticity and reprogramming. [224,225,237,267,268,404]. Lower levels of β-catenin-based epigenetic protection at crucial differentiation sites result in a chromatin state that facilitates cellular reprogramming and transitions between lineages [29,30,64,280,405]. Epigenetic effectors, including histone modifiers and chromatin remodellers, are increasingly seen as central drivers of hepatocyte reprogramming, facilitating the loss of metabolic gene transcription and activation of biliary-promoting networks. Promoters of hepatocyte identity, such as Hnf4α, Hnf6, and C/EBPα, are direct targets of canonical Wnt signalling and repressive chromatin remodelling, and their downregulation appears to prime cells for dedifferentiation and the acquisition of progenitor-like or BEC-like phenotypes.

FACS of mGFP+ (cre-recombined) hepatocytes from both mouse lines revealed a BFP+ plasmid-positive population, confirming plasmid uptake. Unfortunately, BFP expression was too dim and the number of detectable BFP^+ cells too low to allow independent isolation of this subpopulation, necessitating downstream analyses of cre-recombined versus non-recombined cells to assess NICD1/Akt effects. Notably, the mGFP+ populations in NICD1/Akt-treated Gls2CreER-mT/mG mice were significantly higher compared to controls that received only tamoxifen or tamoxifen + backbone plasmid HTVI. This finding indicates that NICD1/Akt upregulation promotes expansion or survival of Gls2-lineage hepatocytes, further supporting their active recruitment into neoplastic processes.

Conversely, the mTom+ population, representing non-cre-recombined cells within the liver lobule, was significantly larger in GSCreER-mT/mG mice treated with NICD1/Akt compared to those given corn oil or corn oil + backbone plasmid HTVI. This supports the Gls2CreER-mT/mG mGFP data described previously, as the Gls2-expressing hepatocyte population would fall within the non-recombined mTom+ cell population in the GSCreER-mT/mG mouse livers. The lack of a significant increase in the number of mGFP+ cells in the GS population mirrors the lack of participation in the neoplasm formation that was observed in the IHC and IF staining. These data provide further evidence that HTVI efficiently delivers both NICD1 and Akt oncogenic drivers non-discriminatorily across hepatocytes throughout the liver lobule, initiating biliary neoplasm formation via the proliferative expansion of the hepatocyte population. The differential participation of discrete hepatocyte subpopulations elucidated by lineage tracing highlights the complex interplay of metabolic state, signalling milieu, and cellular plasticity underpinning the development of iCC.

Activation of NICD1/Akt signalling in periportal Gls2+ hepatocytes appears to trigger a profound loss of mature hepatocyte identity and widespread metabolic and transcriptional reprogramming. The significant downregulation of Hnf6, a master regulator of hepatocyte differentiation, sits at the heart of this shift, being directly linked to the suppression of hepatocyte fate commitment and facilitation of biliary lineage specification, hallmark outcomes of Notch pathway activation [16,406]. Simultaneous decreases in the expression of genes like Cyp2C23, a vital regulator of lipid metabolism and detoxification, and other hepatocyte-enriched transcripts such as Alb and Hnf4α, further illustrate the progressive dismantling of hepatocyte-specific functions [201,218,225,407]. This decline extends well past essential metabolic functions, with reductions in chromatin remodelling factors (Bcl7c and Ino80) and RNA-processing genes (Thoc6 and Pnisr) reinforcing the collapse of mature hepatocyte transcriptional programmes. These molecular events are in line with evidence that disruption of epigenetic regulators and RNA processing machinery often accompanies cellular dedifferentiation or the adoption of a progenitor- or stem-like identity in diverse tissue contexts [408-411].

At the same time, transcriptional rewiring induced by the NICD1/Akt signalling upregulation includes an induction in the expression of genes associated with proliferation, DNA repair, and cell cycle progression, reflecting a shift from a quiescent, functionally specialised hepatocyte state towards a plastic, adaptive programme primed for lineage flexibility [15,17,18,21,22]. This repression of hepatocyte-defining regulators and activation of proliferative and genomic response pathways is consistent with classical models of hepatocyte-to-biliary conversion, where loss of Hnf4α or Hnf6 activity is offset by enhanced Notch-driven biliary determinants and supportive chromatin adaptations [16,97,406,412]. Similar transitions have been observed in liver injury models, where mature hepatocytes undergo partial

dedifferentiation and subsequently re-enter the cell cycle to generate ductal or progenitor-like phenotypes [413,414]. This process underscores how the downregulation of metabolic gene expression is tightly linked to the acquisition of regenerative and lineage-flexible capacities during liver regeneration. Together, these changes indicate that NICD1/Akt activation does not simply impose a biliary fate but instead creates a permissive transcriptional landscape characterised by loss of hepatocytic stability, weakening of chromatin integrity, and engagement of cell cycle regulators.

The cre-recombined Gls2+ hepatocytes subjected to NICD1/Akt were also noted to demonstrate a striking upregulation of mitochondrial genes, including mt-Co3, mt-Nd3, and mt-Atp8. This escalation points to mitochondrial biogenesis and the adoption of high oxidative phosphorylation capacity, a metabolic alteration observed both in regenerative states and in tumour development, which is a signature of the influence of Akt signalling on biosynthetic and survival pathways [354,355,357,389]. Upregulation of Gls2 was particularly interesting given that this gene served as the basis for lineage tracing in both control and NICD1/Akt-treated populations. The elevated Gls2 expression suggests enhanced glutaminolysis, a metabolic adaptation that supplies intermediates to the TCA cycle to support increased biosynthetic and energetic demands during cell proliferation. This phenomenon is well documented in both proliferating liver and cancer cells but would warrant further study [267,274,275,277,415-417].

Although not having reached the pre-determined threshold of statistical significance, there is also detectable upregulation of known biliary lineage marker genes, including Sox9, a well-characterised biliary and progenitor marker whose increased expression marks the initiation of biliary fate acquisition and is essential for BEC differentiation and iCC development [235,397]. The transcriptional changes observed – marked loss of hepatocyte-specific regulators (Hnf6, Hnf4α, Cyp2c23, Alb), induction of proliferative and mitochondrial programs, and modest upregulation of early biliary markers such as Sox9 – reflect a direct reprogramming of mature hepatocytes toward a biliary fate without evidence of a discrete epithelial–mesenchymal transition (EMT) intermediate [115,137,236,237,418]. Classic EMT hallmarks (eg, downregulation of E-cadherin, upregulation of vimentin or N-cadherin) are not appreciably altered in the dataset generated in the present study, and the transition appears to proceed via gradual dismantling of hepatocytic identity and simultaneous engagement of biliary and proliferative gene networks. Thus, NICD1/Akt activation drives a continuum of dedifferentiation and lineage re-specification rather than a two-step EMT-then-transdifferentiation process within periportal Gls2+ hepatocytes. The modest elevation of Mdm2, a critical regulator of p53 signalling, which is known to be a phosphorylation target of Akt, indicates the potential onset of unchecked proliferation and a reduction in apoptosis [419,420]. The increased Gsk3b, Yap1, and Ctnnb1 (β-catenin) expression further

reinforces the activation of key oncogenic pathways, including Hippo/YAP and canonical Wnt/β-catenin signalling, that converge with the NICD1/Akt signalling to promote hepatocyte plasticity and neoplastic transformation [28,29,46,63]. Moreover, Hnf4αos, a long non-coding RNA which regulates hepatocyte differentiation through modulation of Hnf4α expression, shows subtle upregulation, indicating nuanced regulatory adjustments potentially supporting lineage reprogramming [421,422].

It is important to note, however, that there was clear variability between the four biological replicates in the Gls2CreER-mT/mG mice treated with NICD1/Akt HTVI. Several factors could explain this; the first being that differences in transfection efficiency are a common technical challenge in HTVI experiments [78,349-353,394,423]. Thus, the uptake and expression of NICD1/Akt plasmids may have been lower in T1 and T2, resulting in insufficient levels of Notch and Akt signalling to induce the full spectrum of transcriptional changes seen in T3 and T4. Variations in injection parameters, biological heterogeneity between individual animals, or even the timing of sample collection relative to plasmid delivery could all contribute to this inconsistency [78,349-353,394,423]. Alternatively, T1 and T2 may exhibit delayed pathway activation due to slower plasmid processing or protein translation. Because only mGFP+ cells were analysed, these samples could have contained fewer successfully transfected cells, yielding a diluted transcriptional signal more akin to the controls.

To distinguish among these possibilities, several experimental approaches could be employed. First, quantification of NICD1 and Akt transgene expression at the mRNA and protein levels – using qPCR with primers specific to the plasmid-encoded transcripts and Western blotting for the Myc- or HA-tagged proteins – would directly assess uptake and expression efficiency. Second, measurement of mGFP fluorescence intensity and plasmid copy number per cell by digital droplet PCR would reveal whether T1 and T2 have truly had fewer plasmid integrations or lower transgene expression. Third, a time course analysis – sampling at multiple intervals post-HTVI – could determine whether pathway activation in T1 and T2 is delayed by monitoring NICD1/Akt target genes (eg, Hes1, Cyclin D1) via qPCR or immunostaining over time. This observed heterogeneity highlights both the technical and biological challenges associated with *in vivo* manipulation of complex signalling pathways and effectively underscores the importance of including sufficient biological replicates and validating treatment efficacy in future experiments to distinguish true biological variability from technical artefacts.

In contrast, GS+ hepatocytes appear more resistant to full reprogramming, mounting a more limited and stress-focused transcriptional response. The downregulation of Hnf6 in this dataset indicates some suppression of hepatocyte identity, but most of the upregulated genes, such as Fosb and Atf3, are canonical responders to acute cellular stress, injury, and regeneration cues, which signify attempts

at adaptation but do not by themselves denote a full fate change [16,406,424,425]. Trim20b and Agfg2, while less characterised in the liver, are associated in other organ systems with immune modulation and nucleocytoplasmic transport, respectively, which suggests that upregulation following NICD1/Akt activation could signify adaptations in cellular immunity and macromolecular trafficking in response to the stress of oncogenic signalling [426-428]. Among the non-significantly altered genes, upregulation of Ctnnb1 (β-catenin), Yap1, and Akt1 points toward activation of canonical Wnt, Hippo, and PI3K/Akt pathways, all of which are linked to hepatocyte proliferation and tumorigenesis. While these changes did not reach statistical significance, their directionality aligns with the known effects of NICD1/Akt signalling in promoting cellular plasticity and oncogenic transformation in the liver [22,133,390-392,402,429].

Downregulation of metabolic genes such as Bhmt1b (betaine-homocysteine S-methyltransferase) and Aacs (acetoacetyl-CoA synthetase) points to a disturbance in methylation balance and ketone metabolism, which compromises the epigenetic regulation and metabolic stability that are vital for maintaining hepatocyte identity and function [430,431]. Gadd45g, known for its role in cell cycle arrest and DNA damage response, was also downregulated, which may indicate altered proliferative dynamics under NICD1/Akt activation [432]. Downregulation of Hnf4α and Oat, both markers of hepatocyte differentiation, further supports a shift toward a less differentiated, more progenitor-like phenotype [229,281,342,407,421,433]. These transcriptomic alterations appear to emphasise the stress adaptation of the cells, suggesting that the pericentral GS+ population may be initiating some dedifferentiation in the face of oncogenic signals but failing to transition fully toward a biliary phenotype.

Collectively, these data indicate that periportal Gls2+ hepatocytes, which characteristically have lower levels of canonical Wnt signalling, are more readily converted to a biliary phenotype in response to NICD1/Akt signalling through a coordinated decrease in hepatocyte metabolic programmes and upregulation of RNA processing, proliferative, and chromatin-modifying machinery. The GS+ cells, on the other hand, appear to mount a stress response to the NICD1/Akt upregulation but do not undergo a complete fate transition, consistent with the proposed intrinsic resistance conferred by their elevated canonical Wnt signalling activity. Altogether, the transcriptomic evidence highlights that while strong NICD1/Akt signalling can initiate a spectrum of cellular responses, zonal identity and baseline metabolic state ultimately determine the extent of hepatocyte plasticity and susceptibility to reprogramming.

The downregulation of Hnf6 across both Gls2 and GS lineages prompted immunohistochemical validation. The IHC results demonstrate the prominent nuclear expression of Hnf6 in hepatocytes and progenitor-like cells found bordering the lumens of the intrahepatic bile ductules but absence of Hnf6

expression in mature BECs. The observed heterogeneous nuclear expression of Hnf6 within NICD1/Akt-induced neoplasms, with strong positivity in luminal border cells and absence in adjacent neoplastic cells, likely represents dynamic transitional cellular states. This mosaic pattern likely reflects transitional states, where some cells retain hepatocyte-like transcriptional features while others silence Hnf6 as they adopt a more biliary identity [16,434,435]. This heterogeneity parallels normal liver development and injury response, where Hnf6 is transiently expressed during progenitor expansion and lost upon terminal biliary differentiation [412]. Functionally, Hnf6 drives hepatocyte proliferation during liver regeneration by transcriptionally activating key cell cycle regulators through direct binding and activating the promoters of TGFα (hepatocyte mitogen), Cyclin D1 (G1/S-phase progression), and Foxm1 (a regulator of mitosis) [406]. Elevated Hnf6 expression has thus been shown to significantly increase hepatocyte S-phase entry post-partial hepatectomy, while a knockdown of Hnf6 was demonstrated to reduced DNA replication by 50% [406]. This control of proliferation and lineage portrays the role of Hnf6 within a broader transcriptional network governing biliary differentiation, duct morphogenesis, and maintenance of epithelial fate. Thus, in NICD1/Akt-induced neoplasms, Hnf6 expression identifies transitional progenitor-like cells retaining hepatocyte characteristics, while its silencing marks commitment to mature BEC-like fates. The resulting mixture of Hnf6-positive and -negative cells in the neoplasms mirrors normal biliary development and underscores the lineage plasticity central to hepatocyte-to-BEC reprogramming and tumorigenesis. Overall, these findings suggest that although Hnf6 is transiently upregulated in a subset of progenitor-like cells within the neoplasms, the overwhelming shift of a majority of NICD1/Akt-transfected hepatocytes toward Hnf6-negative BEC-like fates produces an overall signature of transcriptional downregulation when NICD1/Akt livers are compared to backbone controls.

To further dissect the role of Hnf6 in NICD1/Akt-driven reprogramming, several complementary experiments could be conducted in future studies. First, employing lineage-specific Cre drivers to induce conditional Hnf6 overexpression or deletion in hepatocytes and biliary epithelial cells *in vivo* would reveal how Hnf6 modulates cell-cycle progression, progenitor expansion, and commitment to biliary versus hepatocyte fates under oncogenic signalling. Second, performing genome-wide chromatin immunoprecipitation followed by high-throughput sequencing (ChIP-seq) for Hnf6 in NICD1/Akt-transfected liver cells would identify direct transcriptional targets and co-regulatory partners that orchestrate the dedifferentiation and biliary specification programs. Finally, leveraging three-dimensional primary murine liver spheroid cultures with inducible Hnf6 expression or knockdown would enable dynamic, real-time imaging and molecular analysis of ductal morphogenesis, the transition from mature hepatocytes to biliary-like cells, and the effects on

spheroid growth, architecture, and regeneration. This integrated approach would clarify how Hnf6 controls the balance between proliferation, lineage plasticity, and differentiation in both normal and neoplastic contexts.

The gene ontology (GO) enrichment analysis conducted on the significantly altered transcripts within the Gls2CreER-mT/mG data revealed a complex transcriptional landscape shaped by the activation of NICD1/Akt signalling. The enrichment across molecular functions (MF) such as nucleic acid binding, oxidoreduction-driven active transmembrane transport, cytochrome c oxidase activity, and NADH dehydrogenase activity indicates heightened mitochondrial respiratory chain function. This metabolic signature, together with enriched transcriptional regulatory and helicase activities, highlights concurrent mitochondrial biogenesis and chromatin remodelling. These features affirm that the hepatocytes are undergoing marked metabolic and epigenetic plasticity, key processes that enable their transition toward a progenitor-like and potentially neoplastic state [436,437].

In the biological process category, the data highlight regulation of metabolic processes, chromatin remodelling, RNA biosynthesis, and mitochondrial ATP synthesis alongside immune modulation, embryonic morphogenesis, and cell cycle control. This diverse enrichment suggests these hepatocytes are experiencing a coordinated reprogramming that sees the cells activating developmental and immune pathways, reflecting their transition from a mature hepatic phenotype toward a more plastic and proliferative state under the oncogenic influence of the NICD1/Akt signalling upregulation [22,435]. These findings align with emerging concepts in liver biology where hepatocytes undergoing dedifferentiation and reprogramming activate developmental programs that mimic those of embryonic progenitors, facilitating tumorigenesis and cellular heterogeneity [438-440].

Conversely, the significantly altered genes identified in the GS lineage exhibit a comparatively focused transcriptomic response with enrichment restricted to betaine-homocysteine S-methyltransferase activity, RNA polymerase II-specific DNA-binding activator activity, and acetoacetate-CoA ligase activity. These functions imply that GS-expressing hepatocytes, while responding to NICD1/Akt signalling, primarily engage methylation reprogramming, transcriptional activation, and altered lipid and ketone body metabolism [52,441]. Expanding the analysis to include terms which had not surpassed the chosen significance level of $p>0.05$ provides a broader view of the transcriptional landscape in these cells, incorporating both highly significant and lower-confidence categories. This broader set highlights some metabolic and gene regulation plasticity but suggests a comparatively restrained response relative to the Gls2 lineage. Enrichment of biological processes like cellular component organisation and primary metabolism reflects the maintenance of fundamental metabolic and

structural features, consistent with GS+ hepatocytes' intrinsic zonal function within the liver lobule [264,330]. Enhanced betaine-homocysteine S-methyltransferase activity suggests a shift in one-carbon metabolism and methyl group transfer, processes linked to oxidative stress adaptation, gene expression regulation through DNA and histone methylation, and methylation homeostasis essential for proliferation and survival [442]. The upregulation of RNA polymerase II-specific transcription activator activity suggests that NICD1/Akt induces transcriptional programs related to cell cycle progression, differentiation, and potentially neoplastic transformation – aligning with Notch and Akt's established roles in promoting proliferation and suppressing apoptosis [22,122,130,133,390,443]. Finally, enriched acetoacetate-CoA ligase activity underscores altered lipid and energy metabolism, particularly ketone body utilisation and fatty acid processing, supporting the increased bioenergetic and biosynthetic demands of proliferating hepatocytes driven by NICD1/Akt signalling [431,444].

Collectively, these data demonstrate that NICD1/Akt co-activation triggers distinct molecular programmes in hepatocytes, which are shaped by their zonal origin – be that periportal or pericentral. The robust mitochondrial, metabolic, and transcriptional reprogramming evident within the periportal Gls2+ lineage contrasts with the comparatively muted, stress-adaptive profile of the GS+ lineage. This dichotomy alludes to this study having successfully exposed an intrinsic hepatocyte heterogeneity, which likely governs plasticity and tumorigenesis susceptibility across the liver lobule. In conclusion, the Gls2 lineage exhibits extensive transcriptomic reprogramming characterised by mitochondrial biogenesis, chromatin remodelling, and progenitor-like features supplanting hepatocyte differentiation markers. Meanwhile, the GS lineage adopts a more conservative, methylation- and metabolism-focused response. Together, these enriched molecular functions suggest that NICD1/Akt upregulation drives hepatocytes into a metabolically active and transcriptionally engaged state that supports proliferation, survival, and neoplastic transformation, consistent with the roles of Notch and Akt signalling in promoting oncogenic processes [22,124,133,236,390].

Following either 24- or 48-hours of transfection, qPCR analysis demonstrated that the upregulation of NICD1/Akt signalling induces a robust lineage reprogramming of the constituent cells from hepatocyte to biliary cell fate. This is evidenced by the significant downregulation of hepatocyte-specific markers Albumin and Hnf4α, alongside the concurrent upregulation of canonical biliary markers including Sox9, K19, and EpCAM [217,397,407,435]. Interestingly, while the classic hepatocyte markers are broadly repressed, the absence of significant changes in Cyp3A4 highlights that suppression of hepatocyte features may be selectively gene-specific or incomplete under certain experimental conditions. This type of heterogeneity in gene regulation has been observed following liver injury and similar genetic manipulation, with cells adopting a biphenotypic state, indicating that some hepatocyte functions may

persist despite global lineage redirection [74,397,445]. Nonetheless, the overall transcriptional profile strongly supports successful induction of biliary identity, closely paralleling molecular adaptations seen during liver development, regeneration, and biliary cancer models [11,15,92,446,447]. The increased expression of the Notch pathway target gene Hes1 not only indicates a shift toward a BEC-like phenotype, but it is also a confirmation that the cells successfully integrated the NICD1 plasmid, activating canonical Notch signalling [17,18,20]. These molecular changes reflect the cooperative interplay between Notch and Akt signalling pathways, which has been documented to suppress key hepatocyte transcription factors like Hnf4α, thus enabling activation of biliary genes, facilitating a cell fate switch toward a BEC lineage [15,397,448]. The finding that lipofectamine-mediated NICD1/Akt transfection in primary murine hepatocyte spheroids recapitulates the hepatocyte phenotypic changes observed following the HTVI *in vivo* establishes this PMHS model as a robust platform for studying hepatocyte lineage plasticity. Notably, Cre-mediated mGFP expression was successfully induced *in vitro* following hydroxytamoxifen treatment in spheroids derived from both Gls2CreER-mT/mG and GSCreER-mT/mG mouse lines. This demonstrates that the PMHS are composed of hepatocytes from all zones of the liver, including the two zones of interest. Additionally, it reiterates data presented in Chapter 3, with the expression of zonated hepatocyte marker genes being maintained *ex vivo*.

This maintenance of zonation underscores the physiological relevance of the spheroid system in modelling distinct hepatocyte populations with their intrinsic spatial identities, which enables precise interrogation of the differential plasticity among zonated hepatocytes and how they respond to oncogenic signals like NICD1/Akt. The controlled experimental environment of this model allows for detailed dissection of cell fate transitions without the confounding influences present in complex tissue contexts [148-151,157,211,262]. Ultimately, the ability to manipulate and isolate discrete hepatocyte subsets provides a powerful means to dissect zonation-dependent traits and the molecular and epigenetic controls of their transdifferentiation, thereby providing a greater understanding of how spatial heterogeneity governs liver regeneration and tumorigenesis.

CHAPTER 6

Conclusions, Limitations, and Future Perspectives

The liver is a uniquely zonated organ, with hepatocytes occupying distinct positions along the porto-central axis, which dictate their metabolic, detoxification, and regenerative roles [55,60,63,260]. This spatial heterogeneity has evolved to maximise the efficient functioning of the organ but also raises important questions about how different hepatocyte populations respond to injury, adapt under stress, or undergo malignant transformation. While zonation is well described at the physiological and metabolic levels, far less is understood about how zonal identity influences hepatocyte cell identity and plasticity — their ability to de-differentiate, reprogramme, and acquire new fates under experimental or pathological stimuli.

In an effort to address this gap in knowledge, this thesis set out to investigate the phenotypic stability, zonation characteristics, and lineage plasticity of hepatocytes by using a combination of complementary *ex vivo* and *in vivo* model systems. Throughout this study, evidence has been presented which demonstrates that hepatocyte fate is strongly influenced by the interplay between zonated position within the liver lobule and the activation of specific oncogenic signalling pathways.

In Chapter 3, it was demonstrated that 3D primary murine hepatocyte spheroid (PMHS) cultures outperform conventional 2D monolayers in maintaining hepatocyte phenotype and function long term *in vitro*. Primary hepatocytes rapidly de-differentiate within 96 hours in 2D culture, rendering them unsuitable for extended investigations of liver-specific processes. Contrastingly, spheroid cultures preserved hepatocyte identity for at least 12 days whilst displaying retention of lobular zonation patterns. The observation that media composition is able to modulate these zonated features confirmed the plasticity of hepatocyte spatial identity and underscored the influence of the microenvironment on liver physiology.

Chapter 4 interrogated the periportal and pericentral hepatocyte subpopulations *in vivo* through the development and characterisation of the Gls2CreER-mT/mG and GSCreER-mT/mG lineage-tracing mouse models. Using Gls2+ and GS+ hepatocytes as markers of the periportal and pericentral zones, respectively, this investigation reinforces published observations of zonated functionality, demonstrating the coordinated contribution of both subpopulations to overall liver homeostasis.

Finally, Chapter 5 explored how the co-upregulation of oncogenic signalling pathways – Notch and Akt – in Gls2CreER-mT/mG and GSCreER-mT/mG mice impacts the lineage plasticity of hepatocytes in zones 1 and 3, respectively. The results of these experiments revealed striking differences between the two hepatocyte subpopulations, with periportal (Gls2+) hepatocytes undergoing extensive

transcriptional and metabolic remodelling in response to NICD1/Akt upregulation, whereas pericentral (GS+) hepatocytes were unable to contribute to tumours and adopted a more conservative, stress-adaptive transcriptional response. The ability of the PMHS model to recapitulate the plasticity observed in the hepatocytes *in vivo* further confirmed the model as being a suitable platform for dissecting fundamental hepatocyte biology in future studies.

An important aspect not directly addressed in this thesis, but crucial to interpreting the behaviour of GS-expressing hepatocytes, is the role of canonical Wnt/β-catenin signalling. Previous published data have shown that Wnt ligands derived from central vein endothelial cells establish and maintain the pericentral identity of GS+ hepatocytes by driving glutamine synthetase expression and repressing periportal gene programmes [65]. Hepatic stellate cells, occupying the space of Disse between the sinusoidal endothelial cells and the hepatocytes, also help to modulate the pericentral zone, defining Wnt signalling through secretion of R-spondin 3 (RSPO3) [3]. In the context of this work, the comparatively suppressed plasticity observed in GS+ hepatocytes following NICD1/Akt upregulation may be a result of the Wnt activity potentially anchoring these hepatocytes in a transcriptional state that constrains their reprogramming potential.

Importantly, Wnt/β-catenin signalling has been described to govern stem and progenitor cell self-renewal, differentiation, and regeneration in multiple organ systems, including the intestine, skin, haematopoietic system, bone, and brain, as well as the liver. In the intestine, for example, Wnt maintains the pool of cycling crypt stem cells and supports their differentiation into specialised epithelial lineages, driving regeneration of the tissue [449,450]. In the skin, Wnt activity is central to regulating the plasticity of epidermal stem cells and hair follicle cycling. During homeostasis, Wnt signals maintain stemness within basal keratinocyte populations and are vital for the activation of hair follicle stem cells, enabling new hair growth in each cycle [383]. Conversely, inhibition or dysregulation of Wnt signalling in this system has been shown to suppress hair follicle regeneration, lead to abnormal epidermal differentiation, or contribute to skin tumorigenesis by allowing aberrant progenitor expansion and/or lineage commitment [383,449,451]. Within the hematopoietic system, Wnt signalling influences hematopoietic stem cell (HSC) fate, proliferation, and lineage plasticity. While low levels of Wnt activity in this system have been observed to support HSC maintenance and self-renewal, much like in the liver, tightly regulated Wnt gradients direct HSCs to differentiate into all mature blood lineages [452]. Dysregulated Wnt signalling is, however, known to interfere with normal haematopoiesis and contributes toward a disruption in self-renewal and differentiation of progenitor cells, leading to leukemic transformation, thus reflecting the pathway's impact on plasticity [377,452,453]. In the central nervous system, Wnt signalling is essential for orchestrating neural crest migration and patterning

during development, driving synaptic remodelling, and facilitating responses to injury – such as axonal regeneration after trauma or disease [385,411]. Imbalances in Wnt activity can disrupt neurodevelopment, hinder repair, or predispose cells to tumorigenesis through the destabilisation of self-renewal programmes.

Beyond regeneration, aberrant Wnt activation has also been observed in several cancers, including those of the liver, colon and lungs. Crosstalk between the Wnt/β-catenin signalling and PI3K/Akt signalling pathways has been implicated in the initiation and progression of hepatocellular carcinoma (HCC), with the complex interactions between pathway components driving stemness in tumour cells, influencing metastases, and conferring resistance to targeted therapies, further suggesting that the Wnt signalling gradient shapes both the hepatocellular subpopulation heterogeneity and propensity for plasticity [376,454,455]. The Wnt pathway also interacts with other signalling networks, including Notch, Hippo/YAP, and TGF-β, in order to mediate phenotypic switching and resistance through the promotion of epithelial-to-mesenchymal transitioning [29-31,63,343,376,403,454,455]. The Wnt signalling gradient is thus not only a fundamental determinant of zonated gene expression but also of the capacity for plastic responses to oncogenic cues.

Recent findings from a preprint by Chung *et al*. (2024) further contextualise the findings of the present study, particularly regarding the impact of metabolic zonation on hepatocyte plasticity and cancer risk [456]. While this work remains to be peer reviewed, it illustrates that the metabolic and spatial environment of hepatocytes directly impacts HCC initiation. In particular, their data demonstrated that zone 3 hepatocytes that had co-mutated Ctnnb1 and tumour-suppressor Arid2 (frequently co-mutated genes in HCC) appeared to be less competitive in terms of proliferation and survival, having been outcompeted by their wild-type neighbours, but they were more tumorigenic [456]. This contrasts with what was observed in the zone 1 Ctnnb1 and Arid2 mutants, as they appeared to be more proliferative than the wild-type cells but less tumorigenic. This supports the idea that metabolic context and zonation – not simply proliferative capacity – govern oncogenic susceptibility. The observations made by Chung *et al*. not only reinforce the present study's findings about zonation-dependent plasticity and transformation but also extend them by pinpointing specific genes (such as GSTM2/3) and pathways (Wnt/β-catenin) that could mechanistically underpin the plasticity and transformation capacity of the Gls2- and GS-expressing hepatocytes [456].

Whilst the present investigation was able to generate several novel insights regarding zonated hepatocyte biology, there were limitations that must be acknowledged. Firstly, although it was determined through statistical analyses that the experiments were adequately powered to detect clear

differences between the lineages in response to the NICD1/Akt upregulation, the possibility remains that minor but biologically relevant variations may not have been captured. In particular, the analyses of hepatocyte subpopulations (Gls2+ vs GS+) would have benefited from more biological replicates in order to delineate subtle aspects of the hepatocytes' functional specialisation more firmly. Additionally, it was technically impossible to collect matched tissue for both FACS sorting and immunohistochemical staining from the same animal due to the *in-situ* perfusion/digestion protocol required for cell isolation. As a result, it was not possible to definitively determine whether the observed differences within experimental groups reflected the underlying biological heterogeneity between mice or if they were partly attributable to technical challenges and variations in transfection efficiencies associated with the hydrodynamic tail vein injection (HTVI) procedure [349,350,352,423].

Another limitation that should be considered, specifically in relation to the PMHS model, is that whilst it does provide a powerful platform to study hepatocyte biology *ex vivo*, it does not fully reflect the complexity of the *in vivo* liver. The absence of non-parenchymal cell types, such as Kupffer cells, hepatic stellate cells, and sinusoidal endothelial cells, eliminates the ability to assess critical cell-cell interactions that help shape hepatocyte behaviour. Similarly, the static nature of spheroid culture within a well of a U-bottom tissue culture plate does not replicate the nutrient and oxygen gradients that are key drivers of zonation *in vivo*. The direct translation of any findings made in the PMHS models into human hepatocytes also complicates the interpretation of the results, given interspecies differences in liver architecture, xenobiotic metabolism, and oncogenic susceptibility.

Thus, a potential next step in terms of the *in vitro* work would be to enhance the physiological complexity of the spheroid system by co-culturing hepatocytes with non-parenchymal liver cells in order to better replicate the multicellular networks that sustain liver function and regeneration. Advancements in microfluidic "liver-on-chip" technologies also offer the exciting potential to impose oxygen, nutrient, and hormone gradients similar to those experienced by the cell *in vivo*, which would also provide a more advanced platform to study zonation [148,155,247,457]. These refinements would improve the translational value of the primary hepatocyte *ex vivo* models, facilitating more accurate *in vitro* study of hepatocellular disease and pharmacological testing.

It should also be considered that the experiments described in this thesis were conducted over relatively short periods, ranging from days to weeks. Whilst these time courses were sufficient to capture acute responses to culture conditions and the NICD1/Akt signalling, such timeframes do not necessarily reflect the chronic processes of regeneration, adaptation, or whole neoplastic progression present within a diseased or damaged liver. Therefore, care must be taken when interpreting the

cellular responses to the upregulation of NICD1/Akt signalling, as both HTVI (*in vivo*) and lipofection (*in vitro) are* effective for experimental purposes but do not truly replicate the stochastic, gradual activation of oncogenes that occurs in human disease. Similarly, while bulk transcriptomic analyses revealed shifts in cellular state, this approach offers only a snapshot of the broader regulatory landscape, as post-translational modifications, signalling network crosstalk, and dynamic chromatin interactions likely contribute significantly to the zonated plasticity of the hepatocytes – analyses of which were unfortunately outside the scope of this thesis. Thus, future work could integrate single-cell multi-omics approaches – including single-cell or single-nuclear RNA-seq, ATAC-seq, and proteomics – to gain a greater overview of the molecular determinants of zonation-dependent plasticity. Epigenetic profiling, in particular, may reveal how chromatin remodelling interacts with metabolic rewiring in order to direct the divergent lineage responses described in this thesis [2,408,411,458,459].

This study primarily examined Notch and Akt signalling, two well-characterised pathways known to drive proliferation and oncogenesis within hepatocytes due to their well-established oncogenic potential and their relevance to liver cancer biology [130,131,133,357]. However, hepatocarcinogenesis is not a single-pathway process; it emerges from the convergence of multiple signalling cascades. Prominent among these are β-catenin signalling [376,454,455], which regulates central metabolic programming and cellular regeneration; Ras/MAPK signalling [67,460], a master regulator of growth and proliferation; and Hippo/Yap/Taz signalling [46-48,133], which integrates mechanical, metabolic, and microenvironmental cues to promote survival and neoplastic expansion. Notably, each of these pathways is known to exhibit some degree of spatial heterogeneity within the liver lobule, either through differential activation gradients or through the zonation of their target gene networks. This raises the possibility that distinct hepatocyte subpopulations may be sensitive to specific oncogenic drivers, resulting in zonally restricted initiation patterns of tumorigenesis. Future studies could, therefore, build upon the work done in this investigation to systematically assess whether the activation of β-catenin, Ras/MAPK, or Hippo/Yap/Taz signalling elicits similarly zonated responses in hepatocytes. To evaluate whether activation of β-catenin, Ras/MAPK, or Hippo/Yap/Taz pathways elicits zonated hepatocyte responses, studies could deploy zone-specific genetic manipulations using Cre lines targeting periportal (zone 1) or pericentral (zone 3) hepatocytes. Alternatively, pharmacological interventions could be used *in vivo* to modulate these pathways and assess their impact on hepatocyte plasticity in different lobular zones. For β-catenin signalling, small molecule inhibitors like ICG-001, which disrupt β-catenin/CBP interaction, could selectively suppress pathway activity [461]. Ras/MAPK signalling can be targeted by clinically available MEK inhibitors such as trametinib or selumetinib to reduce downstream ERK 1/2 activation [462]. When assessing the Hippo/Yap/Taz pathway, emerging inhibitors like verteporfin [463],

which disrupts YAP-TEAD interactions, or novel agents such as IAG933, which selectively blocks YAP/TAZ activity, could be used [464]. The zonation-preserving PMHS model also provides a versatile *ex vivo* platform to investigate Wnt signalling's impact on hepatocyte plasticity. This can be achieved through the co-culturing of hepatocytes with central vein endothelial cells to examine the direct influence of extracellular Wnt ligands. Additionally, this model would also be an excellent vehicle to assess the pharmacological modulators of β-catenin, Ras/MAPK, and Hippo/Yap/Taz signalling in the cells *ex vivo* in real time, enabling the precise identification of pathway effects within a spatially relevant context that mimics *in vivo* zonation.

Another approach to evaluate the impact of oncogenic pathways on hepatocyte plasticity within lobular zones involves the use of conditional knockout or activation strategies targeting key signalling components. By employing the same periportal (Gls2CreER) and pericentral (GSCreER) Cre drivers, precise genetic modifications can be induced in hepatocytes confined to defined zones, enabling detailed analysis of zone-dependent responses and plasticity. For β-catenin, selectively deleting β-catenin or its negative regulator APC can reveal the impact of pathway activation or loss on metabolic gene expression and zonation [34,61]. Similar approaches might target Ras/MAPK components such as Kras or MEK1/2 [67], and Hippo pathway effectors like Yap and Taz [48,304,463,464]. Combining these genetic tools with lineage tracing and spatial transcriptomics would provide a detailed insight into zonation-dependent regulation of hepatocyte identity, plasticity, and oncogenic susceptibility.

The apparent differences in response to stimuli from Gls2+ and GS+ hepatocyte populations shown in this thesis also raise the question of the effects of how metabolites and metabolic pathways may be regulating hepatocyte plasticity. By applying advanced metabolomic profiling, such as mass spectrometry or nuclear magnetic resonance, alongside isotope tracing approaches, the detailed mapping of metabolic fluxes and identification of metabolite changes that accompany lineage switching in hepatocytes may be possible [465-467]. Genetic and pharmacological manipulation of key metabolic enzymes – for example, through conditional knockout models or small-molecule intervention as mentioned above – can directly test the causal influence of specific pathways, such as one-carbon metabolism or ketogenesis, on reprogramming capacity. Integrating these strategies with single-cell transcriptomic and epigenomic platforms, and ultimately with single-cell metabolomics, will help resolve the heterogeneity of hepatocyte plasticity and clarify cross-talk between metabolic state and gene regulation [53,441].

A key avenue for further elucidating the differences in stunted plasticity observed in the pericentral hepatocytes, specifically, involves leveraging CRISPR screens to systematically interrogate the

influence of Wnt pathway components and downstream effectors. Pericentral Wnt signals, predominantly established by endothelial cell-derived ligands such as Wnt2 and Wnt9b, are essential for maintaining central zone identity and function [3,65,380]. Targeting these ligands or their key receptors, including Frizzled family members and LRP5/6, could reveal the extent to which manipulating Wnt signalling modulates plasticity and fate transitions in GS-positive hepatocytes. Additionally, CRISPR-based loss-of-function or activation studies of canonical Wnt targets such as Axin2, Tbx3, Lgr5, Cyclin D1, c-Myc, and negative regulators like Apc would help define their specific roles in regulating zonal stability and lineage commitment. These investigations, particularly when paired with spatial transcriptomics and functional assays, could pinpoint which Wnt-regulated genes act as gatekeepers versus facilitators of pericentral plasticity, thereby opening new therapeutic avenues for liver regeneration and disease modelling.

The Gls2CreER-mT/mG and GSCreER-mT/mG lineage tracing systems developed in this study also have the potential to extend beyond cancer models, offering a valuable platform to explore hepatocyte plasticity in non-malignant disease contexts such as fibrosis, steatosis, and drug-induced liver injury. Previous studies of liver regeneration and injury-induced reprogramming have widely employed chemical injury models to interrogate hepatocyte plasticity [468]. One well-established system is the porphyrinogenic 3,5-diethoxycarbonyl-1,4-dihydrocollidine (DDC) diet, which causes accumulation of porphyrin plugs, induces chronic cholestatic injury, and results in periportal fibrosis with strong activation of ductular reactions [94,98,99,397]. Lineage tracing experiments in this model have demonstrated that genetically labelled hepatocytes can undergo transdifferentiation into biliary epithelial-like cells expressing markers such as EpCAM and K19, highlighting their capacity for hepatocyte-to-biliary reprogramming under injury conditions [92,100]. Another commonly used chemical injury regimen is thioacetamide (TAA) administration, which produces progressive periportal fibrosis, regenerative nodule formation, and, at longer durations, cirrhosis and hepatocellular carcinoma [318,440,469]. Chronic TAA injury has been shown to enhance hepatocyte plasticity by promoting dedifferentiation and senescence-associated states that increase susceptibility to lineage conversion and neoplastic transformation [470,471]. These models have proven particularly useful for uncovering the mechanisms by which hepatocytes adapt and reprogramme in response to sustained injury. For instance, in the DDC model, hepatocyte-derived BEC-like cells have been observed to integrate into bile ducts and contribute directly to regeneration after injury, providing compelling evidence for lineage plasticity in hepatocytes [92,101]. Similarly, prolonged TAA treatment has been associated with hepatocyte-derived cells expressing biliary markers such as Sox9, suggesting a shared injury-induced pathway of lineage switching [468,472]. Thus, DDC and TAA are powerful models for probing transcriptional, epigenetic, and

microenvironmental cues that regulate hepatocyte fate decisions during chronic injury and regeneration. These models could be applied to Gls2- and GSCreER-mT/mG mouse lines in future studies to further investigate how metabolic zonation of the hepatocytes influences their regenerative and reprogramming capacities under pathophysiological conditions.

In summary, by developing a PMHS model that maintains zonated characteristics *ex vivo*, validating previously published spatially distinct metabolic specialisations, and uncovering lineage-specific responses to oncogenic drivers (NICD1/Akt), this thesis demonstrates that hepatocyte zonation is a fundamental determinant of plasticity, stress adaptation, and susceptibility to oncogenic transformation. By situating zonation at the centre of hepatocyte fate determination and liver disease modelling, this work helps to shift the current understanding of hepatocyte biology. Rather than being treated as a homogeneous population, hepatocytes have been revealed here to be dynamic, spatially defined, plastic cells whose responses to oncogenic stimulation offer valuable insight into liver physiology and pathology. Clinically, if certain hepatocyte subtypes are intrinsically more prone to reprogramming, dedifferentiation, or oncogenic transformation, this heterogeneity could explain why particular regions of the liver are disproportionately vulnerable to cancers or chronic disease. Thus, by mapping these spatial propensities, it may help to compile risk assessments for patients with chronic liver injury, guide targeted therapeutic strategies towards the most plastic subpopulations and inform regenerative medicine approaches that seek to harness or suppress hepatocyte reprogramming.

Appendix

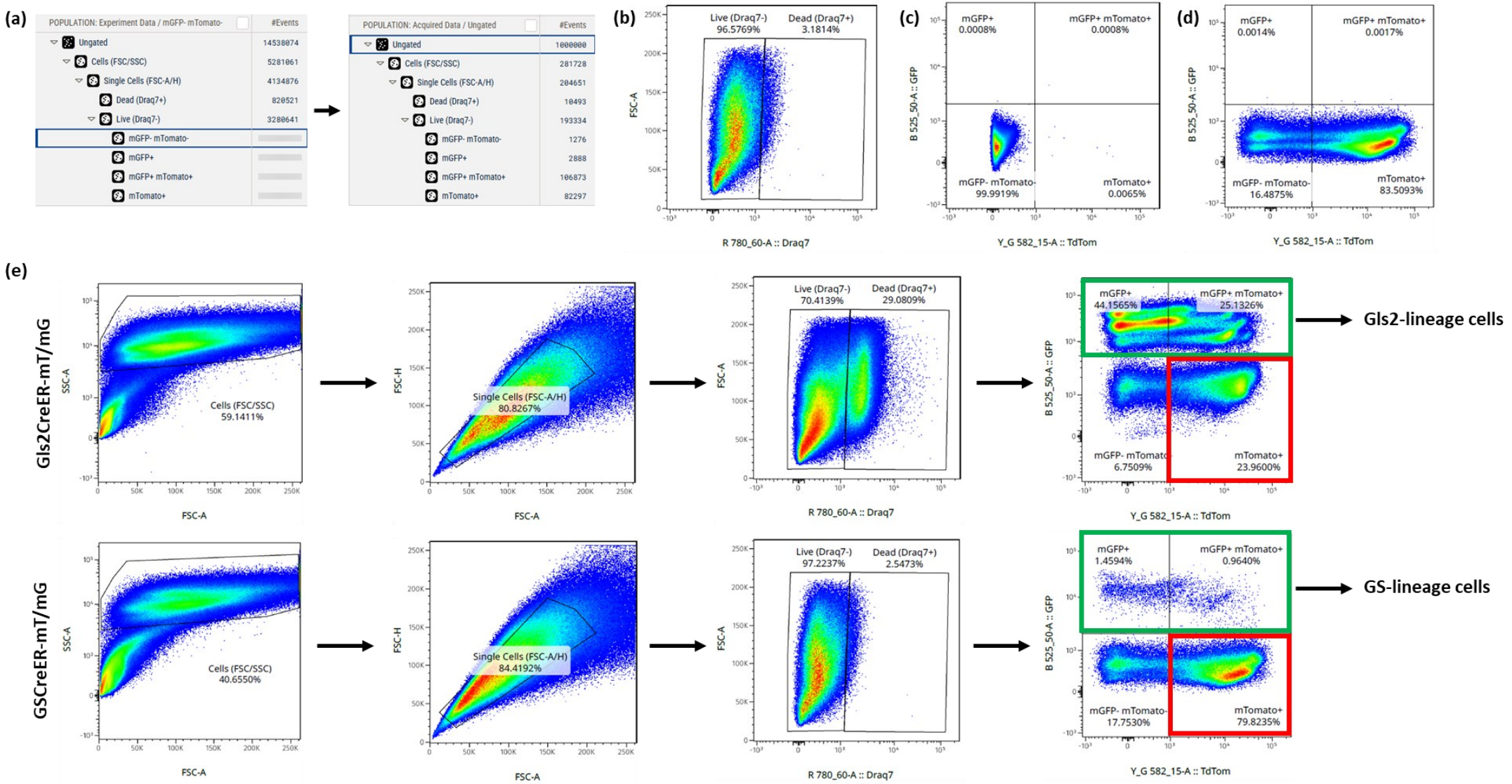
(a)
POPULATION: Experiment Data / mGFP- mTomato-
#Events
Ungated 14538074
Cells (FSC/SSC) 5281061
Single Cells (FSC-A/H) 4134876
Dead (Draq7+) 820521
Live (Draq7-) 3280641
mGFP- mTomato-
mGFP+
mGFP+ mTomato+
mTomato+
POPULATION: Acquired Data / Ungated
#Events
Ungated 1000000
Cells (FSC/SSC) 281728
Single Cells (FSC-A/H) 204651
Dead (Draq7+) 10493
Live (Draq7-) 193334
mGFP- mTomato- 1276
mGFP+ 2888
mGFP+ mTomato+ 106873
mTomato+ 82297
(b)
Live (Draq7-) 96.5769%
Dead (Draq7+) 3.1814%
FSC-A
R 780_60-A :: Draq7
(c)
mGFP+ 0.0008%
mGFP+ mTomato+ 0.0008%
mGFP- mTomato- 99.9919%
mTomato+ 0.0065%
B 525_50-A :: GFP
Y_G 582_15-A :: TdTom
(d)
mGFP+ 0.0014%
mGFP+ mTomato+ 0.0017%
mGFP- mTomato- 16.4875%
mTomato+ 83.5093%
B 525_50-A :: GFP
Y_G 582_15-A :: TdTom
(e)
Gls2CreER-mT/mG
SSC-A
Cells (FSC/SSC) 59.1411%
FSC-A
FSC-H
Single Cells (FSC-A/H) 80.8267%
FSC-A
FSC-A
Live (Draq7-) 70.4139%
Dead (Draq7+) 29.0809%
R 780_60-A :: Draq7
mGFP+ 44.1565%
mGFP+ mTomato+ 25.1326%
mGFP- mTomato- 6.7509%
mTomato+ 23.9600%
B 525_50-A :: GFP
Y_G 582_15-A :: TdTom
Gls2-lineage cells
GSCreER-mT/mG
SSC-A
Cells (FSC/SSC) 40.6550%
FSC-A
FSC-H
Single Cells (FSC-A/H) 84.4192%
FSC-A
FSC-A
Live (Draq7-) 97.2237%
Dead (Draq7+) 2.5473%
R 780_60-A :: Draq7
mGFP+ 1.4594%
mGFP+ mTomato+ 0.9640%
mGFP- mTomato- 17.7530%
mTomato+ 79.8235%
B 525_50-A :: GFP
Y_G 582_15-A :: TdTom
GS-lineage cells

Appendix Figure 1: Representative Corrected Gating Strategy, Controls, and Sorting Hierarchy for Hepatocyte Lineage Tracing. *Representative flow cytometry plots illustrating the sequential gating used to define intact cells, live singlets, and mGFP+/mTomato+ hepatocyte populations for sorting.* ***(a)*** *FlowJo population hierarchy and down-sampling applied during re-analysis to improve debris exclusion and clarify the live/dead and fluorophore-defined gates.* ***(b)*** *Hepatocyte isolation stained with DRAQ7, illustrating the DRAQ7-negative live population used to define the live/dead gate (no fully dead, DRAQ7-positive control sample was acquired for this experiment).* ***(c)*** *Fluorophore-negative hepatocyte control (C57BL/6J, mT/mG-negative) used to define background fluorescence and set mGFP and mTomato negativity thresholds.* ***(d)*** *mTomato-only control (Gls2CreER-mTmG hepatocytes without tamoxifen) used to confirm mTomato detection and gate placement.* ***(e)*** *Sequential sorting strategy for reporter hepatocytes in both Gls2CreER-mT/mG and GSCreER-mT/mG mouse lines, showing gating from total cells (FSC/SSC) to single cells (FSC-A/FSC-H), to live (DRAQ7/FSC) events, and finally to quadrants defining mGFP+ and/or mTomato+ hepatocytes; mGFP+ cells (including those co-expressing mTomato) were sorted to isolate Gls2- or GS-lineage-derived hepatocytes depending on the Cre driver used, while mTomato-only hepatocytes were collected as the negative-lineage control population for downstream analyses.*

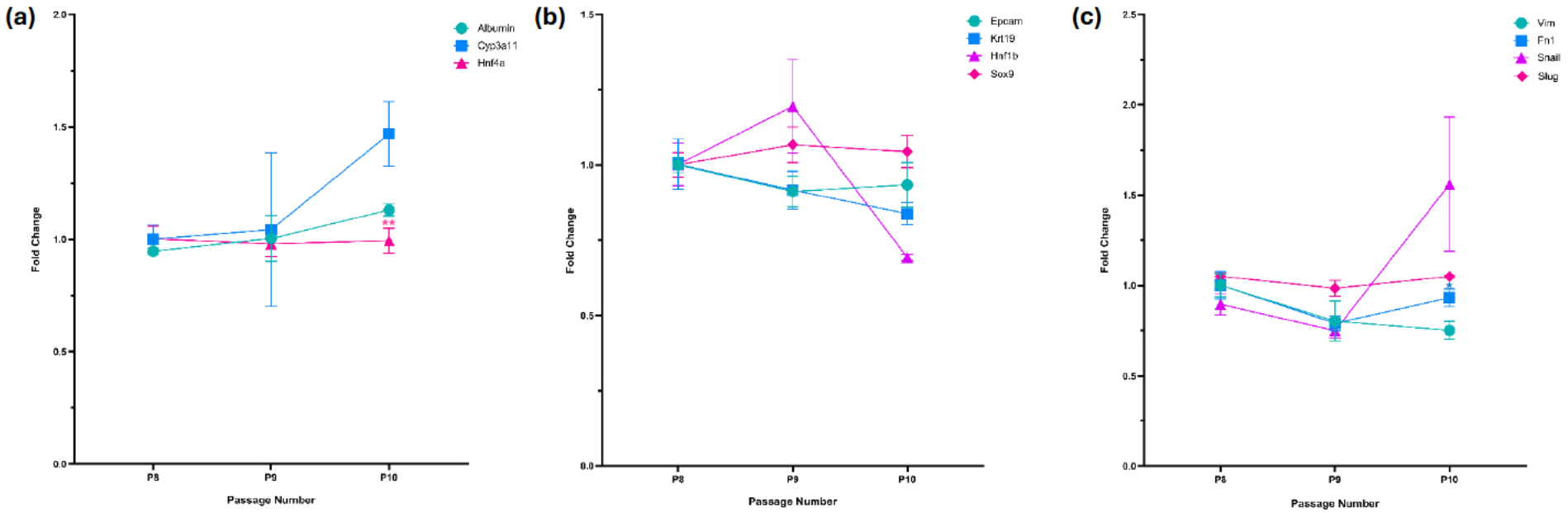

Appendix Figure 2: (a) Hepatocyte, (b) Biliary, and (c) Mesenchymal Gene Expression in Control C57Bl6/J Cholangiocyte Organoids Across Passages. *Cholangiocyte organoids derived from C57BL/6J control mice were used as the control population for hepatocyte, cholangiocyte, and mesenchymal gene expression analyses. RNA was isolated from these control cholangiocyte organoids at sequential passages 8, 9, and 10 for quantification of gene expression over culture time.*

Appendix Table 1: Expression of Hepatocyte, Biliary, and Mesenchymal Gene Markers in Control C57Bl6/J Cholangiocyte Organoids Across Passages (P) 8, 9, and 10. *Mean differences (Mean Diff.), standard error of the mean (Std. Error), and adjusted p-value all calculated through a repeated-measures one-way ANOVA and Tukey HSD multiple comparisons test (*p ≤ 0.05; **p ≤ 0.01).*

	P8-9			P9-10		
	Mean Diff.	**Std. Error**	**p.adj**	**Mean Diff.**	**Std. Error**	**p.adj**
Alb	-0.05667	0.05667	0.6452	-0.1267	0.06741	0.3405
Cyp3A11	-0.04155	0.2316	0.9826	-0.4257	0.2743	0.4305
Hnf4α	0.02167	0.005239	0.0964	-0.01400	0.00100	0.0092**
EpCAM	0.08845	0.02030	0.0877	-0.02210	0.01314	0.3917
K19	0.0860	0.01788	0.0732	0.07803	0.01928	0.1003
Hnf1β	-0.1933	0.08465	0.2591	0.5023	0.08859	0.0537
Sox9	-0.06630	0.01184	0.0550	0.02223	0.01272	0.3737
Vim	0.1985	0.05819	0.1356	0.05170	0.04054	0.5281
Fn1	0.2112	0.04716	0.0834	-0.1408	0.01987	0.0351*
Snail	0.1468	0.05648	0.2127	-0.8109	0.2064	0.1057
Slug	0.06657	0.02098	0.1535	-0.06597	0.02895	0.2599

Appendix Table 2: Identification of Tamoxifen-induced Gene Expression through Comparison of Differentially Expressed Genes in Tamoxifen-treated Gls2CreER-mT/mG Samples and Corn-Oil-treated GSCreER-mT/mG Samples.

Significantly Downregulated Genes from Gls2 mGFP+ (Tamox) vs. GS mGFP+ (Corn Oil) Dataset	**Shared Genes – Assumed to be Influenced by Tamoxifen Treatment**	**Significantly Upregulated Genes from Gls2 mGFP+ (Tamox) vs. GS mTomato+ (Corn Oil) Dataset**
Cyp2d9	Cyp1a2	Trim30b
Cyp2c23	Cyp2a5	Sucnr1
Cyp2c37	Cyp2c29	Mup1
Cyp4a12b	Cyp2c50	Cyp7a1
Cyp2c54	Cyp2e1	ENSMUSG00000139631
Ang	Cyp4a12a	Ugdh
Gls2	ENSMUSG00000124618	Spp1
Cyp2d40	Elovl3	Trim30c

Gm11942	Fcho2	ENSMUSG00000124961
Gstm3	Gas6	Tbx3
Selenbp2	Gm13775	Adh6-ps1
Gm10263	Gm45792	Trim34b
Hsd3b2	Gulo	Adgrf1
Hsd3b5	Lgr5	Gm37518
Cyp7b1	Mup11	Apol7a
Gstm2	Mup15	Gm47689
C6	Mup16	Gm40787
Slc13a3	Mup17	Tnfrsf19
Slc25a30	Mup18	Podn
Cyp2c67	Mup20	Xist
Mup8	Mup21	ENSMUSG00000135760
Slc22a1	Mup7	
Mup3	Mup9	
Tsc22d1	Oat	
C9	Rmdn2	
Ugt2b1	Rnase4	
Hspb1	Slc17a8	
Nat8f5	Slc1a2	
Nat8	Slco1b2	
Lhpp	Susd4	
Tmem254		
Cyp3a25		
Mup14		
Rhbg		
Nox4		
Prodh		
Gm56805		
Gm3734		
ENSMUSG00000123103		
Car3		
ENSMUSG00000131191		
Mcm10		
Aatk		
Ar		

Rcan2		
Slc16a10		
Gna14		
Hspa1b		
Aox3		
Serpine2		
Mup12		
Gm31583		
Aldh2		
Pemt		
Aldh1a1		
Entpd5		
Vcp		
Stmp1		
Errfi1		
Cyp2c38		
Mup-ps3		
Slc43a3		
Gstm1		
Keg1		
Sult2a8		
Notum		
Sp5		
Tgfa		
Ces3a		
Fitm1		
Gsta3		
Gm56821		
Rgn		
Pepd		
Blvrb		
Tdo2		
Ugt2b35		
Aldh3a2		
Mup19		

Appendix Table 3: Differentially Expressed Genes Identified Following the Comparison of mGFP+ Hepatocytes Isolated from Gls2CreER-mT/mG and GSCreER-mT/mG Mouse Livers. *DESeq2 analysis (Benjamini-Hochberg) cutoff of adjusted p<0.05 (-log10 adjusted p<1.3) and log2 fold change > 1/-1.*

Significantly Upregulated Genes in Gls2-Expressing Periportal Hepatocytes	Log2FC	-log10 adj p-value	Significantly Upregulated Genes in GS-Expressing Pericentral Hepatocytes	Log2FC	-log10 adj p-value
Cyp2d9	-3.262493304	16.49621	Slc34a2	5.960625684	22.22475
Cyp2c23	-3.686762821	14.48017	Mmd2	5.763174301	21.02228
Cyp2c37	-3.809237919	13.8729	C1rb	6.468020718	18.25104
Fcho2	-3.094772154	12.90658	Ptgds	6.715355882	16.49621
Cyp4a12b	-10.41853531	12.44009	Cyp2a4	8.309631741	13.75945
Gulo	-3.542823828	12.44009	Cyp2b9	6.539028918	13.56864
Cyp2c54	-3.220232134	10.70115	Cyp4a14	5.702221342	12.6073
Ang	-3.336684936	10.52288	Cyp4a10	3.69987575	12.37986
Gls2	-6.2402555	10.38934	Slc22a27	9.173586971	8.578396
Cyp2d40	-3.29674262	9.568636	GS	4.786524937	8.492144
Gm11942	-3.300229657	9.342944	Isyna1	5.408779957	7.585027
Gstm3	-4.123224995	9.069051	Slc22a26	8.318245992	7.510042
Selenbp2	-3.036162999	9.069051	Ggct	3.59612002	7.235077
Gm10263	-4.554544107	9.042872	Nipal1	5.060086928	6.679854
Hsd3b2	-3.321439202	8.931814	Flnb	2.924285941	6.498941
Hsd3b5	-3.974207614	8.759451	Prtn3	6.165968939	6.49485
Cyp7b1	-3.206305259	7.850781	Ugt2b37	4.604310067	6.25649
Gstm2	-2.992670909	7.204815	H2-Eb1	7.929554815	5.012781
C6	-3.961421507	6.68403	Nedd9	4.747933703	4.730487
Slc13a3	-3.966996174	6.250264	Atp2b2	7.405408382	4.681937
Slc25a30	-2.404975439	5.653647	Tcf24	7.460550307	4.476254
Cyp2c67	-2.506352001	5.204815	Gm6135	3.651498396	4.260428
Mup8	-3.369689239	4.962574	Adamts7	5.210873459	4.176526
Slc22a1	-2.092049949	4.962574	Abcd2	3.80593433	4.074172
Mup3	-2.429943153	4.91364	Plch2	7.434056171	4.020452
Tsc22d1	-2.710703246	4.772113	Gdf15	3.788033544	3.934185
C9	-1.98882237	4.571865	A1bg	7.196162353	3.751997
Ugt2b1	-1.902010305	4.427128	4931408D14Rik	2.176546276	3.704525
Hspb1	-6.422886948	4.383	D17H6S56E-5	4.709774145	3.417146

Nat8f5	-5.134565203	4.149967	Cyp4a31	6.548887025	3.385684
Nat8	-3.938364971	4.083546	Acnat2	3.324244698	3.292417
Lhpp	-3.659123632	4.041914	Krt79	4.96026219	3.279529
Tmem254	-1.836459871	4.041436	Acp1	3.943850473	3.212671
Mup20	-6.535428641	3.99638	Cd63	4.324519589	3.163673
Cyp3a25	-1.924174617	3.99638	Krt4	6.960381026	3.163673
Mup14	-2.944814232	3.98909	Snord118	3.948175183	3.103388
Rhbg	-3.497367641	3.951263	Map3k13	1.98758703	3.084047
Nox4	-3.306225633	3.720929	Gtpbp2	2.838533033	2.959243
Prodh	-1.902989508	3.671215	Gm42047	4.431427289	2.955171
Gm45792	-5.849778615	3.574172	Paxx	2.629041853	2.938514
Gm56805	-2.612907664	3.500664	Mrps12	2.796048455	2.921949
Gm3734	-3.349353983	3.497425	Tff3	3.516415834	2.869297
ENSMUSG00000123103	-7.165224199	3.493395	Uroc1	1.880389313	2.866506
Car3	-2.277614587	3.259207	Tm4sf4	1.708611721	2.724034
ENSMUSG00000131191	-6.955447729	3.213969	Pf4	6.970003237	2.672293
Mcm10	-1.744472741	3.127805	H2-Aa	3.215861092	2.642461
Slco1b2	-1.382063367	2.94798	Cyp39a1	6.327317017	2.642461
Aatk	-6.454037166	2.944622	Fam13a	3.699088202	2.620685
Ar	-4.98162338	2.724034	Cyp3a44	6.656241614	2.569385
Rcan2	-4.167348248	2.608916	Itga6	3.15145335	2.508291
Slc16a10	-1.899073799	2.574837	Igf1os	4.829793562	2.498261
Gna14	-6.095675259	2.507813	Paox	3.647739086	2.467547
Hspa1b	-3.370557343	2.413943	Ehhadh	3.357192729	2.460612
Aox3	-1.684383238	2.283614	Dpy19l3	3.085841023	2.343921
Serpine2	-3.832839629	2.190776	Gm56807	5.892931442	2.287631
Mup12	-4.892676866	2.128889	Gng5c	6.890795377	2.264037
Gm31583	-2.118949691	2.126571	Sulf2	2.620246711	2.252813
Aldh2	-1.805044596	2.126571	Hao2	6.444902918	2.237692
Pemt	-1.889489961	2.072836	Gpat3	5.395783746	2.213364
Aldh1a1	-1.610913419	2.065343	Gm19705	4.813587016	2.190776
Entpd5	-1.528329891	1.991915	Agt	1.28902618	2.180941
Vcp	-2.292720728	1.92597	Gm42428	6.302883807	2.180941
Stmp1	-1.815821214	1.877524	Dsg1c	2.712840468	2.16683
Errfi1	-1.681131134	1.854505	Atp8b5	3.680408774	2.15477

Cyp2c38	-2.02927219	1.847291	Sult5a1	2.732062879	2.079456
Mup-ps3	-6.904692334	1.836285	ENSMUSG00000126988	4.427828487	2.065001
Slc43a3	-3.104357131	1.741503	Tent5a	1.629735577	2.010733
Gstm1	-1.898878383	1.689376	Akr1c18	5.28439198	1.98379
Keg1	-1.471977267	1.67322	Slc16a6	1.820964907	1.972169
Sult2a8	-1.572355522	1.641372	Vnn3	2.124197794	1.972146
Notum	-2.782557434	1.639501	Gm49417	6.892343643	1.972146
Sp5	-6.059408693	1.628558	Fgl1	1.613572736	1.906441
Tgfa	-2.956926422	1.599081	Inf2	2.103255204	1.892379
Ces3a	-1.29504485	1.569212	Gm49594	2.910399888	1.88762
Fitm1	-2.713980578	1.561606	Ube2c	6.268116984	1.88762
Gsta3	-1.922436982	1.561606	Acot4	1.706120401	1.875778
Gm56821	-2.402885914	1.551946	Dynll1	2.264466093	1.875778
Rgn	-2.030682169	1.532906	Gm44066	3.526113205	1.875778
Pepd	-2.528557431	1.53281	Gm7298	8.364039593	1.800407
Blvrb	-1.51354157	1.53281	Aspg	2.273603561	1.794132
Tdo2	-1.439709186	1.53281	H2-T22	2.792794992	1.781864
Ugt2b35	-1.421249006	1.51567	Ly6e	1.289589205	1.767624
Aldh3a2	-1.883596714	1.510073	Baiap2	2.238562782	1.759891
Mup19	-2.823431114	1.50574	App	1.744746083	1.75175
			2610507I01Rik	3.805240993	1.735261
			Abhd2	1.685043743	1.726969
			Flna	4.112068666	1.726969
			Vcam1	3.118205247	1.725686
			Amer2	5.650519343	1.689376
			H2-T24	6.543043161	1.646487
			Phldb1	6.054838394	1.635074
			Cdkn1a	2.422278141	1.628558
			Ppard	3.671245395	1.611566
			Sfxn1	1.352169554	1.561606
			Anxa5	2.517127914	1.556964
			Gm57259	3.267137147	1.551946
			Mup5	3.794450113	1.538961
			Ctps2	6.145656683	1.527212
			ENSMUSG00000141894	3.337662067	1.52073

			Josd2	2.530624967	1.519557
			Mob3a	4.371278232	1.519557
			Mmp14	1.438945812	1.510073

Appendix Table 4: Top 50 genes correlated with Glutaminase 2 (Gls2) or Glutamine Synthetase (GS) expression in hepatocytes, based on RNA-seq data from Ben-Moshe et al. Genes with absolute Pearson correlation coefficients >0.5 were selected, and the overall correlation strength was defined as the sum of absolute correlations with Gls2 and GS.

Genes most correlated with Gls2 expression	Correlation with Gls2	Genes most correlated with GS expression	Correlation with GS
Gls2	1	Glul	1
Odad3	0.945579749	Cldn2	0.961860319
Pcca	0.945473467	Rcan2	0.958138626
Cyp2f2	0.938289821	Slc13a3	0.948115848
Otc	0.934072815	Slc1a2	0.933600822
Uox	0.933659154	Gm57349	0.92150623
Gsap	0.932138987	Slc22a26	0.908667817
Itm2c	0.930231315	Slc43a3	0.905250364
Hsd17b6	0.914522616	Enpp1	0.902783636
Keg1	0.909280507	Gm17087	0.900883373
Nab2	0.908863011	Slc38a10	0.896083173
2810408I11Rik	0.908123428	Gm57094	0.893841744
Got1	0.90692014	Nanp	0.893091489
Eif4h	0.906136093	Serpina7	0.892858458
Csnk1g2	0.90440164	Gm15502	0.888951112
Hal	0.903776154	Cpne8	0.888712502
Las1l	0.897370108	Gm3734	0.88783922
As3mt	0.896873794	ENSMUSG00000137277	0.88514039
Fahd1	0.895052386	Slc22a3	0.884546223
Aldob	0.891125729	Ptpn1	0.883864325
Tdo2	0.889918031	Dusp22	0.881887313
Nadsyn1	0.8898869	Vapb	0.881687166
Mrpl36	0.888998081	Gnl3	0.880623042
Cyp2d41-ps	0.888438011	Glud1	0.878490682
Lsr	0.886883461	Xdh	0.878473647
Gm16573	0.885884033	Cebpd	0.877531562
H2-T23	0.884277381	Rec8	0.877046938
Gm32461	0.884092239	ENSMUSG00000128284	0.87485199
Rnf181	0.884068382	Tbc1d2b	0.87359187
Akr1c12	0.882286091	Egln3	0.87013929

Kynu	0.880687294	Atp13a2	0.869644183
Ctnnbip1	0.880233064	2310030G06Rik	0.868703448
Sucla2	0.879168535	Adgrg2	0.867596641
Gm3809	0.8776975	Aldh3a2	0.866896359
Gm19076	0.876694788	Gm44228	0.864539923
Igfals	0.876548863	Tmem243	0.863624795
Atad3a	0.876491791	Pigo	0.863005751
Aspg	0.876083826	Mcph1	0.862603733
Gm13328	0.875936298	Ddx19b	0.862474502
Gm12728	0.875781524	Gorasp1	0.862432216
Tspan14	0.875353431	Rnase4	0.86198868
Gm12632	0.874120588	Nrn1	0.860632806
Coq9	0.87199998	Cldnd1	0.860166761
ENSMUSG00000139429	0.871110722	Prg4	0.856100529
Gm2451	0.870750605	Gm42855	0.853954097
Vmp1	0.870562902	Gbp10	0.853658029
Tstd3	0.869480094	Clp1	0.85349265
Lman2	0.868489427	Sec63	0.853379913
Arsg	0.866086855	4933404O12Rik	0.851687532
Nudt19	0.865078074	Pex26	0.850413299

Appendix Table 5: Significant Molecular Function and Biological Processes Gene Ontology Enrichment Terms Identified from Bulk RNA-Sequencing of mGFP+ Hepatocytes from Gls2CreER-mT/mG and GSCreER-mT/mG Mice in the Present Study Compared to those Identified to be Gls2 or GS-expression Correlated from the Ben-Moshe et al. Dataset. *Data were filtered using Benjamini-Hochberg multiple test correction (adjusted $p < 0.05$) and only GO terms occurring at a frequency of >5% within the dataset are shown. BP – Biological Processes; MF – Molecular Functions.*

Gls2CreER-mT/mG mGFP+ Hepatocyte GO Terms			
GO Term	**Category**	**Population Frequency**	**q-value**
binding	MF	50%	1.38E-04
catalytic activity	MF	19%	5.30E-18
small molecule binding	MF	19%	8.42E-07
identical protein binding	MF	8.60%	8.43E-04
hydrolase activity	MF	8.30%	1.71E-03
enzyme binding	MF	8.00%	8.93E-03
transporter activity	MF	4.20%	0.0166
transmembrane transporter activity	MF	3.80%	0.0101
lipid binding	MF	3.20%	8.04E-04
protein homodimerization activity	MF	2.80%	1.46E-03
oxidoreductase activity	MF	2.70%	6.06E-17
heme binding	MF	0.56%	1.86E-14
modified amino acid binding	MF	0.40%	1.55E-05
glutathione transferase activity	MF	0.11%	1.67E-06
cellular process	BP	56%	2.15E-08
metabolic process	BP	26%	2.07E-11
regulation of signal transduction	BP	11%	2.57E-03
regulation of cell population proliferation	BP	5.90%	1.89E-03
regulation of programmed cell death	BP	5.70%	2.50E-05
negative regulation of signalling	BP	5.20%	1.93E-03
negative regulation of cell communication	BP	5.20%	1.94E-03
response to xenobiotic stimulus	BP	1.20%	3.82E-04
carboxylic acid transport	BP	1.00%	1.32E-04
hormone metabolic process	BP	0.78%	2.38E-06
epithelial cell proliferation	BP	0.75%	2.69E-03
monosaccharide metabolic process	BP	0.69%	1.91E-04
amide transport	BP	0.57%	9.77E-04
liver development	BP	0.47%	4.77E-04
detoxification	BP	0.37%	4.23E-07
cellular detoxification	BP	0.33%	1.25E-04
purine nucleobase transmembrane transport	BP	0.03%	2.26E-04

GSCreER-mT/mG mGFP+ Hepatocyte GO Terms			
GO Term	**Category**	**Population Frequency**	**q-value**
binding	MF	50%	9.28E-03

protein binding	MF	34%	2.50E-03
catalytic activity	MF	19%	9.20E-10
ion binding	MF	19%	1.68E-03
small molecule binding	MF	19%	1.68E-03
hydrolase activity	MF	8.30%	3.27E-03
transferase activity	MF	7.70%	0.0441
protein-containing complex binding	MF	5.60%	0.011
transporter activity	MF	4.20%	0.0374
transmembrane transporter activity	MF	3.80%	0.0441
oxidoreductase activity	MF	2.70%	3.76E-04
molecular function inhibitor activity	MF	2.00%	0.0391
iron ion binding	MF	0.60%	3.00E-04
heme binding	MF	0.56%	9.85E-04
monooxygenase activity	MF	0.53%	1.07E-06
oxidoreductase activity with incorporation or reduction of molecular oxygen	MF	0.30%	2.85E-07
cellular process	BP	56%	4.69E-08
biological regulation	BP	44%	6.04E-03
regulation of biological process	BP	43%	0.0172
metabolic process	BP	26%	3.06E-08
positive regulation of biological process	BP	22%	5.10E-03
response to stimulus	BP	22%	7.75E-03
cellular component organization or biogenesis	BP	20%	0.0374
developmental process	BP	19%	0.0292
transport	BP	12%	0.0342
anatomical structure development	BP	12%	0.0414
response to chemical	BP	11%	6.42E-03
cellular developmental process	BP	11%	0.0306
response to stress	BP	11%	0.0355
regulation of biological quality	BP	10%	0.0179
cellular response to stimulus	BP	9.60%	0.0451
positive regulation of signalling	BP	6.90%	0.0179
homeostatic process	BP	5.00%	0.0311
response to endogenous stimulus	BP	3.50%	9.70E-03
cell migration	BP	3.30%	2.83E-03
cell adhesion	BP	3.00%	0.0222
positive regulation of catalytic activity	BP	2.00%	3.40E-03
positive regulation of cell development	BP	1.90%	0.0374
regulation of protein kinase activity	BP	1.60%	8.23E-03
regulation of cell cycle phase transition	BP	1.50%	0.0483
inorganic ion homeostasis	BP	1.50%	0.0491
regulation of inflammatory response	BP	1.40%	0.0357
cell surface receptor protein tyrosine kinase signalling pathway	BP	1.40%	0.0374
regulation of small molecule metabolic process	BP	1.30%	2.22E-04
regulation of lipid metabolic process	BP	1.30%	0.0121
positive regulation of protein kinase activity	BP	0.96%	3.77E-03

regulation of reactive oxygen species metabolic process	BP	0.53%	1.84E-03

Ben-Moshe GO Terms Correlated with Gls2 Expression			
GO Term	**Category**	**Population Frequency**	**q-value**
binding	MF	50%	<1E-323
protein binding	MF	34%	<1E-323
small molecule binding	MF	19%	<1E-323
catalytic activity	MF	19%	<1E-323
nucleic acid binding	MF	12%	7.93E-191
hydrolase activity	MF	8.30%	3.16E-166
catalytic activity, acting on a protein	MF	8.00%	1.79E-185
transferase activity	MF	7.70%	4.42E-211
molecular function regulator activity	MF	7.60%	2.82E-101
carbohydrate derivative binding	MF	7.50%	3.40E-189
nucleoside phosphate binding	MF	7.10%	1.44E-221
transcription regulator activity	MF	6.10%	1.63E-63
protein-containing complex binding	MF	5.60%	2.17E-121
molecular adaptor activity	MF	4.60%	5.33E-102
enzyme regulator activity	MF	4.50%	5.59E-103
DNA-binding transcription factor activity	MF	4.50%	2.13E-25
transporter activity	MF	4.20%	4.32E-33
protein-macromolecule adaptor activity	MF	4.00%	4.47E-95
molecular function activator activity	MF	4.00%	3.42E-38
transmembrane transporter activity	MF	3.80%	1.22E-25
cellular process	BP	56%	<1E-323
biological regulation	BP	44%	<1E-323
regulation of biological process	BP	43%	<1E-323
metabolic process	BP	26%	<1E-323
primary metabolic process	BP	22%	<1E-323
regulation of metabolic process	BP	22%	<1E-323
positive regulation of biological process	BP	22%	<1E-323
response to stimulus	BP	22%	8.63E-131
positive regulation of cellular process	BP	21%	<1E-323
cellular component organization or biogenesis	BP	20%	<1E-323

negative regulation of biological process	BP	19%	<1E-323
developmental process	BP	19%	4.29E-248
negative regulation of cellular process	BP	18%	<1E-323
regulation of primary metabolic process	BP	18%	<1E-323
multicellular organismal process	BP	18.00%	3.72E-22
localization	BP	15%	<1E-323
establishment of localization	BP	13%	2.89E-291
anatomical structure development	BP	12%	1.49E-149
response to stress	BP	11.00%	7.76E-193
cellular developmental process	BP	11.00%	1.36E-110
response to chemical	BP	11.00%	1.24E-103
cellular response to stimulus	BP	10%	3.31E-160
regulation of biological quality	BP	10%	9.96E-129
cellular localization	BP	8%	3.70E-248
immune system process	BP	8%	1.55E-30
macromolecule localization	BP	7%	6.33E-210
response to external stimulus	BP	7%	1.50E-34
regulation of molecular function	BP	6%	1.94E-123
response to biotic stimulus	BP	6%	4.42E-31
reproductive process	BP	6%	3.17E-27
anatomical structure morphogenesis	BP	5.40%	1.71E-72
biological process involved in interspecies interaction between organisms	BP	5.10%	2.45E-33
homeostatic process	BP	5.00%	7.69E-93
response to abiotic stimulus	BP	4.40%	1.69E-53
cell motility	BP	4%	5.99E-43
response to endogenous stimulus	BP	3.50%	4.33E-60
chemical homeostasis	BP	3.30%	1.56E-55
cell cycle process	BP	3.00%	2.91E-99

Ben-Moshe GO Terms Correlated with GS Expression			
GO Term	**Category**	**Population Frequency**	**q-value**
binding	MF	50.00%	<1E-323
protein binding	MF	34.00%	<1E-323
small molecule binding	MF	19.00%	<1E-323
catalytic activity	MF	19.00%	<1E-323

nucleic acid binding	MF	12.00%	0.00E+00
hydrolase activity	MF	8.30%	0.00E+00
catalytic activity, acting on a protein	MF	8.00%	0.00E+00
transferase activity	MF	7.70%	0.00E+00
molecular function regulator activity	MF	7.60%	0.00E+00
carbohydrate derivative binding	MF	7.50%	0.00E+00
nucleoside phosphate binding	MF	7.10%	0.00E+00
transcription regulator activity	MF	6.10%	0.00E+00
protein-containing complex binding	MF	5.60%	0.00E+00
molecular adaptor activity	MF	4.60%	0.00E+00
enzyme regulator activity	MF	4.50%	0.00E+00
DNA-binding transcription factor activity	MF	4.50%	0.00E+00
transporter activity	MF	4.20%	0.00E+00
protein-macromolecule adaptor activity	MF	4.00%	0.00E+00
molecular function activator activity	MF	4.00%	0.00E+00
transmembrane transporter activity	MF	3.80%	0.00E+00
cellular process	BP	56.00%	<1E-323
biological regulation	BP	44.00%	<1E-323
regulation of biological process	BP	43.00%	<1E-323
metabolic process	BP	26.00%	<1E-323
primary metabolic process	BP	22.00%	<1E-323
regulation of metabolic process	BP	22.00%	<1E-323
positive regulation of biological process	BP	22.00%	<1E-323
response to stimulus	BP	22.00%	0.00E+00
positive regulation of cellular process	BP	21.00%	<1E-323
cellular component organization or biogenesis	BP	20.00%	<1E-323
developmental process	BP	19.00%	0.00E+00
regulation of primary metabolic process	BP	18.00%	<1E-323
multicellular organismal process	BP	18.00%	0.00E+00
localization	BP	15.00%	<1E-323
establishment of localization	BP	13.00%	0.00E+00
anatomical structure development	BP	12.00%	0.00E+00
response to stress	BP	11.00%	0.00E+00
response to chemical	BP	11.00%	0.00E+00
cellular developmental process	BP	11.00%	0.00E+00

regulation of biological quality	BP	10.00%	0.00E+00
cellular response to stimulus	BP	9.60%	0.00E+00
cellular localization	BP	8.00%	0.00E+00
immune system process	BP	7.70%	0.00E+00
macromolecule localization	BP	6.70%	0.00E+00
response to external stimulus	BP	6.60%	0.00E+00
regulation of molecular function	BP	5.80%	0.00E+00
reproductive process	BP	5.70%	0.00E+00
response to biotic stimulus	BP	5.60%	0.00E+00
anatomical structure morphogenesis	BP	5.40%	0.00E+00
biological process involved in interspecies interaction between organisms	BP	5.10%	0.00E+00
homeostatic process	BP	5.00%	0.00E+00
response to abiotic stimulus	BP	4.40%	0.00E+00
cell motility	BP	4.00%	0.00E+00
response to endogenous stimulus	BP	3.50%	0.00E+00
chemical homeostasis	BP	3.30%	0.00E+00
cell cycle process	BP	3.00%	0.00E+00
microtubule-based process	BP	3.00%	0.00E+00
programmed cell death	BP	2.90%	0.00E+00
cell division	BP	1.40%	0.00E+00

Appendix Table 6: Gene Ontology Enrichment Analysis of mGFP+ Cells Fluorescently Sorted from Gls2CreER-mT/mG and GSCreER-mT/mG Mouse Livers. *Differentially expressed genes were identified through DESeq2 analysis, following which GO Enrichment analysis was conducted on the datasets in Galaxy using a Benjamini-Hochberg multiple test correction (adjusted $p < 0.05$). GO terms were further filtered to show only those occurring at a frequency of >5% within the dataset. BP – Biological Processes; MF – Molecular Functions.*

GO Terms Identified from Gls2CreER-mT/mG mGFP+ Cells			
GO Term	**Category**	**Population Frequency**	**q-value**
binding	MF	60%	0.0294
nucleic acid binding	MF	31%	3.24E-09
zinc ion binding	MF	14%	6.07E-04
transcription regulator activity	MF	14%	2.59E-03
molecular adaptor activity	MF	12%	2.85E-03
protein-macromolecule adaptor activity	MF	9.50%	0.0163
proton transmembrane transporter activity	MF	5.90%	2.40E-06
transcription coactivator activity	MF	5.90%	2.59E-04
oxidoreduction-driven active transmembrane transporter activity	MF	4.10%	2.42E-07
electron transfer activity	MF	4.10%	2.55E-06
active monoatomic ion transmembrane transporter activity	MF	4.10%	5.49E-05
histone binding	MF	4.10%	0.0184
ATP-dependent activity, acting on DNA	MF	3.60%	1.59E-03
cytochrome-c oxidase activity	MF	1.80%	3.06E-04
NADH dehydrogenase (ubiquinone) activity	MF	1.80%	3.10E-03
acetylation-dependent protein binding	MF	1.80%	8.75E-03
purine ribonucleotide transmembrane transporter activity	MF	1.20%	0.0464
metabolic process	BP	46%	9.17E-06
regulation of metabolic process	BP	35%	7.48E-03
regulation of RNA biosynthetic process	BP	27%	8.28E-06
chromatin remodelling	BP	13%	1.72E-05
animal organ development	BP	11%	0.0478
proton transmembrane transport	BP	5.40%	3.27E-05
cell division	BP	4.80%	0.0483
proton motive force-driven mitochondrial ATP synthesis	BP	3.60%	1.45E-04
B cell activation	BP	3.60%	0.039
regulation of stem cell population maintenance	BP	3.00%	2.94E-03
regulation of transforming growth factor beta receptor signalling pathway	BP	3.00%	0.0331
response to calcium ion	BP	3.00%	0.0354
embryonic organ morphogenesis	BP	3.00%	0.0354
host-mediated suppression of symbiont invasion	BP	2.40%	1.64E-03
suppression of viral release by host	BP	1.80%	9.79E-03
regulation of viral entry into host cell	BP	1.80%	9.79E-03

regulation of lipopolysaccharide-mediated signalling pathway	BP	1.80%	0.0226
genomic imprinting	BP	1.80%	0.0226
mRNA transcription by RNA polymerase II	BP	1.80%	0.0483
adult somatic muscle development	BP	1.20%	1.52E-03
positive regulation of alkaline phosphatase activity	BP	1.20%	6.65E-03
establishment of Sertoli cell barrier	BP	1.20%	9.68E-03
regulation of sarcomere organization	BP	1.20%	0.0401
dicarboxylic acid biosynthetic process	BP	1.20%	0.0463
N-terminal protein amino acid acetylation	BP	1.20%	0.0463

GO Terms Identified from GSCreER-mT/mG mGFP+ Cells			
GO Term	**Category**	**Population Frequency**	**q-value**
binding	MF	55%	1E-323
protein binding	MF	38%	1E-323
small molecule binding	MF	22%	7.34E-268
catalytic activity	MF	22%	3.37E-261
nucleic acid binding	MF	13%	1.38E-103
molecular transducer activity	MF	9.60%	8.33E-112
signalling receptor activity	MF	9.60%	8.33E-112
hydrolase activity	MF	9.50%	3.36E-110
catalytic activity, acting on a protein	MF	9.10%	7.10E-108
molecular function regulator activity	MF	8.80%	1.98E-121
transferase activity	MF	8.80%	4.22E-96
carbohydrate derivative binding	MF	8.60%	3.90E-110
transcription regulator activity	MF	6.80%	2.83E-59
protein-containing complex binding	MF	6.40%	1.13E-76
molecular adaptor activity	MF	5.30%	8.61E-62
enzyme regulator activity	MF	5.20%	6.49E-72
DNA-binding transcription factor activity	MF	5.00%	3.80E-39
molecular function activator activity	MF	4.70%	4.55E-62
transporter activity	MF	4.70%	7.97E-41
protein-macromolecule adaptor activity	MF	4.60%	2.02E-58
transmembrane transporter activity	MF	4.30%	4.45E-35
lipid binding	MF	3.60%	1.94E-40
oxidoreductase activity	MF	3.00%	2.31E-27
structural molecule activity	MF	2.70%	1.08E-36
chromatin binding	MF	2.60%	7.69E-28
signalling receptor regulator activity	MF	2.40%	4.93E-31
ATP-dependent activity	MF	2.30%	2.55E-35
catalytic activity, acting on a nucleic acid	MF	2.30%	6.46E-32
molecular function inhibitor activity	MF	2.30%	7.07E-29

odorant binding	MF	1.90%	3.61E-28
primary metabolic process	BP	38%	1E-323
cellular component organization or biogenesis	BP	27%	1E-323

References

1 Malarkey, D. E., Johnson, K., Ryan, L., Boorman, G. & Maronpot, R. R. New insights into functional aspects of liver morphology. *Toxicol Pathol* **33**, 27-34 (2005). https://doi.org/10.1080/01926230590881826

2 Aloia, L. The influence of tissue spatial geometry and functional organisation on liver regeneration. *Semin Cell Dev Biol* **130**, 70-78 (2022). https://doi.org/10.1016/j.semcdb.2021.09.011

3 Sugimoto, A. *et al*. Hepatic stellate cells control liver zonation, size and functions via R-spondin 3. *Nature* **640**, 752-761 (2025). https://doi.org/10.1038/s41586-025-08677-w

4 Sererols-Vinas, L. *et al*. Hepatic Stellate Cells Functional Heterogeneity in Liver Cancer. *Semin Liver Dis* **45**, 33-51 (2025). https://doi.org/10.1055/a-2551-0724

5 Tabibian, J. H., Masyuk, A. I., Masyuk, T. V., O'Hara, S. P. & LaRusso, N. F. Physiology of cholangiocytes. *Compr Physiol* **3**, 541-565 (2013). https://doi.org/10.1002/cphy.c120019

6 Tanaka, M. *et al*. Mouse hepatoblasts at distinct developmental stages are characterized by expression of EpCAM and DLK1: drastic change of EpCAM expression during liver development. *Mech Dev* **126**, 665-676 (2009). https://doi.org/10.1016/j.mod.2009.06.939

7 Si-Tayeb, K., Lemaigre, F. P. & Duncan, S. A. Organogenesis and development of the liver. *Dev Cell* **18**, 175-189 (2010). https://doi.org/10.1016/j.devcel.2010.01.011

8 Sahoo, S., Mishra, A., Diehl, A. M. & Jolly, M. K. Dynamics of a hepatocyte-cholangiocyte decision-making gene regulatory network during liver development and regeneration. *Iscience* **25** (2021). https://doi.org/10.1101/2021.04.22.440352

9 Pu, W. *et al*. Bipotent transitional liver progenitor cells contribute to liver regeneration. *Nat Genet* **55**, 651-664 (2023). https://doi.org/10.1038/s41588-023-01335-9

10 Campbell, S. A. *et al*. Signalling pathways and transcriptional regulators orchestrating liver development and cancer. *Development* **148** (2021). https://doi.org/10.1242/dev.199814

11 Tanimizu, N. & Mitaka, T. Epithelial Morphogenesis during Liver Development. *Cold Spring Harb Perspect Biol* **9** (2017). https://doi.org/10.1101/cshperspect.a027862

12 Chen, T., Oh, S., Gregory, S., Shen, X. & Diehl, A. M. Single-cell omics analysis reveals functional diversification of hepatocytes during liver regeneration. *JCI Insight* **5** (2020). https://doi.org/10.1172/jci.insight.141024

13 Shin, D. & Monga, S. P. Cellular and molecular basis of liver development. *Compr Physiol* **3**, 799-815 (2013). https://doi.org/10.1002/cphy.c120022

14 Boulter, L., Lu, W. Y. & Forbes, S. J. Differentiation of progenitors in the liver: a matter of local choice. *J Clin Invest* **123**, 1867-1873 (2013). https://doi.org/10.1172/JCI66026

15 Zong, Y. *et al*. Notch signaling controls liver development by regulating biliary differentiation. *Development* **136**, 1727-1739 (2009). https://doi.org/10.1242/dev.029140

16 Clotman, F. *et al*. The onecut transcription factor HNF6 is required for normal development of the biliary tract. *Development* **129**, 1819-1828 (2002).

17 Andersson, E. R., Sandberg, R. & Lendahl, U. Notch signaling: simplicity in design, versatility in function. *Development* **138**, 3593-3612 (2011). https://doi.org/10.1242/dev.063610

18 D'Souza, B., Meloty-Kapella, L. & Weinmaster, G. Canonical and non-canonical Notch ligands. *Curr Top Dev Biol* **92**, 73-129 (2010). https://doi.org/10.1016/S0070-2153(10)92003-6

19 D'Souza, B., Miyamoto, A. & Weinmaster, G. The many facets of Notch ligands. *Oncogene* **27**, 5148-5167 (2008). https://doi.org/10.1038/onc.2008.229

20 Kopan, R. & Ilagan, M. X. The canonical Notch signaling pathway: unfolding the activation mechanism. *Cell* **137**, 216-233 (2009). https://doi.org/10.1016/j.cell.2009.03.045

21 Zhou, B. *et al*. Notch signaling pathway: architecture, disease, and therapeutics. *Signal Transduct Target Ther* **7**, 95 (2022). https://doi.org/10.1038/s41392-022-00934-y

22 Adams, J. M. & Jafar-Nejad, H. The Roles of Notch Signaling in Liver Development and Disease. *Biomolecules* **9** (2019). https://doi.org/10.3390/biom9100608
23 Andersson, E. R. *et al*. Mouse Model of Alagille Syndrome and Mechanisms of Jagged1 Missense Mutations. *Gastroenterology* **154**, 1080-1095 (2018). https://doi.org/10.1053/j.gastro.2017.11.002
24 Gilbert, M. A. *et al*. Alagille syndrome mutation update: Comprehensive overview of JAG1 and NOTCH2 mutation frequencies and insight into missense variant classification. *Hum Mutat* **40**, 2197-2220 (2019). https://doi.org/10.1002/humu.23879
25 Geisler, F. *et al*. Liver-specific inactivation of Notch2, but not Notch1, compromises intrahepatic bile duct development in mice. *Hepatology* **48**, 607-616 (2008). https://doi.org/10.1002/hep.22381
26 Lee, D. H. *et al*. LATS-YAP/TAZ controls lineage specification by regulating TGFbeta signaling and Hnf4alpha expression during liver development. *Nat Commun* **7**, 11961 (2016). https://doi.org/10.1038/ncomms11961
27 Bird, T. G. *et al*. TGFbeta inhibition restores a regenerative response in acute liver injury by suppressing paracrine senescence. *Sci Transl Med* **10** (2018). https://doi.org/10.1126/scitranslmed.aan1230
28 Lade, A. G. & Monga, S. P. Beta-catenin signaling in hepatic development and progenitors: which way does the WNT blow? *Dev Dyn* **240**, 486-500 (2011). https://doi.org/10.1002/dvdy.22522
29 Liu, J. *et al*. Wnt/beta-catenin signalling: function, biological mechanisms, and therapeutic opportunities. *Signal Transduct Target Ther* **7**, 3 (2022). https://doi.org/10.1038/s41392-021-00762-6
30 Russell, J. O. & Monga, S. P. Wnt/beta-Catenin Signaling in Liver Development, Homeostasis, and Pathobiology. *Annu Rev Pathol* **13**, 351-378 (2018). https://doi.org/10.1146/annurev-pathol-020117-044010
31 Wild, S. L. *et al*. The Canonical Wnt Pathway as a Key Regulator in Liver Development, Differentiation and Homeostatic Renewal. *Genes (Basel)* **11** (2020). https://doi.org/10.3390/genes11101163
32 Ober, E. A., Verkade, H., Field, H. A. & Stainier, D. Y. Mesodermal Wnt2b signalling positively regulates liver specification. *Nature* **442**, 688-691 (2006). https://doi.org/10.1038/nature04888
33 Reed, K. R. *et al*. B-catenin deficiency, but not Myc deletion, suppresses the immediate phenotypes of APC loss in the liver. *PNAS* **105**, 18919–18923 (2008).
34 Benhamouche, S. *et al*. Apc tumor suppressor gene is the "zonation-keeper" of mouse liver. *Dev Cell* **10**, 759-770 (2006). https://doi.org/10.1016/j.devcel.2006.03.015
35 Qin, K. *et al*. Canonical and noncanonical Wnt signaling: Multilayered mediators, signaling mechanisms and major signaling crosstalk. *Genes Dis* **11**, 103-134 (2024). https://doi.org/10.1016/j.gendis.2023.01.030
36 Valle-Encinas, E. *et al*. Canonical Wnt signalling is activated during BEC-to-hepatocyte conversion in vivo and modulates liver epithelial cell plasticity in hepatic organoids. *BioRxiv* (2020). https://doi.org/10.1101/2020.11.09.374462
37 Kinoshita, T. *et al*. Hepatic differentiation induced by oncostatin M attenuates fetal liver hematopoiesis. *Proceedings of the National Academy of Sciences USA* **96**, 7265–7270 (1999).
38 Miyajima, A. *et al*. Role of Oncostatin M in hematopoiesis and liver development. *Cytokine & Growth Factor Reviews* **11**, 177-183 (2000).
39 Galimi, F. *et al*. Hepatocyte Growth Factor Induces Proliferation and Differentiation of Multipotent and Erythroid Hemopoietic Progenitors *The Journal of Cell Biology* **127**, 1743-1754 (1994).
40 Tauran, Y. *et al*. A novel agonist for the HGF receptor MET promotes differentiation of human pluripotent stem cells into hepatocyte-like cells. *Dev Growth Differ* **64**, 527-536 (2022). https://doi.org/10.1111/dgd.12818

41 Suzuki, A., Iwama, A., Miyashita, H., Nakauchi, H. & Taniguchi, H. Role for growth factors and extracellular matrix in controlling differentiation of prospectively isolated hepatic stem cells. *Development* **130**, 2513-2524 (2003). https://doi.org/10.1242/dev.00459

42 Wallace, K., Marek, C. J., Hoppler, S. & Wright, M. C. Glucocorticoid-dependent transdifferentiation of pancreatic progenitor cells into hepatocytes is dependent on transient suppression of WNT signalling. *J Cell Sci* **123**, 2103-2110 (2010). https://doi.org/10.1242/jcs.070722

43 Fairhall, E. A. *et al*. Glucocorticoid-induced pancreatic-hepatic trans-differentiation in a human cell line in vitro. *Differentiation* **102**, 10-18 (2018). https://doi.org/10.1016/j.diff.2018.05.003

44 Hu, W. *et al*. Individual-specific functional epigenomics reveals genetic determinants of adverse metabolic effects of glucocorticoids. *Cell Metab* **33**, 1592-1609 e1597 (2021). https://doi.org/10.1016/j.cmet.2021.06.004

45 Mueller, K. M. *et al*. Hepatic growth hormone and glucocorticoid receptor signaling in body growth, steatosis and metabolic liver cancer development. *Mol Cell Endocrinol* **361**, 1-11 (2012). https://doi.org/10.1016/j.mce.2012.03.026

46 Fitamant, J. *et al*. YAP Inhibition Restores Hepatocyte Differentiation in Advanced HCC, Leading to Tumor Regression. *Cell Rep* **10**, 1692-1707 (2015). https://doi.org/10.1016/j.celrep.2015.02.027

47 Russell, J. O. & Camargo, F. D. Hippo signalling in the liver: role in development, regeneration and disease. *Nat Rev Gastroenterol Hepatol* **19**, 297-312 (2022). https://doi.org/10.1038/s41575-021-00571-w

48 Shi, H. *et al*. Complex roles of Hippo-YAP/TAZ signaling in hepatocellular carcinoma. *J Cancer Res Clin Oncol* **149**, 15311-15322 (2023). https://doi.org/10.1007/s00432-023-05272-2

49 Halpern, K. B. *et al*. Single-cell spatial reconstruction reveals global division of labour in the mammalian liver. *Nature* **542**, 352-356 (2017). https://doi.org/10.1038/nature21065

50 Adler, M., Korem Kohanim, Y., Tendler, A., Mayo, A. & Alon, U. Continuum of Gene-Expression Profiles Provides Spatial Division of Labor within a Differentiated Cell Type. *Cell Syst* **8**, 43-52 e45 (2019). https://doi.org/10.1016/j.cels.2018.12.008

51 Ben-Moshe, S. *et al*. Spatial sorting enables comprehensive characterization of liver zonation. *Nat Metab* **1**, 899-911 (2019). https://doi.org/10.1038/s42255-019-0109-9

52 Chen, F., Schonberger, K. & Tchorz, J. S. Distinct hepatocyte identities in liver homeostasis and regeneration. *JHEP Rep* **5**, 100779 (2023). https://doi.org/10.1016/j.jhepr.2023.100779

53 Cheng, X. *et al*. Glucagon contributes to liver zonation. *Proc Natl Acad Sci U S A* **115**, E4111-E4119 (2018). https://doi.org/10.1073/pnas.1721403115

54 Panday, R., Monckton, C. P. & Khetani, S. R. The Role of Liver Zonation in Physiology, Regeneration, and Disease. *Semin Liver Dis* **42**, 1-16 (2022). https://doi.org/10.1055/s-0041-1742279

55 Paris, J. & Henderson, N. C. Liver zonation, revisited. *Hepatology* **76**, 1219-1230 (2022). https://doi.org/10.1002/hep.32408

56 Pu, W. & Zhou, B. Hepatocyte generation in liver homeostasis, repair, and regeneration. *Cell Regen* **11**, 2 (2022). https://doi.org/10.1186/s13619-021-00101-8

57 Bar-Peled, L. & Kory, N. Principles and functions of metabolic compartmentalization. *Nat Metab* **4**, 1232-1244 (2022). https://doi.org/10.1038/s42255-022-00645-2

58 McEnerney, L. *et al*. Dual modulation of human hepatic zonation via canonical and non-canonical Wnt pathways. *Exp Mol Med* **49**, e413 (2017). https://doi.org/10.1038/emm.2017.226

59 Liang, Y. *et al*. Temporal analyses of postnatal liver development and maturation by single-cell transcriptomics. *Dev Cell* **57**, 398-414 e395 (2022). https://doi.org/10.1016/j.devcel.2022.01.004

60 Ma, R., Martinez-Ramirez, A. S., Borders, T. L., Gao, F. & Sosa-Pineda, B. Metabolic and non-metabolic liver zonation is established non-synchronously and requires sinusoidal Wnts. *Elife* **9** (2020). https://doi.org/10.7554/eLife.46206
61 Burke, Z. D. *et al*. Spatiotemporal regulation of liver development by the Wnt/beta-catenin pathway. *Sci Rep* **8**, 2735 (2018). https://doi.org/10.1038/s41598-018-20888-y
62 Colletti, M. *et al*. Convergence of Wnt signaling on the HNF4alpha-driven transcription in controlling liver zonation. *Gastroenterology* **137**, 660-672 (2009). https://doi.org/10.1053/j.gastro.2009.05.038
63 Goel, C., Monga, S. P. & Nejak-Bowen, K. Role and Regulation of Wnt/beta-Catenin in Hepatic Perivenous Zonation and Physiological Homeostasis. *Am J Pathol* **192**, 4-17 (2022). https://doi.org/10.1016/j.ajpath.2021.09.007
64 Monga, S. P. beta-Catenin Signaling and Roles in Liver Homeostasis, Injury, and Tumorigenesis. *Gastroenterology* **148**, 1294-1310 (2015). https://doi.org/10.1053/j.gastro.2015.02.056
65 Preziosi, M., Okabe, H., Poddar, M., Singh, S. & Monga, S. P. Endothelial Wnts regulate beta-catenin signaling in murine liver zonation and regeneration: A sequel to the Wnt-Wnt situation. *Hepatol Commun* **2**, 845-860 (2018). https://doi.org/10.1002/hep4.1196
66 Wei, Y. *et al*. Liver homeostasis is maintained by midlobular zone 2 hepatocytes. *Science* **371** (2021). https://doi.org/10.1126/science.abb1625
67 Delire, B. & Starkel, P. The Ras/MAPK pathway and hepatocarcinoma: pathogenesis and therapeutic implications. *Eur J Clin Invest* **45**, 609-623 (2015). https://doi.org/10.1111/eci.12441
68 Wei, G. *et al*. Erk and MAPK signaling is essential for intestinal development through Wnt pathway modulation. *Development* **147** (2020). https://doi.org/10.1242/dev.185678
69 Wortzel, I. & Seger, R. The ERK Cascade: Distinct Functions within Various Subcellular Organelles. *Genes Cancer* **2**, 195-209 (2011). https://doi.org/10.1177/1947601911407328
70 Hildebrandt, F. *et al*. Spatial Transcriptomics to define transcriptional patterns of zonation and structural components in the mouse liver. *Nat Commun* **12**, 7046 (2021). https://doi.org/10.1038/s41467-021-27354-w
71 Cunningham, R. P. & Porat-Shliom, N. Liver Zonation - Revisiting Old Questions With New Technologies. *Front Physiol* **12**, 732929 (2021). https://doi.org/10.3389/fphys.2021.732929
72 Gola, A. *et al*. Commensal-driven immune zonation of the liver promotes host defence. *Nature* **589**, 131-136 (2021). https://doi.org/10.1038/s41586-020-2977-2
73 Bravo Gonzalez-Blas, C. *et al*. Single-cell spatial multi-omics and deep learning dissect enhancer-driven gene regulatory networks in liver zonation. *Nat Cell Biol* **26**, 153-167 (2024). https://doi.org/10.1038/s41556-023-01316-4
74 Clotman, F. *et al*. Control of liver cell fate decision by a gradient of TGF beta signaling modulated by Onecut transcription factors. *Genes Dev* **19**, 1849-1854 (2005). https://doi.org/10.1101/gad.340305
75 Liu, Y. *et al*. Onecut1 partially contributes to the liver progenitor cell transition and acquisition of metastatic potential in hepatocellular carcinoma. *BioRxiv Preprint* (2022). https://doi.org/10.1101/2022.09.20.508738
76 Bao, Y. *et al*. Acetaminophen-Induced Liver Injury Alters Expression and Activities of Cytochrome P450 Enzymes in an Age-Dependent Manner in Mouse Liver. *Drug Metab Dispos* **48**, 326-336 (2020). https://doi.org/10.1124/dmd.119.089557
77 Pittala, S., Krelin, Y., Kuperman, Y. & Shoshan-Barmatz, V. A Mitochondrial VDAC1-Based Peptide Greatly Suppresses Steatosis and NASH-Associated Pathologies in a Mouse Model. *Mol Ther* **27**, 1848-1862 (2019). https://doi.org/10.1016/j.ymthe.2019.06.017
78 Wang, H. & Chen, X. Hydrodynamic Injection for Developing NASH Model. *Methods Mol Biol* **2455**, 31-39 (2022). https://doi.org/10.1007/978-1-0716-2128-8_3
79 Aizarani, N. *et al*. A human liver cell atlas reveals heterogeneity and epithelial progenitors. *Nature* **572**, 199-204 (2019). https://doi.org/10.1038/s41586-019-1373-2

80 Batts, K. P. Iron overload syndromes and the liver. *Mod Pathol* **20 Suppl 1**, S31-39 (2007). https://doi.org/10.1038/modpathol.3800715
81 Covelli, C. *et al*. Pathology of autoimmune hepatitis. *Pathologica* **113**, 185-193 (2021). https://doi.org/10.32074/1591-951X-241
82 Terziroli Beretta-Piccoli, B., Mieli-Vergani, G. & Vergani, D. Autoimmmune hepatitis. *Cell Mol Immunol* **19**, 158-176 (2022). https://doi.org/10.1038/s41423-021-00768-8
83 Hessien, M. H., El-Sharkawi, I. M., El-Barbary, A. A., El-Beltagy, D. M. & Snyder, N. Non-invasive index of liver fibrosis induced by alcohol, thioacetamide and Schistosomal infection in mice. *BMC Gastroenterol* **10**, 53 (2010). https://doi.org/10.1186/1471-230X-10-53
84 Wallace, M. C. *et al*. Standard operating procedures in experimental liver research: thioacetamide model in mice and rats. *Lab Anim* **49**, 21-29 (2015). https://doi.org/10.1177/0023677215573040
85 MacParland, S. A. *et al*. Single cell RNA sequencing of human liver reveals distinct intrahepatic macrophage populations. *Nat Commun* **9**, 4383 (2018). https://doi.org/10.1038/s41467-018-06318-7
86 Ramachandran, P. *et al*. Resolving the fibrotic niche of human liver cirrhosis at single-cell level. *Nature* **575**, 512-518 (2019). https://doi.org/10.1038/s41586-019-1631-3
87 Lu, W. Y. & Forbes, S. J. Telomerase Activity Links to Regenerative Capacity of Hepatocytes. *Transplantation* **102**, 1587-1588 (2018). https://doi.org/10.1097/TP.0000000000002346
88 Wang, B., Zhao, L., Fish, M., Logan, C. Y. & Nusse, R. Self-renewing diploid Axin2+ cells fuel homeostatic renewal of the liver. *Nature* **524**, 180-185 (2015).
89 Sun, T. *et al*. AXIN2(+) Pericentral Hepatocytes Have Limited Contributions to Liver Homeostasis and Regeneration. *Cell Stem Cell* **26**, 97-107 e106 (2020). https://doi.org/10.1016/j.stem.2019.10.011
90 May, S. *et al*. Absent expansion of AXIN2+ hepatocytes and altered physiology in Axin2CreERT2 mice challenges the role of pericentral hepatocytes in homeostatic liver regeneration. *J Hepatol* **78**, 1028-1036 (2023). https://doi.org/10.1016/j.jhep.2023.01.009
91 Aoshima, K. & Tanimizu, N. Lineage plasticity and reprogramming of epithelial cells during tissue injury and regeneration-lessons from the lineage plasticity of hepatocytes and cholangiocytes induced by liver injury–. *Regenerative Therapy* **29**, 447-454 (2025). https://doi.org/10.1016/j.reth.2025.04.008
92 Yanger, K. *et al*. Robust cellular reprogramming occurs spontaneously during liver regeneration. *Genes Dev* **27**, 719-724 (2013). https://doi.org/10.1101/gad.207803.112
93 Li, L. *et al*. Kupffer-cell-derived IL-6 is repurposed for hepatocyte dedifferentiation via activating progenitor genes from injury-specific enhancers. *Cell Stem Cell* **30**, 283-299 e289 (2023). https://doi.org/10.1016/j.stem.2023.01.009
94 Fickert, P. *et al*. A new xenobiotic-induced mouse model of sclerosing cholangitis and biliary fibrosis. *Am J Pathol* **171**, 525-536 (2007). https://doi.org/10.2353/ajpath.2007.061133
95 Pose, E., Sancho-Bru, P. & Coll, M. 3,5-Diethoxycarbonyl-1,4-Dihydrocollidine Diet: A Rodent Model in Cholestasis Research. *Methods in Molecular Biology* **1981**, 249–257 (2019).
96 Li, W. *et al*. A Homeostatic Arid1a-Dependent Permissive Chromatin State Licenses Hepatocyte Responsiveness to Liver-Injury-Associated YAP Signaling. *Cell Stem Cell* **25**, 54-68 e55 (2019). https://doi.org/10.1016/j.stem.2019.06.008
97 Merrell, A. J. *et al*. Dynamic Transcriptional and Epigenetic Changes Drive Cellular Plasticity in the Liver. *Hepatology* **74**, 444-457 (2021). https://doi.org/10.1002/hep.31704
98 Clerbaux, L.-A. *et al*. in *Experimental Animal Models of Human Diseases - An Effective Therapeutic Strategy* Ch. Chapter 8, (2018).
99 Jiang, A. *et al*. Loss of Wnt Secretion by Macrophages Promotes Hepatobiliary Injury after Administration of 3,5-Diethoxycarbonyl-1, 4-Dihydrocollidine Diet. *Am J Pathol* **189**, 590-603 (2019). https://doi.org/10.1016/j.ajpath.2018.11.010

100 Tarlow, B. D. *et al*. Bipotential adult liver progenitors are derived from chronically injured mature hepatocytes. *Cell Stem Cell* **15**, 605-618 (2014). https://doi.org/10.1016/j.stem.2014.09.008
101 Font-Burgada, J. *et al*. Hybrid Periportal Hepatocytes Regenerate the Injured Liver without Giving Rise to Cancer. *Cell* **162**, 766-779 (2015). https://doi.org/10.1016/j.cell.2015.07.026
102 Li, D., Li, W. & Hui, L. Hybrid hepatocyte: A newly identified player for regeneration in hepatic injuries. *Hepatology* **64**, 2244-2246 (2016). https://doi.org/10.1002/hep.28837
103 Ang, C. H. *et al*. Self-maintenance of zonal hepatocytes during adult homeostasis and their complex plasticity upon distinct liver injuries. *Cell Rep* **44**, 115093 (2025). https://doi.org/10.1016/j.celrep.2024.115093
104 Arino, S. *et al*. Ductular reaction-associated neutrophils promote biliary epithelium proliferation in chronic liver disease. *J Hepatol* **79**, 1025-1036 (2023). https://doi.org/10.1016/j.jhep.2023.05.045
105 Desmet, V., Roskams, T. & Van Eyken, P. Ductular reaction in the liver. *Pathol Res Pract* **191**, 513-524 (1995). https://doi.org/10.1016/s0344-0338(11)80870-8
106 Sato, K. *et al*. Ductular Reaction in Liver Diseases: Pathological Mechanisms and Translational Significances. *Hepatology* **69**, 420-430 (2019). https://doi.org/10.1002/hep.30150
107 Desmet, V. J. Ductal plates in hepatic ductular reactions. Hypothesis and implications. II. Ontogenic liver growth in childhood. *Virchows Arch* **458**, 261-270 (2011). https://doi.org/10.1007/s00428-011-1049-2
108 Nagahama, Y. *et al*. Contributions of hepatocytes and bile ductular cells in ductular reactions and remodeling of the biliary system after chronic liver injury. *Am J Pathol* **184**, 3001-3012 (2014). https://doi.org/10.1016/j.ajpath.2014.07.005
109 Aguilar-Bravo, B. *et al*. Ductular Reaction Cells Display an Inflammatory Profile and Recruit Neutrophils in Alcoholic Hepatitis. *Hepatology* **69**, 2180-2195 (2019). https://doi.org/10.1002/hep.30472
110 Mavila, N., Siraganahalli Eshwaraiah, M. & Kennedy, J. Ductular Reactions in Liver Injury, Regeneration, and Disease Progression-An Overview. *Cells* **13** (2024). https://doi.org/10.3390/cells13070579
111 Sato, K., Pham, L., Glaser, S., Francis, H. & Alpini, G. Pathophysiological Roles of Ductular Reaction in Liver Inflammation and Hepatic Fibrogenesis. *Cell Mol Gastroenterol Hepatol* **15**, 803-805 (2023). https://doi.org/10.1016/j.jcmgh.2022.11.006
112 Furuyama, K. *et al*. Continuous cell supply from a Sox9-expressing progenitor zone in adult liver, exocrine pancreas and intestine. *Nat Genet* **43**, 34-41 (2011). https://doi.org/10.1038/ng.722
113 Sorrentino, G. Microenvironmental control of the ductular reaction: balancing repair and disease progression. *Cell Death Dis* **16**, 246 (2025). https://doi.org/10.1038/s41419-025-07590-4
114 Nejak-Bowen, K. If It Looks Like a Duct and Acts Like a Duct: On the Role of Reprogrammed Hepatocytes in Cholangiopathies. *Gene Expr* **20**, 19-23 (2020). https://doi.org/10.3727/105221619X15664105014956
115 Choi, S. S. & Diehl, A. M. Epithelial-to-mesenchymal transitions in the liver. *Hepatology* **50**, 2007-2013 (2009). https://doi.org/10.1002/hep.23196
116 Manco, R. *et al*. Reactive cholangiocytes differentiate into proliferative hepatocytes with efficient DNA repair in mice with chronic liver injury. *J Hepatol* **70**, 1180-1191 (2019). https://doi.org/10.1016/j.jhep.2019.02.003
117 Espanol-Suner, R. *et al*. Liver progenitor cells yield functional hepatocytes in response to chronic liver injury in mice. *Gastroenterology* **143**, 1564-1575 e1567 (2012). https://doi.org/10.1053/j.gastro.2012.08.024
118 Raven, A. *et al*. Cholangiocytes act as facultative liver stem cells during impaired hepatocyte regeneration. *Nature* **547**, 350-354 (2017). https://doi.org/10.1038/nature23015

119 Bae, J. S. *et al.* Expression of K19 and K7 in dysplastic nodules and hepatocellular carcinoma. *Oncol Lett* **4**, 213-220 (2012). https://doi.org/10.3892/ol.2012.731
120 Yuan, S., Norgard, R. J. & Stanger, B. Z. Cellular Plasticity in Cancer. *Cancer Discov* **9**, 837-851 (2019). https://doi.org/10.1158/2159-8290.CD-19-0015
121 Lim, B. *et al.* Active repression of cell fate plasticity by PROX1 safeguards hepatocyte identity and prevents liver tumorigenesis. *Nat Genet* **57**, 668-679 (2025). https://doi.org/10.1038/s41588-025-02081-w
122 Guest, R. V. *et al.* Cell lineage tracing reveals a biliary origin of intrahepatic cholangiocarcinoma. *Cancer Res* **74**, 1005-1010 (2014). https://doi.org/10.1158/0008-5472.CAN-13-1911
123 Abou-Alfa, G. K. *et al.* Advances in cholangiocarcinoma research: report from the third Cholangiocarcinoma Foundation Annual Conference. *J Gastrointest Oncol* **7**, 819-827 (2016). https://doi.org/10.21037/jgo.2016.11.11
124 Fan, B. *et al.* Cholangiocarcinomas can originate from hepatocytes in mice. *J Clin Invest* **122**, 2911-2915 (2012). https://doi.org/10.1172/JCI63212
125 Ilyas, S. I. *et al.* Cholangiocarcinoma - novel biological insights and therapeutic strategies. *Nat Rev Clin Oncol* **20**, 470-486 (2023). https://doi.org/10.1038/s41571-023-00770-1
126 Sempoux, C. *et al.* Intrahepatic cholangiocarcinoma: new insights in pathology. *Semin Liver Dis* **31**, 49-60 (2011). https://doi.org/10.1055/s-0031-1272839
127 Shaib, Y. H., El-Serag, H. B., Davila, J. A., Morgan, R. & McGlynn, K. A. Risk factors of intrahepatic cholangiocarcinoma in the United States: a case-control study. *Gastroenterology* **128**, 620-626 (2005). https://doi.org/10.1053/j.gastro.2004.12.048
128 Wang, T. *et al.* Cellular heterogeneity and transcriptomic profiles during intrahepatic cholangiocarcinoma initiation and progression. *Hepatology* **76**, 1302-1317 (2022). https://doi.org/10.1002/hep.32483
129 Zhu, Y. & Kwong, L. N. Insights Into the Origin of Intrahepatic Cholangiocarcinoma From Mouse Models. *Hepatology* **72**, 305-314 (2020). https://doi.org/10.1002/hep.31200
130 Wang, J. *et al.* Notch2 controls hepatocyte-derived cholangiocarcinoma formation in mice. *Oncogene* **37**, 3229-3242 (2018). https://doi.org/10.1038/s41388-018-0188-1
131 Guest, R. V. *et al.* Notch3 drives development and progression of cholangiocarcinoma. *Proc Natl Acad Sci U S A* **113**, 12250-12255 (2016). https://doi.org/10.1073/pnas.1600067113
132 Minnis-Lyons, S. E. *et al.* Notch-IGF1 signaling during liver regeneration drivesbiliary epithelial cell expansion and inhibitshepatocyte differentiation. *Science Signaling* **14**, 1-11 (2021).
133 Hu, S. *et al.* NOTCH-YAP1/TEAD-DNMT1 Axis Drives Hepatocyte Reprogramming Into Intrahepatic Cholangiocarcinoma. *Gastroenterology* **163**, 449-465 (2022). https://doi.org/10.1053/j.gastro.2022.05.007
134 Bell, C. C. *et al.* Comparison of Hepatic 2D Sandwich Cultures and 3D Spheroids for Long-term Toxicity Applications: A Multicenter Study. *Toxicol Sci* **162**, 655-666 (2018). https://doi.org/10.1093/toxsci/kfx289
135 de Hoyos-Vega, J. M., Hong, H. J., Stybayeva, G. & Revzin, A. Hepatocyte cultures: From collagen gel sandwiches to microfluidic devices with integrated biosensors. *APL Bioeng* **5**, 041504 (2021). https://doi.org/10.1063/5.0058798
136 Kaur, I. *et al.* Primary Hepatocyte Isolation and Cultures: Technical Aspects, Challenges and Advancements. *Bioengineering (Basel)* **10** (2023). https://doi.org/10.3390/bioengineering10020131
137 Tonooka, Y., Takaku, T., Toyoshima, M., Takahashi, Y. & Kitamoto, S. Suppression of the Epithelial-Mesenchymal Transition and Maintenance of the Liver Functions in Primary Hepatocytes through Dispersion Culture within a Dome-Shaped Collagen Matrix. *Biol Pharm Bull* **47**, 1241-1247 (2024). https://doi.org/10.1248/bpb.b24-00180
138 Choi, H. J. & Choi, D. Successful mouse hepatocyte culture with sandwich collagen gel formation. *J Korean Surg Soc* **84**, 202-208 (2013). https://doi.org/10.4174/jkss.2013.84.4.202

139 Dunn, J. C. Y., Tompkins, R. G. & Yarmush, M. L. Long-Term in Vitro Function of Adult Hepatocytes in a Collagen Sandwich Configuration. *Biotechnology Progress* **7**, 237-245 (1991).
140 Dunn, J. C. Y., Yarmush, M. L., Koebe, H. G. & Tompkins, R. G. Hepatocyte Function and Extracellular Matrix Geometry: Long-term Culture in a Sandwich Configuration. *FASEB*, 174-177 (1989).
141 Gijbels, E., Vanhaecke, T. & Vinken, M. Establishment of Sandwich Cultures of Primary Human Hepatocytes. *Methods in Molecular Biology* **1981**, 325-333 (1981).
142 Kern, A., Bader, A., Pichlmayr, R. & Sewing, K. F. Drug Metabolism in Hepatocyte Sandwich Cultures of Rats and Humans *Biochemical Pharmacology* **54**, 761-772 (1997).
143 Seidemann, L. *et al.* Optimization of extracellular matrix for primary human hepatocyte cultures using mixed collagen-Matrigel matrices. *EXCLI J* **22**, 12-34 (2023). https://doi.org/10.17179/excli2022-5459
144 Deharde, D. *et al.* Bile canaliculi formation and biliary transport in 3D sandwich-cultured hepatocytes in dependence of the extracellular matrix composition. *Arch Toxicol* **90**, 2497-2511 (2016). https://doi.org/10.1007/s00204-016-1758-z
145 Gupta, K. *et al.* Bile canaliculi contract autonomously by releasing calcium into hepatocytes via mechanosensitive calcium channel. *Biomaterials* **259**, 120283 (2020). https://doi.org/10.1016/j.biomaterials.2020.120283
146 Ng, S. *et al.* Improved hepatocyte excretory function by immediate presentation of polarity cues. *Tissue Eng* **12**, 2181-2191 (2006). https://doi.org/10.1089/ten.2006.12.2181
147 Bell, C. C. *et al.* Characterization of primary human hepatocyte spheroids as a model system for drug-induced liver injury, liver function and disease. *Sci Rep* **6**, 25187 (2016). https://doi.org/10.1038/srep25187
148 Bialkowska, K., Komorowski, P., Bryszewska, M. & Milowska, K. Spheroids as a Type of Three-Dimensional Cell Cultures-Examples of Methods of Preparation and the Most Important Application. *Int J Mol Sci* **21** (2020). https://doi.org/10.3390/ijms21176225
149 Cox, C. R., Lynch, S., Goldring, C. & Sharma, P. Current Perspective: 3D Spheroid Models Utilizing Human-Based Cells for Investigating Metabolism-Dependent Drug-Induced Liver Injury. *Front Med Technol* **2**, 611913 (2020). https://doi.org/10.3389/fmedt.2020.611913
150 Fey, S. J. & Wrzesinski, K. Determination of drug toxicity using 3D spheroids constructed from an immortal human hepatocyte cell line. *Toxicol Sci* **127**, 403-411 (2012). https://doi.org/10.1093/toxsci/kfs122
151 Gaskell, H. *et al.* Characterization of a functional C3A liver spheroid model. *Toxicol Res (Camb)* **5**, 1053-1065 (2016). https://doi.org/10.1039/c6tx00101g
152 Ha, D.-H., Thi, P. M., Chaudhary, P. & Jeong, J.-H. Efficient Formation of Three Dimensional Spheroids of Primary Hepatocytes Using Micropatterned Multi-Well Plates. *Macromolecular Research* **27**, 938-943 (2019). https://doi.org/10.1007/s13233-019-7103-7
153 Handin, N. *et al.* Conditions for maintenance of hepatocyte differentiation and function in 3D cultures. *iScience* **24**, 103235 (2021). https://doi.org/10.1016/j.isci.2021.103235
154 Sato, K. *et al.* Organoids and Spheroids as Models for Studying Cholestatic Liver Injury and Cholangiocarcinoma. *Hepatology* **74**, 491-502 (2021). https://doi.org/10.1002/hep.31653
155 Vinci, M. *et al.* Advances in establishment and analysis of three-dimensional tumor spheroid-based functional assays for target validation and drug evaluation. *BMC Biol* **10**, 29 (2012). https://doi.org/10.1186/1741-7007-10-29
156 Subramanian, K. *et al.* Spheroid culture for enhanced differentiation of human embryonic stem cells to hepatocyte-like cells. *Stem Cells Dev* **23**, 124-131 (2014). https://doi.org/10.1089/scd.2013.0097
157 Nautiyal, M. *et al.* Characterization of primary mouse hepatocyte spheroids as a model system to support investigations of drug-induced liver injury. *Toxicol In Vitro* **70**, 105010 (2021). https://doi.org/10.1016/j.tiv.2020.105010

158 Chen, J. *et al*. An in vitro 3D spheroid model with liver steatosis and fibrosis on microwell arrays for drug efficacy evaluation. *J Biotechnol* **399**, 153-163 (2025). https://doi.org/10.1016/j.jbiotec.2025.01.019
159 Tanimizu, N. *et al*. Generation of mouse hepatobiliary organoids from hepatocyte progenitors and cholangiocytes isolated from healthy adult mouse liver. *Nature communications* **12**, 3390 (2021). https://doi.org/10.21203/rs.3.pex-1510/v1
160 Vyas, D. *et al*. Self-assembled liver organoids recapitulate hepatobiliary organogenesis in vitro. *Hepatology* **67**, 750-761 (2018). https://doi.org/10.1002/hep.29483
161 Wu, F. *et al*. Generation of hepatobiliary organoids from human induced pluripotent stem cells. *J Hepatol* **70**, 1145-1158 (2019). https://doi.org/10.1016/j.jhep.2018.12.028
162 Dowbaj, A. M. *et al*. Mouse liver assembloids model periportal architecture and biliary fibrosis. *Nature* **644**, 473-482 (2025). https://doi.org/10.1038/s41586-025-09183-9
163 Huch, M., Knoblich, J. A., Lutolf, M. P. & Martinez-Arias, A. The hope and the hype of organoid research. *Development* **144**, 938-941 (2017). https://doi.org/10.1242/dev.150201
164 Huch, M. & Koo, B. K. Modeling mouse and human development using organoid cultures. *Development* **142**, 3113-3125 (2015). https://doi.org/10.1242/dev.118570
165 Kim, Y. *et al*. Liver organoids: Current advances and future applications for hepatology. *Clin Mol Hepatol* **31**, S327-S348 (2025). https://doi.org/10.3350/cmh.2024.1040
166 Caiazza, C., Parisi, S. & Caiazzo, M. Liver Organoids: Updates on Disease Modeling and Biomedical Applications. *Biology (Basel)* **10** (2021). https://doi.org/10.3390/biology10090835
167 Harrison, S. P. *et al*. Liver Organoids: Recent Developments, Limitations and Potential. *Front Med (Lausanne)* **8**, 574047 (2021). https://doi.org/10.3389/fmed.2021.574047
168 Panwar, A., Das, P. & Tan, L. P. 3D Hepatic Organoid-Based Advancements in LIVER Tissue Engineering. *Bioengineering (Basel)* **8** (2021). https://doi.org/10.3390/bioengineering8110185
169 Peng, W. C., Kraaier, L. J. & Kluiver, T. A. Hepatocyte organoids and cell transplantation: What the future holds. *Exp Mol Med* **53**, 1512-1528 (2021). https://doi.org/10.1038/s12276-021-00579-x
170 Peng, W. C. *et al*. Inflammatory Cytokine TNFalpha Promotes the Long-Term Expansion of Primary Hepatocytes in 3D Culture. *Cell* **175**, 1607-1619 e1615 (2018). https://doi.org/10.1016/j.cell.2018.11.012
171 Hendriks, D. *et al*. Engineered human hepatocyte organoids enable CRISPR-based target discovery and drug screening for steatosis. *Nat Biotechnol* **41**, 1567-1581 (2023). https://doi.org/10.1038/s41587-023-01680-4
172 Park, Y. *et al*. Three-Dimensional Organoids as a Model to Study Nonalcoholic Fatty Liver Disease. *Semin Liver Dis* **42**, 423-433 (2022). https://doi.org/10.1055/a-1934-5588
173 Wei, J., Zhang, W. & Zhao, B. Human liver organoid: modeling liver steatosis and beyond. *Cell Regen* **12**, 17 (2023). https://doi.org/10.1186/s13619-023-00161-y
174 Guan, Y. *et al*. A human multi-lineage hepatic organoid model for liver fibrosis. *Nat Commun* **12**, 6138 (2021). https://doi.org/10.1038/s41467-021-26410-9
175 Arino, S. *et al*. Patient-derived liver organoids recapitulate liver epithelial heterogeneity and enable precision modeling of alcohol-related liver disease. *J Hepatol* (2025). https://doi.org/10.1016/j.jhep.2025.07.014
176 Broutier, L. *et al*. Human primary liver cancer-derived organoid cultures for disease modeling and drug screening. *Nat Med* **23**, 1424-1435 (2017). https://doi.org/10.1038/nm.4438
177 Dong, R., Zhang, B. & Zhang, X. Liver organoids: an in vitro 3D model for liver cancer study. *Cell Biosci* **12**, 152 (2022). https://doi.org/10.1186/s13578-022-00890-8
178 Hu, H. *et al*. Long-Term Expansion of Functional Mouse and Human Hepatocytes as 3D Organoids. *Cell* **175**, 1591-1606 e1519 (2018). https://doi.org/10.1016/j.cell.2018.11.013
179 Akbari, S. *et al*. Robust, Long-Term Culture of Endoderm-Derived Hepatic Organoids for Disease Modeling. *Stem Cell Reports* **13**, 627-641 (2019). https://doi.org/10.1016/j.stemcr.2019.08.007

180 Ramli, M. N. B. *et al*. Human Pluripotent Stem Cell-Derived Organoids as Models of Liver Disease. *Gastroenterology* **159**, 1471-1486 e1412 (2020). https://doi.org/10.1053/j.gastro.2020.06.010
181 Akbari, S., Arslan, N., Senturk, S. & Erdal, E. Next-Generation Liver Medicine Using Organoid Models. *Front Cell Dev Biol* **7**, 345 (2019). https://doi.org/10.3389/fcell.2019.00345
182 Tadokoro, T. *et al*. Human iPSC–liver organoid transplantation reducesfibrosis through immunomodulation. *Science Translational Medicine* **16**, 1-12 (2024).
183 Zhou, V. X., Lolas, M. & Chang, T. T. Direct orthotopic implantation of hepatic organoids. *J Surg Res* **211**, 251-260 (2017). https://doi.org/10.1016/j.jss.2016.12.028
184 Gong, D. *et al*. Advances, challenges and future applications of liver organoids in experimental regenerative medicine. *Front Med (Lausanne)* **11**, 1521851 (2024). https://doi.org/10.3389/fmed.2024.1521851
185 Hu, Y. *et al*. Research progress and application of liver organoids for disease modeling and regenerative therapy. *J Mol Med (Berl)* **102**, 859-874 (2024). https://doi.org/10.1007/s00109-024-02455-3
186 JacksonLaboratory. *STOCK Gls2em1(cre/ERT2)Hzhu/J Strain #036247*, 2025).
187 JacksonLaboratory. *STOCK Glulem1(cre/ERT2)Hzhu/J Strain #036248*, 2025).
188 Muzumdar, M. D., Tasic, B., Miyamichi, K., Li, L. & Luo, L. A global double-fluorescent Cre reporter mouse. *Genesis* **45**, 593-605 (2007). https://doi.org/10.1002/dvg.20335
189 Berry, M. N. & Friend, D. S. High-yield Preparation of Isolated Rat Liver Parenchymal Cells: A Biochemical and Fine Structural Study. *The Journal of Cell Biology* **48**, 506-520 (1969).
190 Lee, S. M., Schelcher, C., Demmel, M., Hauner, M. & Thasler, W. E. Isolation of human hepatocytes by a two-step collagenase perfusion procedure. *J Vis Exp* (2013). https://doi.org/10.3791/50615
191 Jung, Y., Zhao, M. & Svensson, K. J. Isolation, culture, and functional analysis of hepatocytes from mice with fatty liver disease. *STAR Protoc* **1**, 100222 (2020). https://doi.org/10.1016/j.xpro.2020.100222
192 Charni-Natan, M. & Goldstein, I. Protocol for Primary Mouse Hepatocyte Isolation. *STAR Protoc* **1**, 100086 (2020). https://doi.org/10.1016/j.xpro.2020.100086
193 Seglen, P. O. Preparation of isolated rat liver cells. *Methods Cell Biol* **13**, 29-83 (1976). https://doi.org/10.1016/s0091-679x(08)61797-5
194 Kreamer, B. L. *et al*. Use of low-speed, Iso-density Percoll Centrifugation Method to Increase the Viability of Isoalted Rat Hepatocyte Preparations. *In Vitro Cellular & Developmental Biology* **22** (1986).
195 Wang, L. & Boyer, J. L. The maintenance and generation of membrane polarity in hepatocytes. *Hepatology* **39**, 892-899 (2004). https://doi.org/10.1002/hep.20039
196 Tocan, V. *et al*. Hepatocyte polarity establishment and apical lumen formation are organized by Par3, Cdc42, and aPKC in conjunction with Lgl. *J Biol Chem* **297**, 101354 (2021). https://doi.org/10.1016/j.jbc.2021.101354
197 QIAGEN. (QIAGEN, 2019).
198 Invitrogen. (ThermoFischer Scientific, 2018).
199 Roche. (Roche, 2015).
200 Pfaffl, M. W. A new mathematical model for relative quantification in real-time RT–PCR. *Nucleic Acids Res* **29** (2001).
201 Li, Y., Ross-Viola, J. S., Shay, N. F., Moore, D. D. & Ricketts, M. L. Human CYP3A4 and murine Cyp3A11 are regulated by equol and genistein via the pregnane X receptor in a species-specific manner. *J Nutr* **139**, 898-904 (2009). https://doi.org/10.3945/jn.108.103572
202 Promega. (2009).
203 Bankhead, P. *et al*. QuPath: Open source software for digital pathology image analysis. *Sci Rep* **7**, 16878 (2017). https://doi.org/10.1038/s41598-017-17204-5

204 Aronovich, E. L., McIvor, R. S. & Hackett, P. B. The Sleeping Beauty transposon system: a non-viral vector for gene therapy. *Hum Mol Genet* **20**, R14-20 (2011). https://doi.org/10.1093/hmg/ddr140
205 Guirguis, F. *et al.* Consistent Delivery of Adeno-Associated Virus via Lateral Tail-Vein Injection in Adult Mice. *J Vis Exp* (2024). https://doi.org/10.3791/66934
206 Yano, J., Lilly, E. A., Noverr, M. C. & Fidel, P. L. A Contemporary Warming/Restraining Device for Efficient Tail Vein Injections in a Murine Fungal Sepsis Model. *J Vis Exp* (2020). https://doi.org/10.3791/61961
207 Hillman-Jackson, J. *et al.* Using Galaxy to perform large-scale interactive data analyses. *Curr Protoc Bioinformatics* **Chapter 10**, 10 15 11-10 15 47 (2012). https://doi.org/10.1002/0471250953.bi1005s38
208 Rowe, C. *et al.* Proteome-wide analyses of human hepatocytes during differentiation and dedifferentiation. *Hepatology* **58**, 799-809 (2013). https://doi.org/10.1002/hep.26414
209 Baiocchini, A. *et al.* Extracellular Matrix Molecular Remodeling in Human Liver Fibrosis Evolution. *PLoS One* **11**, e0151736 (2016). https://doi.org/10.1371/journal.pone.0151736
210 Dunn, J. C. Y., Tompkins, R. G. & Yarmush, M. L. Hepatocytes in Collagen Sandwich : Evidence for Transcriptional and Translational Regulation. *The Journal of Cell Biology* **116**, 1043-1053 (1992).
211 Chua, A. C. Y. *et al.* Hepatic spheroids used as an in vitro model to study malaria relapse. *Biomaterials* **216**, 119221 (2019). https://doi.org/10.1016/j.biomaterials.2019.05.032
212 Arterburn, L. M., Zurlo, J., Yager, J. D., Overton, R. M. & Heifetz, A. A. A Morphological Study of Differentiated Hepatocytes In Vitro. *Hepatology* **22** (1995).
213 Nelson, L. J. *et al.* Human Hepatic HepaRG Cells Maintain an Organotypic Phenotype with High Intrinsic CYP450 Activity/Metabolism and Significantly Outperform Standard HepG2/C3A Cells for Pharmaceutical and Therapeutic Applications. *Basic Clin Pharmacol Toxicol* **120**, 30-37 (2017). https://doi.org/10.1111/bcpt.12631
214 Nelson, L. J. *et al.* Profiling the impact of medium formulation on morphology and functionality of primary hepatocytes in vitro. *Sci Rep* **3**, 2735 (2013). https://doi.org/10.1038/srep02735
215 Toyoda, H. *et al.* Changes to hepatocyte ploidy and binuclearity profiles during human chronic viral hepatitis. *Gut* **54**, 297-302 (2005). https://doi.org/10.1136/gut.2004.043893
216 Sceter, G., Schwarze, P. E. & Segle, P. O. Shift From Polyploidizing to Nonpolyploidizing Growth in Carcinogen-Treated Rat Liver. *Journal of the National Cancer Institute* **80** (1988).
217 Battle, M. A. *et al.* Hepatocyte nuclear factor 4a orchestrates expression of cell adhesion proteins during the epithelial transformation of the developing liver. *PNAS* **103**, 8419–8424 (2006).
218 Buyl, K., De Kock, J., Bolleyn, J., Rogiers, V. & Vanhaecke, T. Measurement of Albumin Secretion as Functionality Test in Primary Hepatocyte Cultures. *Methods in Molecular Biology* **1250**, 303-308 (2015).
219 Higuchi, Y. *et al.* Functional polymer-dependent 3D culture accelerates the differentiation of HepaRG cells into mature hepatocytes. *Hepatol Res* **46**, 1045-1057 (2016). https://doi.org/10.1111/hepr.12644
220 Nicolas, C. T. *et al.* Hepatocyte spheroids as an alternative to single cells for transplantation after ex vivo gene therapy in mice and pig models. *Surgery* **164**, 473-481 (2018). https://doi.org/10.1016/j.surg.2018.04.012
221 Grubman, S. A. *et al.* Regulation of intracellular pH by immortalized human intrahepatic biliary epithelial cell lines. *American Journal of Physiology-Gastrointestinal and Liver Physiology* **266** (1994).
222 López-Terrada, D., Cheung, S. W., Finegold, M. J. & Knowles, B. B. Hep G2 is a hepatoblastoma-derived cell line. *Human Pathology* **40**, 1512-1515 (2009). https://doi.org/10.1016/j.humpath.2009.06.015

223 Hammad, S. *et al.* Protocols for staining of bile canalicular and sinusoidal networks of human, mouse and pig livers, three-dimensional reconstruction and quantification of tissue microarchitecture by image processing and analysis. *Arch Toxicol* **88**, 1161-1183 (2014). https://doi.org/10.1007/s00204-014-1243-5

224 Lopez de la Oliva, A. R. *et al.* Nuclear Translocation of Glutaminase GLS2 in Human Cancer Cells Associates with Proliferation Arrest and Differentiation. *Sci Rep* **10**, 2259 (2020). https://doi.org/10.1038/s41598-020-58264-4

225 Ghafoory, S. *et al.* Zonation of nitrogen and glucose metabolism gene expression upon acute liver damage in mouse. *PLoS One* **8**, e78262 (2013). https://doi.org/10.1371/journal.pone.0078262

226 Kaestner, K. H. In the Zone: How a Hepatocyte Knows Where It Is. *Gastroenterology* **137**, 425-427 (2009).

227 Scheidecker, B. *et al.* Induction of in vitro Metabolic Zonation in Primary Hepatocytes Requires Both Near-Physiological Oxygen Concentration and Flux. *Front Bioeng Biotechnol* **8**, 524 (2020). https://doi.org/10.3389/fbioe.2020.00524

228 Hempel, M. *et al.* Pathological implications of cadherin zonation in mouse liver. *Cell Mol Life Sci* **72**, 2599-2612 (2015). https://doi.org/10.1007/s00018-015-1861-y

229 Ginguay, A., Cynober, L., Curis, E. & Nicolis, I. Ornithine Aminotransferase, an Important Glutamate-Metabolizing Enzyme at the Crossroads of Multiple Metabolic Pathways. *Biology (Basel)* **6** (2017). https://doi.org/10.3390/biology6010018

230 Berry, M. N. & Simpson, F. O. Fine Structure of Cells Isolated From Adult Mouse LIver. *The Journal of Cell Biology* **15**, 9-17 (1962).

231 Gijbels, E., Vanhaecke, T. & Vinken, M. Establishment of Sandwich Cultures of Primary Human Hepatocytes. *Methods Mol Biol* **1981**, 325-333 (2019). https://doi.org/10.1007/978-1-4939-9420-5_21

232 Karsdal, M. A. *et al.* Novel insights into the function and dynamics of extracellular matrix in liver fibrosis. *Am J Physiol Gastrointest Liver Physiol* **308**, G807-830 (2015). https://doi.org/10.1152/ajpgi.00447.2014

233 Page, J. L. *et al.* Gene expression profiling of extracellular matrix as an effector of human hepatocyte phenotype in primary cell culture. *Toxicol Sci* **97**, 384-397 (2007). https://doi.org/10.1093/toxsci/kfm034

234 Dianat, N. *et al.* Generation of functional cholangiocyte-like cells from human pluripotent stem cells and HepaRG cells. *Hepatology* **60**, 700-714 (2014). https://doi.org/10.1002/hep.27165

235 O'Neill, K. E. *et al.* Hepatocyte-ductal transdifferentiation is mediated by reciprocal repression of SOX9 and C/EBPalpha. *Cell Reprogram* **16**, 314-323 (2014). https://doi.org/10.1089/cell.2014.0032

236 Larue, L. & Bellacosa, A. Epithelial-mesenchymal transition in development and cancer: role of phosphatidylinositol 3' kinase/AKT pathways. *Oncogene* **24**, 7443-7454 (2005). https://doi.org/10.1038/sj.onc.1209091

237 Ramirez-Pena, E. *et al.* The Epithelial to Mesenchymal Transition Promotes Glutamine Independence by Suppressing GLS2 Expression. *Cancers (Basel)* **11** (2019). https://doi.org/10.3390/cancers11101610

238 Miura, S. *et al.* Hepatocytes differentiate into intestinal epithelial cells through a hybrid epithelial/mesenchymal cell state in culture. *Nat Commun* **15**, 3940 (2024). https://doi.org/10.1038/s41467-024-47869-2

239 Andersen, J. T. *et al.* Extending serum half-life of albumin by engineering neonatal Fc receptor (FcRn) binding. *J Biol Chem* **289**, 13492-13502 (2014). https://doi.org/10.1074/jbc.M114.549832

240 Rozga, J., Piątek, T. & Małkowski, P. in *Transfusion Medicine and Hemotherapy* Vol. 36 Ch. 5, 399-407 (2009).

241 Govaere, O. *et al.* Keratin 19: a key role player in the invasion of human hepatocellular carcinomas. *Gut* **63**, 674-685 (2014). https://doi.org/10.1136/gutjnl-2012-304351
242 Mishra, L. *et al.* Liver stem cells and hepatocellular carcinoma. *Hepatology* **49**, 318-329 (2009). https://doi.org/10.1002/hep.22704
243 Rhee, H. *et al.* Keratin 19 Expression in Hepatocellular Carcinoma Is Regulated by Fibroblast-Derived HGF via a MET-ERK1/2-AP1 and SP1 Axis. *Cancer Res* **78**, 1619-1631 (2018). https://doi.org/10.1158/0008-5472.CAN-17-0988
244 Takano, M. *et al.* Keratin 19 as a key molecule in progression of human hepatocellular carcinomas through invasion and angiogenesis. *BMC Cancer* **16**, 903 (2016). https://doi.org/10.1186/s12885-016-2949-y
245 Oshima, R. G. Apoptosis and keratin intermediate filaments. *Cell Death Differ* **9**, 486-492 (2002). https://doi.org/10.1038/sj.cdd.4400988
246 Sharma, P. *et al.* Keratin 19 regulates cell cycle pathway and sensitivity of breast cancer cells to CDK inhibitors. *Sci Rep* **9**, 14650 (2019). https://doi.org/10.1038/s41598-019-51195-9
247 Royo, F. *et al.* Three-Dimensional Hepatocyte Spheroids: Model for Assessing Chemotherapy in Hepatocellular Carcinoma. *Biomedicines* **12** (2024). https://doi.org/10.3390/biomedicines12061200
248 Lu, Z. H. *et al.* CD25 is a novel marker of hepatic bile canaliculus. *Int J Surg Pathol* **20**, 455-461 (2012). https://doi.org/10.1177/1066896912444158
249 McCaughan, G. W., Wickson, J. E., Creswick, P. F. & Gorrell, M. D. Identification of the bile canalicular cell surface molecule GP110 as the ectopeptidase dipeptidyl peptidase IV: an analysis by tissue distribution, purification and N-terminal amino acid sequence. *Hepatology* **11**, 534-544 (1990). https://doi.org/10.1002/hep.1840110403
250 Bebelman, M. P. *et al.* Hepatocyte apical bulkheads provide a mechanical means to oppose bile pressure. *J Cell Biol* **222** (2023). https://doi.org/10.1083/jcb.202208002
251 Treyer, A. & Musch, A. Hepatocyte polarity. *Compr Physiol* **3**, 243-287 (2013). https://doi.org/10.1002/cphy.c120009
252 Gadd, V. L., Aleksieva, N. & Forbes, S. J. Epithelial Plasticity during Liver Injury and Regeneration. *Cell Stem Cell* **27**, 557-573 (2020). https://doi.org/10.1016/j.stem.2020.08.016
253 Duivenvoorde, L. P. M., Louisse, J., Pinckaers, N. E. T., Nguyen, T. & van der Zande, M. Comparison of gene expression and biotransformation activity of HepaRG cells under static and dynamic culture conditions. *Sci Rep* **11**, 10327 (2021). https://doi.org/10.1038/s41598-021-89710-6
254 Ueyama, T., Tsuji, S., Sugiyama, T. & Tada, M. Fluorometric evaluation of CYP3A4 expression using improved transgenic HepaRG cells carrying a dual-colour reporter for CYP3A4 and CYP3A7. *Sci Rep* **7**, 2874 (2017). https://doi.org/10.1038/s41598-017-03146-5
255 Kitaoka, S., Hatogai, J., Ochiai, W. & Sugiyama, K. Zonation of the drug-metabolizing enzyme cytochrome P450 3A in infant mice begins in pre-weaning period. *The Journal of Toxicological Sciences* **43**, 223-227 (2018).
256 van Herwaarden, A. E. *et al.* Knockout of cytochrome P450 3A yields new mouse models for understanding xenobiotic metabolism. *J Clin Invest* **117**, 3583-3592 (2007). https://doi.org/10.1172/JCI33435
257 Keinan, O. *et al.* Glycogen metabolism links glucose homeostasis to thermogenesis in adipocytes. *Nature* **599**, 296-301 (2021). https://doi.org/10.1038/s41586-021-04019-8
258 Roach, P. J., Depaoli-Roach, A. A., Hurley, T. D. & Tagliabracci, V. S. Glycogen and its metabolism: some new developments and old themes. *Biochem J* **441**, 763-787 (2012). https://doi.org/10.1042/BJ20111416
259 Ahn, J. *et al.* Human three-dimensional in vitro model of hepatic zonation to predict zonal hepatotoxicity. *J Biol Eng* **13**, 22 (2019). https://doi.org/10.1186/s13036-019-0148-5
260 Gebhardt, R. Metabolic Zonation of the Liver: Regulation and Implications for Liver Function. *Pharmacology & Therapeutics* **53**, 275-354 (1992).

261 Boon, L., Geerts, W. J., Jonker, A., Lamers, W. H. & Van Noorden, C. J. High protein diet induces pericentral glutamate dehydrogenase and ornithine aminotransferase to provide sufficient glutamate for pericentral detoxification of ammonia in rat liver lobules. *Histochemistry and cell biology* **111**, 445-452 (1999).
262 Li, F., Cao, L., Parikh, S. & Zuo, R. Three-Dimensional Spheroids With Primary Human Liver Cells and Differential Roles of Kupffer Cells in Drug-Induced Liver Injury. *J Pharm Sci* **109**, 1912-1923 (2020). https://doi.org/10.1016/j.xphs.2020.02.021
263 Messner, S., Agarkova, I., Moritz, W. & Kelm, J. M. Multi-cell type human liver microtissues for hepatotoxicity testing. *Arch Toxicol* **87**, 209-213 (2013). https://doi.org/10.1007/s00204-012-0968-2
264 Kurosaki, S. *et al*. Cell fate analysis of zone 3 hepatocytes in liver injury and tumorigenesis. *JHEP Rep* **3**, 100315 (2021). https://doi.org/10.1016/j.jhepr.2021.100315
265 Siller, R., Greenhough, S., Naumovska, E. & Sullivan, G. J. Small-molecule-driven hepatocyte differentiation of human pluripotent stem cells. *Stem Cell Reports* **4**, 939-952 (2015). https://doi.org/10.1016/j.stemcr.2015.04.001
266 Wang, W. *et al*. Evaluation of AXIN1 and AXIN2 as targets of tankyrase inhibition in hepatocellular carcinoma cell lines. *Sci Rep* **11**, 7470 (2021). https://doi.org/10.1038/s41598-021-87091-4
267 Hu, W. *et al*. Glutaminase 2, a novel p53 target gene regulating energy metabolism and antioxidant function. *Proc Natl Acad Sci U S A* **107**, 7455-7460 (2010). https://doi.org/10.1073/pnas.1001006107
268 Suzuki, S. *et al*. Phosphate-activated glutaminase (GLS2), a p53-inducible regulator of glutamine metabolism and reactive oxygen species. *Proc Natl Acad Sci U S A* **107**, 7461-7466 (2010). https://doi.org/10.1073/pnas.1002459107
269 Chun, Y. & Kim, J. AMPK-mTOR Signaling and Cellular Adaptations in Hypoxia. *Int J Mol Sci* **22** (2021). https://doi.org/10.3390/ijms22189765
270 Garcia, D. & Shaw, R. J. AMPK: Mechanisms of Cellular Energy Sensing and Restoration of Metabolic Balance. *Mol Cell* **66**, 789-800 (2017). https://doi.org/10.1016/j.molcel.2017.05.032
271 Garza-Lombo, C., Schroder, A., Reyes-Reyes, E. M. & Franco, R. mTOR/AMPK signaling in the brain: Cell metabolism, proteostasis and survival. *Curr Opin Toxicol* **8**, 102-110 (2018). https://doi.org/10.1016/j.cotox.2018.05.002
272 Smiles, W. J. *et al*. New developments in AMPK and mTORC1 cross-talk. *Essays Biochem* **68**, 321-336 (2024). https://doi.org/10.1042/EBC20240007
273 Fleming, K. E. & Wanless, I. R. Glutamine synthetase expression in activated hepatocyte progenitor cells and loss of hepatocellular expression in congestion and cirrhosis. *Liver Int* **33**, 525-534 (2013). https://doi.org/10.1111/liv.12099
274 Liu, P. *et al*. Glutamine synthetase promotes tumor invasion in hepatocellular carcinoma through mediating epithelial-mesenchymal transition. *Hepatol Res* **50**, 246-257 (2020). https://doi.org/10.1111/hepr.13433
275 Shen, Y. *et al*. Glutamine metabolism: from proliferating cells to cardiomyocytes. *Metabolism* **121**, 154778 (2021). https://doi.org/10.1016/j.metabol.2021.154778
276 Villar, V. H. *et al*. Hepatic glutamine synthetase controls N(5)-methylglutamine in homeostasis and cancer. *Nat Chem Biol* **19**, 292-300 (2023). https://doi.org/10.1038/s41589-022-01154-9
277 Dai, W. *et al*. Glutamine synthetase limits beta-catenin-mutated liver cancer growth by maintaining nitrogen homeostasis and suppressing mTORC1. *J Clin Invest* **132** (2022). https://doi.org/10.1172/JCI161408
278 Delgado, T. C., de Las Heras, J. & Martinez-Chantar, M. L. Understanding gut-liver axis nitrogen metabolism in Fatty Liver Disease. *Front Endocrinol (Lausanne)* **13**, 1058101 (2022). https://doi.org/10.3389/fendo.2022.1058101

279 Frieg, B., Gorg, B., Gohlke, H. & Haussinger, D. Glutamine synthetase as a central element in hepatic glutamine and ammonia metabolism: novel aspects. *Biol Chem* **402**, 1063-1072 (2021). https://doi.org/10.1515/hsz-2021-0166
280 Sekine, S., Lan, B. Y., Bedolli, M., Feng, S. & Hebrok, M. Liver-specific loss of beta-catenin blocks glutamine synthesis pathway activity and cytochrome p450 expression in mice. *Hepatology* **43**, 817-825 (2006). https://doi.org/10.1002/hep.21131
281 Couchet, M. *et al*. Ornithine Transcarbamylase - From Structure to Metabolism: An Update. *Front Physiol* **12**, 748249 (2021). https://doi.org/10.3389/fphys.2021.748249
282 Kirpich, I. A. *et al*. Integrated hepatic transcriptome and proteome analysis of mice with high-fat diet-induced nonalcoholic fatty liver disease. *J Nutr Biochem* **22**, 38-45 (2011). https://doi.org/10.1016/j.jnutbio.2009.11.009
283 Aumailley, L. *et al*. Combined transcriptomics and proteomics unveil the impact of vitamin C in modulating specific protein abundance in the mouse liver. *Biol Res* **57**, 26 (2024). https://doi.org/10.1186/s40659-024-00509-x
284 Michel, G., Yu, Y., Chang, T. & Yee, J. K. Site-specific gene insertion mediated by a Cre-loxP-carrying lentiviral vector. *Mol Ther* **18**, 1814-1821 (2010). https://doi.org/10.1038/mt.2010.150
285 Schmidt, E. E., Taylor, D. S., Prigge, J. R., Barnett, S. & Capecchi, M. R. Illegitimate Cre-dependent chromosomerearrangements in transgenicmouse spermatids. *PNAS* **97**, 13702–13707 (2000).
286 Semprini, S. *et al*. Cryptic loxP sites in mammalian genomes: genome-wide distribution and relevance for the efficiency of BAC/PAC recombineering techniques. *Nucleic Acids Res* **35**, 1402-1410 (2007). https://doi.org/10.1093/nar/gkl1108
287 Alvarez-Aznar, A. *et al*. Tamoxifen-independent recombination of reporter genes limits lineage tracing and mosaic analysis using CreER(T2) lines. *Transgenic Res* **29**, 53-68 (2020). https://doi.org/10.1007/s11248-019-00177-8
288 Bohin, N., Carlson, E. A. & Samuelson, L. C. Genome Toxicity and Impaired Stem Cell Function after Conditional Activation of CreER(T2) in the Intestine. *Stem Cell Reports* **11**, 1337-1346 (2018). https://doi.org/10.1016/j.stemcr.2018.10.014
289 Higashi, A. Y. *et al*. Direct hematological toxicity and illegitimate chromosomal recombination caused by the systemic activation of CreERT2. *J Immunol* **182**, 5633-5640 (2009). https://doi.org/10.4049/jimmunol.0802413
290 Payne, S., De Val, S. & Neal, A. Endothelial-Specific Cre Mouse Models: Is Your Cre CREdibile? *Arteriosclerosis, thrombosis, and vascular biology* **38**, 2550-2561 (2018).
291 Rossi, M. *et al*. Warning regarding hematological toxicity of tamoxifen activated CreERT2 in young Rosa26CreERT2 mice. *Sci Rep* **13**, 5976 (2023). https://doi.org/10.1038/s41598-023-32633-1
292 Gravdal, K., Halvorsen, O. J., Haukaas, S. A. & Akslen, L. A. A switch from E-cadherin to N-cadherin expression indicates epithelial to mesenchymal transition and is of strong and independent importance for the progress of prostate cancer. *Clin Cancer Res* **13**, 7003-7011 (2007). https://doi.org/10.1158/1078-0432.CCR-07-1263
293 Tian, X. *et al*. Generation of a self-cleaved inducible Cre recombinase for efficient temporal genetic manipulation. *EMBO J* **39**, e102675 (2020). https://doi.org/10.15252/embj.2019102675
294 Hosur, V. *et al*. Large-Scale Genome-Wide Optimization and Prediction of the Cre Recombinase System for Precise Genome Manipulation in Mice. *Res Sq* (2024). https://doi.org/10.21203/rs.3.rs-4595968/v1
295 Andrews, T. S. *et al*. Single-Cell, Single-Nucleus, and Spatial RNA Sequencing of the Human Liver Identifies Cholangiocyte and Mesenchymal Heterogeneity. *Hepatol Commun* **6**, 821-840 (2022). https://doi.org/10.1002/hep4.1854
296 Carlessi, R. *et al*. Single-nucleus RNA sequencing of pre-malignant liver reveals disease-associated hepatocyte state with HCC prognostic potential. *Cell Genom* **3**, 100301 (2023). https://doi.org/10.1016/j.xgen.2023.100301

297 Van Melkebeke, L. *et al*. Comparison of the single-cell and single-nucleus hepatic myeloid landscape within decompensated cirrhosis patients. *Front Immunol* **15**, 1346520 (2024). https://doi.org/10.3389/fimmu.2024.1346520
298 Richter, M. L. *et al*. Single-nucleus RNA-seq2 reveals functional crosstalk between liver zonation and ploidy. *Nat Commun* **12**, 4264 (2021). https://doi.org/10.1038/s41467-021-24543-5
299 He, L. *et al*. Application of single-cell RNA sequencing technology in liver diseases: a narrative review. *Ann Transl Med* **9**, 1598 (2021). https://doi.org/10.21037/atm-21-4824
300 Wang, S. Protocol to obtain high-quality single-cell RNA-sequencing data from mouse liver cells using centrifugation. *STAR Protoc* **3**, 101824 (2022). https://doi.org/10.1016/j.xpro.2022.101824
301 Donocoff, R. S., Teteloshvili, N., Chung, H., Shoulson, R. & Creusot, R. J. Optimization of tamoxifen-induced Cre activity and its effect on immune cell populations. *Sci Rep* **10**, 15244 (2020). https://doi.org/10.1038/s41598-020-72179-0
302 Reinert, R. B. *et al*. Tamoxifen-Induced Cre-loxP Recombination Is Prolonged in Pancreatic Islets of Adult Mice. *PLoS One* **7**, e33529 (2012). https://doi.org/10.1371/journal.pone.0033529
303 Sohal, D. S. *et al*. Temporally Regulated and Tissue-Specific Gene Manipulations in the Adult and Embryonic Heart Using a Tamoxifen-Inducible Cre Protein. *Circulation Research* (2001).
304 Yovchev, M. *et al*. Experimental Model for Successful Liver Cell Therapy by Lenti TTR-YapERT2 Transduced Hepatocytes with Tamoxifen Control of Yap Subcellular Location. *Sci Rep* **6**, 19275 (2016). https://doi.org/10.1038/srep19275
305 Lipov, E. G., Joshi, J. R. & Sanders, S. A new mechanism of action for tamoxifen *The Lancet Oncology* **10**, 542 (2009).
306 Wiseman, H. Tamoxifen: new membranemediated mechanisms of action and therapeutic advances. *Trends in pharmacological sciences* **15**, 83-89 (1994).
307 Kliewer, S. A. & Willson, T. M. Regulation of xenobiotic and bile acid metabolism by the nuclear pregnane X receptor. *Journal of Lipid Research* **43**, 359-364 (2002). https://doi.org/10.1016/s0022-2275(20)30141-3
308 Pavek, P. Pregnane X Receptor (PXR)-Mediated Gene Repression and Cross-Talk of PXR with Other Nuclear Receptors via Coactivator Interactions. *Front Pharmacol* **7**, 456 (2016). https://doi.org/10.3389/fphar.2016.00456
309 Desai, P. B. *et al*. Induction of cytochrome p450 3a4 in primary human hepatocytes and activation of the human pregnane x receptor by tamoxifen and 4-hydroxytamoxifen. *Drug Metabolism And Disposition* **30** (2002).
310 Jiang, Y. *et al*. Pregnane X Receptor Regulates Liver Size and Liver Cell Fate by Yes-Associated Protein Activation in Mice. *Hepatology* **69**, 343-358 (2019). https://doi.org/10.1002/hep.30131
311 Sane, R. S., Buckley, D. J., Buckley, A. R., Nallani, S. C. & Desai, P. B. Role of human pregnane X receptor in tamoxifen- and 4-hydroxytamoxifen-mediated CYP3A4 induction in primary human hepatocytes and LS174T cells. *Drug Metab Dispos* **36**, 946-954 (2008). https://doi.org/10.1124/dmd.107.018598
312 Tripathi, R., Aggarwal, T. & Fredriksson, R. SLC38A10 Transporter Plays a Role in Cell Survival Under Oxidative Stress and Glutamate Toxicity. *Front Mol Biosci* **8**, 671865 (2021). https://doi.org/10.3389/fmolb.2021.671865
313 Ming, W. H. *et al*. Pregnane X receptor activation alleviates renal fibrosis in mice via interacting with p53 and inhibiting the Wnt7a/beta-catenin signaling. *Acta Pharmacol Sin* **44**, 2075-2090 (2023). https://doi.org/10.1038/s41401-023-01113-7
314 Liu, Z. *et al*. Short-term tamoxifen treatment has long-term effects on metabolism in high-fat diet-fed mice with involvement of Nmnat2 in POMC neurons. *FEBS Lett* **592**, 3305-3316 (2018). https://doi.org/10.1002/1873-3468.13240
315 Li, M. *et al*. Tamoxifen induced hepatic steatosis in high-fat feeding rats through SIRT1-Foxo1 suppression and LXR-SREBP1c activation. *Toxicol Res (Camb)* **11**, 673-682 (2022). https://doi.org/10.1093/toxres/tfac043

316 Zhao, F. *et al.* The effect and mechanism of tamoxifen-induced hepatocyte steatosis in vitro. *Int J Mol Sci* **15**, 4019-4030 (2014). https://doi.org/10.3390/ijms15034019
317 Horton, J. D., Goldstein, J. L. & Brown, M. S. SREBPs: activators of the complete program of cholesterol and fatty acid synthesis in the liver. *Journal of Clinical Investigation* **109**, 1125-1131 (2002). https://doi.org/10.1172/jci0215593
318 Fourcot, A. *et al.* Gas6 deficiency prevents liver inflammation, steatohepatitis, and fibrosis in mice. *Am J Physiol Gastrointest Liver Physiol* **300**, G1043-1053 (2011). https://doi.org/10.1152/ajpgi.00311.2010
319 Miki, Y. *et al.* Comparative effects of raloxifene, tamoxifen and estradiol on human osteoblasts in vitro: estrogen receptor dependent or independent pathways of raloxifene. *J Steroid Biochem Mol Biol* **113**, 281-289 (2009). https://doi.org/10.1016/j.jsbmb.2009.01.010
320 Lichter-Konecki, U. Defects of the urea cycle. *Translational Science of Rare Diseases* **1**, 23-43 (2016). https://doi.org/10.3233/trd-160002
321 Knopf, J. L., Gallagher, J. F. & Held, W. A. Differential, Multihormonal Regulation of the Mouse Major Urinary Protein Gene Family in the Liver. *Molecular and Cellular Biology* **3**, 2232-2240 (1983).
322 Penn, D. J., Zala, S. M. & Luzynski, K. C. Regulation of Sexually Dimorphic Expression of Major Urinary Proteins. *Frontiers in Physiology* **13** (2022). https://doi.org/10.3389/fphys.2022.822073
323 Watson, B. R. *et al.* Spatial transcriptomics of healthy and fibrotic human liver at single-cell resolution. *Nat Commun* **16**, 319 (2025). https://doi.org/10.1038/s41467-024-55325-4
324 Suo, Y., Thimme, R. & Bengsch, B. Spatial single-cell omics: new insights into liver diseases. *Gut* (2025). https://doi.org/10.1136/gutjnl-2024-332105
325 Yakubovsky, O. *et al.* A spatial transcriptomics atlas of live donors reveals unique zonation patterns in the healthy human liver. *bioRxiv* (2025). https://doi.org/10.1101/2025.02.22.639181
326 Hussain, S. I. *et al.* Structural and functional implications of SLC13A3 and SLC9A6 mutations: an in silico approach to understanding intellectual disability. *BMC Neurol* **23**, 353 (2023). https://doi.org/10.1186/s12883-023-03397-y
327 Weiner, I. D., Miller, R. T. & Verlander, J. W. Localization of the ammonium transporters, Rh B glycoprotein and Rh C glycoprotein, in the mouse liver. *Gastroenterology* **124**, 1432-1440 (2003). https://doi.org/10.1016/s0016-5085(03)00277-4
328 Xu, J., Kulkarni, S. R., Li, L. & Slitt, A. L. UDP-glucuronosyltransferase expression in mouse liver is increased in obesity- and fasting-induced steatosis. *Drug Metab Dispos* **40**, 259-266 (2012). https://doi.org/10.1124/dmd.111.039925
329 Liu, Y., Hyde, A. S., Simpson, M. A. & Barycki, J. J. Emerging regulatory paradigms in glutathione metabolism. *Adv Cancer Res* **122**, 69-101 (2014). https://doi.org/10.1016/B978-0-12-420117-0.00002-5
330 Clinkenbeard, E. L., Butler, J. E. & Spear, B. T. Pericentral activity of alpha-fetoprotein enhancer 3 and glutamine synthetase upstream enhancer in the adult liver are regulated by beta-catenin in mice. *Hepatology* **56**, 1892-1901 (2012). https://doi.org/10.1002/hep.25819
331 Kiseleva, Y. V. *et al.* Molecular pathways of liver regeneration: A comprehensive review. *World J Hepatol* **13**, 270-290 (2021). https://doi.org/10.4254/wjh.v13.i3.270
332 Lin, Y. H. *et al.* IGFBP2 expressing midlobular hepatocytes preferentially contribute to liver homeostasis and regeneration. *Cell Stem Cell* **30**, 665-676 e664 (2023). https://doi.org/10.1016/j.stem.2023.04.007
333 Gebhardt, R., Baldysiak-Figiel, A., Krugel, V., Ueberham, E. & Gaunitz, F. Hepatocellular expression of glutamine synthetase: an indicator of morphogen actions as master regulators of zonation in adult liver. *Prog Histochem Cytochem* **41**, 201-266 (2007). https://doi.org/10.1016/j.proghi.2006.12.001
334 Wongkittichote, P., Ah Mew, N. & Chapman, K. A. Propionyl-CoA carboxylase - A review. *Mol Genet Metab* **122**, 145-152 (2017). https://doi.org/10.1016/j.ymgme.2017.10.002

335 Torres, N., Martinez, L., Aleman, G., Bourges, H. & Tovar, A. R. Histidase expression is regulated by dietary protein at the pretranslational level in rat liver. *J Nutr* **128**, 818-824 (1998). https://doi.org/10.1093/jn/128.5.818

336 Pang, L. *et al*. A stable liver-specific urate oxidase gene knockout hyperuricemia mouse model finds activated hepatic de novo purine biosynthesis and urate nephropathy. *Biochim Biophys Acta Mol Basis Dis* **1870**, 167009 (2024). https://doi.org/10.1016/j.bbadis.2023.167009

337 Lu, J. *et al*. Knockout of the urate oxidase gene provides a stable mouse model of hyperuricemia associated with metabolic disorders. *Kidney Int* **93**, 69-80 (2018). https://doi.org/10.1016/j.kint.2017.04.031

338 Mersaoui, S. Y. *et al*. Arsenic 3 methyltransferase (AS3MT) automethylates on cysteine residues in vitro. *Arch Toxicol* **96**, 1371-1386 (2022). https://doi.org/10.1007/s00204-022-03248-8

339 Camara, A. K. S., Zhou, Y., Wen, P. C., Tajkhorshid, E. & Kwok, W. M. Mitochondrial VDAC1: A Key Gatekeeper as Potential Therapeutic Target. *Front Physiol* **8**, 460 (2017). https://doi.org/10.3389/fphys.2017.00460

340 Matsumoto, K. *et al*. Claudin 2 deficiency reduces bile flow and increases susceptibility to cholesterol gallstone disease in mice. *Gastroenterology* **147**, 1134-1145 e1110 (2014). https://doi.org/10.1053/j.gastro.2014.07.033

341 Petrenko, O. *et al*. Transcriptomic signatures of progressive and regressive liver fibrosis and portal hypertension. *iScience* **27**, 109301 (2024). https://doi.org/10.1016/j.isci.2024.109301

342 Stanulovic, V. S. *et al*. Hepatic HNF4alpha deficiency induces periportal expression of glutamine synthetase and other pericentral enzymes. *Hepatology* **45**, 433-444 (2007). https://doi.org/10.1002/hep.21456

343 Perrimon, N., Pitsouli, C. & Shilo, B. Z. Signaling mechanisms controlling cell fate and embryonic patterning. *Cold Spring Harb Perspect Biol* **4**, a005975 (2012). https://doi.org/10.1101/cshperspect.a005975

344 Matz-Soja, M., Hovhannisyan, A. & Gebhardt, R. Hedgehog signalling pathway in adult liver: a major new player in hepatocyte metabolism and zonation? *Med Hypotheses* **80**, 589-594 (2013). https://doi.org/10.1016/j.mehy.2013.01.032

345 Matz-Soja, M. *et al*. Hedgehog signaling is a potent regulator of liver lipid metabolism and reveals a GLI-code associated with steatosis. *Elife* **5** (2016). https://doi.org/10.7554/eLife.13308

346 Moron, M. S., Depierre, J. W. & Mannervik, B. Levels of Glutathione, Glutathione Reductase and Glutathione S-Transferase Activities in Rat Lung and Liver. *Biochimica et Biophysica Acta* **582**, 67-78 (1979).

347 Sun, A. S. & Cederbaum, A. I. Oxidoreductase Activities in Normal Rat Liver, Tumor-bearing Rat Liver, and Hepatoma HC-2521. *Cancer Research* **40**, 4677-4681 (1980).

348 Jeliazkova, P. *et al*. Canonical Notch2 signaling determines biliary cell fates of embryonic hepatoblasts and adult hepatocytes independent of Hes1. *Hepatology* **57**, 2469-2479 (2013). https://doi.org/10.1002/hep.26254

349 Bonamassa, B., Hai, L. & Liu, D. Hydrodynamic gene delivery and its applications in pharmaceutical research. *Pharm Res* **28**, 694-701 (2011). https://doi.org/10.1007/s11095-010-0338-9

350 Budker, V. G. *et al*. Mechanism of plasmid delivery by hydrodynamic tail vein injection. II. Morphological studies. *J Gene Med* **8**, 874-888 (2006). https://doi.org/10.1002/jgm.920

351 Chen, X. & Calvisi, D. F. Hydrodynamic transfection for generation of novel mouse models for liver cancer research. *Am J Pathol* **184**, 912-923 (2014). https://doi.org/10.1016/j.ajpath.2013.12.002

352 Huang, M., Sun, R., Huang, Q. & Tian, Z. Technical Improvement and Application of Hydrodynamic Gene Delivery in Study of Liver Diseases. *Front Pharmacol* **8**, 591 (2017). https://doi.org/10.3389/fphar.2017.00591

353 Kim, M. J. & Ahituv, N. The hydrodynamic tail vein assay as a tool for the study of liver promoters and enhancers. *Methods Mol Biol* **1015**, 279-289 (2013). https://doi.org/10.1007/978-1-62703-435-7_18
354 Guo, J. *et al*. Evaluation of the effect of GSK-3beta on liver cancer based on the PI3K/AKT pathway. *Front Cell Dev Biol* **12**, 1431423 (2024). https://doi.org/10.3389/fcell.2024.1431423
355 Shamsan, E. *et al*. The role of PI3k/AKT signaling pathway in attenuating liver fibrosis: a comprehensive review. *Front Med* **11**, 1389329 (2024). https://doi.org/10.3389/fmed.2024.1389329
356 Katsube, K. & Sakamoto, K. Notch in vertebrates--molecular aspects of the signal. *Int J Dev Biol* **49**, 369-374 (2005). https://doi.org/10.1387/ijdb.041950kk
357 Ho, C. *et al*. AKT (v-akt murine thymoma viral oncogene homolog 1) and N-Ras (neuroblastoma ras viral oncogene homolog) coactivation in the mouse liver promotes rapid carcinogenesis by way of mTOR (mammalian target of rapamycin complex 1), FOXM1 (forkhead box M1)/SKP2, and c-Myc pathways. *Hepatology* **55**, 833-845 (2012). https://doi.org/10.1002/hep.24736
358 Kharas, M. G. *et al*. Constitutively active AKT depletes hematopoietic stem cells and induces leukemia in mice. *Blood* **115**, 1406-1415 (2010). https://doi.org/10.1182/blood-2009-06-229443
359 Lotto, J. *et al*. Single-Cell Transcriptomics Reveals Early Emergence of Liver Parenchymal and Non-parenchymal Cell Lineages. *Cell* **183**, 702-716 e714 (2020). https://doi.org/10.1016/j.cell.2020.09.012
360 Wang, S. *et al*. Region-specific cellular and molecular basis of liver regeneration after acute pericentral injury. *Cell Stem Cell* **31**, 341-358 e347 (2024). https://doi.org/10.1016/j.stem.2024.01.013
361 Wang, H., Zhou, Y., Yu, L., Liu, Z. & Zheng, S. Advanced omics approaches in liver transplant settings: current applications and future prospectives. *Front Immunol* **16**, 1564248 (2025). https://doi.org/10.3389/fimmu.2025.1564248
362 Sun, Y. *et al*. Asparagine protects pericentral hepatocytes during acute liver injury. *J Clin Invest* **133** (2023). https://doi.org/10.1172/JCI163508
363 Tanimizu, N., Ichinohe, N., Suzuki, H. & Mitaka, T. Prolonged oxidative stress and delayed tissue repair exacerbate acetaminophen-induced liver injury in aged mice. *Aging* **12** (2020).
364 Oliveira, L. C. *et al*. Autoimmune hepatitis, HLA and extended haplotypes. *Autoimmun Rev* **10**, 189-193 (2011). https://doi.org/10.1016/j.autrev.2010.09.024
365 Jin, C. *et al*. Single-cell RNA sequencing reveals the pro-inflammatory roles of liver-resident Th1-like cells in primary biliary cholangitis. *Nat Commun* **15**, 8690 (2024). https://doi.org/10.1038/s41467-024-53104-9
366 Lleo, A., Leung, P. S. C., Hirschfield, G. M. & Gershwin, E. M. The Pathogenesis of Primary Biliary Cholangitis: A Comprehensive Review. *Semin Liver Dis* **40**, 34-48 (2020). https://doi.org/10.1055/s-0039-1697617
367 Tanaka, A. Current understanding of primary biliary cholangitis. *Clin Mol Hepatol* **27**, 1-21 (2021). https://doi.org/10.3350/cmh.2020.0028
368 Xin, J. *et al*. Spatial transcriptomics analysis of zone-dependent hepatic ischemia-reperfusion injury murine model. *Commun Biol* **6**, 194 (2023). https://doi.org/10.1038/s42003-023-04564-0
369 Abu Rmilah, A. *et al*. Understanding the marvels behind liver regeneration. *Wiley Interdiscip Rev Dev Biol* **8**, e340 (2019). https://doi.org/10.1002/wdev.340
370 Hindley, C. J., Mastrogiovanni, G. & Huch, M. The plastic liver: differentiated cells, stem cells, every cell? *J Clin Invest* **124**, 5099-5102 (2014). https://doi.org/10.1172/JCI78372
371 Lin, S. *et al*. Distributed hepatocytes expressing telomerase repopulate the liver in homeostasis and injury. *Nature* **556**, 244-248 (2018). https://doi.org/10.1038/s41586-018-0004-7
372 Huang, R., Zhang, X., Gracia-Sancho, J. & Xie, W. F. Liver regeneration: Cellular origin and molecular mechanisms. *Liver Int* **42**, 1486-1495 (2022). https://doi.org/10.1111/liv.15174

373 Pu, W. *et al*. Mfsd2a+ hepatocytes repopulate the liver during injury and regeneration. *Nat Commun* **7**, 13369 (2016). https://doi.org/10.1038/ncomms13369
374 Gribben, C. *et al*. Acquisition of epithelial plasticity in human chronic liver disease. *Nature* **630**, 166-173 (2024). https://doi.org/10.1038/s41586-024-07465-2
375 Schaub, J. R. *et al*. De novo formation of the biliary system by TGFbeta-mediated hepatocyte transdifferentiation. *Nature* **557**, 247-251 (2018). https://doi.org/10.1038/s41586-018-0075-5
376 Leung, R. W. H. & Lee, T. K. W. Wnt/beta-Catenin Signaling as a Driver of Stemness and Metabolic Reprogramming in Hepatocellular Carcinoma. *Cancers (Basel)* **14** (2022). https://doi.org/10.3390/cancers14215468
377 Yu, M. *et al*. The evolving roles of Wnt signaling in stem cell proliferation and differentiation, the development of human diseases, and therapeutic opportunities. *Genes Dis* **11**, 101026 (2024). https://doi.org/10.1016/j.gendis.2023.04.042
378 Colozza, G., Park, S. Y. & Koo, B. K. Clone wars: From molecules to cell competition in intestinal stem cell homeostasis and disease. *Exp Mol Med* **54**, 1367-1378 (2022). https://doi.org/10.1038/s12276-022-00854-5
379 Flanagan, D. J., Austin, C. R., Vincan, E. & Phesse, T. J. Wnt Signalling in Gastrointestinal Epithelial Stem Cells. *Genes (Basel)* **9** (2018). https://doi.org/10.3390/genes9040178
380 Tian, A., Benchabane, H., Wang, Z. & Ahmed, Y. Regulation of Stem Cell Proliferation and Cell Fate Specification by Wingless/Wnt Signaling Gradients Enriched at Adult Intestinal Compartment Boundaries. *PLoS Genet* **12**, e1005822 (2016). https://doi.org/10.1371/journal.pgen.1005822
381 Meng, P., Zhu, M., Ling, X. & Zhou, L. Wnt signaling in kidney: the initiator or terminator? *J Mol Med (Berl)* **98**, 1511-1523 (2020). https://doi.org/10.1007/s00109-020-01978-9
382 Zhou, D., Tan, R. J., Fu, H. & Liu, Y. Wnt/beta-catenin signaling in kidney injury and repair: a double-edged sword. *Lab Invest* **96**, 156-167 (2016). https://doi.org/10.1038/labinvest.2015.153
383 Choi, Y. S. *et al*. Distinct functions for Wnt/beta-catenin in hair follicle stem cell proliferation and survival and interfollicular epidermal homeostasis. *Cell Stem Cell* **13**, 720-733 (2013). https://doi.org/10.1016/j.stem.2013.10.003
384 Mulligan, K. A. & Cheyette, B. N. Wnt signaling in vertebrate neural development and function. *J Neuroimmune Pharmacol* **7**, 774-787 (2012). https://doi.org/10.1007/s11481-012-9404-x
385 Oliva, C. A., Vargas, J. Y. & Inestrosa, N. C. Wnts in adult brain: from synaptic plasticity to cognitive deficiencies. *Front Cell Neurosci* **7**, 224 (2013). https://doi.org/10.3389/fncel.2013.00224
386 Gessert, S. & Kuhl, M. The multiple phases and faces of wnt signaling during cardiac differentiation and development. *Circ Res* **107**, 186-199 (2010). https://doi.org/10.1161/CIRCRESAHA.110.221531
387 Li, Y. *et al*. The molecular mechanisms of cardiac development and related diseases. *Signal Transduct Target Ther* **9**, 368 (2024). https://doi.org/10.1038/s41392-024-02069-8
388 Tian, Y., Cohen, E. D. & Morrisey, E. E. The importance of Wnt signaling in cardiovascular development. *Pediatr Cardiol* **31**, 342-348 (2010). https://doi.org/10.1007/s00246-009-9606-z
389 Calvisi, D. F. *et al*. Increased lipogenesis, induced by AKT-mTORC1-RPS6 signaling, promotes development of human hepatocellular carcinoma. *Gastroenterology* **140**, 1071-1083 (2011). https://doi.org/10.1053/j.gastro.2010.12.006
390 Cigliano, A., Wang, J., Chen, X. & Calvisi, D. F. Role of the Notch signaling in cholangiocarcinoma. *Expert Opin Ther Targets* **21**, 471-483 (2017). https://doi.org/10.1080/14728222.2017.1310842
391 Sirica, A. E. Notching Up on the Cellular Origins of Intrahepatic Cholangiocarcinoma. *Hepatology* **57**, 1668-1671 (2013).
392 South, A. P., Cho, R. J. & Aster, J. C. The double-edged sword of Notch signaling in cancer. *Semin Cell Dev Biol* **23**, 458-464 (2012). https://doi.org/10.1016/j.semcdb.2012.01.017

393 Zender, S. *et al*. A critical role for notch signaling in the formation of cholangiocellular carcinomas. *Cancer Cell* **23**, 784-795 (2013). https://doi.org/10.1016/j.ccr.2013.04.019
394 Sebestyen, M. G. *et al*. Mechanism of plasmid delivery by hydrodynamic tail vein injection. I. Hepatocyte uptake of various molecules. *J Gene Med* **8**, 852-873 (2006). https://doi.org/10.1002/jgm.921
395 Gentric, G., Celton-Morizur, S. & Desdouets, C. Polyploidy and liver proliferation. *Clin Res Hepatol Gastroenterol* **36**, 29-34 (2012). https://doi.org/10.1016/j.clinre.2011.05.011
396 Miyaoka, Y. *et al*. Hypertrophy and unconventional cell division of hepatocytes underlie liver regeneration. *Curr Biol* **22**, 1166-1175 (2012). https://doi.org/10.1016/j.cub.2012.05.016
397 Tanimizu, N., Nishikawa, Y., Ichinohe, N., Akiyama, H. & Mitaka, T. Sry HMG box protein 9-positive (Sox9+) epithelial cell adhesion molecule-negative (EpCAM-) biphenotypic cells derived from hepatocytes are involved in mouse liver regeneration. *J Biol Chem* **289**, 7589-7598 (2014). https://doi.org/10.1074/jbc.M113.517243
398 Means, A. L., Xu, Y., Zhao, A., Ray, K. C. & Gu, G. A CK19(CreERT) knockin mouse line allows for conditional DNA recombination in epithelial cells in multiple endodermal organs. *Genesis* **46**, 318-323 (2008). https://doi.org/10.1002/dvg.20397
399 Obiorah, I. E. *et al*. Prognostic Implications of Arginase and Cytokeratin 19 Expression in Hepatocellular Carcinoma After Curative Hepatectomy: Correlation With Recurrence-Free Survival. *Gastroenterology Res* **12**, 78-87 (2019). https://doi.org/10.14740/gr1156
400 Zhuo, J. *et al*. The distinct responsiveness of cytokeratin 19-positive hepatocellular carcinoma to regorafenib. *Cell Death Dis* **12**, 1084 (2021). https://doi.org/10.1038/s41419-021-04320-4
401 Sekiya, S. & Suzuki, A. Intrahepatic cholangiocarcinoma can arise from Notch-mediated conversion of hepatocytes. *J Clin Invest* **122**, 3914-3918 (2012). https://doi.org/10.1172/JCI63065
402 Boulter, L. *et al*. Macrophage-derived Wnt opposes Notch signaling to specify hepatic progenitor cell fate in chronic liver disease. *Nat Med* **18**, 572-579 (2012). https://doi.org/10.1038/nm.2667
403 Fan, J. *et al*. Noncanonical Wnt signaling plays an important role in modulating canonical Wnt-regulated stemness, proliferation and terminal differentiation of hepatic progenitors. *Oncotarget* **8**, 27105-27119 (2017).
404 Velazquez-Villegas, L. A. *et al*. PPARalpha Downregulates Hepatic Glutaminase Expression in Mice Fed Diets with Different Protein:Carbohydrate Ratios. *J Nutr* **146**, 1634-1640 (2016). https://doi.org/10.3945/jn.116.232868
405 Russell, J. O. *et al*. Hepatocyte-Specific beta-Catenin Deletion During Severe Liver Injury Provokes Cholangiocytes to Differentiate Into Hepatocytes. *Hepatology* **69**, 742-759 (2019). https://doi.org/10.1002/hep.30270
406 Tan, Y., Yoshida, Y., Hughes, D. E. & Costa, R. H. Increased Expression of Hepatocyte Nuclear Factor 6 Stimulates Hepatocyte Proliferation during Mouse Liver Regeneration. *Gastroenterology* **130**, 1283–1300 (2006).
407 Parviz, F. *et al*. Hepatocyte nuclear factor 4α controls the development of a hepatic epithelium and liver morphogenesis. *Nature Genetics* **34** (2003).
408 Chen, T. & Dent, S. Y. Chromatin modifiers and remodellers: regulators of cellular differentiation. *Nat Rev Genet* **15**, 93-106 (2014). https://doi.org/10.1038/nrg3607
409 Mossink, B., Negwer, M., Schubert, D. & Nadif Kasri, N. The emerging role of chromatin remodelers in neurodevelopmental disorders: a developmental perspective. *Cell Mol Life Sci* **78**, 2517-2563 (2021). https://doi.org/10.1007/s00018-020-03714-5
410 Singh, P. N. P., Madha, S., Leiter, A. B. & Shivdasani, R. A. Cell and chromatin transitions in intestinal stem cell regeneration. *Genes Dev* **36**, 684-698 (2022). https://doi.org/10.1101/gad.349412.122

411 Ye, Y. *et al.* Chromatin remodeling during in vivo neural stem cells differentiating to neurons in early Drosophila embryos. *Cell Death Differ* **24**, 409-420 (2017). https://doi.org/10.1038/cdd.2016.135
412 Tian, M. *et al.* Role of HNF6 in liver homeostasis and pathophysiology. *Mol Med* **31**, 48 (2025). https://doi.org/10.1186/s10020-025-01105-9
413 Aguilar-Bravo, B. *et al.* Hepatocyte dedifferentiation profiling in alcohol-related liver disease identifies CXCR4 as a driver of cell reprogramming. *J Hepatol* **79**, 728-740 (2023). https://doi.org/10.1016/j.jhep.2023.04.013
414 Mu, X. *et al.* Hepatocellular carcinoma originates from hepatocytes and not from the progenitor/biliary compartment. *J Clin Invest* **125**, 3891-3903 (2015). https://doi.org/10.1172/JCI77995
415 Jin, J., Byun, J. K., Choi, Y. K. & Park, K. G. Targeting glutamine metabolism as a therapeutic strategy for cancer. *Exp Mol Med* **55**, 706-715 (2023). https://doi.org/10.1038/s12276-023-00971-9
416 Jin, L., Alesi, G. N. & Kang, S. Glutaminolysis as a target for cancer therapy. *Oncogene* **35**, 3619-3625 (2016). https://doi.org/10.1038/onc.2015.447
417 Li, T., Copeland, C. & Le, A. Glutamine Metabolism in Cancer. *Adv Exp Med Biol* **1311**, 17-38 (2021). https://doi.org/10.1007/978-3-030-65768-0_2
418 Hishida, T. *et al.* In vivo partial cellular reprogramming enhances liver plasticity and regeneration. *Cell Rep* **39**, 110730 (2022). https://doi.org/10.1016/j.celrep.2022.110730
419 Carr, M. I. & Jones, S. N. Regulation of the Mdm2-p53 signaling axis in the DNA damage response and tumorigenesis. *Transl Cancer Res* **5**, 707-724 (2016). https://doi.org/10.21037/tcr.2016.11.75
420 Chibaya, L., Karim, B., Zhang, H. & Jones, S. N. Mdm2 phosphorylation by Akt regulates the p53 response to oxidative stress to promote cell proliferation and tumorigenesis. *Proc Natl Acad Sci U S A* **118** (2021). https://doi.org/10.1073/pnas.2003193118
421 Hayhurst, G. P., Lee, Y. H., Lambert, G., Ward, J. M. & Gonzalez, F. J. Hepatocyte nuclear factor 4alpha (nuclear receptor 2A1) is essential for maintenance of hepatic gene expression and lipid homeostasis. *Mol Cell Biol* **21**, 1393-1403 (2001). https://doi.org/10.1128/MCB.21.4.1393-1403.2001
422 Jin, J. *et al.* Correlations of Long Noncoding RNA HNF4A-AS1 Alternative Transcripts with Liver Diseases and Drug Metabolism. *Drug Metab Dispos* **52**, 1345-1355 (2024). https://doi.org/10.1124/dmd.124.001873
423 Suda, T. *et al.* Hydrodynamic Delivery: Characteristics, Applications, and Technological Advances. *Pharmaceutics* **15** (2023). https://doi.org/10.3390/pharmaceutics15041111
424 Hai, T., Wolford, C. C. & Chang, Y. S. ATF3, a hub of the cellular adaptive-response network, in the pathogenesis of diseases: is modulation of inflammation a unifying component? *Gene Expr* **15**, 1-11 (2010). https://doi.org/10.3727/105221610x12819686555015
425 Ohnishi, Y. N. *et al.* FosB is essential for the enhancement of stress tolerance and antagonizes locomotor sensitization by DeltaFosB. *Biol Psychiatry* **70**, 487-495 (2011). https://doi.org/10.1016/j.biopsych.2011.04.021
426 Kawai, T. & Akira, S. Regulation of innate immune signalling pathways by the tripartite motif (TRIM) family proteins. *EMBO Molecular Medicine* **3**, 513-527 (2011). https://doi.org/10.1002/emmm.201100160
427 Yang, W., Gu, Z., Zhang, H. & Hu, H. To TRIM the Immunity: From Innate to Adaptive Immunity. *Front Immunol* **11**, 02157 (2020). https://doi.org/10.3389/fimmu.2020.02157
428 Watanabe, A. *et al.* Arf GTPase-activating proteins SMAP1 and AGFG2 regulate the size of Weibel-Palade bodies and exocytosis of von Willebrand factor. *Biol Open* **10** (2021). https://doi.org/10.1242/bio.058789

429 Ntziachristos, P., Lim, J. S., Sage, J. & Aifantis, I. From fly wings to targeted cancer therapies: a centennial for notch signaling. *Cancer Cell* **25**, 318-334 (2014). https://doi.org/10.1016/j.ccr.2014.02.018

430 da Silva, R. P., Eudy, B. J. & Deminice, R. One-Carbon Metabolism in Fatty Liver Disease and Fibrosis: One-Carbon to Rule Them All. *J Nutr* **150**, 994-1003 (2020). https://doi.org/10.1093/jn/nxaa032

431 Queathem, E. D. *et al*. Ketogenesis supports hepatic polyunsaturated fatty acid homeostasis via fatty acid elongation. *bioRxiv* (2024). https://doi.org/10.1101/2024.07.09.602593

432 Ou, D. L. *et al*. Growth arrest DNA damage-inducible gene 45 gamma expression as a prognostic and predictive biomarker in hepatocellular carcinoma. *Oncotarget* **6** (2015).

433 Girard, R. *et al*. The transcription factor hepatocyte nuclear factor 4A acts in the intestine to promote white adipose tissue energy storage. *Nat Commun* **13**, 224 (2022). https://doi.org/10.1038/s41467-021-27934-w

434 Glaser, S. *et al*. Differential transcriptional characteristics of small and large biliary epithelial cells derived from small and large bile ducts. *Am J Physiol Gastrointest Liver Physiol* **299**, G769-777 (2010). https://doi.org/10.1152/ajpgi.00237.2010

435 Tachmatzidi, E. C., Galanopoulou, O. & Talianidis, I. Transcription Control of Liver Development. *Cells* **10** (2021). https://doi.org/10.3390/cells10082026

436 Wallace, D. C. Mitochondria and cancer. *Nat Rev Cancer* **12**, 685-698 (2012). https://doi.org/10.1038/nrc3365

437 Iwafuchi-Doi, M. & Zaret, K. S. Cell fate control by pioneer transcription factors. *Development* **143**, 1833-1837 (2016). https://doi.org/10.1242/dev.133900

438 Sia, D., Villanueva, A., Friedman, S. L. & Llovet, J. M. Liver Cancer Cell of Origin, Molecular Class, and Effects on Patient Prognosis. *Gastroenterology* **152**, 745-761 (2017). https://doi.org/10.1053/j.gastro.2016.11.048

439 Pek, N. M. Q., Liu, K. J., Nichane, M. & Ang, L. T. Controversies Surrounding the Origin of Hepatocytes in Adult Livers and the in Vitro Generation or Propagation of Hepatocytes. *Cell Mol Gastroenterol Hepatol* **11**, 273-290 (2021). https://doi.org/10.1016/j.jcmgh.2020.09.016

440 Holczbauer, A., Wangensteen, K. J. & Shin, S. Cellular origins of regenerating liver and hepatocellular carcinoma. *JHEP Rep* **4**, 100416 (2022). https://doi.org/10.1016/j.jhepr.2021.100416

441 Kim, M., Delgado, E. & Ko, S. DNA methylation in cell plasticity and malignant transformation in liver diseases. *Pharmacol Ther* **241**, 108334 (2023). https://doi.org/10.1016/j.pharmthera.2022.108334

442 Perez-Miguelsanz, J. *et al*. Betaine homocysteine S-methyltransferase emerges as a new player of the nuclear methionine cycle. *Biochim Biophys Acta Mol Cell Res* **1864**, 1165-1182 (2017). https://doi.org/10.1016/j.bbamcr.2017.03.004

443 Kadonaga, J. T. Regulation of RNA Polymerase II Transcription by Sequence-Specific DNA Binding Factors<RNA polymerase II-specific transcription. *Cell* **116**, 247-257 (2004).

444 Stern, J. R. A Role of Acetoacetyl-CoA Synthetase in Acetoacetate Utilization by Rat Liver Cell Fractions. *Biochemical and Biophysical Research Communications* **44** (1971).

445 Raynaud, P., Carpentier, R., Antoniou, A. & Lemaigre, F. P. Biliary differentiation and bile duct morphogenesis in development and disease. *Int J Biochem Cell Biol* **43**, 245-256 (2011). https://doi.org/10.1016/j.biocel.2009.07.020

446 Shiojiri, N. & Mizuno, T. Differentiation of functional hepatocytes and biliary epithelial cells from immature hepatocytes of the fetal mouse in vitro. *Anatomy and Embryology* **187**, 221-229 (1993).

447 Sekiya, S. & Suzuki, A. Hepatocytes, rather than cholangiocytes, can be the major source of primitive ductules in the chronically injured mouse liver. *Am J Pathol* **184**, 1468-1478 (2014). https://doi.org/10.1016/j.ajpath.2014.01.005

448 Tanimizu, N. *et al*. Hepatic biliary epithelial cells acquire epithelial integrity but lose plasticity to differentiate into hepatocytes in vitro during development. *J Cell Sci* **126**, 5239-5246 (2013). https://doi.org/10.1242/jcs.133082
449 Haegebarth, A. & Clevers, H. Wnt signaling, lgr5, and stem cells in the intestine and skin. *Am J Pathol* **174**, 715-721 (2009). https://doi.org/10.2353/ajpath.2009.080758
450 Yeung, T. M., Chia, L. A., Kosinski, C. M. & Kuo, C. J. Regulation of self-renewal and differentiation by the intestinal stem cell niche. *Cell Mol Life Sci* **68**, 2513-2523 (2011). https://doi.org/10.1007/s00018-011-0687-5
451 Bai, R. *et al*. The Roles of WNT Signaling Pathways in Skin Development and Mechanical-Stretch-Induced Skin Regeneration. *Biomolecules* **13** (2023). https://doi.org/10.3390/biom13121702
452 Cain, C. J. & Manilay, J. O. Hematopoietic stem cell fate decisions are regulated by Wnt antagonists: comparisons and current controversies. *Exp Hematol* **41**, 3-16 (2013). https://doi.org/10.1016/j.exphem.2012.09.006
453 Ring, A., Kim, Y. M. & Kahn, M. Wnt/catenin signaling in adult stem cell physiology and disease. *Stem Cell Rev Rep* **10**, 512-525 (2014). https://doi.org/10.1007/s12015-014-9515-2
454 Gajos-Michniewicz, A. & Czyz, M. WNT/beta-catenin signaling in hepatocellular carcinoma: The aberrant activation, pathogenic roles, and therapeutic opportunities. *Genes Dis* **11**, 727-746 (2024). https://doi.org/10.1016/j.gendis.2023.02.050
455 Wang, K., Qiu, X., Zhao, Y., Wang, H. & Chen, L. The Wnt/beta-catenin signaling pathway in the tumor microenvironment of hepatocellular carcinoma. *Cancer Biol Med* **19**, 305-318 (2021). https://doi.org/10.20892/j.issn.2095-3941.2021.0306
456 Chung, A. *et al*. Liver cancer initiation is dependent on metabolic zonation but decoupled from premalignant clonal expansion. *bioRxiv* (2024). https://doi.org/10.1101/2024.01.10.575013
457 Rizki-Safitri, A. *et al*. Prospect of in vitro Bile Fluids Collection in Improving Cell-Based Assay of Liver Function. *Front Toxicol* **3**, 657432 (2021). https://doi.org/10.3389/ftox.2021.657432
458 Aloia, L. *et al*. Epigenetic remodelling licences adult cholangiocytes for organoid formation and liver regeneration. *Nat Cell Biol* **21**, 1321-1333 (2019). https://doi.org/10.1038/s41556-019-0402-6
459 Nikopoulou, C. *et al*. Spatial and single-cell profiling of the metabolome, transcriptome and epigenome of the aging mouse liver. *Nat Aging* **3**, 1430-1445 (2023). https://doi.org/10.1038/s43587-023-00513-y
460 Moon, H. & Ro, S. W. Ras Mitogen-activated Protein Kinase Signaling and Kinase Suppressor of Ras as Therapeutic Targets for Hepatocellular Carcinoma. *J Liver Cancer* **21**, 1-11 (2021). https://doi.org/10.17998/jlc.21.1.1
461 Gang, E. J. *et al*. Small-molecule inhibition of CBP/catenin interactions eliminates drug-resistant clones in acute lymphoblastic leukemia. *Oncogene* **33**, 2169-2178 (2014). https://doi.org/10.1038/onc.2013.169
462 Ram, T. *et al*. MEK inhibitors in cancer treatment: structural insights, regulation, recent advances and future perspectives. *RSC Med Chem* **14**, 1837-1857 (2023). https://doi.org/10.1039/d3md00145h
463 Wang, C. *et al*. Verteporfin inhibits YAP function through up-regulating 14-3-3σ sequestering YAP in the cytoplasm. *Am J Cancer Res* **6** (2016).
464 Chapeau, E. A. *et al*. Direct and selective pharmacological disruption of the YAP-TEAD interface by IAG933 inhibits Hippo-dependent and RAS-MAPK-altered cancers. *Nat Cancer* **5**, 1102-1120 (2024). https://doi.org/10.1038/s43018-024-00754-9
465 Markley, J. L. *et al*. The future of NMR-based metabolomics. *Curr Opin Biotechnol* **43**, 34-40 (2017). https://doi.org/10.1016/j.copbio.2016.08.001
466 Lane, A. N., Higashi, R. M. & Fan, T. W. NMR and MS-based Stable Isotope-Resolved Metabolomics and Applications in Cancer Metabolism. *Trends Analyt Chem* **120** (2019). https://doi.org/10.1016/j.trac.2018.11.020

467 Jang, C., Chen, L. & Rabinowitz, J. D. Metabolomics and Isotope Tracing. *Cell* **173**, 822-837 (2018). https://doi.org/10.1016/j.cell.2018.03.055

468 Guest, R. V., Boulter, L., Dwyer, B. J. & Forbes, S. J. Understanding liver regeneration to bring new insights to the mechanisms driving cholangiocarcinoma. *NPJ Regen Med* **2**, 13 (2017). https://doi.org/10.1038/s41536-017-0018-z

469 Reichert, D. *et al*. Improved Recovery from Liver Fibrosis by Crenolanib. *Cells* **10** (2021). https://doi.org/10.3390/cells10040804

470 Huck, I., Gunewardena, S., Espanol-Suner, R., Willenbring, H. & Apte, U. Hepatocyte Nuclear Factor 4 Alpha Activation Is Essential for Termination of Liver Regeneration in Mice. *Hepatology* **70**, 666-681 (2019). https://doi.org/10.1002/hep.30405

471 Jang, J. H., Kang, K. J., Kim, Y. H., Kang, Y. N. & Lee, I. S. Reevaluation of experimental model of hepatic fibrosis induced by hepatotoxic drugs: an easy, applicable, and reproducible model. *Transplant Proc* **40**, 2700-2703 (2008). https://doi.org/10.1016/j.transproceed.2008.07.040

472 Ko, S., Russell, J. O., Molina, L. M. & Monga, S. P. Liver Progenitors and Adult Cell Plasticity in Hepatic Injury and Repair: Knowns and Unknowns. *Annu Rev Pathol* **15**, 23-50 (2020). https://doi.org/10.1146/annurev-pathmechdis-012419-032824